CANADIAN THESES ON MICROFICHE

I.S.B.N.

THESES CANADIENNES SUR MICROFICHE

National Library of Canada
Collections Development Branch

Canadian Theses on
Microfiche Service

Ottawa, Canada
K1A 0N4

Bibliothèque nationale du Canada
Direction du développement des collections

Service des thèses canadiennes
sur microfiche

## NOTICE

The quality of this microfiche is heavily dependent upon the quality of the original thesis submitted for microfilming. Every effort has been made to ensure the highest quality of reproduction possible.

If pages are missing, contact the university which granted the degree.

Some pages may have indistinct print especially if the original pages were typed with a poor typewriter ribbon or if the university sent us a poor photocopy.

Previously copyrighted materials (journal articles, published tests, etc.) are not filmed.

Reproduction in full or in part of this film is governed by the Canadian Copyright Act, R.S.C. 1970, c. C-30. Please read the authorization forms which accompany this thesis.

## AVIS

La qualité de cette microfiche dépend grandement de la qualité de la thèse soumise au microfilmage. Nous avons tout fait pour assurer une qualité supérieure de reproduction.

S'il manque des pages, veuillez communiquer avec l'université qui a conféré le grade.

La qualité d'impression de certaines pages peut laisser à désirer, surtout si les pages originales ont été dactylographiées à l'aide d'un ruban usé ou si l'université nous a fait parvenir une photocopie de mauvaise qualité.

Les documents qui font déjà l'objet d'un droit d'auteur (articles de revue, examens publiés, etc.) ne sont pas microfilmés.

La reproduction, même partielle, de ce microfilm est soumise à la Loi canadienne sur le droit d'auteur, SRC 1970, c. C-30. Veuillez prendre connaissance des formules d'autorisation qui accompagnent cette thèse.

THIS DISSERTATION
HAS BEEN MICROFILMED
EXACTLY AS RECEIVED

LA THÈSE A ÉTÉ
MICROFILMÉE TELLE QUE
NOUS L'AVONS REÇUE

NL-339 (r. 82/08)

Canada

0-315-08917-2

National Library of Canada | Bibliothèque nationale du Canada

28 Canadian Theses Division | Division des thèses canadiennes

Ottawa, Canada
K1A 0N4

56834

## PERMISSION TO MICROFILM — AUTORISATION DE MICROFILMER

• Please print or type — Écrire en lettres moulées ou dactylographier

Full Name of Author — Nom complet de l'auteur

ROGER CHEUNG-LUP NG

Date of Birth — Date de naissance

NOVEMBER 25, ~~1952~~ 1953.

Country of Birth — Lieu de naissance

HONG KONG

Permanent Address — Résidence fixe

8404 - 14 AVENUE,
EDMONTON, ALBERTA, CANADA T6K 1X4

Title of Thesis — Titre de la thèse

CORRELATION BASED DATA PROCESSING FOR SIMULTANEOUS MULTIELEMENT ANALYSIS BY INDUCTIVELY COUPLED PLASMA EMISSION SPECTROSCOPY

University — Université

UNIVERSITY OF ALBERTA, EDMONTON, ALBERTA, CANADA

Degree for which thesis was presented — Grade pour lequel cette thèse fut présentée

Ph.D.

Year this degree conferred — Année d'obtention de ce grade

1982

Name of Supervisor — Nom du directeur de thèse

GARY HORLICK

Permission is hereby granted to the NATIONAL LIBRARY OF CANADA to microfilm this thesis and to lend or sell copies of the film.

The author reserves other publication rights, and neither the thesis nor extensive extracts from it may be printed or otherwise reproduced without the author's written permission.

L'autorisation est, par la présente, accordée à la BIBLIOTHÈQUE NATIONALE DU CANADA de microfilmer cette thèse et de prêter ou de vendre des exemplaires du film.

L'auteur se réserve les autres droits de publication; ni la thèse ni de longs extraits de celle-ci ne doivent être imprimés ou autrement reproduits sans l'autorisation écrite de l'auteur.

Date

March 29, 1982

Signature

R. Cheung-Lup Ng

NL-91 (4/77)

THE UNIVERSITY OF ALBERTA

# CORRELATION BASED DATA PROCESSING FOR SIMULTANEOUS MULTIELEMENT ANALYSIS BY INDUCTIVELY COUPLED PLASMA EMISSION SPECTROSCOPY

by

© ROGER C.L. NG

A THESIS

SUBMITTED TO THE FACULTY OF GRADUATE STUDIES AND RESEARCH

IN PARTIAL FULFILMENT OF THE REQUIREMENTS FOR THE DEGREE

OF DOCTOR OF PHILOSOPHY

IN

DEPARTMENT OF CHEMISTRY

EDMONTON, ALBERTA

SPRING, 1982

THE UNIVERSITY OF ALBERTA

RELEASE FORM

NAME OF AUTHOR Roger C.L. Ng

TITLE OF THESIS Correlation Based Data Processing for Simultaneous Multielement Analysis by Inductively Coupled Plasma Emission Spectroscopy

DEGREE FOR WHICH THESIS WAS PRESENTED Ph.D.

YEAR THIS DEGREE GRANTED 1982

Permission is hereby granted to THE UNIVERSITY OF ALBERTA LIBRARY to reproduce single copies of this thesis and to lend or sell such copies for private, scholarly or scientific research purposes only.

The author reserves other publication rights, and neither the thesis nor extensive extracts from it may be printed or otherwise reproduced without the author's written permission.

(Signed) Ng Cheung Lup

Permanent Address:
8404 - 14 Avenue
Edmonton, Alberta. T6K 1X4

Dated February 18, 1982

THE UNIVERSITY OF ALBERTA

FACULTY OF GRADUATE STUDIES AND RESEARCH

The undersigned certify that they have read, and recommend to the Faculty of Graduate Studies and Research for acceptance, a thesis entitled CORRELATION BASED DATA PROCESSING FOR SIMULTANEOUS MULTIELEMENT ANALYSIS BY INDUCTIVELY COUPLED PLASMA EMISSION SPECTROSCOPY submitted by ROGER C.L. NG in partial fulfilment of the reguirements for the degree of Doctor of Philosophy in Analytical Chemistry.

Gary Horlick
G. Horlick, Supervisor

F.F. Cantwell

D.G. Fisher

P. Kebarle

D.L. Rabenstein

R.C. Fry
R.C. Fry, External Examiner

Date February 18, 1982

To my mother and

the memory of my father

## ABSTRACT

With the advent of inductively coupled plasma (ICP) emission spectroscopy, vast amounts of analytical information can be obtained simultaneously. However, only a small fraction of this information is actually utilized by the conventional detection systems such as direct reading type spectrometers when coupled to the ICP. In our laboratory, measurement systems based on photodiode array and Fourier transform spectrometers which are capable of simultaneously acquiring several hundred Angstroms of continuous spectral information from the ICP have been developed. Given such spectrochemical measurement systems, one then needs effective software and hardware systems to fully utilize the large amounts of spectral data available from these systems. Correlation based methods are found to be particularly simple and effective.

In this thesis, theoretical and practical aspects of correlation techniques as applied to spectral data processing are discussed. Simply speaking, correlation analysis involves the use of a function (correlation mask) to extract desirable analytical information from raw experimental data. A unique correlation data point can be obtained by performing a point-to-point multiplication between the correlation mask and the raw spectral data at zero phase shift. The summation of these products represents

the consolidation of all the desirable spectral information into a single point. With the proper choice of correlation masks, the relative and absolute magnitudes of this correlation data point indicate the qualitative and quantitative information for the analyte-of-interest.

The correlation procedure is applied to analytical data obtained with the ICP-photodiode array spectrometer and the ICP-Fourier transform spectrometer systems. It is shown that this technique can be utilized to process complex spectral patterns for specific information via a software approach. This includes the identification and quantitation of sought-for analyte. Because of the simplicity of this method, the possibility of implementing correlation analysis for automatic computer interpretation of spectral data is evaluated.

Finally, the power of correlation techniques is then further illustrated with the development of a real time data processing system for interferometric signals. In this case, hardware implementation of correlation analysis is achieved with the aid of a low cost microcomputer and a high speed electronic multiplier-accumulator chip.

ACKNOWLEDGEMENT

I would like to extend my sincere thanks and appreciation to Professor Gary Horlick for his continuous support and advice, and Dr. Robert Hall for his expert suggestions on the operation of the interferometer system during the initial stage of this study.

I would also like to thank my sister, Fanny for her assistance in typing the thesis.

Finally, I have to thank my wife, Amy and my lovely daughter, Tania for their understanding and patience during the course of my graduate studies.

TABLE OF CONTENTS


| Chapter | | Page |
|---|---|---|
| I | Introduction | |
| | A. An Ideal Spectrochemical Measurement System | 1 |
| | B. Atomic Emission Spectroscopy | 3 |
| | Inductively Coupled Plasma | 5 |
| | C. Multielement Analysis Spectrometers | 9 |
| | D. Correlation Based Signal Processing | 17 |
| II | Theoretical and Practical Aspects of Correlation Analysis | |
| | A. What is Correlation? | 23 |
| | B. Correlation and Fourier Transformation | 25 |
| | Computer Software | 26 |
| | Utilization of Fast Fourier Transform Algorithms | 27 |
| | Inverse Fourier Transformation | 35 |
| | C. Cross-correlation | 42 |
| | D. Auto-correlation | 47 |
| | E. Convolution | 50 |
| | F. Information at $\tau = 0$ Point of the Cross-correlation Function | 56 |
| III | Correlation Based Data Processing for the ICP-Photodiode Array Spectrometer System | |
| | A. Introduction | 63 |

Chapter | Page

B. The ICP-Photodiode Array Spectrometer System . . . . . 64
C. Simple Cross-correlation Masks . . . . . 67
D. Cross-correlation Masks for Complex Spectra. . . . . 73
E. Conclusions. . . . . 84

IV Correlation Based Data Processing for the ICP-Fourier Transform Spectrometer System
A. Introduction . . . . . 91
B. The Experimental System. . . . . 93
C. Use of a Fourier Transform Spectrometer as a Simultaneous Detection System for the ICP
(a) General Considerations . . . . . 102
(b) Noise Studies of the ICP by a Fourier Transform Spectrometer . . . . . 105
(c) Analytical Improvement of the ICP-FT Spectrometer System Using a Mixed Gas ICP. . . . . 109
(d) Conclusion . . . . . 121
D. Cross-correlation Masks for Processing Interferograms . . . . . 125
E. Elemental Analysis Using Cross-correlation Techniques . . . . . 133

| Chapter | | Page |
|---|---|---|
| | Qualitative Aspects . . . . . | 133 |
| | Quantitative Aspects. . . . . | 158 |
| | F. Conclusions . . . . . | 167 |
| V | A Real Time Correlation Based Data Processing System for Interferometric Signals | |
| | A. Introduction to Real Time Data Processing Systems for Interferometric Signals . . . | 170 |
| | B. Rockwell AIM 65/TRW Multiplier-Accumulator Data Processing System. . . . . | 172 |
| | Rockwell AIM 65 Microcomputer . . . . . | 174 |
| | Interferometer Control and Measurement Electronics . . . . . | 177 |
| | Start Pulse and Clock Control Circuitry . | 180 |
| | Analog to Digital Conversion Circuitry. . | 182 |
| | TRW Multiplier-Accumulator. . . . . | 184 |
| | Data Multiplexing Circuitry . . . . . | 187 |
| | Computer Software . . . . . | 189 |
| | C. Evaluation of the Rockwell AIM 65/TRW MAC Data Processing System. . . . . | 196 |
| | Qualitative Aspects . . . . . | 196 |
| | Quantitative Aspects. . . . . | 202 |
| | D. Conclusions and Prospects . . . . . | 207 |
| VI | Summary. . . . . | 211 |

Page

Footnotes . . . . . 215

Bibliography . . . . . 216

Appendix I Alternate Methods of Recycling Fast Fourier Transform Algorithms . . . . . 225

Appendix II Modifications of the Michelson Interferometer . . . . . 233

Appendix III Computer Software . . . . . 239

## LIST OF TABLES


| Table | Description | Page |
|---|---|---|
| 1 | Components of the ICP-PDA spectrometer system. | 66 |
| 2 | Detectors used in the ICP-Fourier transform spectrometer system. | 99 |
| 3 | Various components of the ICP-Fourier transform spectrometer system. | 101 |
| 4 | Recommended ICP source at different spectral regions. | 123 |
| 5 | Most sensitive ICP emission line for 70 elements. | 137 |
| 6 | Most sensitive ICP emission line for 70 elements within the spectral window of 240-260 nm. | 147 |
| 7 | Some ICP emission lines for aluminium, cobalt, iron, nickel, palladium and vanadium (240 nm - 360 nm). | 151 |
| 8 | Percent relative standard deviation data for different data processing methods. (10 ppm vanadium, ten readings) | 166 |
| 9 | Binary equivalence of the correlation masks. | 192 |
| 10 | Decimal equivalence of the correlation masks as generated by the BASIC program. | 194 |

| Table | Description | Page |
|---|---|---|
| 11 | Memory map of the AIM 65 microcomputer. | 195 |
| 12 | Some spectral lines in the near IR-visible region. | 197 |
| 13 | Most sensitive ICP spectral lines of magnesium, scandium, tin and thallium within the 240-360 nm window. | 203 |

LIST OF FIGURES


| Figure | Description | Page |
|---|---|---|
| 1 | Schematic diagram of an ICP discharge. | 7 |
| 2 | (a) Zinc, (b) cadmium and (c) boron spectra. | 19 |
| 3 | Cross-correlation patterns for the (a) zinc, (b) cadmium and (c) boron spectra with the zinc spectrum. | 20 |
| 4 | A simple line spectrum used as the input data array for the FFT implementation. | 29 |
| 5 | (a) Real and (b) imaginary output arrays for Scheme 1 implementation of the FFT. | 30 |
| 6 | (a) Real and (b) imaginary output arrays for Scheme 2 implementation of the FFT. | 32 |
| 7 | A single peak spectrum. | 33 |
| 8 | (a) Real, (b) imaginary and (c) amplitude output arrays for the single peak spectrum with Scheme 2 FFT implementation. | 34 |
| 9 | (a) Real and (b) imaginary output arrays for the single peak spectrum with Scheme 1 FFT implementation. | 36 |
| 10 | (a) Real, (b) imaginary and (c) amplitude output arrays for Scheme 3 inverse FFT implementation. | 38 |
| 11 | (a) Real, (b) imaginary and (c) amplitude output arrays for Scheme 4 inverse FFT implementation. | 41 |

| Figure | Description | Page |
|---|---|---|
| 12 | Flow chart for Fourier domain cross-correlation. | 43 |
| 13 | (a) Function one and (b) function two for cross-correlation operation. (c) Cross-correlation function as calculated by the procedure outlined in Figure 12. | 44 |
| 14 | Cross-correlation function resulting from function one * function two. | 46 |
| 15 | Cross-correlation function resulting from function two * function one. | 48 |
| 16 | Flow chart for Fourier domain auto-correlation. | 49 |
| 17 | Flow chart for simplified Fourier domain auto-correlation. | 51 |
| 18 | (a) Function to be auto-correlated. (b) Auto-correlation function as calculated by the procedure outlined in Figure 17. | 52 |
| 19 | Auto-correlation function for the function shown in Figure 18(a). | 53 |
| 20 | (a) An input peak signal. (b) Low pass filter response function. | 55 |
| 21 | Convolution function resulting from the peak signal and the low pass filter response function. | 57 |

| Figure | Description | Page |
|---|---|---|
| 22 | Sample spectrum containing cadmium and zinc. | 59 |
| 23 | Correlation patterns for the sample spectrum with the (a) zinc, (b) cadmium and (c) boron spectra. | 61 |
| 24 | Vanadium spectral intensity and binary cross-correlation masks. | 68 |
| 25 | Vanadium analytical curves determined using spectral intensity cross-correlation masks. Threshold (a) 0%, (b) 20%, (c) 40%, (d) 60% and (e) 80%. | 70 |
| 26 | Vanadium analytical curves determined using binary cross-correlation masks. Thresholds (a) 20%, (b) 40%, (c) 60% and (d) 80%. | 72 |
| 27 | Nickel spectral intensity and binary cross-correlation masks. | 74 |
| 28 | Spectrum of nickel (1000 ppm) and vanadium (180 ppm). | 76 |
| 29 | Vanadium minus nickel difference spectrum. | 77 |
| 30 | Vanadium spectral intensity and binary cross-correlation masks minus any nickel information. | 79 |
| 31 | Nickel minus vanadium difference spectrum. | 80 |

| Figure | Description | Page |
|---|---|---|
| 32 | Nickel spectral intensity and binary cross-correlation masks minus any vanadium information. | 81 |
| 33 | Detection of nickel in the presence of vanadium using nickel spectral intensity cross-correlation masks. Thresholds (a) 0%, (b) 20%, (c) 40%, (d) 60% and (e) 80%. | 82 |
| 34 | Detection of nickel in the presence of vanadium using vanadium stripped nickel spectral intensity cross-correlation masks. Thresholds (a) 0%, (b) 20%, (c) 40%, (d) 60% and (e) 80%. | 83 |
| 35 | Detection of nickel in the presence of vanadium using nickel binary cross-correlation masks. Thresholds (a) 20%, (b) 40%, (c) 60% and (d) 80%. | 85 |
| 36 | Detection of nickel in the presence of vanadium using vanadium stripped nickel binary cross-correlation masks. Thresholds (a) 20%, (b) 40%, (c) 60% and (d) 80%. | 86 |
| 37 | Vanadium analytical curves determined using nickel stripped vanadium spectral intensity cross-correlation masks. Thresholds (a) 0%, (b) 20%, (c) 40%, (d) 60% and (e)80%. | 87 |

| Figure | Description | Page |
|---|---|---|
| 38 | Vanadium analytical curves determined using nickel stripped vanadium binary cross-correlation masks. Thresholds (a) 20%, (b) 40%, (c) 60% and (d) 80%. | 88 |
| 39 | Block diagram of the ICP-Fourier transform spectrometer system. | 94 |
| 40 | Schematic diagram of the Michelson interferometer. | 96 |
| 41 | Block diagram of the Michelson interferometer setup. | 97 |
| 42 | Spectrum illustrating the presence of proportional noise originated from the ICP. | 107 |
| 43 | Sodium (500 ppm) spectrum obtained using a conventional argon ICP. | 111 |
| 44 | Sodium (500 ppm) spectrum obtained using a 50% argon / 50% nitrogen ICP. | 113 |
| 45 | Analytical working curve for lithium obtained using an argon/nitrogen ICP. | 115 |
| 46 | Background of the argon ICP in the visible region. | 116 |
| 47 | Background of the argon/nitrogen ICP in the visible region. | 117 |
| 48 | Analytical working curve of calcium obtained using a 50% argon/50% nitrogen ICP. | 118 |

| Figure | Description | Page |
|---|---|---|
| 49 | Calcium (10 ppm) spectrum obtained using a helium/argon ICP. | 120 |
| 50 | Analytical working curve of magnesium obtained using a conventional argon ICP. | 122 |
| 51 | Interferogram resulting from a He-Ne laser. | 128 |
| 52 | Cross-correlation between cosine waves of (a) same frequency and (b) different frequencies. | 130 |
| 53 | A multielement interferogram containing lithium, sodium, potassium, rubidium and cesium. | 134 |
| 54 | Multielement spectrum containing lithium, sodium, potassium, rubidium and cesium emission lines. | 136 |
| 55 | Results of cross-correlation analysis on the multielement alkali metal interferogram utilizing analog cross-correlation masks. | 139 |
| 56 | Results of cross-correlation analysis for the multielement alkali metal interferogram utilizing square cross-correlation masks. | 140 |
| 57 | A multielement interferogram containing vanadium, cobalt, nickel, and iron. | 142 |
| 58 | Multielement spectrum containing vanadium, cobalt, nickel and iron emission lines. | 143 |

| Figure | Description | Page |
|---|---|---|
| 59 | (a) Cobalt, (b) nickel, (c) iron and (d) vanadium spectra. | 144 |
| 60 | Results of cross-correlation analysis for the multielement transition metal interferogram using Table 5 for the generation of analog cross-correlation masks. | 146 |
| 61 | Results of cross-correlation analysis for the multielement transition metal interferogram using Table 6 for the generation of analog cross-correlation masks. | 149 |
| 62 | Secondary cross-correlation analysis results for (a) aluminium, (b)cobalt, (c) iron, (d) nickel, (e) palladium and (f) vanadium utilizing analog cross-correlation masks. | 152 |
| 63 | Results of the alternate secondary cross-correlation analysis for (a) aluminium, (b) cobalt, (c) iron, (d) nickel, (e) palladium and (f) vanadium utilizing analog cross-correlation masks. | 154 |
| 64 | Results of cross-correlation analysis for the multielement transition metal interferogram using Table 6 for the generation of square cross-correlation masks. | 155 |

| Figure | Description | Page |
|---|---|---|
| 65 | Secondary cross-correlation analysis results for (a) aluminium, (b) cobalt, (c) iron, (d) nickel, (e) palladium and (f) vanadium utilizing square cross-correlation masks. | 156 |
| 66 | Results of the alternate secondary cross-correlation analysis for (a) aluminium, (b) cobalt, (c) iron, (d) nickel, (e) palladium and (f) vanadium utilizing square cross-correlation masks. | 157 |
| 67 | Linear analytical curves for lithium obtained by (a) square and (b) analog cross-correlation masks. | 159 |
| 68 | Linear analytical curves for nickel obtained by cross-correlation analysis with analytical information corresponding to (a) 310.17, 341.48, 305.08; (b) 310.17, 341.48; (c) 310.17 nm. | 161 |
| 69 | Detection of nickel and vanadium in the presence of each other with cross-correlation masks corresponding to (a) 310.17, 341.48, 305.08; (b) 309.31, 311.07, 310.23 nm. | 162 |
| 70 | Detection of nickel and vanadium in the presence of each other with cross-correlation masks corresponding to (a) 341.48, 305.08; (b) 309.31, 311.07 nm. | 164 |

| Figure | Description | Page |
|---|---|---|
| 71 | Analytical working curve for vanadium obtained in the presence of cobalt, nickel and iron by cross-correlation analysis. | 165 |
| 72 | Comparsion between Fourier transform and correlation data processing methods. | 168 |
| 73 | Block diagram of the Rockwell AIM 65 microcomputer/TRW multiplier-accumulator data processing system. | 173 |
| 74 | Rockwell AIM 65 microcomputer R6522 Versatile Interface Adapter configuration. | 176 |
| 75 | Timing diagram for the Michelson interferometer/Rockwell AIM 65 microcomputer system. | 178 |
| 76 | Start pulse and clock control circuitry. | 181 |
| 77 | Analog to digital conversion circuitry. | 183 |
| 78 | TRW multiplier-accumulator configuration. | 186 |
| 79 | Block diagram of the data multiplexing circuitry. | 188 |
| 80 | Two-line to four-line decoder of the data multiplexing circuitry. | 190 |
| 81 | Multiplexing circuitry between the AIM 65 microcomputer and the TRW multiplier-accumulator. | 191 |
| 82 | Cross-correlation analysis on a He-Ne laser signal. | 198 |

| Figure | Description | Page |
|---|---|---|
| 83 | A magnesium hollow cathode lamp spectrum. | 199 |
| 84 | Cross-correlation analysis on a magnesium hollow cathode lamp signal. | 201 |
| 85 | Secondary cross-correlation analysis on the magnesium hollow cathode lamp signal. | 204 |
| 86 | "Analytical working curve" for the He-Ne laser (632.8 nm). | 205 |
| 87 | "Analytical working curve" for magnesium (285.2 nm). | 206 |
| 88 | (a) Real, (b) imaginary and (c) amplitude output arrays for Scheme 5 inverse FFT implementation. | 226 |
| 89 | (a) Real, (b) imaginary and (c) amplitude output arrays for Scheme 6 inverse FFT implementation. | 227 |
| 90 | Pseudo interferogram obtained by reflecting the real output array of the Scheme 2 FFT about itself. | 229 |
| 91 | (a) Real, (b) imaginary and (c) amplitude output arrays for Scheme 7 inverse FFT implementation. | 230 |
| 92 | Modified photomultiplier tube dynode chain circuitry. | 234 |

| Figure | Description | Page |
|---|---|---|
| 93 | Flow chart for the FORTRAN FFT program. | 240 |
| 94 | Flow chart for the BASIC program. | 247 |
| 95 | Flow chart for the ASSEMBLER program. | 251 |

# CHAPTER I

## Introduction

### A. An Ideal Spectrochemical Measurement System

A typical spectrochemical measurement can be subdivided into three basic operations: an encoding step, a decoding step, and a processing step. At the encoding step, analytical information about the composition of a sample is encoded in the form of electromagnetic radiation. This part of the system is usually classified as the source and a common example is the use of flames in atomic emission, absorption or fluorescence spectrometry. At the decoding step, electromagnetic radiation carrying the analytical information is measured. This task is carried out by a spectrometer. In many cases, the processing step simply means the human interpretation of the spectral data obtained. With the advent of advanced electronic technology, a computer is usually incorporated into the system with the appropriate supporting data reduction software. It is then possible to obtain the desirable analytical results within a relatively short period of time. In addition, the computer may also act as a controller for the whole system as demanded by the user.

Analytical spectroscopists have been in search of an "ideal" system ever since the need for spectrochemical measurement arose. Although it is unlikely that an "ideal"

system will ever appear, it is worthwhile to look at some of the desirable characteristics of the "ideal" system to act as a standard towards which all "real" systems should strive.

An ideal atomic spectrochemical measurement system should have the capability of obtaining analytical information for all elements at all concentration levels and the data obtained should be a linear function of the concentration with no interference effects. In addition, accurate and precise results are desirable. The measurement system should also be applicable to all types of samples without much sample preparation. The instrument used to carry out the analysis should be compact, reliable, low cost and easy to maintain. With the ever increasing load of samples to be analysed, emphasis must also be placed on the necessity of the system to perform multielement analysis simultaneously and for final analytical results to be obtained in a short period of time. This implies that efficient data processing methods must be employed.

Among all the techniques that have been used to carry out the encoding step necessary for spectrochemical measurements, the observation of emitted radiation from free atoms generated from the sample offers the most

promise of providing an "ideal" system. Simultaneous multi-element analysis is possible with optical emission spectroscopy in a relatively simple manner. The only requirement is an energetic source to generate excited free atoms and/or ions from a sample. In the next section, an almost ideal excitation source for atomic emission spectrometry (AES), the inductively coupled plasma (ICP), will be introduced and described.

B. Atomic Emission Spectroscopy

The principal excitation sources for AES are listed below:

(a) Flames.

(b) Sparks.

(c) Direct current (d.c.) arcs.

(d) Plasmas.

(e) Glow discharge lamps.

(f) Hollow cathode discharges.

(g) Lasers.

Excitation sources based on glow discharge lamps, hollow cathode discharges and lasers have had somewhat limited usage in AES while d.c. arcs and sparks, together with the classical thermal excitation provided by high temperature flames such as nitrous oxide-acetylene, are

widely used in many applications. However, during the past decade, exceptional growth has occurred in the area of plasma emission spectroscopy. These energetic sources, especially the ICP are likely to be used for years to come as they approximate, in many ways, the ideal spectroscopic source.

By definition, plasmas are gases in which a portion of the atoms or molecules is ionized. The plasma sources that have been utilized in AES can be classified into:

(a) D.c. plasma jets.

(b) Capactively coupled microwave plasmas (CMP).

(c) Microwave induced plasmas (MIP).

(d) Inductively coupled plasma (ICP).

An excellent description of these various kinds of plasma excitation source can be found in the article by Butler et al. (1). Comparison between these plasma sources along with a general review of plasma spectroscopy have also been presented by Greenfield et al. (2,3) and Boumans et al. (4). These references should be consulted for more details.

The analytical performance of the ICP has been compared with the other plasma sources and with various established spectroscopic methods such as flame AES, flame

and furnace atomic absorption spectrometry, arc AES and x-ray fluorescence spectrometry by Boumans (5). The overall assessment was based on the analytical capability to perform direct solid analysis, direct liquid analysis, multielement analysis, trace analysis, precise analysis and accurate analysis. He concluded that the ICP is the method of choice although it suffers from the incapability of performing direct quantitative solid sample analysis. This clearly explains why the ICP occupies such an important role in AES at the present time. This can be verified by the degree of commercialization and ever increasing analytical applications of the ICP.

Inductively Coupled Plasma: The ICP was developed from a low pressure discharge described by Bobat (6) in 1947 to the present atmospheric pressure gas discharge. The first ICP discharge sustained at atmospheric pressure was generated by Reed (7,8) in 1961. Reed used argon as the plasma gas and his system was applied to the manufacture of crystals from refractory materials. The easy vaporization of powders ($Al_2O_3$) injected into the discharge led to the suggestion that the ICP might have potential as an excitation source for AES. In 1964, the analytical application of the ICP discharge was first reported by Greenfield et al. (9). Shortly after, Fassel and Wendt (10)

published their own independent work on the ICP. Since then, an explosive growth in the use of ICP has occurred.

A schematic diagram of the ICP discharge (11) is shown in Figure 1. It consists of an ICP torch which is composed of three concentric quartz tubes. The torch is placed within a water cooled copper coil to which a radiofrequency (7-50 MHz, a typical value is 27.12 MHz) current is applied. The power output of the radiofrequency generator is usually in the range of one to three kilowatts, though some ICP systems operate at power levels as high as ten kilowatts. The ICP is initiated with the aid of a Tesla coil. It provides a seed of electrons which interact with the oscillating magnetic field (see Figure 1) produced by the high frequency current to further ionize the plasma support gas (normally argon) thereby forming a stable discharge. The temperature of the plasma discharge in the central core is about 10,000 $^{o}$K. Three flows of gas, usually argon, are introduced to the torch. The plasma gas (or coolant gas) is introduced tangentially at about 15 liters per minute (lpm) and is intended to sustain the discharge in an annular shape and to prevent the outer quartz tube from melting. The auxiliary gas (0-1 lpm) is used to raise or lower the plasma discharge and in some cases, this flow of gas is not necessary. Samples, in the form of fine aerosol are

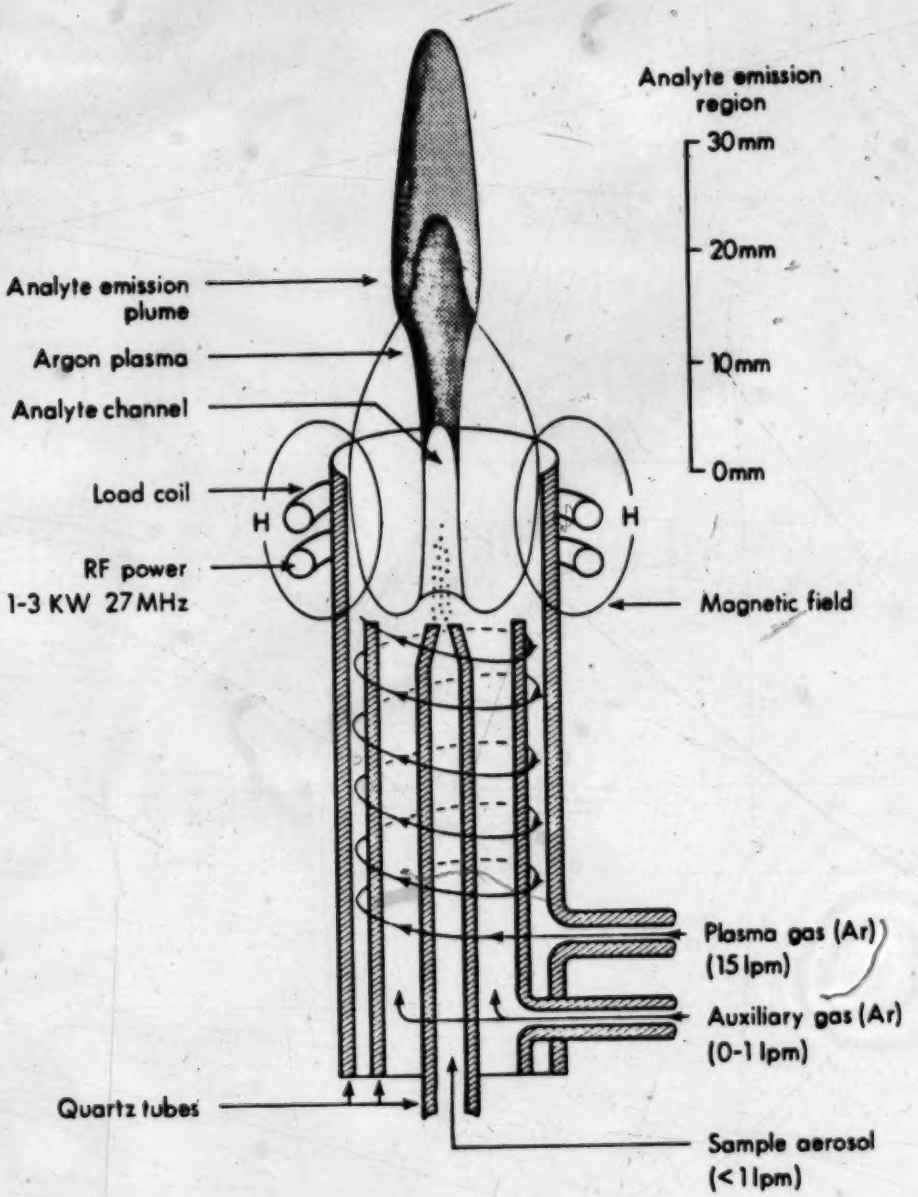


FIGURE 1. Schematic diagram of an ICP discharge.

introduced into the discharge with the aerosol carrier or nebulizer gas through the central tube of the ICP torch. The optimal emission region of the plasma is normally around 15 mm above the copper coil depending however on the operating conditions and the sought-for analyte (12).

Some of the desirable characteristics offered by the ICP as an encoding device in a spectrochemical measurement system are: good sensitivity and low detection limits for most of the elements, high precision and accuracy in the results obtained, linear response with respect to analyte concentration of up to five orders of magnitude, and low interference effects. In a sense, the ICP closely approximates the "ideal" spectroscopic source other than the fact that at the present time it only produces good analytical results for liquid samples and it is relatively expensive. Also as a result of the high excitation energy available in the ICP, spectral interferences can be a serious problem. However, the ICP does provide the spectroscopist with an excellent excitation source for spectrochemical measurements. The next problem is how to extract and utilize the vast amount of analytical information available from the ICP. In other words, what kind of spectrometer should be used to decode the analytical spectrochemical information generated by the ICP?

C. Multielement Analysis Spectrometers

In order to fully utilize the spectral information available from the ICP, wide continuous spectral coverage by the spectrometer is highly desirable. Furthermore, simultaneous detection capability is necessary for efficient spectral analysis. This is also essential for background correction which is a major consideration when using an ICP. A true background or spectral correction procedure can only be implemented if simultaneous spectral coverage can be achieved.

In general, spectrometers commonly used in AES can be subdivided into two main types:

(a) Dispersive type.

(b) Non-dispersive type.

Dispersive type spectrometers have been conveniently grouped into four categories by Boumans (13). The list is reproduced below because it gives a general idea of the various kinds of dispersive spectrometer that are available.

(a) Polychromators, one-dimensional dispersion with fixed optical components:

(i) large polychromators (direct readers) with multiple exit slit and multiple detector (photomultiplier tube, PMT) or multiple

exit slit and single detector (PMT) or a single movable exit slit and a single detector (PMT);

(ii) large or small polychromators with exit slits replaced by multiple arrays of photodiodes, each consisting of a few photodiodes for measurements of the line peak and the background.

(b) Echelle spectrometers, two dimensional dispersion with fixed optical components:

( i) multiple exit slit and single detector (PMT) design, "spinning encoding disk";

(ii) multiple exit slit and multiple detector design, cassette with fixed apertures, mirrors and PMTs;

(iii) with television camera tube (and image converter;

(iv) with image dissector.

(c) Spectrographs, one dimensional dispersion with photographic detection completed with:

( i) manual microphotometer;

(ii) recording microphotometer;

(iii) computerized automatic microphotometer.

(d) Monochromators, one-dimensional dispersion with

mechanically movable optical component(s) for wavelength adjustment:

(i) single exit slit and single detector (PMT) design with wavelength control as follows:

- -manual
- -scanning
- -slewing and programmable with precision mechanical device
- -slewing and programmable with computer or microprocessor;

(ii) without exit slit, with television camera or self-scanning linear photodiode array.

Among the dispersive type spectrometers, there is no doubt about the capability of spectrographs in covering a wide spectral region, simultaneously and continuously. In fact, spectrographs, which use photographic detection can record thousands of spectral lines within a short period of time. However, the major drawback in the use of spectrographs is that time consuming readout procedures are required. Although computerized automatic microphotometers such as those developed by Witner et al. (14) and by Walthall (15) have appeared to minimize the problem, good quantitative results are still difficult to obtain. These disadvantages can be overcome by the use of detectors

such as photomultiplier tubes (PMTs). With the use of these detectors, electronic readout can be instantaneous. Linear response over 5-6 orders of magnitude with good quantitative results can be obtained with PMTs. However, with the use of PMTs which are essentially single channel detectors, wide spectral coverage capability is lost. In order to combine the advantages offered by PMTs and photographic detectors, direct reading type spectrometers were introduced. In this case, up to sixty channels of PMTs can be configured in the focal plane of a polychromator for simultaneous detection of spectral information. The major disadvantages offered by the use of this type of spectrometer are: non-trivial alignment procedures for each channel, limited PMT channels because of physical limitations in the focal plane of the polychromator, the instrument is bulky and expensive, and it is difficult to change to new channels. These, combined with the fact that continuous spectral coverage is not possible for background correction are some of the reasons for the appearance of slew scan type spectrometers. For slew scan type spectrometers, a single channel detector is used to scan through the entire spectral region. This is achieved either by moving the optical components of a monochromator or by moving the detector along the focal curve of a polychromator. In this way, continuous

spectral coverage can be achieved. However, precise alignment of the detector at a particular spectral wavelength for analysis is not easy even with the help of a computer. Furthermore, the capability of simultaneous detection of signals is lost. Much time is spent in scanning through the entire spectral region in search of the sought-for analytical information.

So, the problem of combining simultaneous, continuous and wide spectral detection with good quantitative measurement characteristics into a single spectrometer has puzzled spectroscopists for a long time. With the arrival of electronic image detectors such as self-scanning photodiode arrays, image dissectors and television camera type detectors, an extensive investigation on the feasibility of these kinds of detectors for analytical applications has begun. These detectors are essentially the electronic versions of photographic detectors. They were developed to combine the advantages offered by both PMTs and photographic detectors, although the goal is not quite reached at the present time. These devices are capable of simultaneous coverage of a limited spectral region with instantaneous electronic readout. Within the last few years, developments in this area have produced image detectors such as the intensified photodiode array with a sensitivity comparable to PMTs.

The major drawbacks of the image detectors are high cost and limited spectral coverage. Despite this, these electronic devices have found numerous applications in the development of an "ideal" spectrometer. Of particular interest is the replacement of single channel detectors such as PMTs with image detectors. They can be used in the direct reading type spectrometers such as those developed by Boumans (16,17) or slew scan type spectrometers developed by Horlick et al. (18,19), Fry (20), Yates et al. (21) and Furuta (22). With these configurations, simultaneous coverage within a narrow spectral region for background correction is possible. In order to extend the spectral coverage of these detectors, the use of Echelle spectrometers which produce two dimensional spectra combined with the use of two dimensional image detectors has been reported. This configuration was first reported by Margoshes (23) in 1970 and since then, several versions have been developed (24-27). With the tremendous progress in electronic technology, it is likely that the potential of the image sensors in the development of an "ideal" spectrometer is not fully developed.

All the spectrometers mentioned above belong to the dispersive catagory. Another approach is to dispense with the dispersive system completely and make use of the

multiplex technique. With this technique, spectral information is encoded so that a single detector can be used to simultaneously measure a wide spectral region. The most common examples are Fourier transform spectroscopy (FTS) and Hadamard transform spectroscopy (HTS). In the case of HTS, a dispersive element is still used. In fact it is very similar to a direct reading spectrometer and is listed under the dispersive type spectrometers by Boumans. The only difference with the HTS is that a single detector (PMT) is used and discrete spectral information from various exit slits of a polychromator are multiplexed into the single detector. Since a multiplex advantage is not realized in the UV-visible-near IR region where detector noise is not the limiting factor, HTS does not offer a better alternative to the conventional dispersive type spectrometers when coupled to the ICP. However, in the case of FTS, wide continuous spectral information can be obtained simultaneously. The use of a FT spectrometer to carry out atomic emission spectrochemical measurement has been discussed in detail by Horlick, Hall and Yuen (28). It appears that the major drawback of the FTS when used in conjunction with the ICP is the dynamic range problem. This limitation is due to the multiplex property of the technique. Every single data point contains information covering the whole spectral

region and must stay within the scale of the measurement electronics system in order to obtain proper analytical information concerning the sample. The dynamic range problem exists if the sample gives a very intense emission at a particular wavelength. This intense emission will limit the amplification of the signal and emission from weak spectral lines is difficult to detect. With the use of the ICP, the dynamic range problem due to strong background emission can essentially render some spectral regions analytically useless as reported by Hall (33). This can now be resolved with the use of a mixed gas ICP. Further discussion of this problem can be found in Chapter VI.

In conclusion, there is no definite answer as to which design is the "ideal" spectrometer. However, one thing that can be said is that simultaneous and continuous spectral coverage is a major feature of an "ideal" instrument.

In our laboratory, spectrometers based on photodiode arrays and Fourier transform techniques capable of simultaneous multielement analysis have been developed. The photodiode array spectrometer can simultaneously measure 1024 spectral resolution elements and the Fourier transform spectrometer, 4096 spectral resolution elements. Compared to multichannel polychromators which may have 20 to 50 channels the measurement capability of these new

systems represents a major increase in capability. Given this new level of spectral information measurement capability one then needs effective software and hardware systems to fully utilize such large amounts of spectral data. A basic step in the processing problem is the detection of the spectral information characteristic of the chemical species. In atomic emission spectrometry this typically involves the detection and quantitation of a specific combination of spectral peaks in a complex multiline spectrum.

In this thesis, correlation techiques as applied to the data processing step of the spectrochemical measurement systems based on ICP-photodiode array spectrometer and ICP-Fourier transform spectrometer will be presented. Correlation techniques were chosen because they are simple and highly effective in processing complex data arrays.

D. Correlation Based Signal Processing

Correlation techniques have long been used to measure and process signals in physics, chemistry and engineering. An early work concerning the application of correlation analysis to the detection of periodic communication signals was reported by Lee et al. (63). This topic was reviewed in some detail in 1960 (64). Correlation techniques, again

applied to communications, have also been described by Lange (65). Many of the applications of correlation techniques to chemical data have been reviewed and presented by Horlick and Hietfje (38). Interested readers should refer to this review and the references cited for full details.

Correlation techniques can be effectively applied to spectrochemical data. In particular, the signal detection aspects of correlation analysis look promising for achieving computerized automatic detection of spectral information. The power of correlation techniques for signal detection is best illustrated with an example.

Three atomic emission spectra are shown in Figure 2 for zinc, cadmium and boron all measured in the same spectral region (~220 nm) with the photodiode array spectrometer described in Chapter III. The wavelength axis has been left off on purpose to emphasize the fact that knowledge of it is unnecessary for spectral identification using cross-correlation techniques. Let us choose zinc as the sought-for spectral information. The complete cross-correlation patterns for zinc-zinc, zinc-cadmium, zinc-boron are shown in Figure 3. The exact computation of these cross-correlation functions will be described in the next chapter.

Cross-correlation patterns can be intuitively evaluated

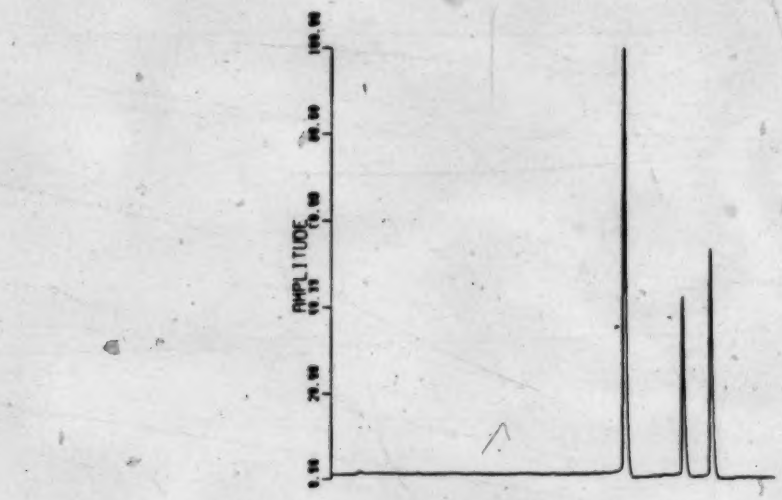


(a)

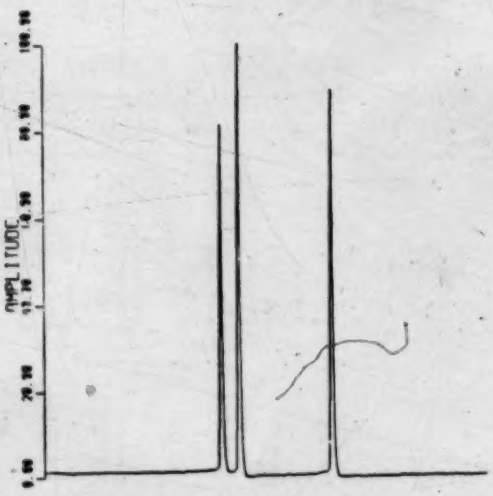


(b)

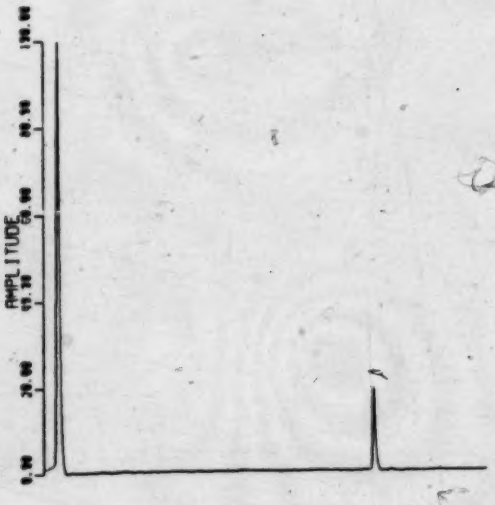


(c)

FIGURE 2. (a) Zinc, (b) cadmium and (c) boron spectra.

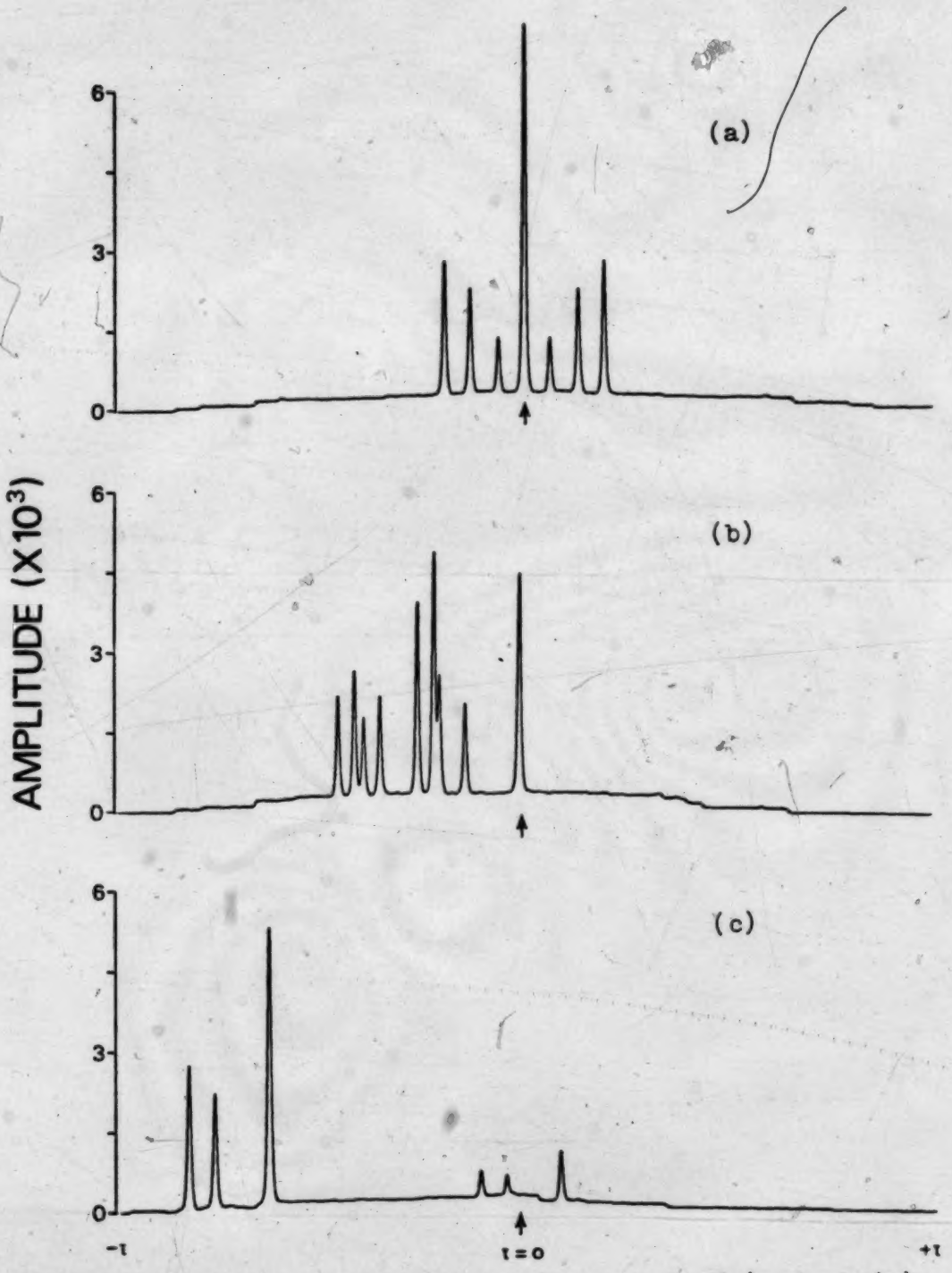


FIGURE 3. Cross-correlation patterns for the (a) zinc, (b) cadmium and (c) boron spectra with the zinc spectrum[1].

by envisioning the correlating pattern, the zinc spectrum in this case, to be slowly translated across the other spectral patterns. The value of the cross-correlation function at any particular displacement is the sum of the products of the two functions at that displacement, in a sense, their mutual areas. A unique point is the point of zero displacement, i.e. when the wavelength axes of the two spectral patterns exactly coincide. This point is often designated the $\tau = 0$ point. A large relative value of the cross-correlation function at $\tau = 0$ indicates a high degree of similarity between the two patterns. This is clearly indicated in Figure 3 by the cross-correlation pattern of zinc with itself. Note the relatively large central value and the symmetry characteristic of an auto-correlation pattern (Figure 3a). Thus the relative magnitude of the $\tau = 0$ point can be used to indicate detection of a spectral pattern. Note that the other cross-correlation patterns have no distinct maximum at $\tau = 0$ although the zinc-cadmium cross-correlation pattern does contain a peak near $\tau = 0$ indicating that two lines of zinc and cadmium must exist at essentially the same wavelength. Such is the case as zinc has a line at 213 nm and cadmium a line at 214 nm in this region.

The absolute magnitude of the $\tau = 0$ point is also

important in that it represents the consolidation into a single value of all the quantitative information about the sought-for constituent. Thus rather than quantifying zinc on the basis of a single spectral intensity, the $\tau = 0$ value represents the summation of the quantitative information from all spectral lines, thus more completely utilizing the available spectral information.

Correlation techniques can be further extended to process complex patterns for specific analytical information. This task includes the identification and quantitation of sought-for analyte with the proper use of cross-correlation functions. Further details and examples of correlation techniques as applied to atomic emission spectrometry will be presented later in Chapter II. First, the theory of correlation analysis will be reviewed. In addition the mathematical computation of the cross-correlation functions will be presented. A software approach of implementing cross-correlation techniques for processing spectral data obtained from an ICP-photodiode array spectrometer system and an ICP-Fourier transform spectrometer system will be described in Chapter III and IV respectively. A real time data processing system for interferometric signals utilizing cross-correlation techniques implemented in a hardware approach will be described in Chapter V.

# CHAPTER II

## Theoretical and Practical Aspects of Correlation Analysis

The basis of correlation techniques, as applied to chemistry, has been well documented in the literature (34-39). In this chapter, correlation theory based on these references will be summarized and presented. For a detailed description of the theory and its applications to chemical data measurement, the review by Horlick and Hieftje (38) should be consulted. As will be shown later, the full correlation operation can be carried out with the aid of Fourier transformation. The practical computation of the correlation function via the Fourier transformation route will be illustrated with particular attention paid to the manipulation of input and output data arrays.

### A. What is Correlation?

Simply stated, correlation analysis provides information about the coherence within a signal or between two signals. The correlation function of two signals is obtained by evaluating the time averaged or integrated product of the two signals as a function of their relative displacement. Mathematically, correlation can be expressed as:

$$C_{ab}(\tau) = \lim_{T\to\infty} \frac{1}{2T} \int_{-T}^{+T} a(t)b(t\pm\tau)dt \qquad \text{(i)}$$

where $C_{ab}(\tau)$ is the correlation function between the two signals a(t) and b(t) and $\tau$ is their relative displacement. The signals can be a function of essentially any variable, for example, wavelength, retardation, frequency, accelerating voltage, time etc. Thus, if a and b are considered to be functions of time, the correlation function $C_{ab}$ will be related to and plotted against the relative time delay between the two signals.

In most situations, correlation is implemented on digitized signals. For digitized signals, the calculation of the correlation function can be expressed by the following summation:

$$C_{ab}(n\Delta t) = \sum_{t} a(t)b(t \pm n\Delta t) \qquad n=0,1,2,3,..... \quad (ii)$$

The signals can only be displaced some integral number of the sampling interval, $\Delta t$. Thus, the displacement $n\Delta t$ is equivalent to $\tau$ in Equation i.

There are two basic correlation operations: auto-correlation and cross-correlation. These, together with a special kind of correlation operation, convolution, will be treated individually later. First, the relationship between correlation and Fourier transformation must be defined.

B. Correlation and Fourier Transformation

The ready availability of digital computers has facilitated software approaches to correlation. In particular, the fast Fourier transform (FFT) algorithm (40) has essentially revolutionized the extent to which correlation techniques can be implemented on computers and indeed many correlation based techniques are more commonly referred to as Fourier transform techniques. The power and range of applicability of some of these techniques are generally well known and documented in several books (41-45). In addition to providing a convenient route for the implementation of correlation, a knowledge of Fourier transforms also aids the utilization and understanding of correlation operations. An important theorem concerning correlation states that correlation of two waveforms is equivalent to multiplication of their Fourier transforms followed by inverse Fourier transformation of the product. Schematically, this sequence can be represented in the following way:

$$a(t) \quad * \quad b(t) \quad = \quad c_{ab}(\tau) \qquad \text{(iii)}$$

$$\downarrow \qquad \text{FOURIER TRANSFORMATION} \qquad \downarrow \qquad \uparrow \text{INVERSE FOURIER TRANSFORMATION}$$

$$A(f) \quad x \quad B(f) \quad = \quad C_{AB}(f) \qquad \text{(iv)}$$

The asterisk in Equation iii is merely a common shorthand way to represent correlation; Equation iii is therefore identical to Equation i. Notice that in Equations iii and iv, cross-correlation is shown to involve a multiplication process in the Fourier domain. Simple as this aspect of correlation might seem, it is of paramount importance. A large fraction of software and hardware methods for obtaining the correlation function rely on the Fourier transform method because of its speed and relative simplicity.

Several versions of the FFT abound in the literature and in program libraries and utilization of these sub-routines may, at first, seem trivial. However, subtleties and pit falls exist with respect to data pretreatment, data post-treatment, inverse Fourier transformation and manipulation of real and imaginary arrays that can cause considerable grief to the uninitiated. Thus, the utilization and recycling of FFT algorithms will be discussed before correlation analysis is illustrated.

Computer Software: All calculations were carried out using a FORTRAN FFT program which is based on a Cooley-Tukey FFT algorithm (40) first suggested by Gentleman and Sande (43). The complete program listing with flowchart is included in Appendix III. This program can be operated

with or without a sorting routine which will be explained later. The maximum number of points that can be processed with the DEC PDP 11/10 minicomputer running under an RT-11 operating system is 4096 due to the in core memory size (32 K) limitation. Detailed documentation can be found along with the program. All the figures are 1024 points unless otherwise specified. They were displayed and plotted with a VT-11 screen and a Zeta incremental plotter.

Utilization of Fast Fourier Transform Algorithms: All FFT algorithms require real and imaginary input data arrays. However, in the vast majority of situations, the prospective user has a simple array of data to process; for example, a digitized optical spectrum. Thus the user is immediately faced with the problem of how to fill up the real and imaginary input arrays of the FFT with the array of data. With most FFT algorithms, it is recommended that the data array be placed in the real input array and that the imaginary input array be filled with zeros. This is illustrated in the following scheme with R and I representing the real and imaginary arrays.

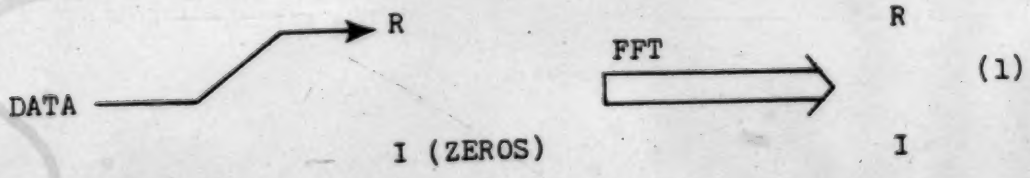


(1)

A data array which is a simple line spectrum generated by the computer is used for illustration and is shown in Figure 4. If this data array is placed in the real input array of the FFT and zeros in the imaginary input array the resulting real and imaginary outputs, after a 1024-point FFT, appear as shown in Figure 5.

An alternate method of filling the real and imaginary input arrays with data to be transformed is to put the odd points, i.e., 1, 3, 5, 7... of the data array into the real input array and the even points, i.e., 2, 4, 6, 8... of the data array into the imaginary input array. This scheme is outlined below:

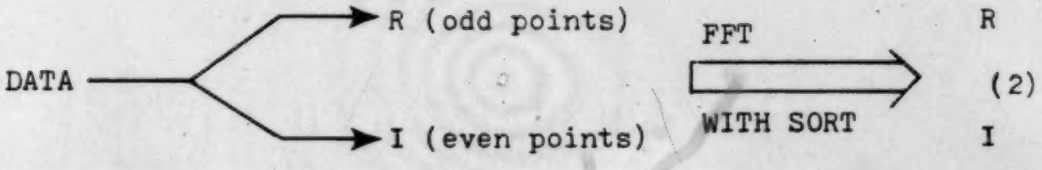


When this method is used the FFT must be followed by a sorting routine in order to generate the correct real and imaginary outputs (46).

This method provides for very efficient use of the FFT algorithm as N data points can be transformed using an N/2 FFT. However, this approach is normally carried out so as to keep the transform size identical to the data array. This is easily accomplished by filling out each

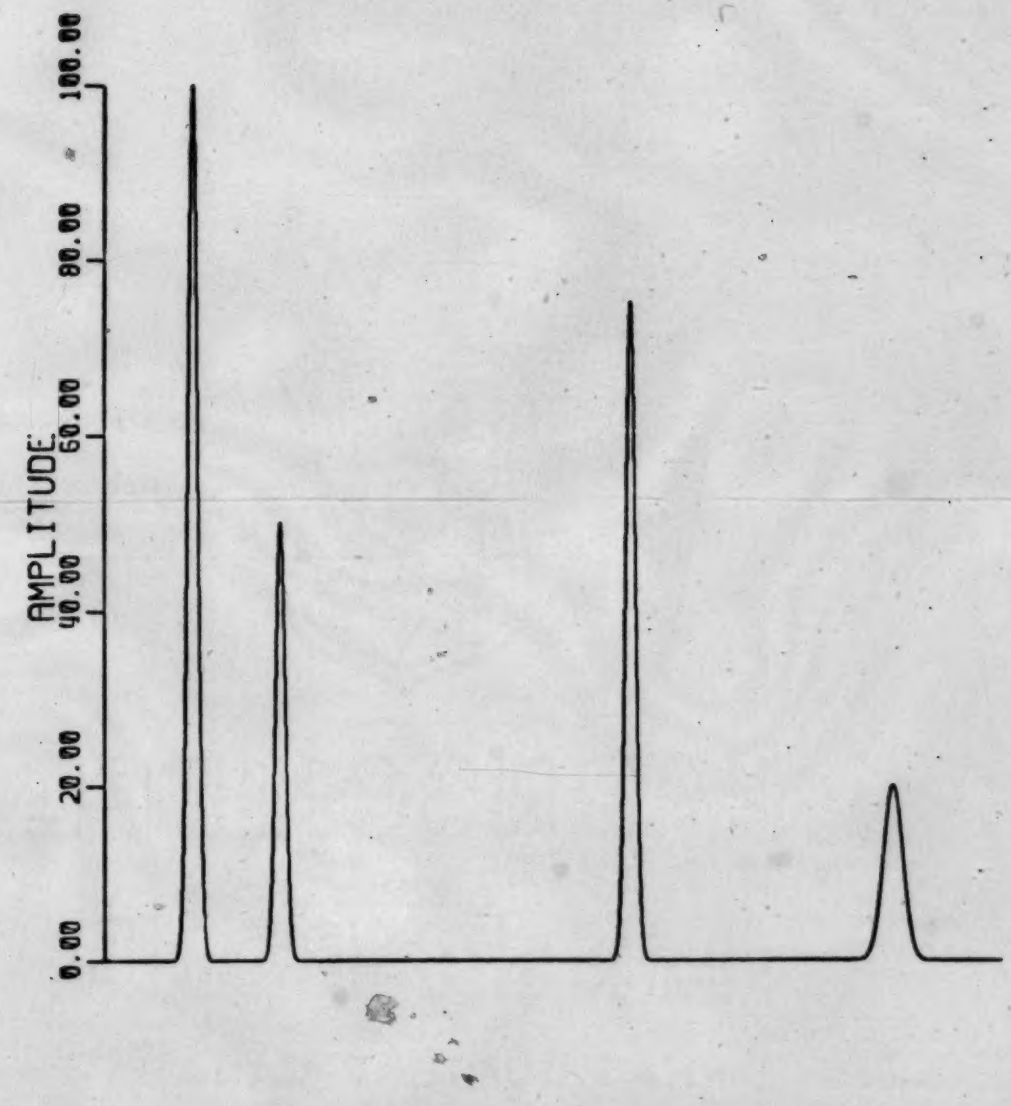


FIGURE 4. A simple line spectrum used as the input data array for the FFT implementation.

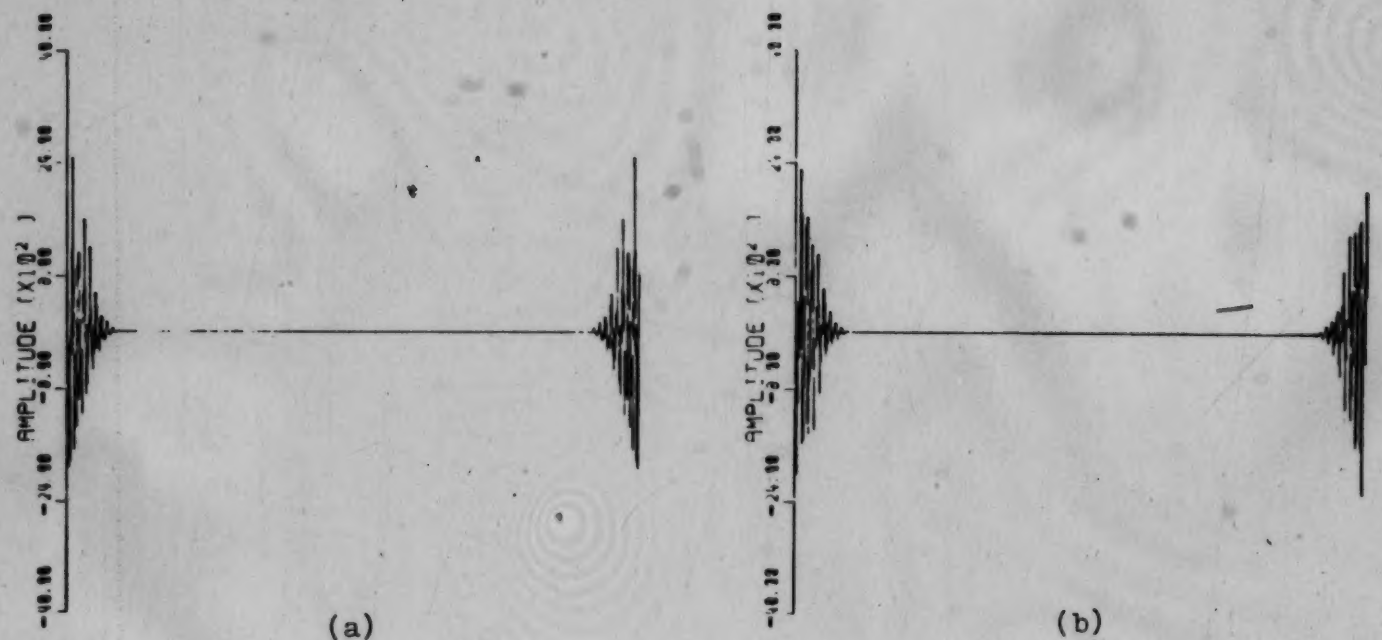


FIGURE 5. (a) Real and (b) imaginary output arrays for Scheme 1 implementation of the FFT.

input data array to N with zeros after placing the N/2 odd and even points in the real and imaginary inputs.

The results of this approach are illustrated in Figure 6. The same input data as that illustrated in Figure 4 was used. The 512 odd points were placed in the real input array and the 512 even points in the imaginary array. Both input arrays were then filled out to 1024 with zeros and a 1024-point FFT calculated followed by the sort routine.

Both Schemes 1 and 2 are equally valid approaches to setting up the real and imaginary input arrays of the FFT algorithm starting with a simple data array. However, Scheme 2 is usually preferred because the real and imaginary outputs are intuitively easier to interpret in that the end of each output array represents the Nyquist frequency rather than the center of the array as for Scheme 1. For example, the FFT outputs resulting from Scheme 2 implementation for a single peak spectrum shown in Figure 7 are illustrated in Figure 8. The real and imaginary FFT outputs are damped cosine and sine waves. The functional form and extent of the damping are directly related to the position of the peak along the horizontal axis (wavelength axis in the case of optical spectrum) relative to the origin. The amplitude output

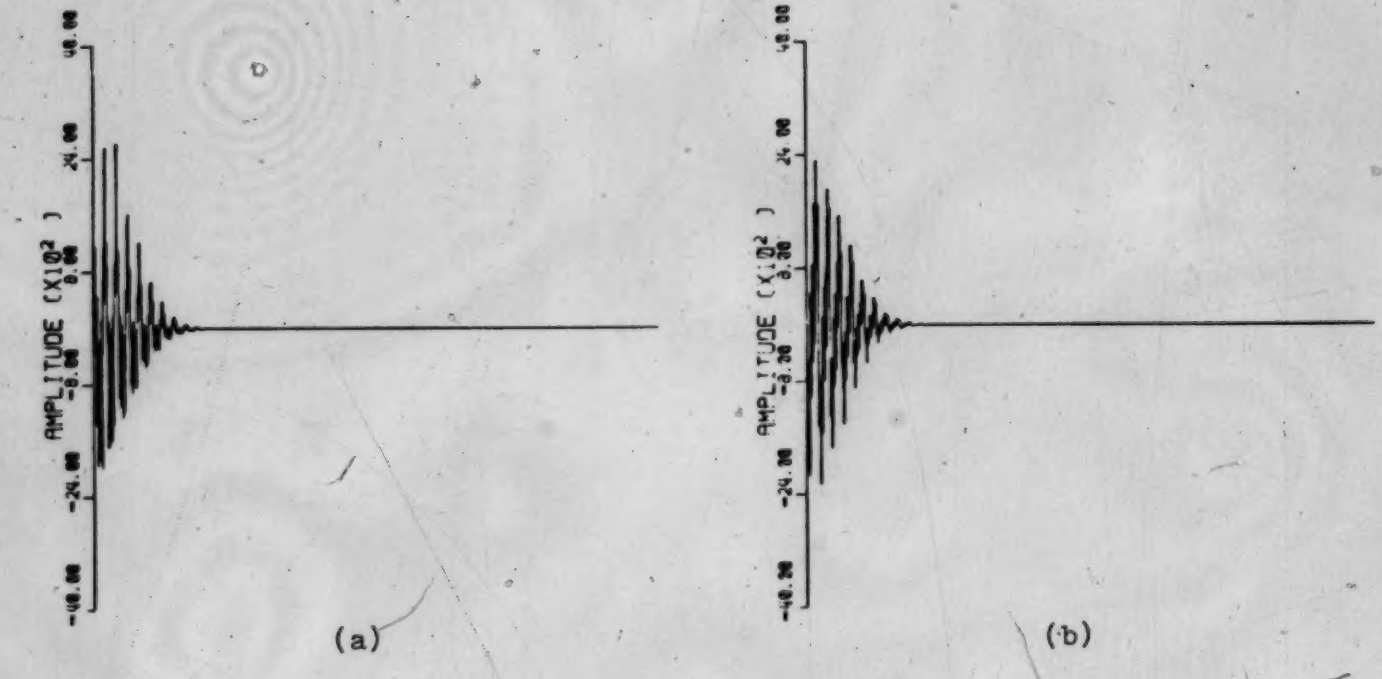


FIGURE 6. (a) Real and (b) imaginary output arrays for Scheme 2 implementation of the FFT.

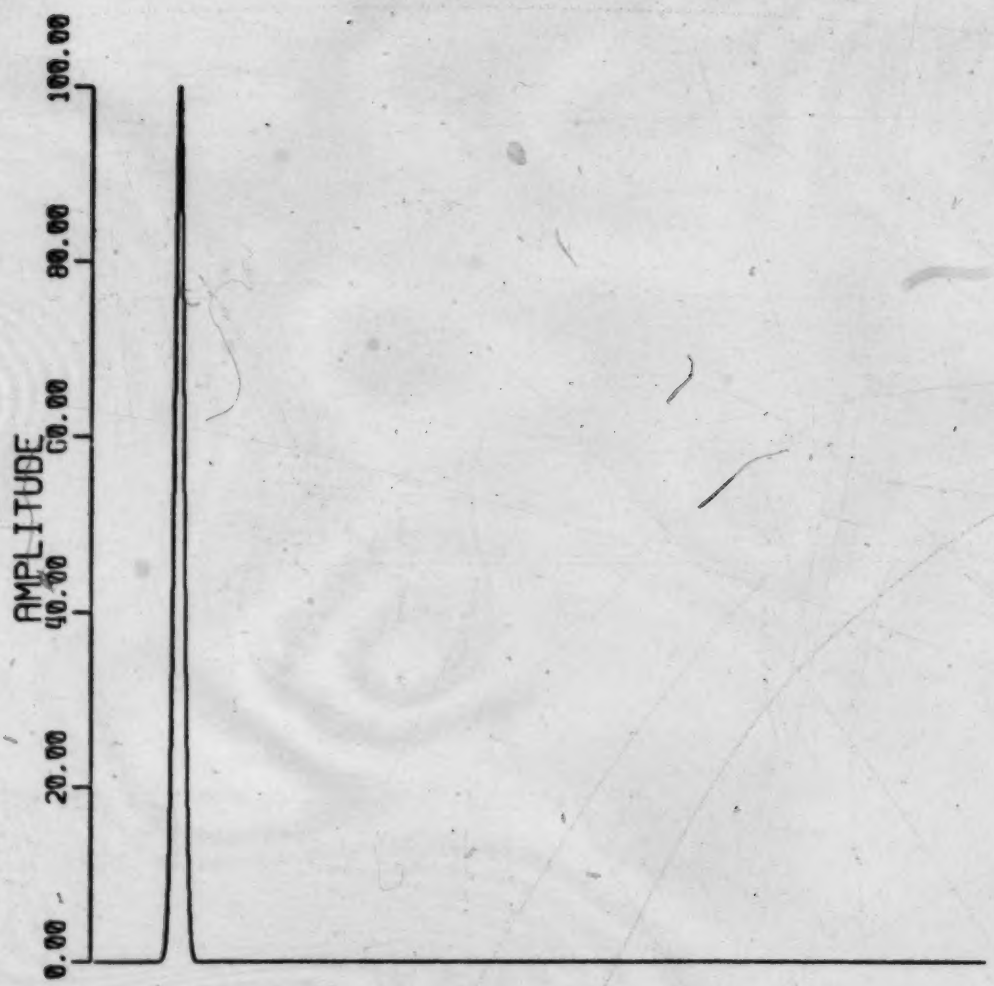


FIGURE 7. A single peak spectrum.

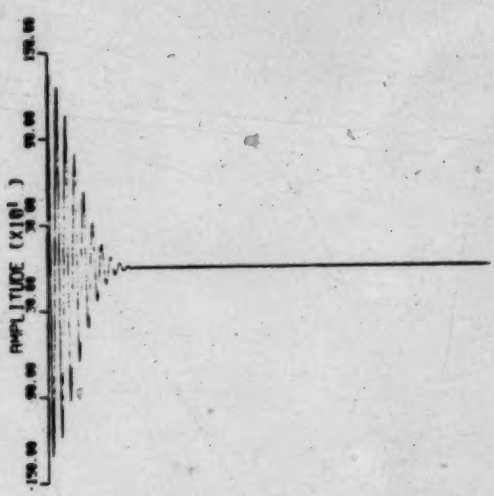


(a)

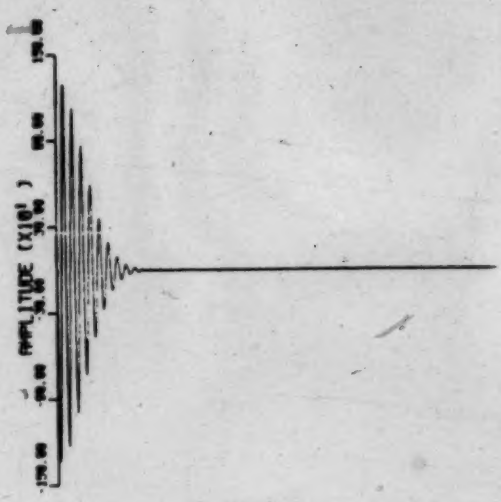


(b)

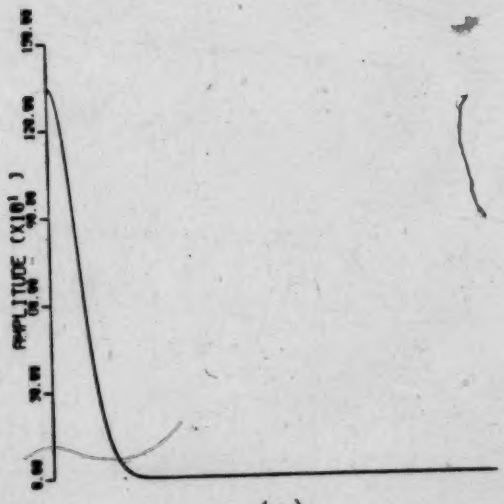


(c)

FIGURE 8. (a) Real, (b) imaginary and (c) amplitude output arrays for the single peak spectrum with Scheme 2 FFT implementation.

array $[(R^2 + I^2)^{1/2}]$ is shown in Figure 8(c). It represents the amplitude of the Fourier components making up the original data, the single peak spectrum. In all cases, these outputs, using Scheme 1, would be complicated by information at each end of the output arrays. This is illustrated in Figure 9. These are the real and imaginary output arrays of the single peak spectrum obtained using Scheme 1 implementation.

Inverse Fourier Transformation: With a great many Fourier transform data processing methods, data is transformed, manipulated in the transform domain, and then re-transformed (inverse Fourier transformation) back to the original domain. The basis for these methods involves the fact that convolutions, cross-correlations, and auto-correlations can all be performed as multiplications in the Fourier domain as pointed out earlier in this chapter.

A number of subtleties exist in implementing inverse Fourier transformations that may give many a novice considerable frustration. Several alternate routes are possible depending both on the original method of Fourier transformation (Scheme 1 or 2) and on the nature of the processing carried out in the Fourier domain. The main confusion centers around the exact manipulation of the

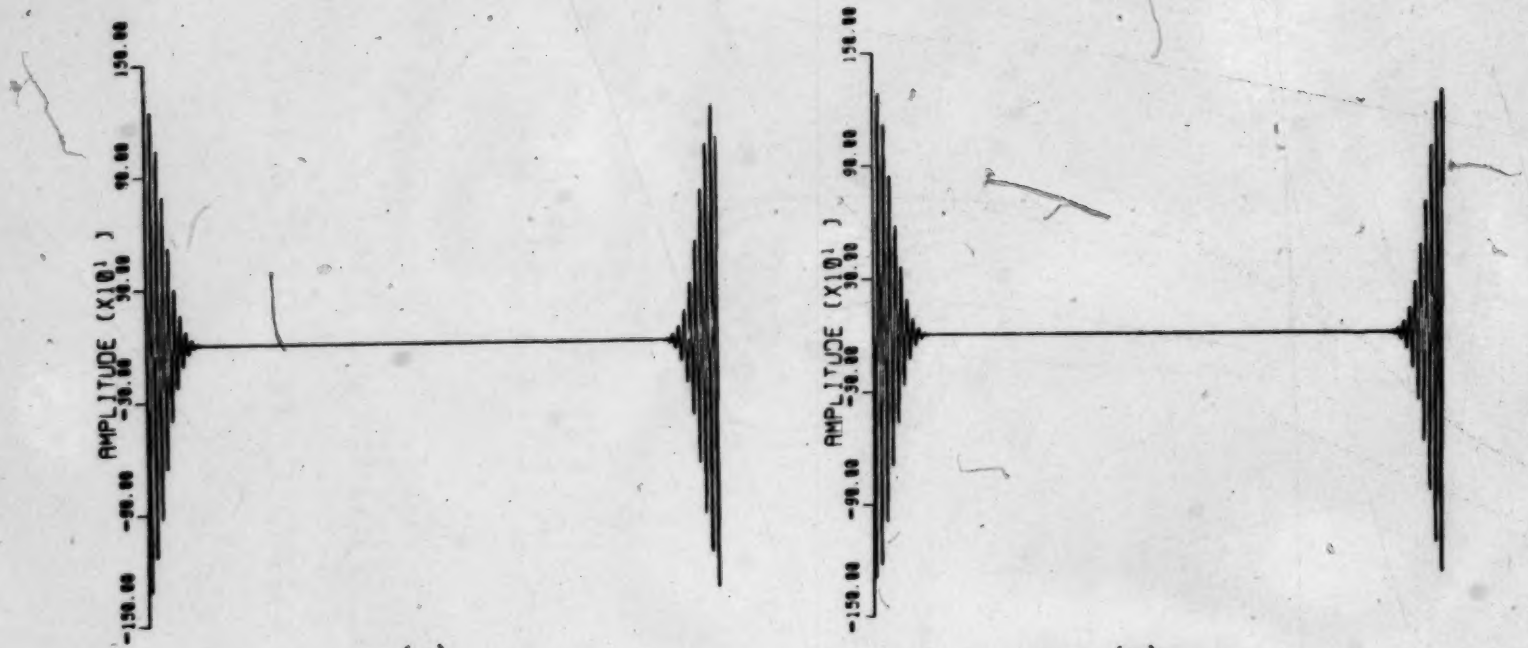


(a) (b)

FIGURE 9. (a) Real and (b) imaginary output arrays for the single peak spectrum with Scheme 1 FFT implementation.

explicit real and imaginary arrays that are generated after the first FFT.

The standard route for recycling the FFT when Scheme 1 is used to set up the input arrays for the first transform is shown below:

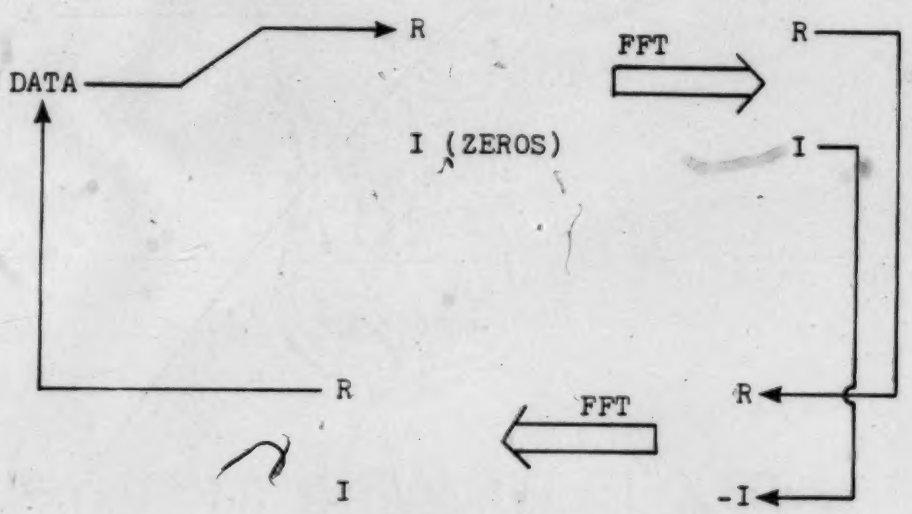


(3)

The real output array from the first FFT is used as the real input for the second FFT and the negative of the imaginary output array from the first FFT is used as the imaginary input for the second FFT. The real, imaginary and amplitude output arrays of the second FFT using Scheme 3 are shown in Figure 10. The original data is the line

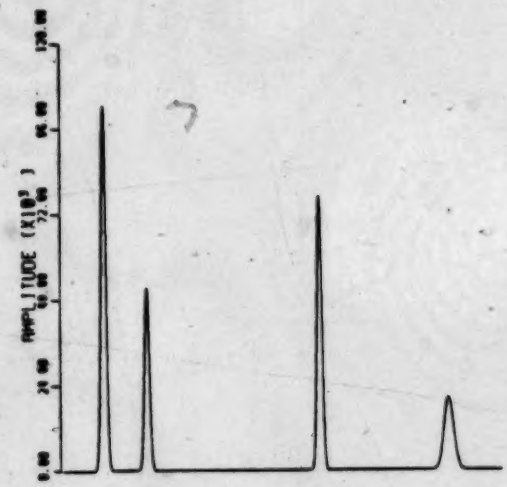


(a)

(b)

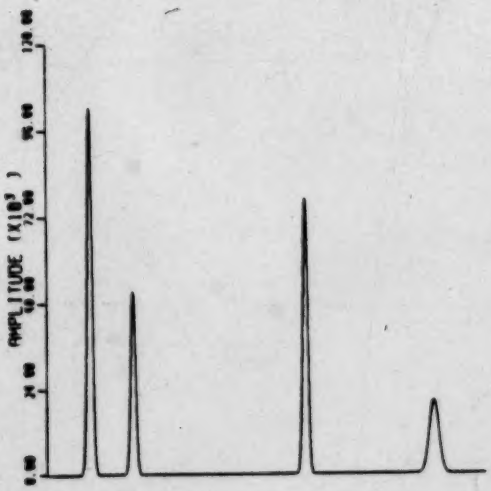


(c)

FIGURE 10. (a) Real, (b) imaginary and (c) amplitude output arrays for Scheme 3 inverse FFT implementation.

spectrum illustrated in Figure 4. In this case the real and the amplitude output arrays both contain the original data.

When Scheme 2 (even-odd point method) is used to set up the original input arrays, recycling is carried out as outlined below:

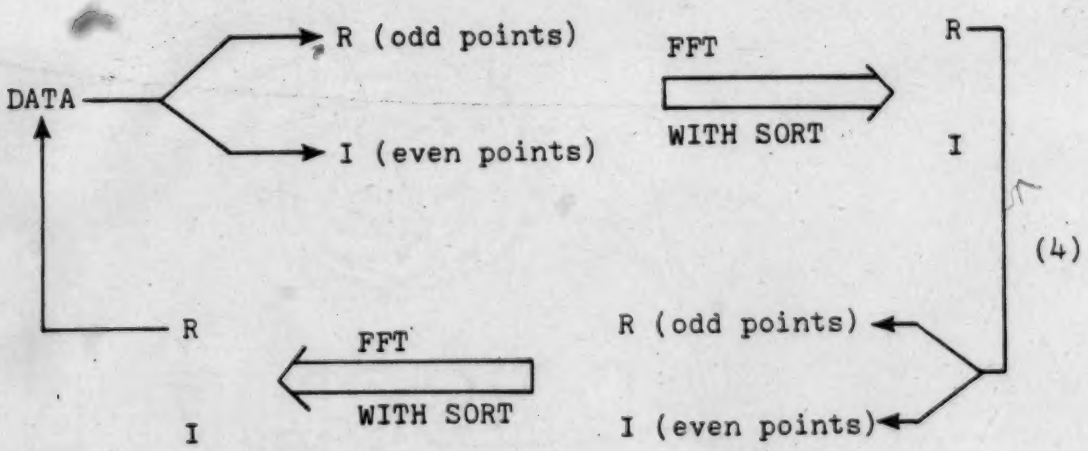


In this case recycling is implemented using only the real output of the first FFT as a single input to the second FFT. It is sorted odd points into the real input array and even points into the imaginary array as is standard for Scheme 2. These arrays are again filled out with

zeros to the N value of the transform. The real, imaginary and amplitude output arrays of the second FFT are shown in Figure 11, again for the case in which the original data is the line spectrum shown in Figure 4. Now only the real output array contains the original data.

In addition to Scheme 4, several other recycling implementations when Scheme 2 is used as the primary FFT method have been tried. These results will be presented in Appendix I as they may aid others in sorting out FFT problems and options.

Though the same pattern of the original spectrum can be obtained using different versions of inverse FFT, one has to watch out for the change in amplitude. In general, the amplitude of the resulting spectrum is increased by a factor which is equal to half of the number of relevant data points inputted for the inverse FFT. For example, in Scheme 3 the amplitude of the final spectrum is a factor of 1024 higher than the original spectrum since there are 2 x 1024 (real and imaginary) data points inputted for the inverse FFT. In Scheme 4, the amplitude is out by a factor of 512 because only one 1024 data array has been used. Thus, amplitude adjustment is necessary whenever an inverse FFT is implemented. This applies to correlation operations if the Fourier transformation

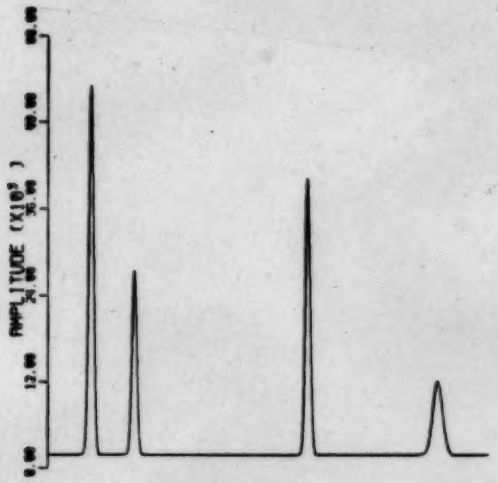


(a)

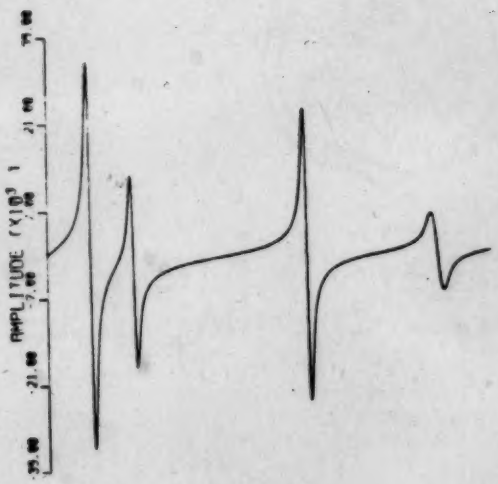


(b)

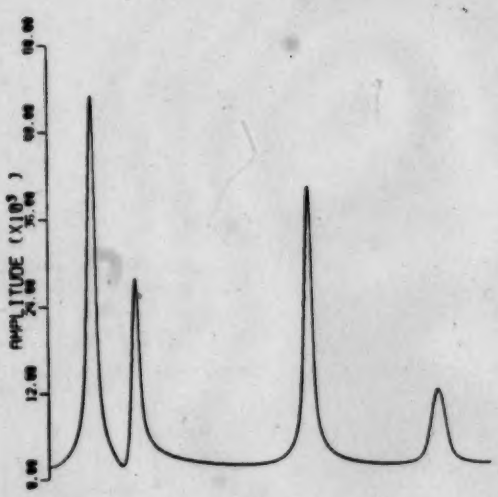


(c)

FIGURE 11. (a) Real, (b) imaginary and (c) amplitude output arrays for Scheme 4 inverse FFT implementation.

route is chosen.

C. Cross-correlation

A cross-correlation function is obtained if the two signals, a(t) and b(t) in Equation i (see Section A) are different. This operation is used to check for similarities between the two signals.

Full cross-correlation in the Fourier domain requires complete systematic utilization of the real and imaginary arrays of the FFT algorithms. The basic general scheme that is used for full cross-correlation operations is shown in Figure 12. The two functions to be correlated (function one and function two) are processed with the sorting FFT algorithm. Each will produce real and imaginary arrays; R1, I1 and R2, I2. A complex mathematical multiplication is then performed. The product now consists of real, (R1R2 + I1I2) and imaginary, (R2I1 - R1I2) parts. These are inputted into the appropriate real and imaginary input arrays of the non-sorting FFT algorithm. In the case of the imaginary array, the negative is taken. The resultant correlation function will then be available in the real output array resulting from the non-sorting FFT algorithm. The whole operation is illustrated in Figure 13 with two simple functions. The functions shown in

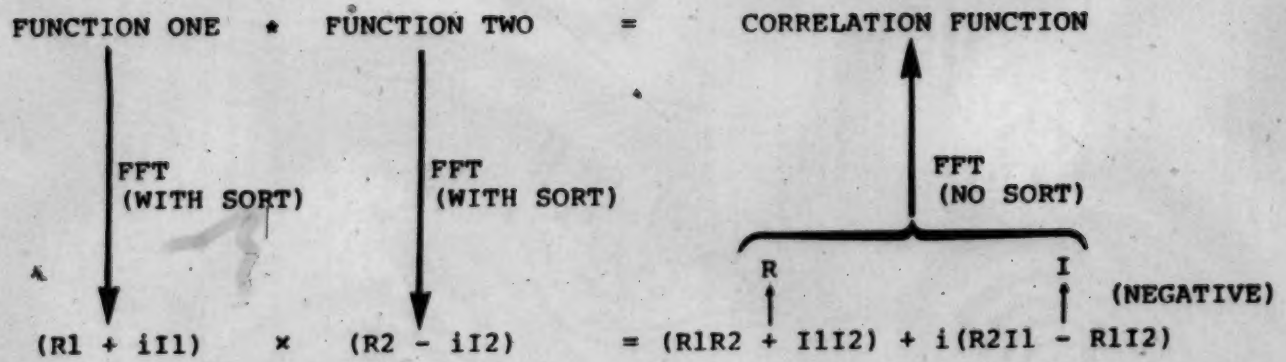


FIGURE 12. Flow chart for Fourier domain cross-correlation.

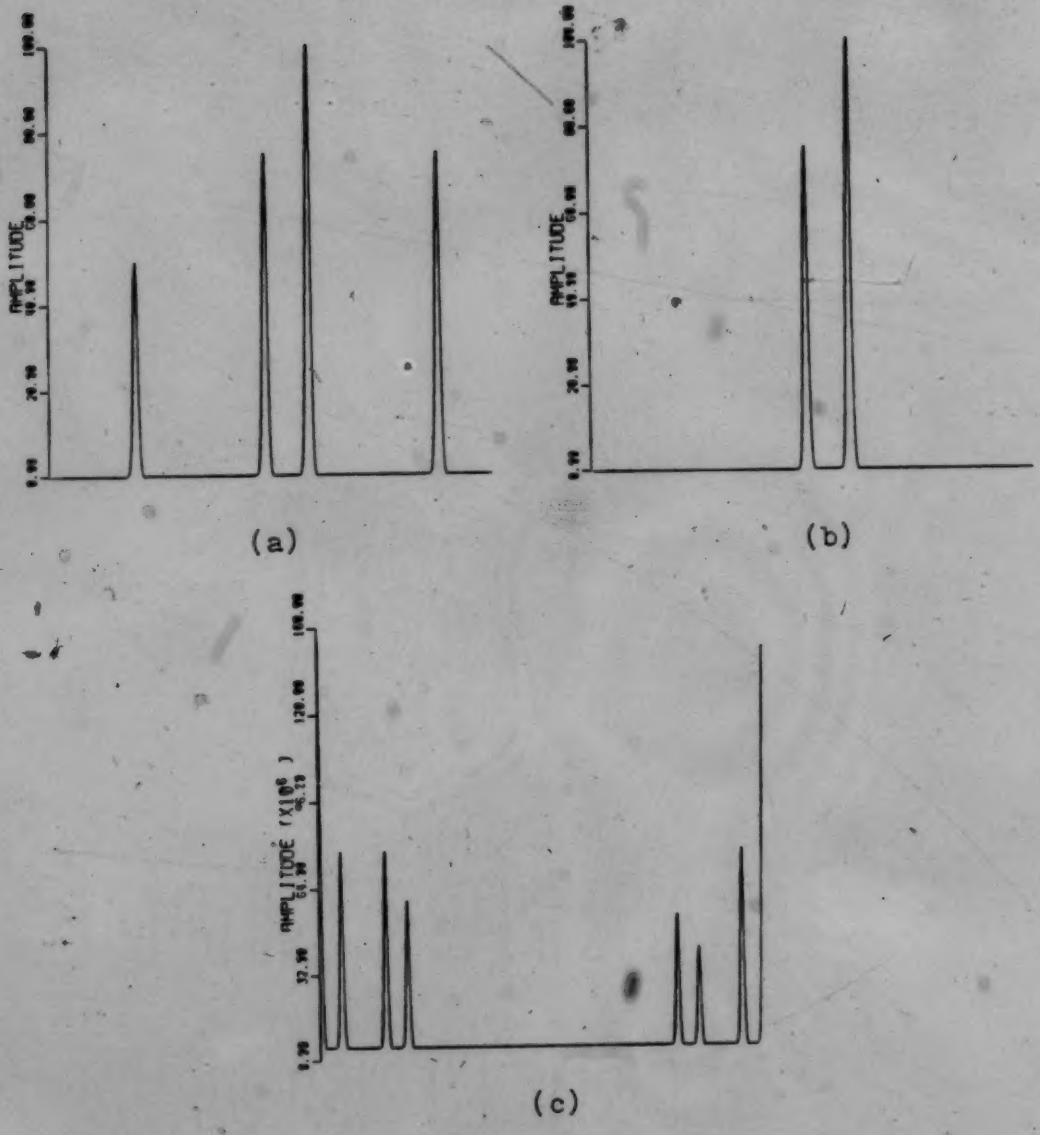


FIGURE 13. (a) Function one and (b) function two for cross-correlation operation. (c) Cross-correlation function as calculated by the procedure outlined in Figure 12.

Figures 13(a) and 13(b) are simple spectral patterns.

Cross-correlation patterns can be intuitively evaluated by envisioning one of the functions, for example function two to be slowly translated across function one. The value of the cross-correlation function at any particular displacement is the sum of the products of the two functions at that displacement, in a sense, their mutual area. In this particular example, when the two functions are cross-correlated, the resulting correlation function obtained in the real output array as shown in Figure 13(c) is out of sequence when plotting against a scale running from a negative displacement ($-\tau$) to a positive displacement ($+\tau$). The actual correlation pattern of the two functions is shown in Figure 14. It is obtained after proper rearrangement of the data array. Rearrangement simply means the interchange of the upper 512 points with the lower 512 points of the function which contains the correlation information shown in Figure 13(c).

At this point, the distinction between $a(t) * b(t)$ and $b(t) * a(t)$ correlation operations should be made. This is best illustrated by the above mentioned example. If the two functions are interchanged in the correlation operation, the resultant correlation function will then be the mirror image of the one obtained previously. This

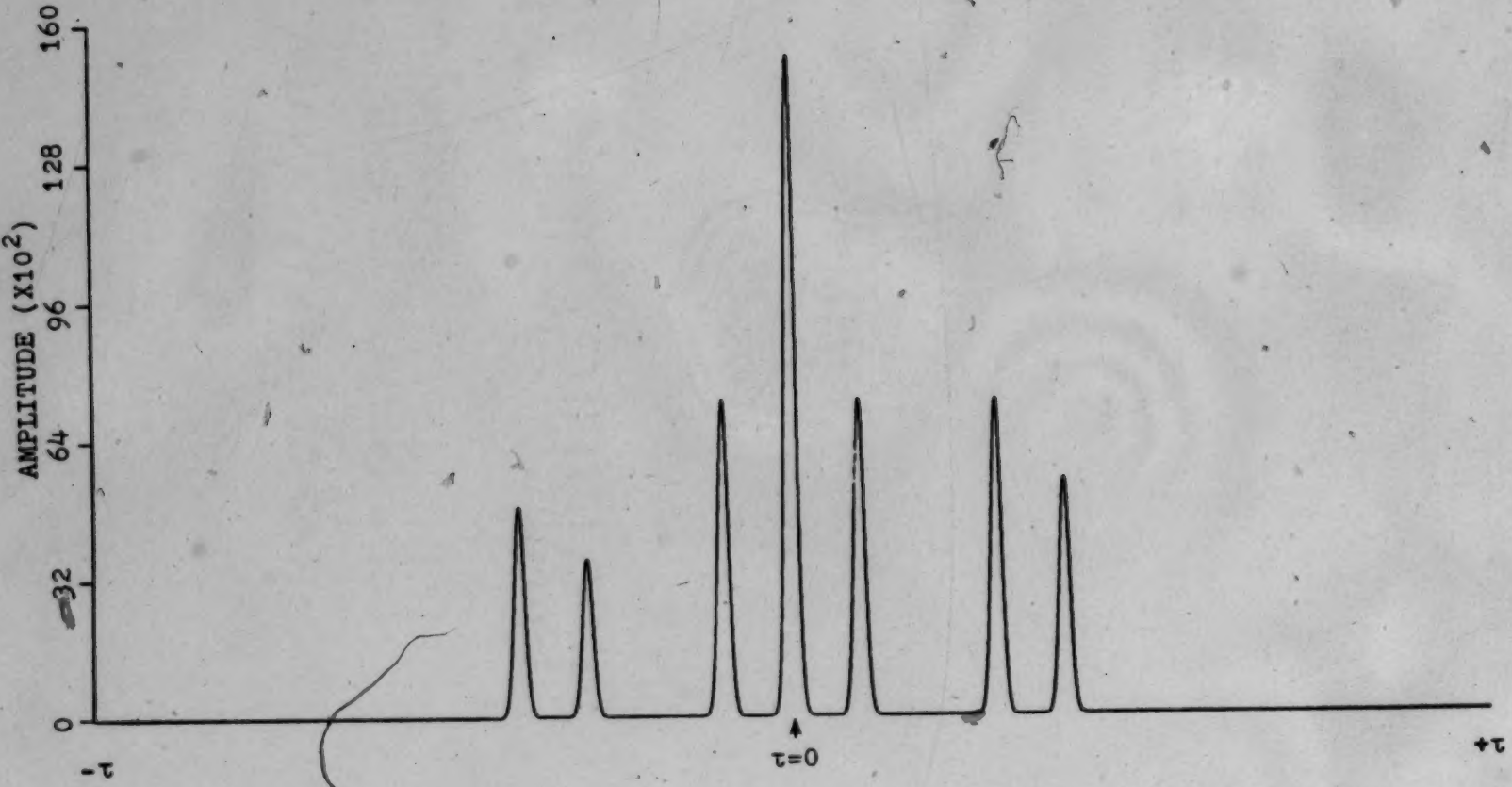


FIGURE 14. Cross-correlation function resulting from function one * function two.

is shown in Figure 15. Thus, care must be exercised when performing full cross-correlation operations as to which signal among the two is displaced.

D. Auto-correlation

Auto-correlation is cross-correlation of a function with itself. If the two signals, a(t) and b(t) in Equation i are identical, the function obtained is called an auto-correlation function. It is used to check whether coherence exists within a signal. It can be represented by the following equation:

$$C_{aa}(\tau) = \lim_{T\to\infty} \frac{1}{2T} \int_{-T}^{+T} a(t)a(t\pm\tau)dt \qquad (v)$$

where $C_{aa}(\tau)$ is the auto-correlation function for the signal a(t) and $\tau$ is the relative displacement.

In the case of digitized signals, the equation becomes:

$$C_{aa}(n\Delta t) = \sum_{t} a(t)a(t\pm n\Delta t) \qquad n=0,1,2,3,..... \quad (vi)$$

Auto-correlation can be implemented by the scheme shown in Figure 16. It is somewhat simpler than cross-correlation in that only two FFT's need to be carried out and there is no imaginary cross product. The multiplication

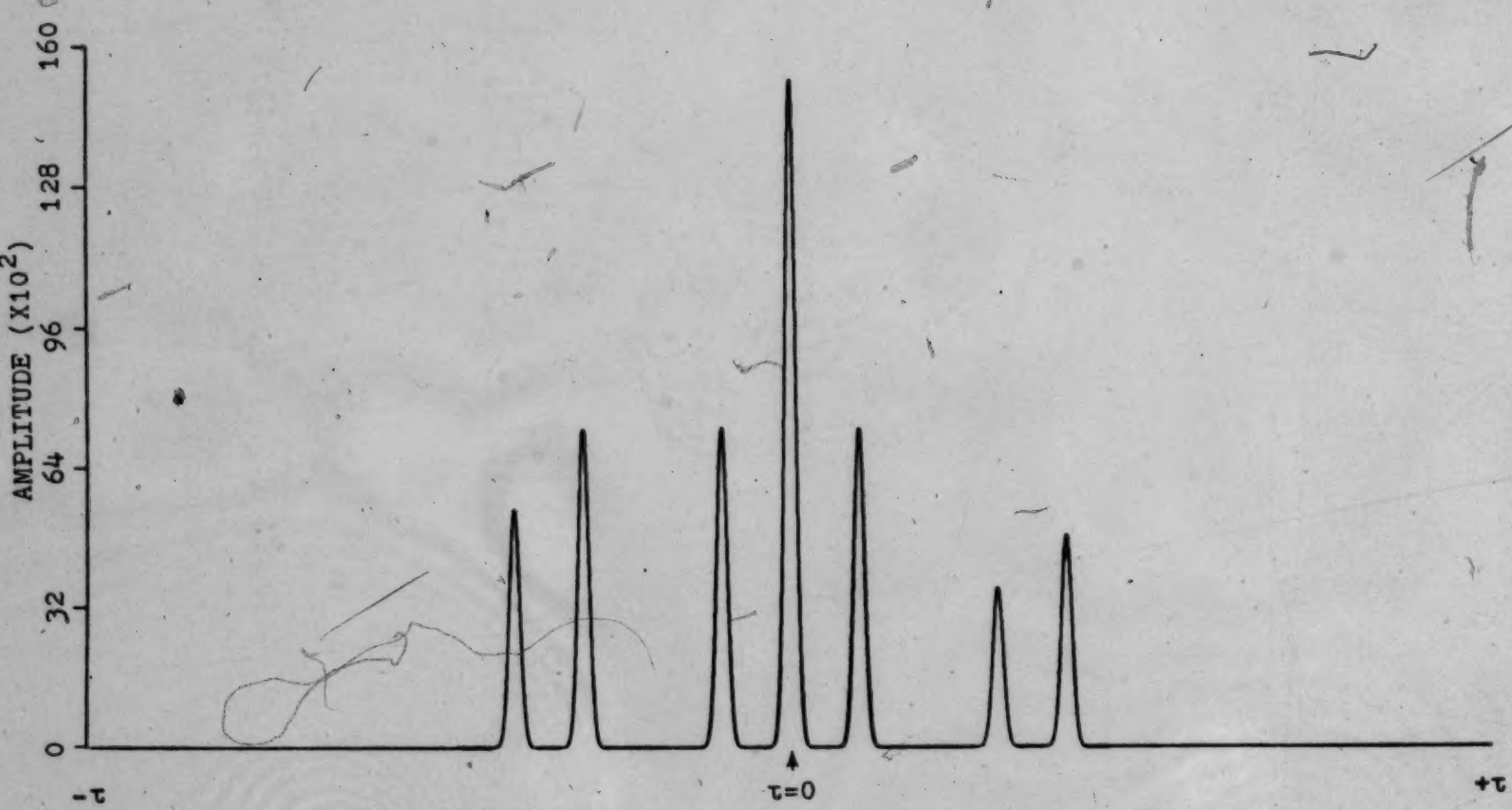


FIGURE 15. Cross-correlation function resulting from function two * function one.

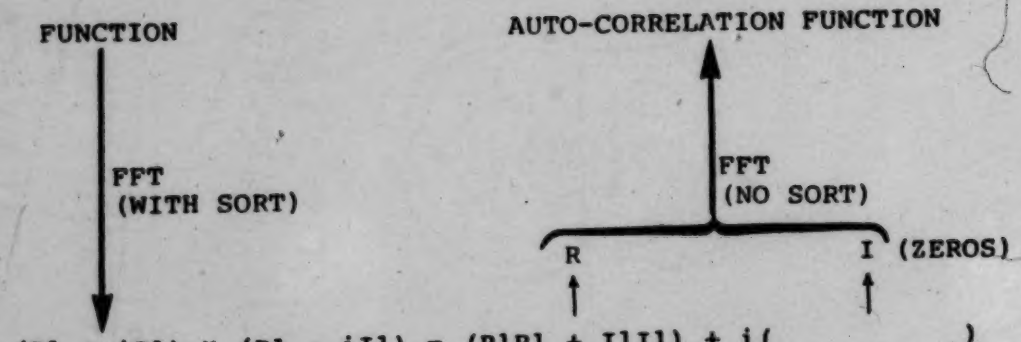


FIGURE 16. Flow chart for Fourier domain auto-correlation.

product which contains only real terms will generate the auto-correlation function in the real output array resulting from the non-sorting FFT algorithm. In this case, the imaginary input array for the non-sorting FFT algorithm is filled with zeros. The rearrangement of the correlation function output array is necessary as in the case of cross-correlation. An even simpler route is possible for auto-correlation using only the sorting FFT algorithm and this is illustrated in Figure 17. A simple spectral pattern and its corresponding auto-correlation function are shown in Figure 18. The full auto-correlation function as depicted in Figure 19 can be obtained simply by reflecting the resulting function in Figure 18(b) about the origin.

E. Convolution

A number of the aspects of correlation that have been introduced are perhaps more familiar to the reader under the term convolution. However, convolution, an operation which occurs during the generation or measurement of all signals, can be considered to be merely a special kind of correlation process. Mathematically, convolution can be expressed as:

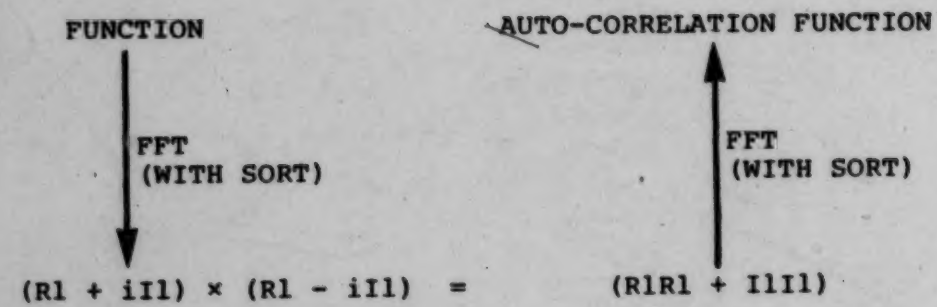


FIGURE 17. Flow chart for simplified Fourier domain auto-correlation.

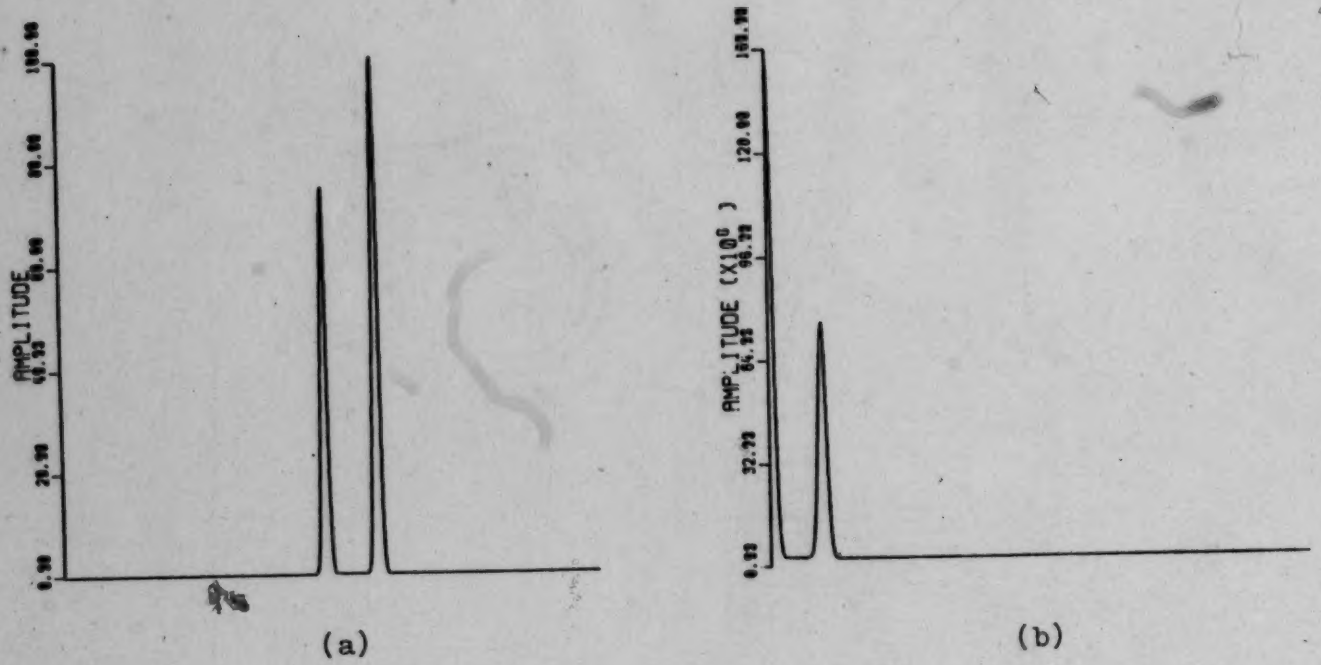


(a) (b)

FIGURE 18. (a) Function to be auto-correlated. (b) Auto-correlation function as calculated by the procedure outlined in Figure 17.

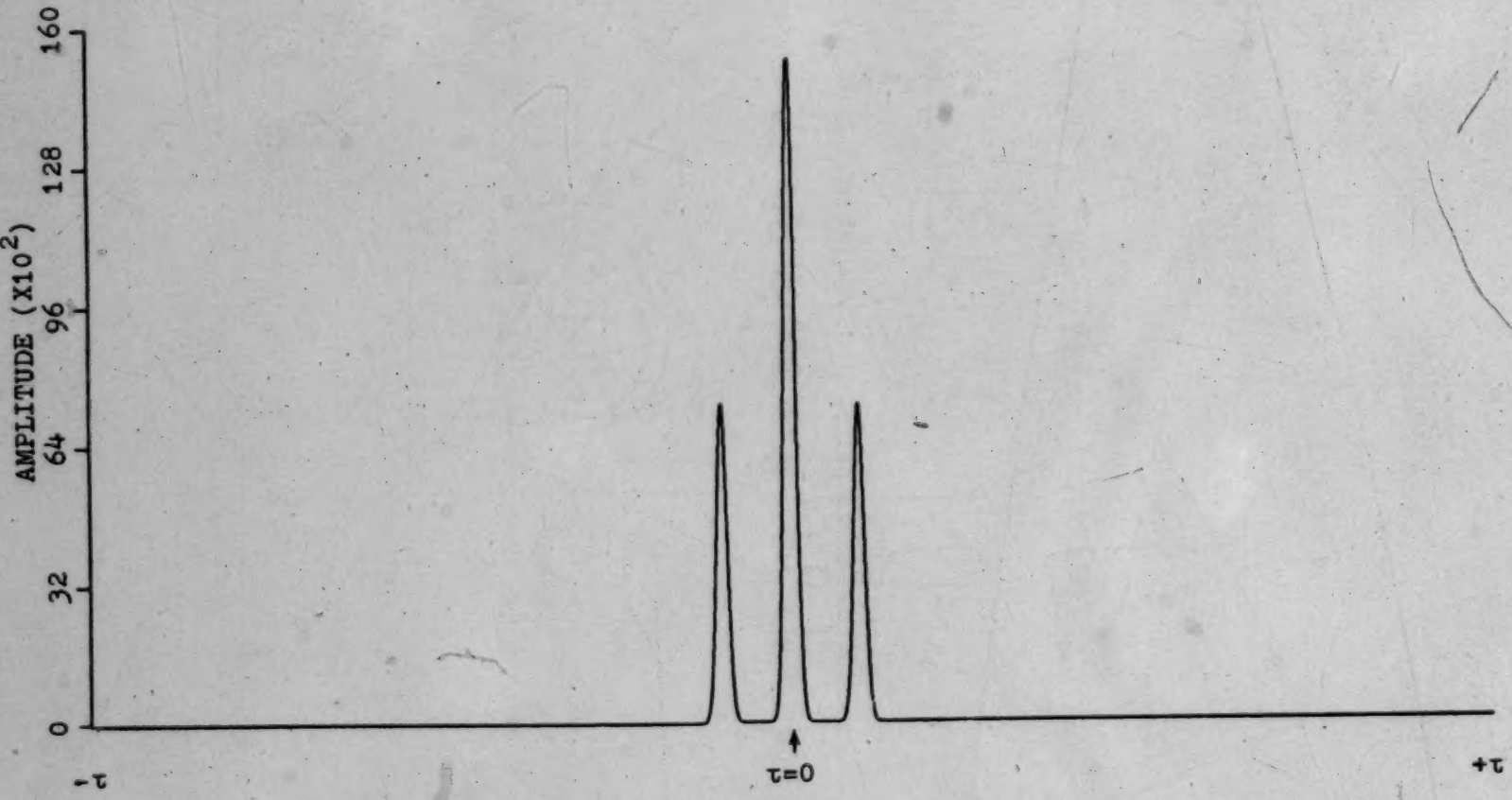


FIGURE 19. Auto-correlation function for the function shown in Figure 18(a).

$$CON_{ab}(\tau) = \lim_{T\to\infty} \frac{1}{2T} \int_{-T}^{+T} a(t)b(-t\pm\tau)dt \qquad \text{(vii)}$$

or

$$CON_{ab}(n\Delta t) = \sum_{t} a(t)b(-t\pm n\Delta t) \qquad n=0,1,2,3,..... \quad \text{(viii)}$$

If Equations vii and i are compared, their only difference is observed to be a minus sign in front of the t of the b function. The effect of this minus sign is to reverse the b(t) function (from left to right) on the time axis before it is multiplied by a(t). The rest of the shifting, multiplying and averaging procedures are identical to those employed in correlation. Therefore, correlation and convolution are identical, except that in convolution, one of the signals is first reversed.

The reason for this can be best understood with the aid of an example. Consider the effect of an instrument response function on a signal. A peak input signal and a low pass filter response function typical of amplifiers and recorders are shown in Figure 20. By convention / tradition both the signal and the response function are expressed with the time increasing to the right. However, if we imagine the input signal entering the instrument it

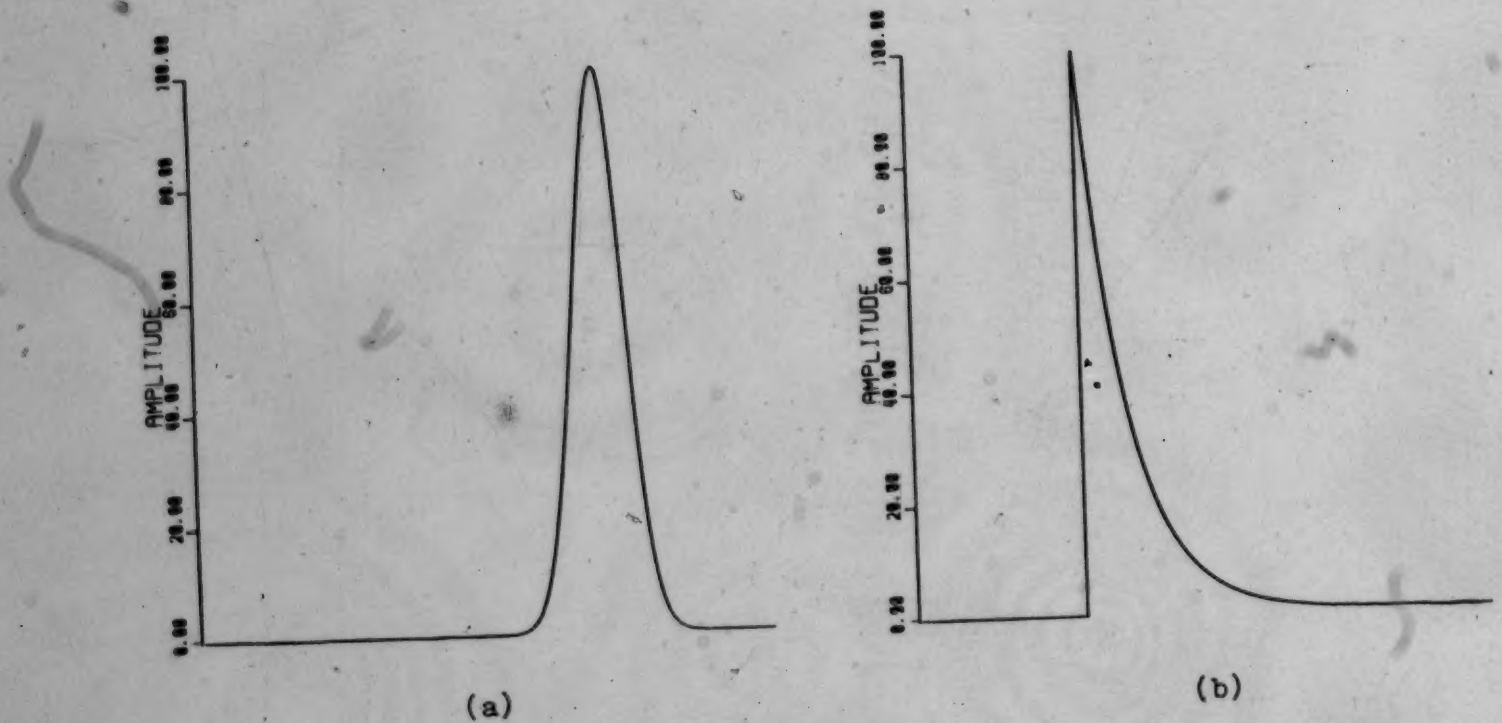


(a) (b)

FIGURE 20. (a) An input peak signal. (b) Low pass filter response function.

is apparent that the left side of the signal would enter first. Thus, in order to use the correlation operation to assess the effect of the instrument on the signal either the signal or the response function must be reversed from left to right before evaluation. It is conventional to reverse the response function. Thus, convolution is cross-correlation with reversal of the response function before evaluating the correlation function. The convolution function of the peak signal and the low pass filter response function obtained using the same flow chart (Figure 12) as in the case of cross-correlation is illustrated in Figure 21. The response function is reversed before the full cross-correlation operation.

From these considerations, convolution can be seen to be merely a special kind of correlation and can often be implemented and utilized in similar ways. In fact, in those many instances in which the response function is symmetrical, its inversion produces no change, so that correlation and convolution provide identical results.

F. Information at $\tau = 0$ Point of the Cross-correlation Function

In the previous chapter, the power of correlation analysis for spectral identification of relatively simple spectra has been illustrated. The $\tau = 0$ points of the

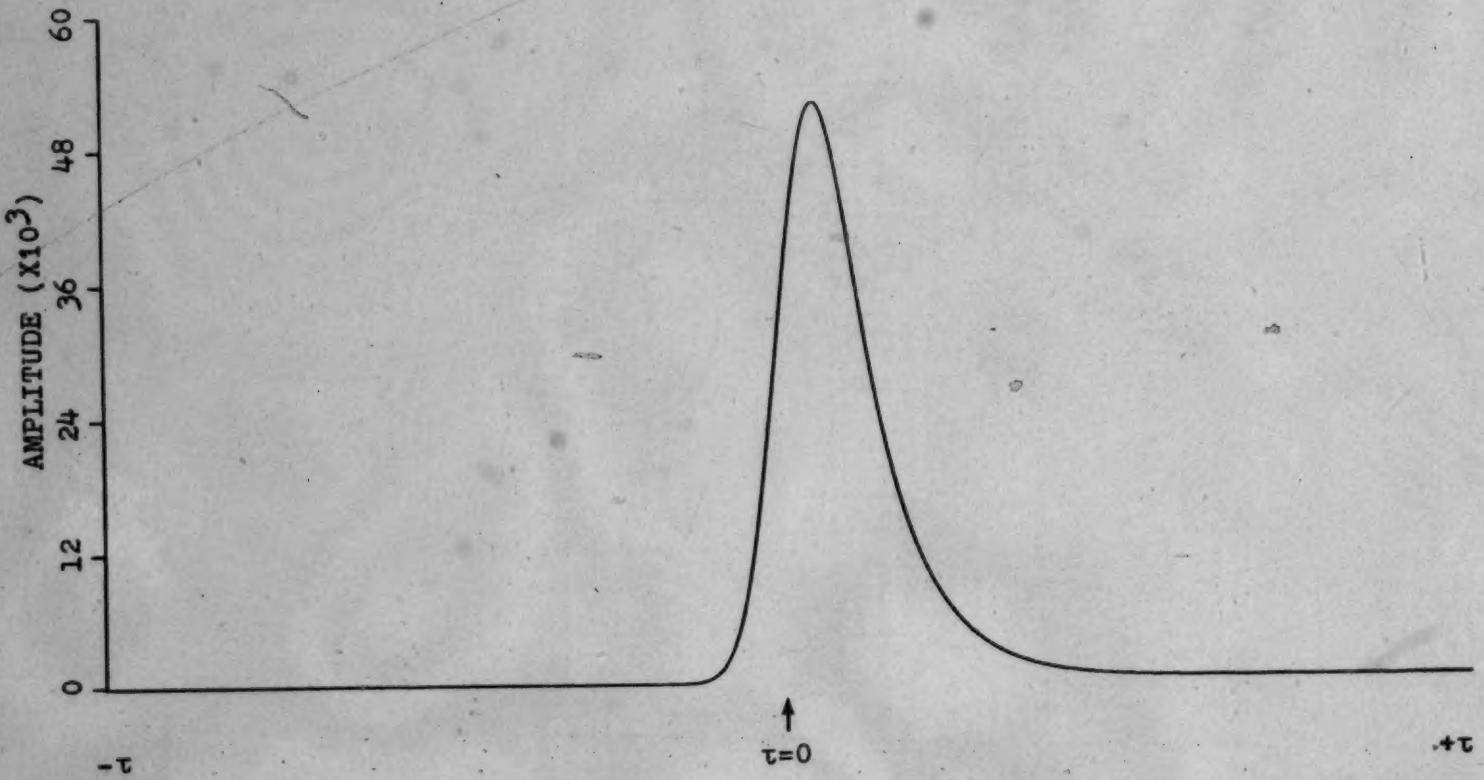


FIGURE 21. Convolution function resulting from the peak signal and the low pass filter response function.

cross-correlation functions contain quantitative and qualitative analytical information corresponding to the sought-for analyte. In this section, another example is given to further illustrate that in many cases, full cross-correlation functions need not be evaluated. As long as the two functions that undergo cross-correlation operation are in phase, the cross-correlation function at the $\tau = 0$ point contains all the relevant analytical information required. This is best illustrated with a more practical example: the qualitative and quantitative analysis of a multielement sample spectrum. A spectrum containing cadmium and zinc is shown in Figure 22. This, together with the zinc, cadmium and boron spectra shown in Figure 2 were measured with the ICP-photodiode array spectrometer system in the same spectral region (~220 nm). The experimental details in obtaining these spectra will be given in the next chapter.

The spectrum containing cadmium and zinc information is cross-correlated with the pure zinc, cadmium and boron spectra individually. At this point, the term "correlation mask" should be introduced. It simply represents the function used to mask out desirable analytical information from a sample spectrum by correlation techniques. In this particular example, cross-correlation masks are essentially the zinc,

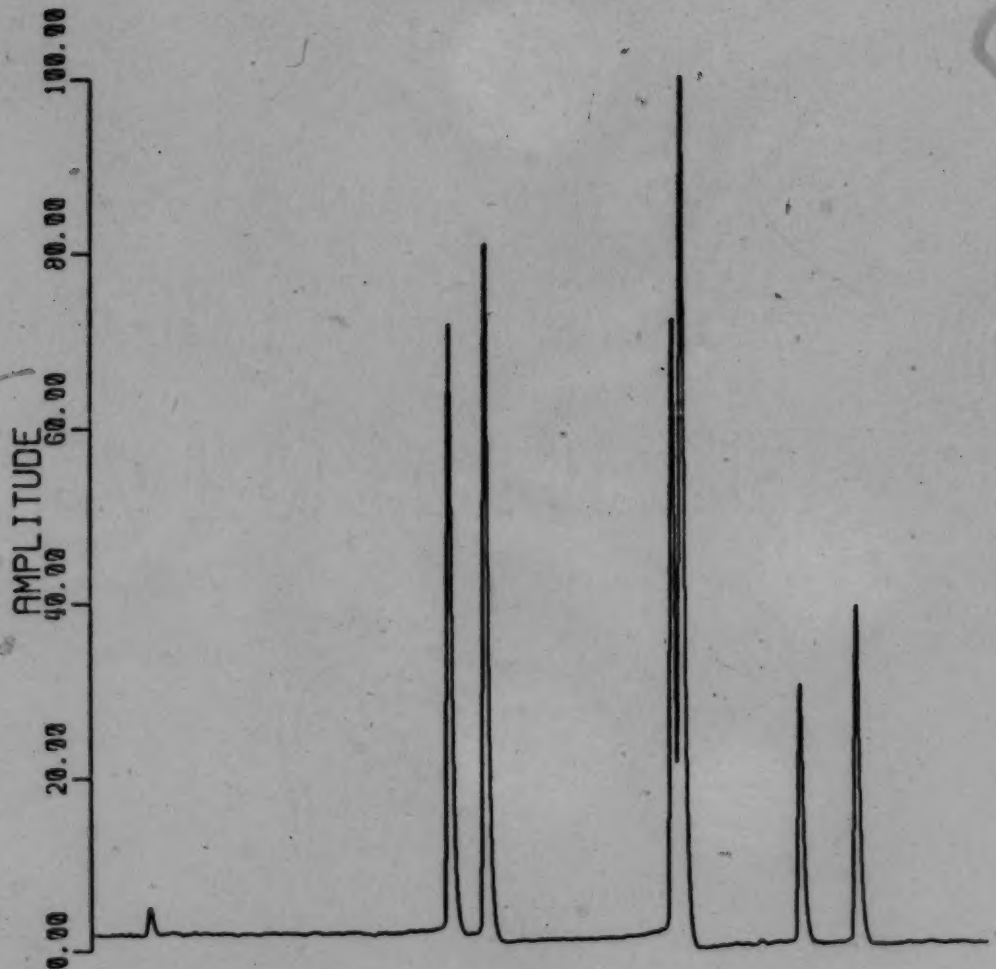


FIGURE 22. Sample spectrum containing cadmium and zinc.

cadmium and boron spectra which are used to extract zinc, cadmium and boron information respectively. This terminology will be frequently used throughout this thesis. The results of the cross-correlation operations is shown in Figure 23. The relatively high magnitude of the $\tau = 0$ points corresponding to zinc and cadmium correlation masks clearly indicates the presence of zinc and cadmium spectral information in the sample. In the case of boron, no distinct high $\tau = 0$ point is observed indicating the unlikelihood that boron is present in the sample. The absolute magnitude of the $\tau = 0$ point will provide the quantitative information corresponding to the specific correlation mask used. As long as the amplitude of the cross-correlation mask remains constant, the magnitude of the $\tau = 0$ point will be linearly proportional to the quantity of the sought-for information present in the signal.

This example is given here merely to stress the capability of spectral identification and quantitation using the cross-correlation technique. The $\tau = 0$ point can be utilized as opposed to the full cross-correlation operation as long as the correlation mask and the signal are in phase. Full cross-correlation or scanning between the signal and the mask is not necessary. In the subsequent chapters, correlation based data processing utilizing the

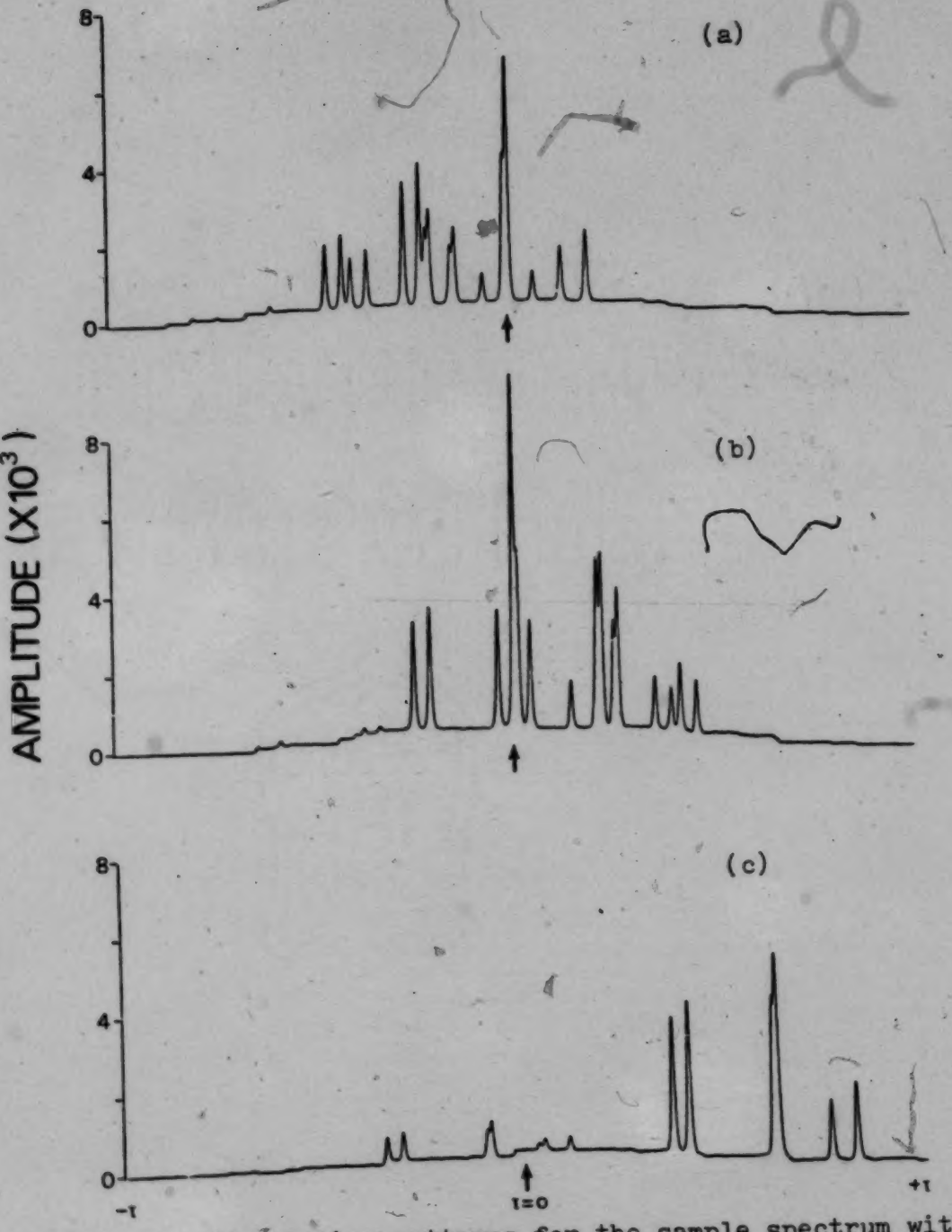


FIGURE 23. Correlation patterns for the sample spectrum with the (a) zinc, (b) cadmium and (c) boron spectra.

$\tau = 0$ value of the full cross-correlation function as applied to multielement atomic emission signals originating from an ICP source will be illustrated and discussed.

# CHAPTER III

## Correlation Based Data Processing for the ICP-Photodiode Array Spectrometer System

### A. Introduction

Cross-correlation techniques have been effectively applied to the computerized automatic detection of spectral information (36,48,49). The basic approach as outlined in the last chapter involves cross-correlation of the raw spectral signal with a noise free mask of the sought-for spectral pattern. In this chapter the concepts of cross-correlation methods for spectral pattern detection as applied to atomic emission spectra measured with a 1024-element photodiode array spectrometer coupled to an ICP will be outlined and then several analog and binary spectral masks will be evaluated as to their effectiveness for spectral signal detection. In particular, special attention is paid to the effectiveness of cross-correlation techniques in cases where spectral interference is severe. This is important because when electronic image detectors (50-55) are coupled to spectrometers, spectral resolution is often sacrificed in order to achieve reasonable wavelength coverage.

The cross-correlation techniques will be illustrated for the determination of nickel or/and vanadium. This system was chosen because the determination of both elements

is of prime importance for the petroleum industry (56-58). Besides, both nickel and vanadium yield complex spectra which result in several spectral overlaps. An evaluation of the effectiveness of correlation analysis for the automatic processing of spectrochemical data obtained by an image sensor can thus be made.

B. The ICP-Photodiode Array Spectrometer System

A commercially available radiofrequency (27.12 MHz) inductively coupled plasma which is capable of delivering a maximum power of 5 KW was used as the source for all the atomic emission spectra described in this chapter. The plasma was imaged onto the entrance slit of the photodiode array spectrometer using a UV grade quartz lens of ten centimeters focal length. The whole experimental setup was located on an optical rail bed similar in concept to the one suggested by Walters (59).

The 1024-element self scanning photodiode array spectrometer has been described in the literature (18,75). A brief description of the spectrometer is included below for completeness. For full details, references cited should be consulted.

A 1024-element photodiode array was placed horizontally along the exit focal curve of a monochromator. The

monochromator is of the Czerny-Turner design and has a focal length of 35 centimeters. The standard diffraction grating provides approximately 500 Å of spectral coverage for the array detector. The physical length of the array is approximately one inch while the individual photodiode measures 0.001 inch wide by 0.017 inch tall. During data acquisition, the photodiode array was cooled to about -20°C with the use of a Peltier cooler. This significantly reduces dark current of the array and enables the integration time to be varied from milliseconds to seconds depending on the magnitude of the signal. The photodiode array spectrometer was coupled to a PDP 11/10 minicomputer. The complete system with the supporting software has been recently described by Hull (60) and will not be repeated here.

The analog signal obtained from the spectrometer was electronically filtered and amplified with a differential amplifier prior to analog-to-digital conversion. The analog-to-digital converter was contained in the PDP 11 Laboratory Peripheral System. The equipment used for this study is summarized in Table 1.

The atomic emission spectra of nickel and vanadium were obtained at an ICP power level of 1.5 KW with the coolant gas flowing at about 15 liters per minute (lpm). The auxiliary gas flow was completely shut off. A

TABLE 1. Components of the ICP-PDA spectrometer system.

| Item | Source |
|---|---|
| Inductively Coupled Plasma | |
| ICP 5000 Matching Box | Plasma Therm, Inc. |
| ICP RF Generator HFS 5000D | Plasma Therm, Inc. |
| Photodiode Array Spectrometer | |
| 1024 Element Photodiode Array | Reticon Corporation |
| Monochromator EU 700-70 | Heath |
| Monochromator Electronic Control Unit EU 700-51 | Heath |
| Peltier Cooler CP 1.4-71-06 | Materials Electronic Products Corp. |
| Differential Amplifier AM 502 | Tektronix |
| Computer | |
| PDP 11/10 16-bit Minicomputer (RT-11 Operating System, 16K Core Memory) | Digital Equipment Corporation (DEC) |
| Cartridge Disk Drive RK-05J | DEC |
| Video Terminal VT-55 | DEC |
| Decwriter II | DEC |
| Laboratory Peripheral System LPS 11 | DEC |
| Zeta 100/1200 Series Incremental Plotter | Zeta Research Corporation |

conventional cross-flow nebulizer was utilized with the gas flowing at about 1 lpm. The observation height of the plasma was approximately 15 mm above the load coil. The spectrometer was set so that it covered approximately from 275 to 325 nanometers. All the spectra obtained were averaged over ten seconds unless otherwise specified.

C. Simple Cross-correlation Masks

The first step in the generation of a cross-correlation mask for the detection of specific spectral information is the measurement of a spectrum of the sought-for element. The atomic emission spectrum of vanadium is shown at the bottom of Figure 24. The wavelength axis was left off. When utilizing cross-correlation techniques it is not necessary to define the wavelength axis, the specificity is built into the measured vanadium cross-correlation mask.

This complete spectrum can be used as a cross-correlation mask to detect vanadium in subsequent measurements. Only the $\tau = 0$ point need be evaluated which can be generated by multiplying this spectral intensity cross-correlation mask and subsequent spectra together point-by-point and adding up the products. Such a procedure can be used to establish an analytical curve plotting the magnitude of the $\tau = 0$ cross-correlation point versus concentration. Such an analytical curve is shown

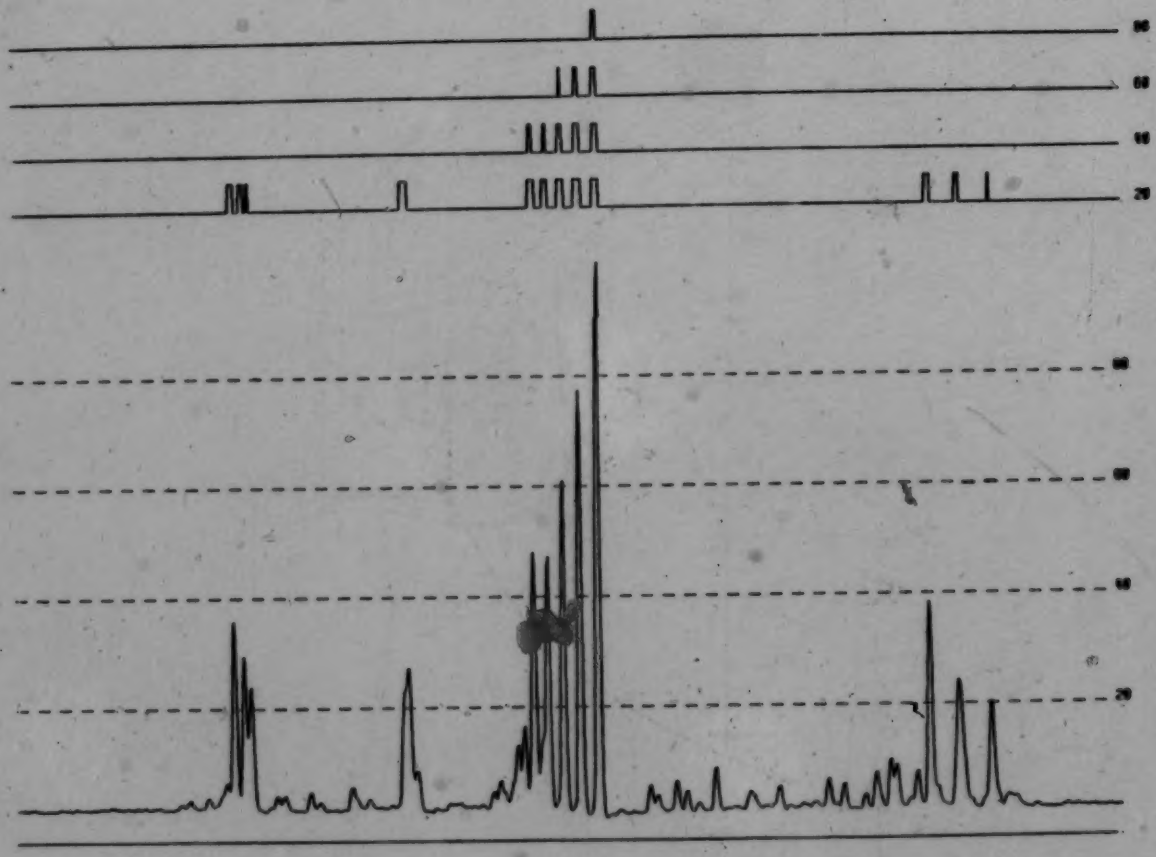

FIGURE 24. Vanadium spectral intensity and binary cross-correlation masks.

in Figure 25. Alternate masks may be generated using threshold levels. Several such levels are indicated in Figure 24 superimposed on the vanadium spectrum. Now, in the generation of the $\tau = 0$ value, cross-correlation products are only evaluated when the vanadium mask value exceeds the specified threshold. With the 80% threshold value the measurement reduces to essentially a conventional single peak intensity measurement as might normally be carried out in setting up an analytical curve. The analytical curves for various threshold levels are also shown in Figure 25. As less and less vanadium information is used to establish the analytical curve the sensitivity, as indicated by the slope of the analytical curve, is reduced. Thus the full cross-correlation mask provides the most sensitive measurement of vanadium.

The full cross-correlation mask also provides the most precise measurement of vanadium. Ten vanadium spectra at the 10 ppm level were measured and the $\tau = 0$ cross-correlation points evaluated using the masks with various thresholds. The percent relative standard deviation (rsd) of the ten $\tau = 0$ values ranged from 11.6% for the 80% threshold mark to 8.3% for the full (0% threshold) cross-correlation mask.

An interesting alternative to the "spectral intensity"

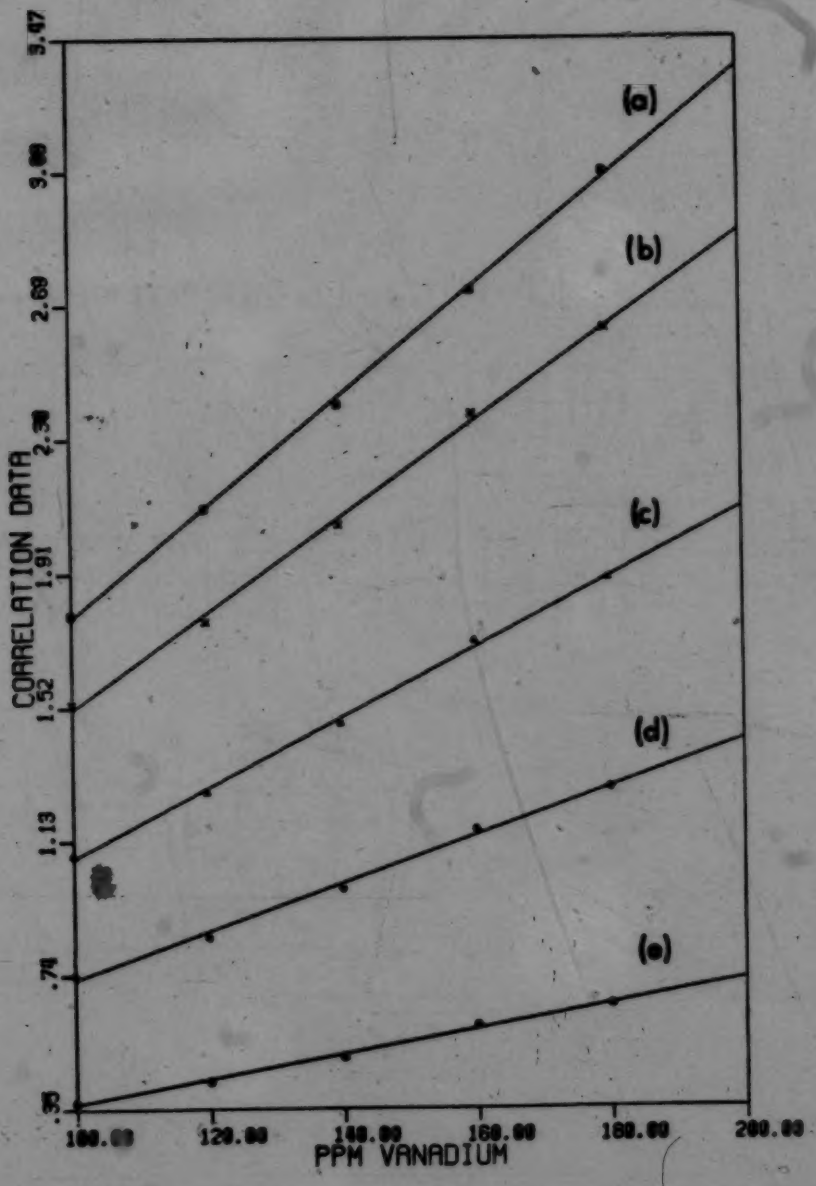


FIGURE 25. Vanadium analytical curves determined using spectral intensity cross-correlation masks. Threshold (a) 0%, (b) 20%, (c) 40%, (d) 60% and (e) 80%.

masks depicted at the bottom of Figure 24 are the binary masks shown at the top of Figure 24. A binary cross-correlation mask is generated by first setting a threshold and then every spectral intensity greater than or equal to the threshold value is set equal to binary 1 and every value less than the threshold is set equal to binary 0. Binary masks for thresholds of 20%, 40%, 60% and 80% are shown at the top of Figure 24.

Several advantages accrue to the utilization of binary cross-correlation masks. The evaluation of the $\tau = 0$ point is now considerably simpler as the multiplication step is not required. The $\tau = 0$ cross-correlation of the binary mask and a measured vanadium spectrum amounts to a gated integration of specific spectral intensities. Analytical curves established using the binary masks are shown in Figure 26 and are comparable to those shown in Figure 25. Also the precision of the $\tau = 0$ value is essentially the same for the binary and intensity masks. At a threshold value of 20%, the percent rsd of the ten $\tau = 0$ values for the 10 ppm vanadium spectra was 8.7% for the spectral intensity mask and 8.5% for the corresponding binary mask.

In addition to allowing simpler evaluation of the cross-correlation values the binary masks occupy considerably less storage space in a computing system than

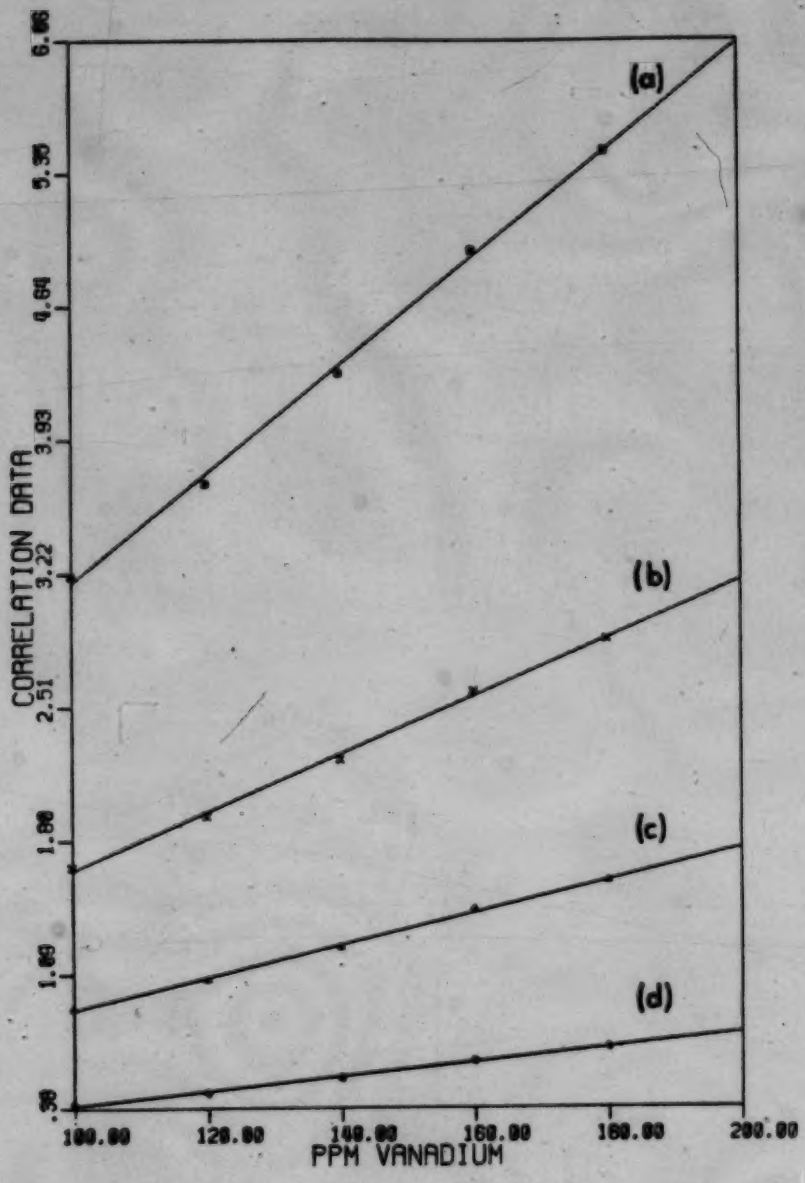


FIGURE 26. Vanadium analytical curves determined using binary cross-correlation masks. Thresholds (a) 20%, (b) 40%, (c) 60% and (d) 80%.

the spectral intensity masks. This could facilitate implementation of cross-correlation methods with simple ROM (Read Only Memory) based microprocessor systems. Also integrated circuit subsystems are now available specifically designed to carry out the cross-correlation between a stored binary pattern and an input analog signal (61). Utilization of these subsystems would allow essentially real time evaluation of $\tau = 0$ cross-correlation values.

The analogous spectral intensity and binary cross-correlation masks for nickel in this exact same spectral region are shown in Figure 27. They can be used for the determination of nickel in a manner analogous to that just discussed for vanadium.

These cross-correlation masks are good for spectral identification and quantification for relatively simple analysis. When analytical information is required for samples of complex nature, spectral interference is a major problem. In the next section cross-correlation masks with built-in specificity for a particular analytical problem, determination of vanadium or nickel in a mixture of two, will be illustrated.

## D. Cross-correlation Masks for Complex Spectra

Consider the problem of generating cross-correlation

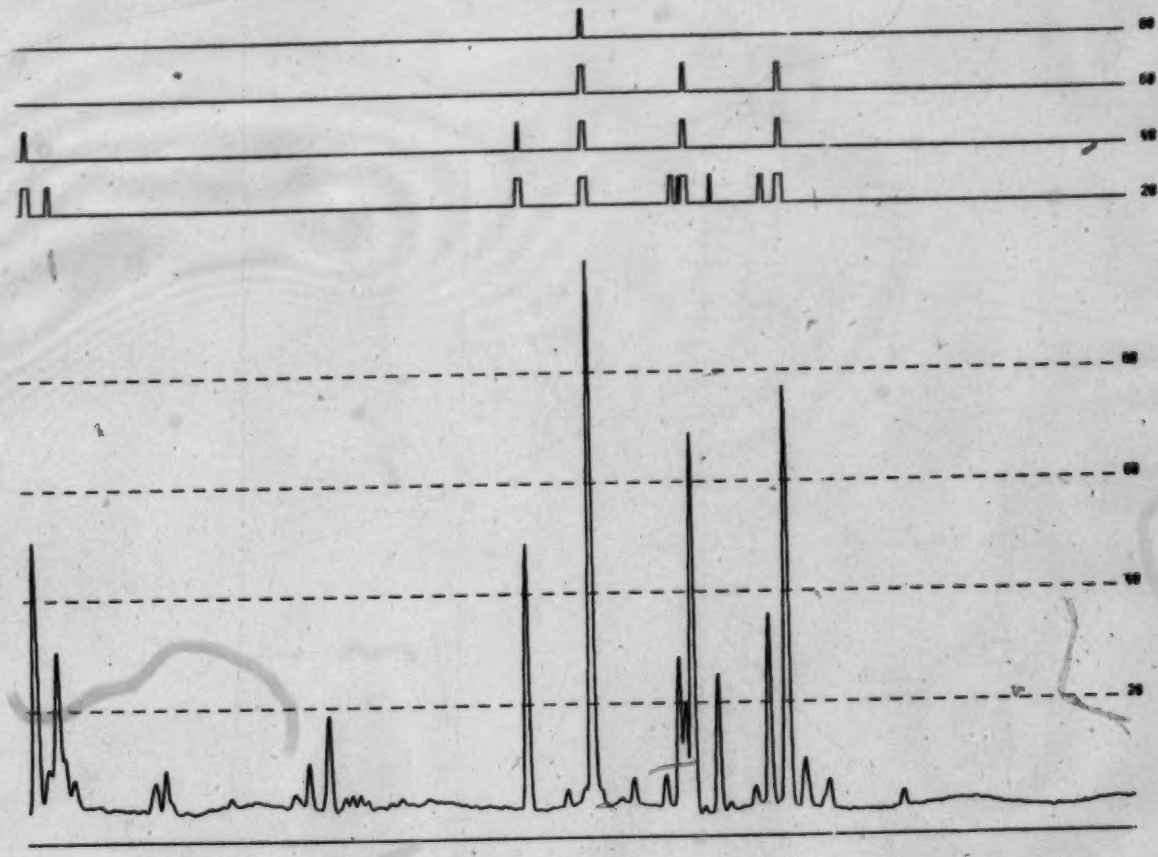

FIGURE 27. Nickel spectral intensity and binary cross-correlation masks.

masks for the determination of either nickel or vanadium in the presence of each other. The spectrum of a solution containing both nickel and vanadium is shown in Figure 28. Several lines overlap, the most serious being the overlap of the most intense line of nickel in this region (310.1 nm) with the second most intense vanadium line (310.2 nm).

A spectral intensity cross-correlation mask specific for vanadium in the presence of nickel can be constructed by stripping a vanadium spectrum with a nickel spectrum. This is easily accomplished by subtracting a nickel spectrum from a vanadium spectrum as shown in Figure 29. Such an operation is very easy to perform in a precise manner using the computer coupled photodiode array spectrometer. Depending on the degree of spectral overlap, the amount of stripping can be easily adjusted. In this example, the stripping was carried out using a nickel spectrum whose maximum intensity was twice that of the maximum intensity in the vanadium spectrum. This was accomplished by computer software on stored spectra. The remaining features in the vanadium spectrum (above a threshold of zero) can be used to set up specific spectral intensity and binary cross-correlation masks that will detect vanadium in the presence of nickel and will not respond to any nickel information. These masks are shown

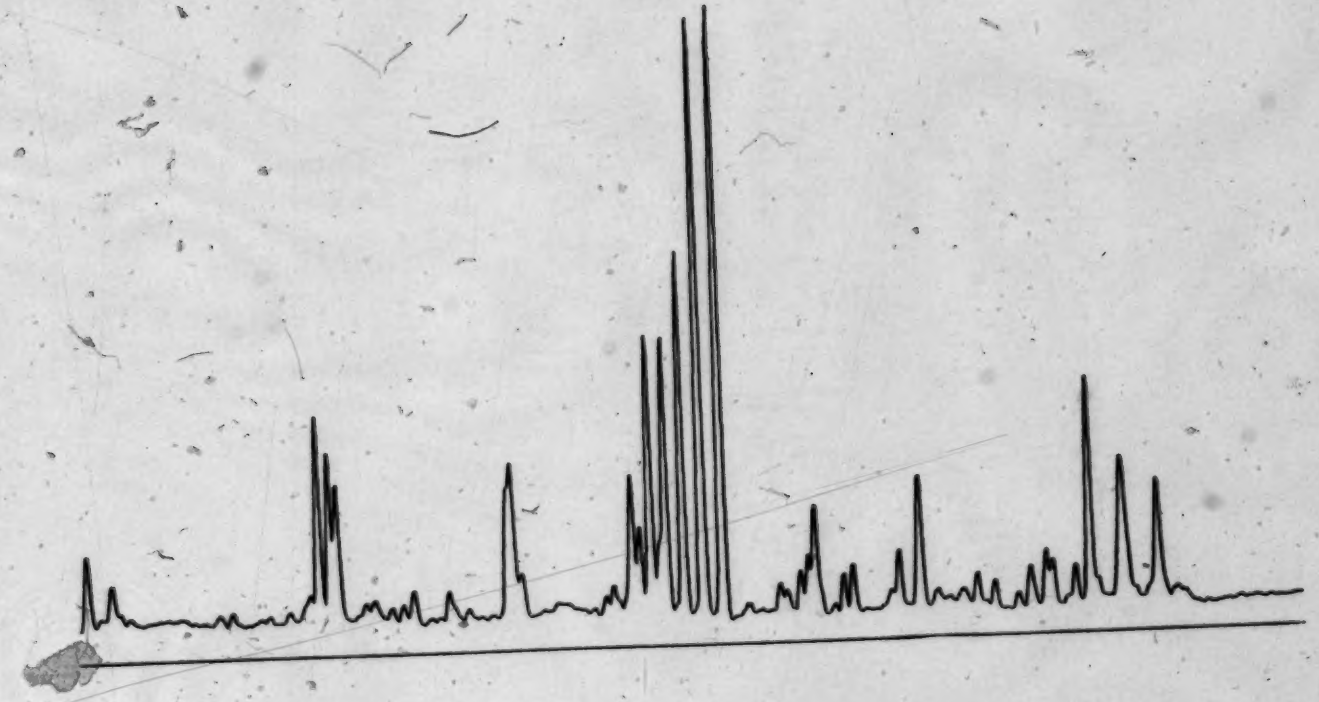

FIGURE 28. Spectrum of nickel (1000 ppm) and vanadium (180 ppm).

FIGURE 29. Vanadium minus nickel difference spectrum.

in Figure 30. The analogous procedure can be used to set up cross-correlation masks for the detection of nickel in the presence of vanadium and the results are shown in Figures 31 and 32. Thus with the measurement capability of the photodiode array spectrometer it is relatively easy to set up, in an essentially automatic fashion, cross-correlation masks for the analysis of mixtures. Again, note that knowledge of the wavelength axis or even where lines overlap is not required. The stripping procedure automatically removes the overlapped spectral intensities.

The $\tau = 0$ value of the cross-correlation function was evaluated for spectra obtained of solutions containing a constant amount of nickel (1000 ppm) and increasing amounts of vanadium (100 to 200 ppm) using cross-correlation masks generated from a nickel spectrum and a vanadium stripped nickel spectrum. The responses of these spectral intensity correlation masks are shown in Figure 33 and 34 respectively with various threshold levels. In all cases, pure nickel spectral intensity cross-correlation masks do extract undesirable vanadium information from the signal as indicated by the slope of the graphs in Figure 33. The vanadium stripped nickel cross-correlation masks do not respond to vanadium information as illustrated in Figure

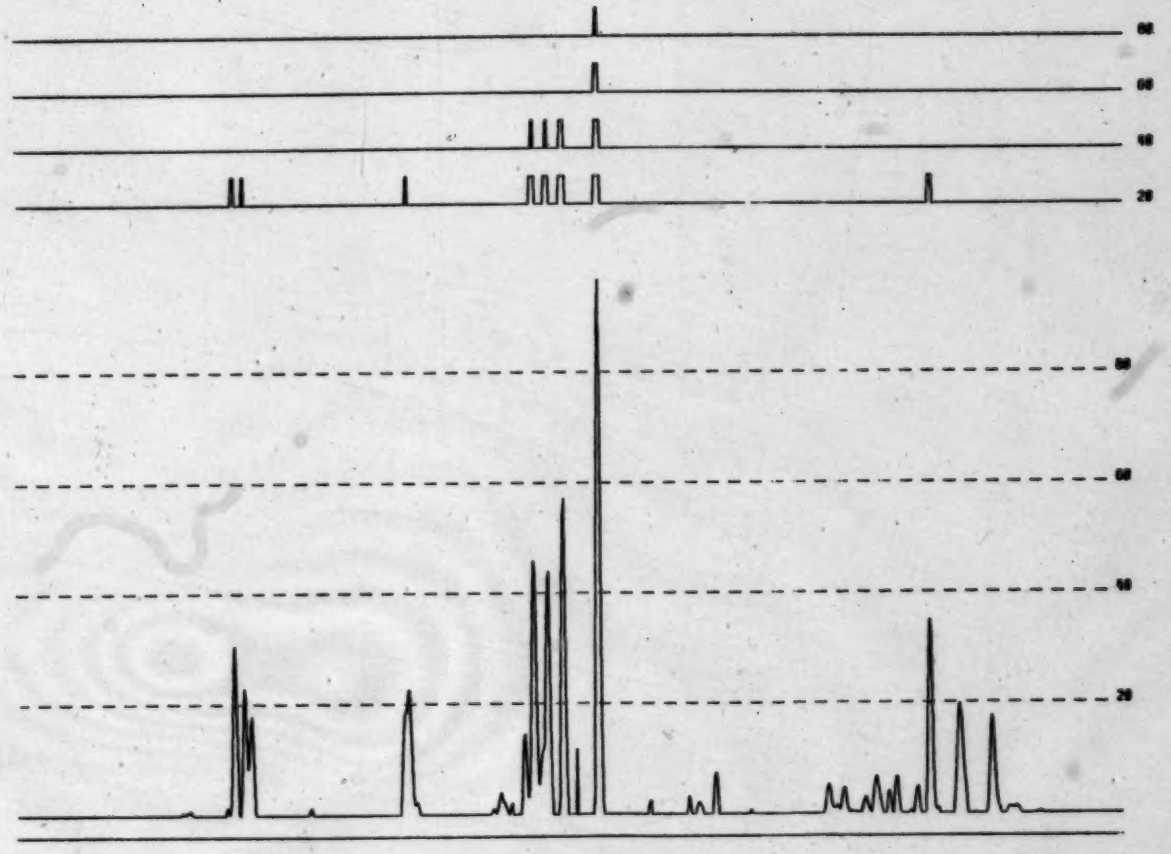

FIGURE 30. Vanadium spectral intensity and binary cross-correlation masks minus any nickel information.

FIGURE 31. Nickel minus vanadium difference spectrum.

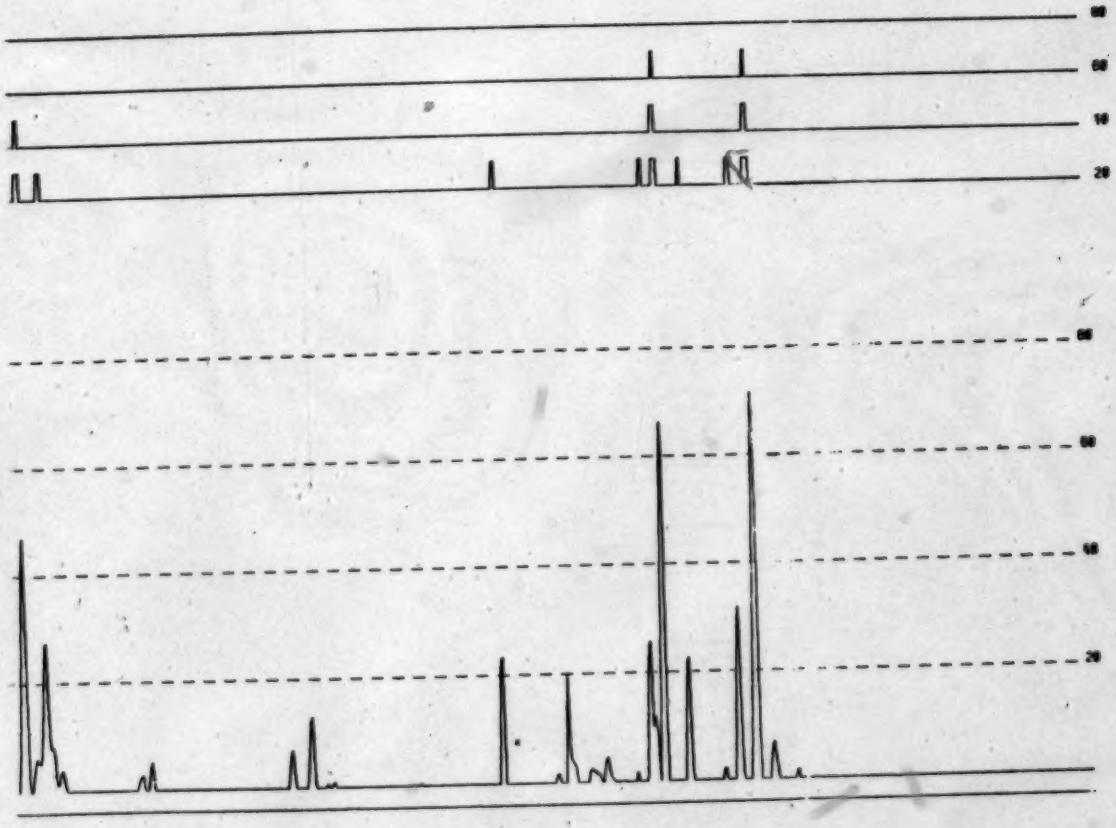

FIGURE 32. Nickel spectral intensity and binary cross-correlation masks minus any vanadium information.

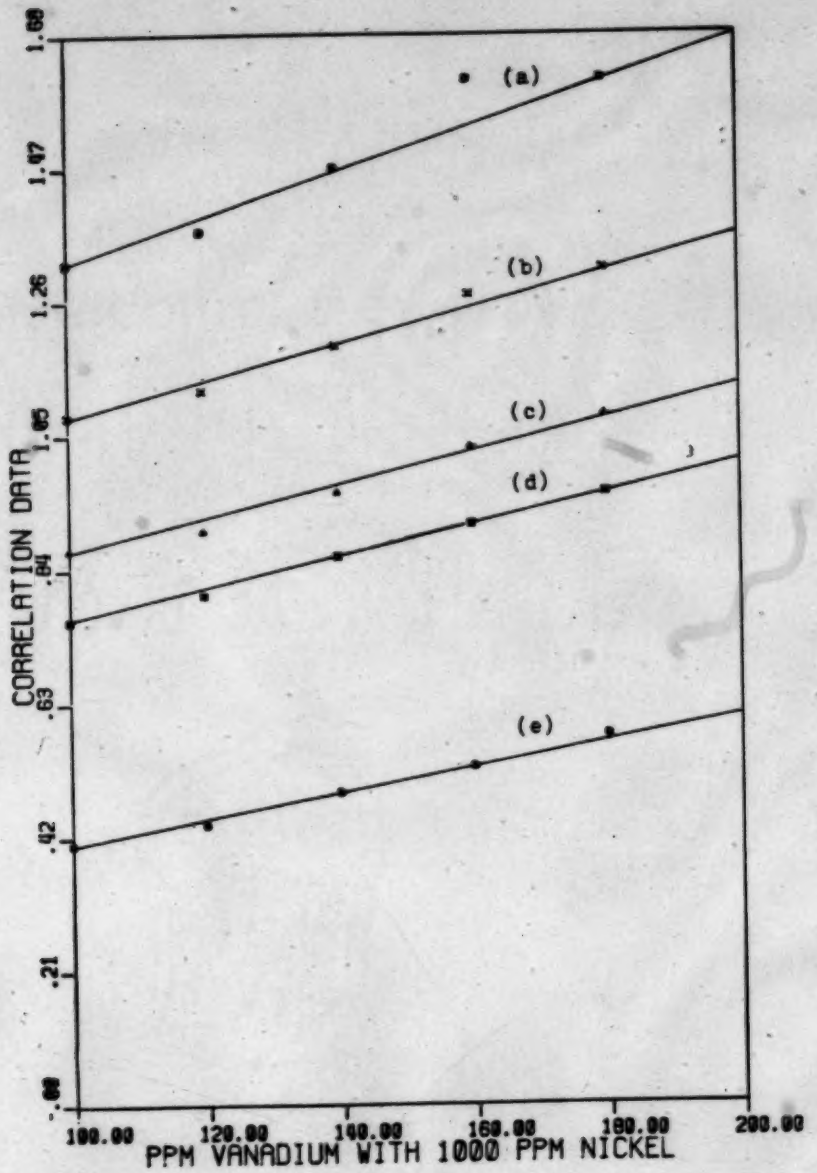


FIGURE 33. Detection of nickel in the presence of vanadium using nickel spectral intensity cross-correlation masks. Thresholds (a) 0%, (b) 20%, (c) 40%, (d) 60% and (e) 80%.

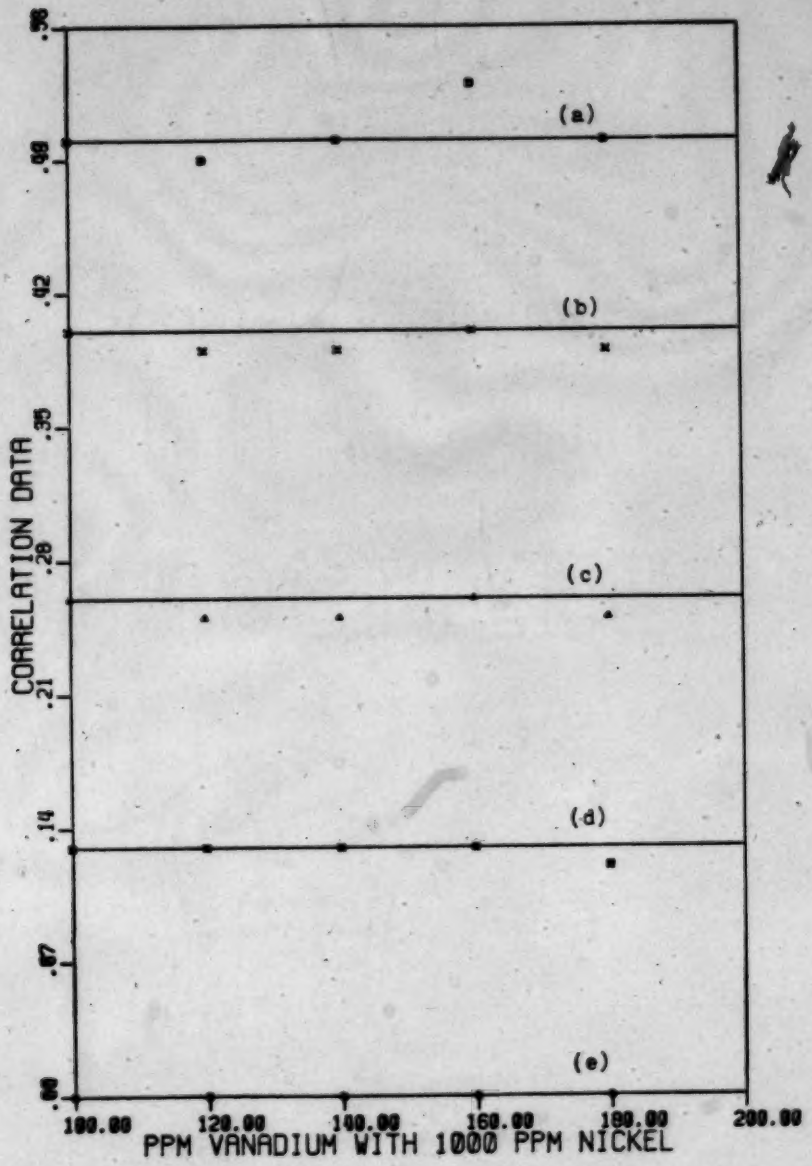


FIGURE 34. Detection of nickel in the presence of vanadium using vanadium stripped nickel spectral intensity cross-correlation masks. Thresholds (a) 0%, (b) 20%, (c) 40%, (d) 60% and (e) 80%.

34. Similar results are obtained for binary cross-correlation masks at different threshold levels, these are illustrated in Figures 35 and 36. Linear working curves for these cross-correlation masks are illustrated for the determination of vanadium in the presence of nickel as shown in Figures 37 and 38.

At this point, one can envision correlation masks designed to implement more complex decisions than simply the detection of a single element. This can be achieved by simultaneously assessing several elemental species and their relative concentrations. In this way, correlation masks with specificity built-in can be generated for a specific analytical problem.

One has to keep in mind that the correlation masks generated as mentioned above can overcome the problem of spectral interferences, they do not compensate for the true chemical interferences arising due to the matrix of the sample.

## E. Conclusions

From the fact that the performance of binary correlation masks is comparable to the spectral intensity correlation masks in all aspects, a preliminary investigation to generate binary cross-correlation masks from a library

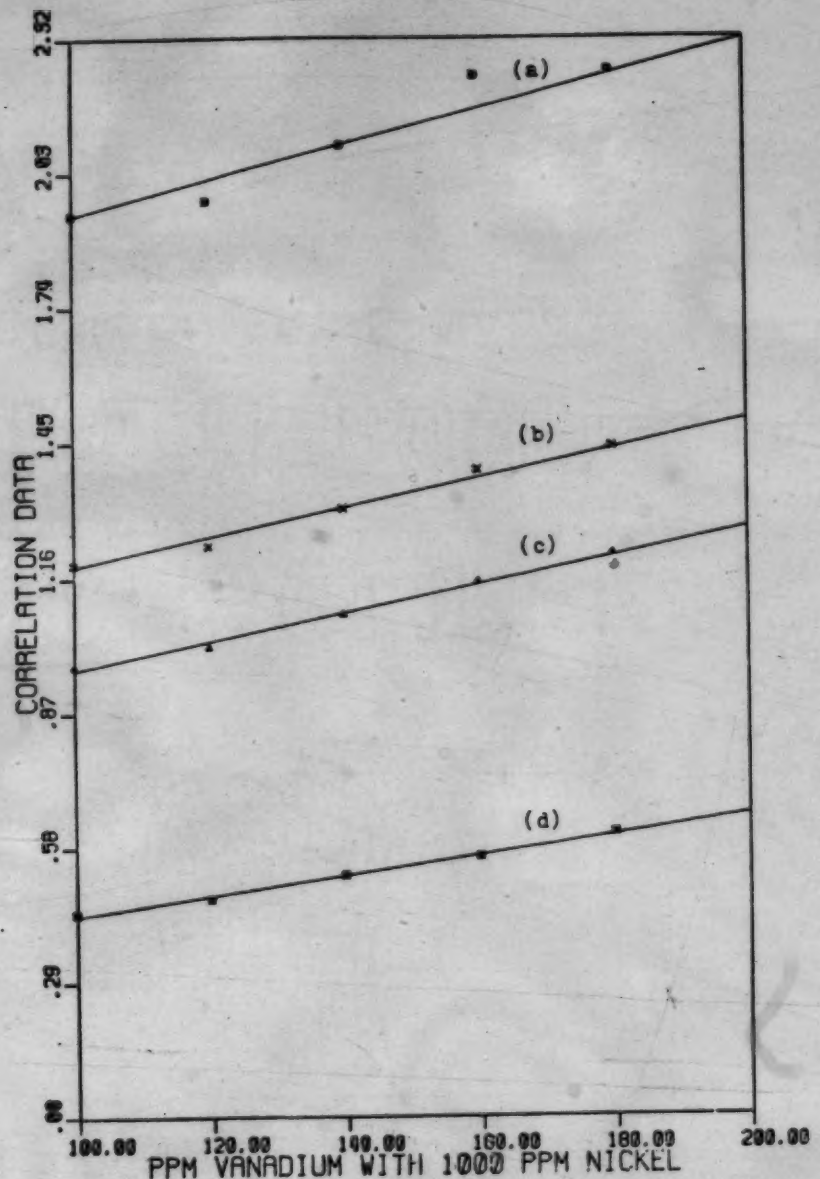


FIGURE 35. Detection of nickel in the presence of vanadium using nickel binary cross-correlation masks. Thresholds (a) 20%, (b) 40%, (c) 60% and (d) 80%.

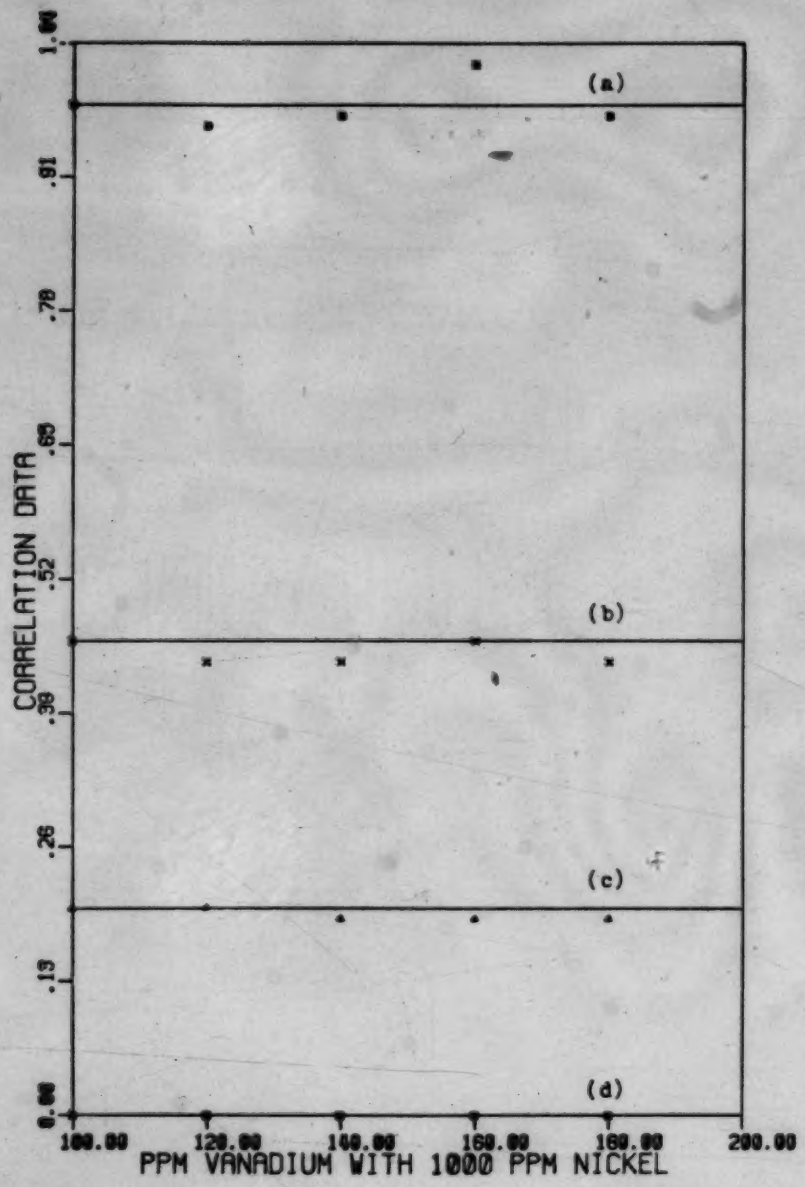


FIGURE 36. Detection of nickel in the presence of vanadium using vanadium stripped nickel binary cross-correlation masks. Thresholds (a) 20%, (b) 40%, (c) 60% and (d) 80%.

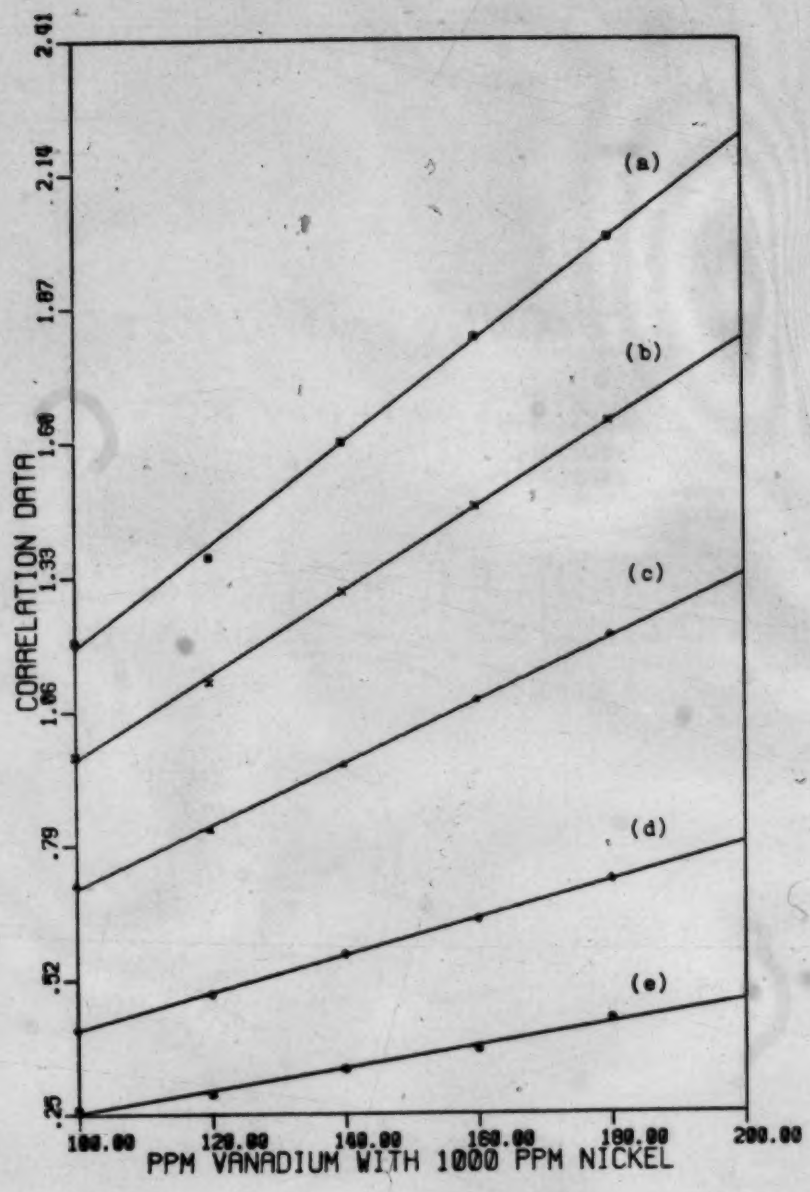


FIGURE 37. Vanadium analytical curves determined using nickel stripped vanadium spectral intensity cross-correlation masks. Thresholds (a) 0%, (b) 20%, (c) 40%, (d) 60% and (e) 80%.

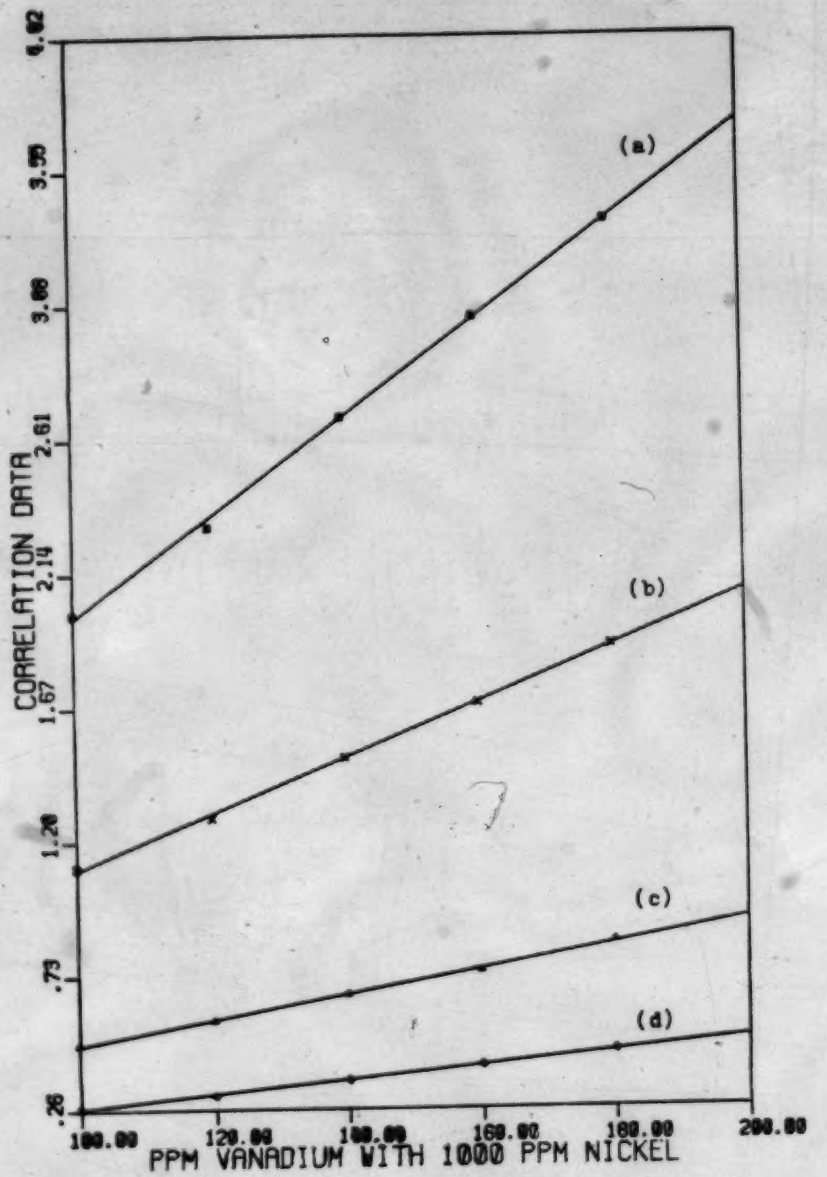


FIGURE 38. Vanadium analytical curves determined using nickel stripped vanadium binary cross-correlation masks. Thresholds (a) 20%, (b) 40%, (c) 60% and (d) 80%.

of spectral line wavelengths by computer software was attempted. This was accomplished by calibrating the spectral window covered by the photodiode array with some standards that emit known spectral lines within the particular spectral window. Appropriate correlation masks were then generated for data processing. This has not been very successful because of difficulties in exactly calibrating the photodiodes to corresponding wavelengths. This is due to the fact that the dispersion of the monochromator varies slightly with wavelength. If this would have been successful, it would partially solve the problem of limited spectral coverage by the array detector. The monochromator can be slew scanned and calibrated before cross-correlation masks for specific analytical problem will be generated for data processing.

Based on the results obtained in this study, experimentally generated cross-correlation masks can be very powerful. However, more spectral coverage by the image detector is necessary in order to fully extend the advantage of correlation analysis. Image sensor based spectrometers utilizing area arrays and Echelle spectrometers are now being developed that could eliminate this limitation.

The fact that the knowledge of wavelength axis is not necessary may help spectroscopists to further extend the analytical capability of this system. Spectral information can be packed into the detector without regard to the wavelength axis to fully utilize the size limited array detector (62). The task of extracting the specific spectral pattern for each element can then be handled by cross-correlation techniques even with severe spectral overlaps. Without cross-correlation analysis, human interpretation would be fairly difficult since all the spectral information does not necessary follow the wavelength axis.

Correlation analysis does not limit itself to be used as an effective data reduction tool for the photodiode array spectrometer system, it can also be implemented in a similar concept for other spectrometers based on different image detectors. In the next two chapters, cross-correlation techniques are utilized to process spectral data arrays in the form of interferograms generated by Fourier transform spectrometers. With this kind of spectrometer, wide spectral coverage and precise wavelength calibration can be obtained in contrast to the dispersive-based detector system such as the photodiode array. Thus, the potential of correlation techniques can be further extended.

# CHAPTER IV

## Correlation Based Data Processing for the ICP-Fourier Transform Spectrometer System

### A. Introduction

Simultaneous wavelength detection capability is one of the chief advantages offered by a Fourier transform spectrometer when coupled to an ICP. A vast amount of analytical information is available within a relatively short period of time. Thus, effective data processing is of prime importance when the system is utilized in multielement atomic emission spectroscopy. This statement is also true in other fields of spectrochemical measurement utilizing an FT spectrometer as the detection system, such as in the area of infrared spectroscopy where the FT spectrometer finds most of its application.

The time domain signal (i.e. the interferogram) obtained from the spectrometer is normally processed through the fast Fourier transform (FFT) mathematical algorithm described earlier in Chapter II. This step is necessary before human interpretation of the spectral data is possible. The FFT, when utilized has imposed certain limitations on the efficiency of the data processing routine, in addition to the requirement of a certain computer memory size for the processing of the spectral data. In the case of a large number of data

points for high resolution work, a large computer memory is desirable.

Hardware development in computer technology, such as the array processor, has tremendously reduced FT computation time required by the computer. But, these devices are usually very expensive. In the case of long interferograms, techniques such as decimation in time (76-78) where interferograms are processed in segments rather than as a whole giant block of data can be employed. However, software development was found to be non-trivial (33). The laboratory computer can also be interfaced to a large central computer for efficient processing of large blocks of data points. In these cases, efficient data processing will be hindered by the time used to transfer data between devices. In view of the above comments, a simpler, alternate method to efficiently process the spectrochemical information obtained from the ICP-FT spectrometer system is sought. Capability of the data processing method to perform real time analysis is of prime consideration. The adaptation of the method to automatic interpretation of spectral data is also important. Correlation is the answer.

Correlation techniques have been applied to process interferograms (33,79,80). In this study, the feasibility

of the cross-correlation function at the $\tau = 0$ point as the data processor for multielement atomic emission interferograms will be investigated. The advantage of the precise wavenumber axis provided by the FT spectrometer will be utilized. This enables cross-correlation masks to be generated by the software of a small laboratory computer for extraction of analytical information directly from the time domain signal without going through the FFT process. As mentioned above, the possibility of real time data processing and automatic interpretation of spectral data will be assessed.

In order to fully appreciate this study, a general discussion on the use of the FT spectrometer as a detection system for the ICP is included in this chapter. Particular attention is paid to the dynamic range problem imposed by the use of the FT spectrometer.

## B. The Experimental System

A block diagram of the experimental setup is illustrated in Figure 39. The inductively coupled plasma, Michelson interferometer and all the related optics were mounted on an optical rail bed similar to the one designed by Walters (59,81). The rail bed was in turn placed on a vibration isolation table which was air-floated

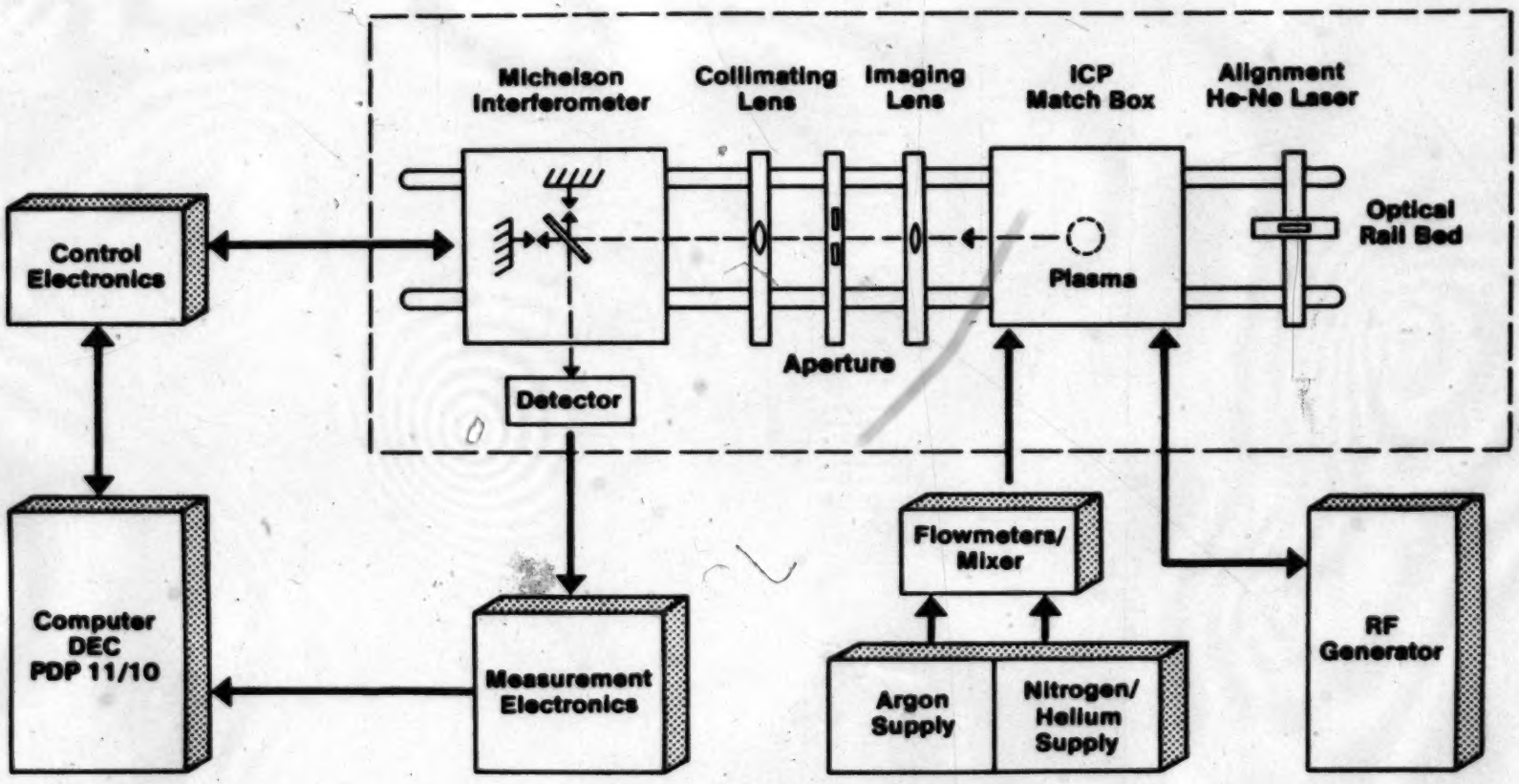


FIGURE 39. Block diagram of the ICP-Fourier transform spectrometer system.

whenever experimental data were being taken. This system provides precise alignment with the aid of a He-Ne laser and the excellent stability that is required for the operation of the interferometer. This setup is advantageous because alignment between the plasma and the interferometer, together with the internal optical alignment within the interferometer is very critical especially when it is being used in the ultraviolet region because of the short wavelengths that are involved.

The Michelson interferometer with its control electronics used in this study has been well documented in the literature (28,32,33). For the latest modifications of the interferometer system, refer to Appendix II. A schematic diagram of the interferometer design and a block diagram of how the interferometer operates are included for completeness in Figure 40 and 41. The inductively coupled plasma is commercially available and is capable of a maximum power output of three kilowatts. The operating conditions for the ICP are similar to those described in Chapter III. In some cases, gases other than argon such as nitrogen or helium have been introduced into the coolant stream of the plasma. In these cases, analytical data were obtained under a mixed gas plasma condition. Mixed gas plasmas were initiated using the

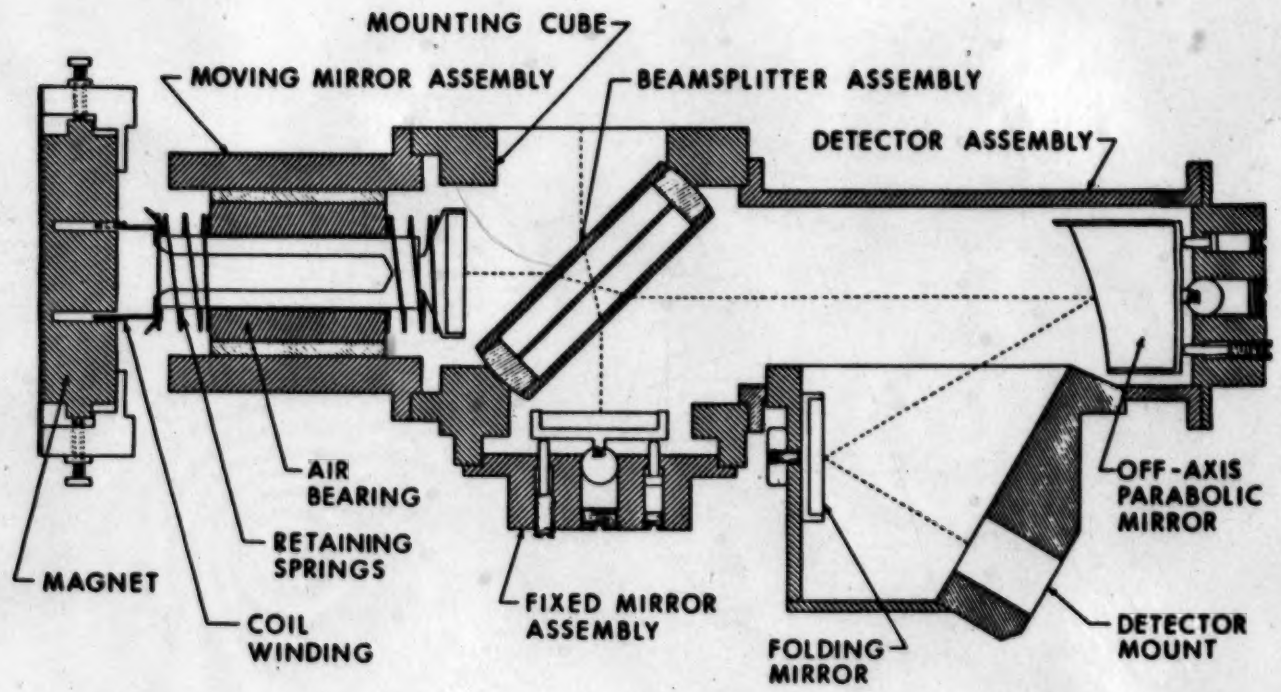


FIGURE 40. Schematic diagram of the Michelson interferometer.

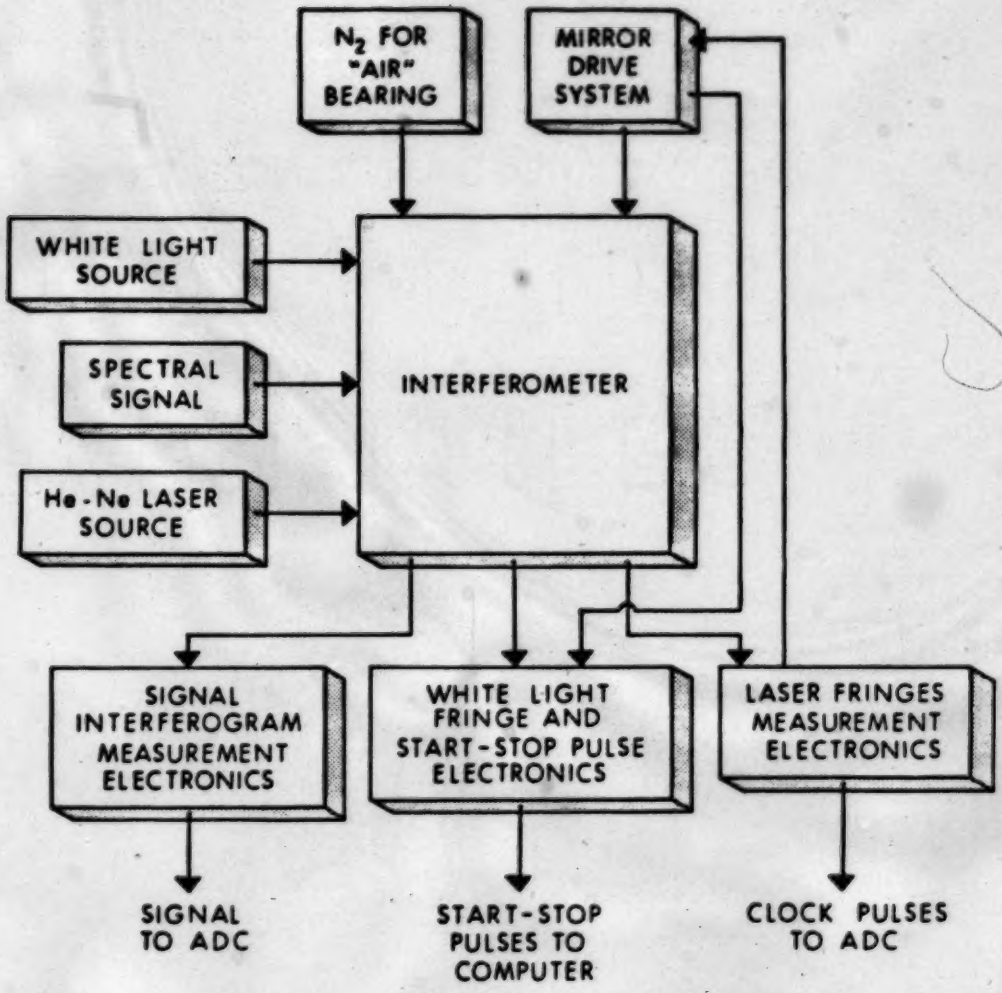


FIGURE 41. Block diagram of the Michelson interferometer setup.

conventional argon and were then slowly crossed over to the mixed gas condition with the aid of a flowmeter. Further discussion on the use of the mixed gas plasma will appear later in this chapter.

A small region of the plasma was spatially selected by a 10 cm focal length quartz imaging lens and a 5 mm circular aperture. The radiation passed by the aperture was collimated by another quartz lens of 12 mm focal length before it reached the interferometer. This optical link between the ICP and the interferometer is not the only alternative. Currently, an all mirror based optical interface is being considered.

Different detectors can be used in conjunction with the interferometer, depending on the spectral region of interest. A summary of the different detectors that have been used to cover the near IR-visible-UV spectral region is included in Table 2. Due to the fact that the present beamsplitter in the interferometer does not operate below 250 nm, the solar blind PMT detector is sometimes replaced by a combination of the visible PMT and a solar blind optical filter (Oriel 5786) which has a spectral response from 250 nm to 360 nm. This enables a gain in sensitivity of several orders of magnitude. However, with UV studies below 250 nm, the combination

TABLE 2. Detectors used in the ICP-Fourier transform spectrometer system.

| Detector | Spectral Response | Peak Response (nm) |
|---|---|---|
| Solar Blind PMT (Hamamatsu R166) | 160 - 320 | 220 |
| UV-VIS PMT (RCA 1P28) | 200 - 650 | 300 |
| Silicon Diode (Electro-nuclear Lab., Inc. 626) | 400 - 1100 | 850 |

is not feasible.

The analog signal was fed into a current amplifier, electronic filter and a low noise amplifier before the analog to digital conversion was performed by the Laboratory Peripheral System that was interfaced to a PDP 11/10 minicomputer. All the interferograms were averaged over twenty five scans and output through an incremental plotter. Signals in the spectral domain obtained by the FFT of the interferograms were obtained using the software developed by Hall (33). Detailed descriptions of the individual programs can be found in reference 33. Sources of the equipment that have been used in this system are summarized in Table 3.

Two spectral systems were used for this correlation study. In one system the multielement signal obtained from a solution of nickel (1000 ppm), vanadium (100 ppm), cobalt (2500 ppm) and iron (1000 ppm) was studied. This signal was measured using the 1P28 PMT combined with the solar blind filter and a conventional argon ICP. The second system studied was the multielement spectrum of the alkali elements (1 ppm sodium, 2 ppm potassium, 0.1 ppm lithium, 10 ppm rubidium and 5 ppm cesium). This signal was measured using a silicon diode detector and a mixed gas nitrogen / argon ICP.

TABLE 3. Various components of the ICP-Fourier transform spectrometer system.

| Item | Source |
|---|---|
| Vibrational Isolation System 22-4485 | Ealing Corporation |
| Inductively Coupled Plasma | |
| ICP 2500 Matching Box | Plasma Therm, Inc. |
| ICP RF Generator HFP 2500D | Plasma Therm, Inc. |
| Flowmeters 605 | Matheson |
| Michelson Interferometer | Chemistry, U. of Alberta |
| Signal Measurement Electronics | |
| Current Amplifier 427 | Keithley Instruments |
| Variable Electronic Filter 3343 | Krohn Hite |
| Low Noise Amplifier PAR 225 | Princeton Applied Reseach |
| Computer | |
| PDP 11/10 16-bit Minicomputer | Digital Equipment Corporation (DEC) |
| (RT-11 Operating System, 32K Core Memory) | |
| Cartridge Disk Drive RK-05J | DEC |
| Graphics VT-11 | DEC |
| Decwriter II | DEC |
| Laboratory Peripheral System LPS 11 | DEC |
| Zeta 100/1200 Series Incremental Plotter | Zeta Research Corporation |

C. Use of a Fourier Transform Spectrometer as a Simultaneous Detection System for the ICP

(a) General Considerations

When an FT spectrometer which is essentially a Michelson interferometer is utilized as a measurement system for atomic emission spectroscopy, it offers various advantages over the conventional detection systems. Most of all, its wide and continuous spectral coverage is unmatched by any other spectrometer. In addition to this, high resolution can be achieved in a compact system, the resolution function can be controlled by the use of apodization techniques (32) and accurate and precise wavelength calibration is inherent in the nature of the instrumentation. All these, with the computerization of the system, provide a simplicity and flexibility that cannot be matched by other systems.

Like most systems, the FT spectrometer is not without problems. One of the problems being aliasing, which refers to the phenomenon of undersampling of the signal. This problem exists especially when the spectrometer is being utilized in the ultraviolet-visible near IR region. It can certainly impose spurious information when dealing with broadband information. However, with atomic emission spectrochemical measurements,

line spectra are normally obtained. Yuen and Horlick (32,82) showed that alaising can be used advantageously if it is carefully considered and manipulated. Another problem deals with the degradation of the signal-to-noise ratio when the spectrometer is used in the UV-visible region. However, signal-to-noise ratio is often not the overwhelming consideration when carrying out a spectrochemical measurement.

The necessity of carrying out the FFT data processing could be considered a drawback of the system because of the requirement of computer and software overhead. With the remarkable progress in computer technology, this problem will certainly be phased out. Above all, a simpler, alternate data processing approach based on correlation techniques can be utilized. This correlation technique can be implemented in real time even in the case of long interferograms. Furthermore, it can be utilized in such a way that automatic computer interpretation of spectral data is possible. Full details on this technique will be described in this and the following chapter.

By far, the most severe drawback that limits the practical use of the ICP-FT spectrometer system for real sample analysis is the presence of a dynamic range

problem. This limitation is due to the multiplex property of the spectrometer. Every single data point contains information covering the whole spectral response of the system and the signal must stay within the scale of the data acquisition system in order to obtain proper analytical information concerning the sample. The dynamic range problem is realized if the sample gives a very intense emission at a particular wavelength. This intense emission will thus limit the amplification of the signal and emission at some other weak spectral lines will thus be very difficult to detect. In a sense, the detection of weak signals is limited by the bit resolution of the analog-to-digital converter being used. This is why it is called the dynamic range limitation. This problem can be partially overcome to a certain extent by the use of optical or electronic filters. However, when the FT spectrometer is coupled to the ICP, a serious problem arises because of the presence of very intense plasma background (line and continum) extending from the UV to near IR region. Detection capability of the system may be severly limited by this background. Use of optical or electronic filters to resolve the problem is out of question in certain spectral region because of the enormous background

and the close proximity of the spectral lines. Another important consideration is the "visibility" of the noise present in the ICP by the FT spectrometer. This is very important with respect to the use of the spectrometer as a simultaneous multielement detection system for the ICP. A little bit of insight into this is essential as the way the noise shows up in the signal may again impose the dynamic range limitation. We shall discuss these problems in the following sections.

(b) Noise Studies of the ICP by a Fourier Transform Spectrometer

Spectral information available from the ICP is encoded as a time domain signal by the FT spectrometer. Input radiation is modulated at different frequencies according to their wavelengths. In order to obtain a spectrum, the time domain signal must be transformed through the FT algorithm. In this way, it is analgous to noise power spectra (83-88). Thus, one can predict the superimposition of the desirable signal with the noise.

Winefordner et al. (88) have demonstrated that the plasma consists of 1/f, 60 Hz and a proportional noise centered around 200-500 Hz under the normal operating condition of the plasma. The exact frequency of the proportional noise depends on the plasma conditions. For

example, if the power of the plasma increases, the frequency of the proportional noise also increases. Work in our laboratory has shown similar noise behaviour of the ICP (87) and the proportional noise is suspected to be due to the asymmetrical rotation of the plasma. Because of the periodic nature of these noise sources, careful electronic filtering must be applied to the signal obtained from the spectrometer, or a dynamic range limitation due to the presence of the noise spikes will occur. The low frequency noises, (1/f and 60 Hz) are not of major concern when applying the FT spectrometer to the ICP as they can be effectively filtered out electronically. The proportional noise spike does create a problem if one is not aware of its high amplitude. An example is shown in Figure 42. This is a spectrum obtained using the silicon diode detector. The proportional noise spike as indicated by the arrow can be seen near 17400 $cm^{-1}$ corresponding to about 400 Hz. Its presence in the signal will certainly impose the dynamic range problem for any analytical application[2]. The other spectral lines shown in Figure 42 are due to the plasma background (mostly argon and oxygen lines from 400-800 nm) and will be discussed later in this section. Because of the fact that the frequency of this noise spike is fairly

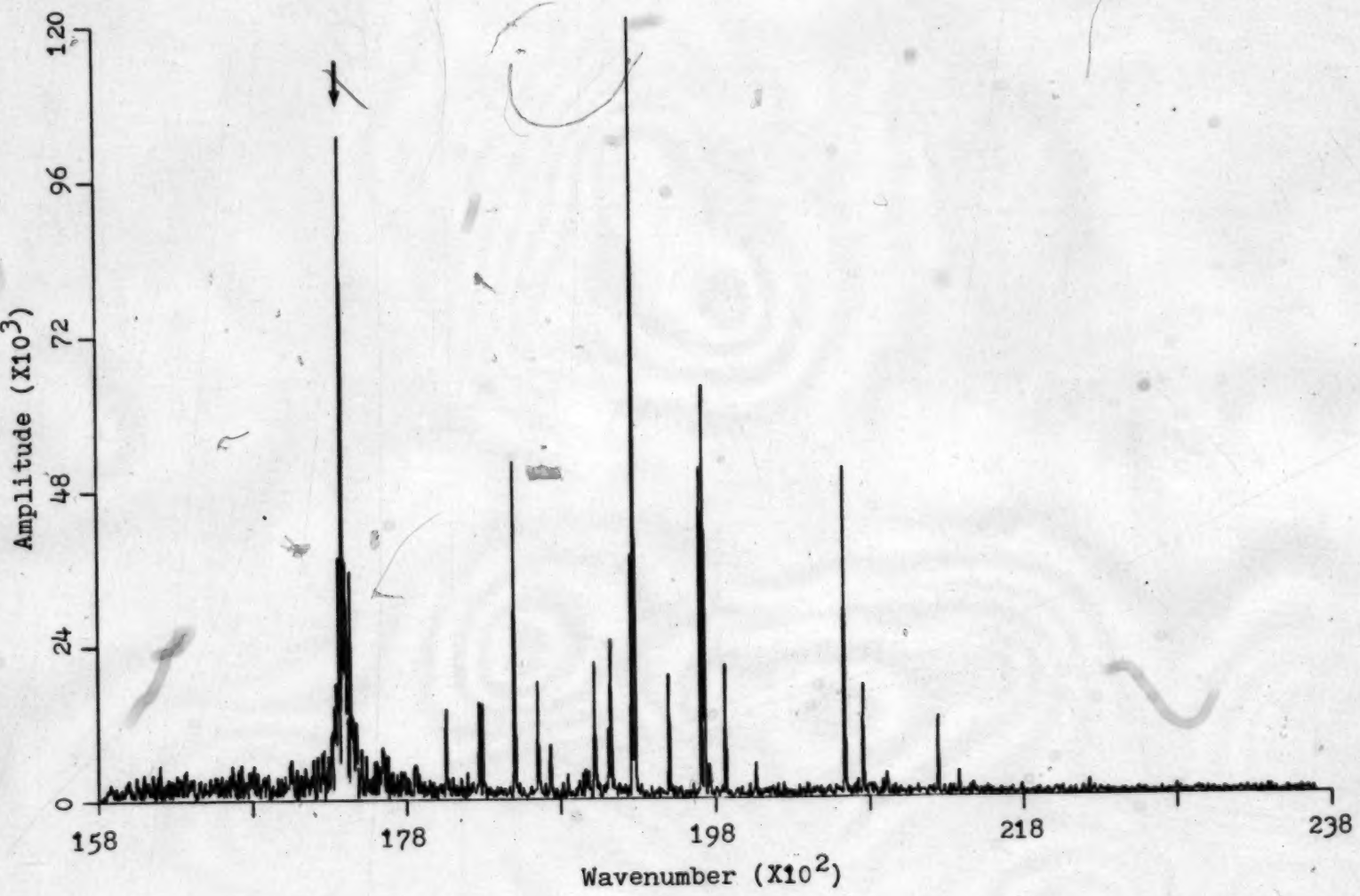


FIGURE 42. Spectrum illustrating the presence of proportional noise originated from the ICP.

close to the frequency of the signal (1KHz-30KHz), a better than average electronic filter must be employed to prevent the noise interference on the signal. A variable electronic filter (Krohn-Hite, Model 3343) capable of 48 dB/octave rolloff per channel is employed. This will completely eliminate the proportional noise from interfering with the signal. Other means of eliminating the proportional noise are available. These include the use of a variable notch filter or a long, extended ICP torch (87) in place of the conventional design. As mentioned before, the proportional noise does change in frequency as one changes the operating condition of the plasma. Thus, the notch filter does require frequent resetting if it is being employed in the system. A long ICP torch simply means an extension of the outer quartz tube to about 5 cm above the load coil and emission of the plasma passes through the quartz before it reaches the spectrometer. Loss of spectral signal, especially in the UV region is anticipated. Based on these facts, the Krohn-Hite electronic filter has been incorporated into the measurement electronics for the signal coming out from the FT spectrometer.

As a summary, while utilizing the FT spectrometer as a detection system for the ICP, one has to be aware

of the noise present in the system as it will show up superimposed with the signal spectrum. The presence of noise spikes in the spectrum may impose the dynamic range limitation on the determination of trace elements. The solution to this problem is the use of a good electronic filter. Let us turn to the problem of dynamic range due to the intense plasma background and the use of a mixed gas ICP as a partial solution to this limitation.

(c) Analytical Improvement of the ICP-FT Spectrometer System Using a Mixed Gas ICP

The use of gases other than argon to sustain the plasma discharge can be traced back to the early stage of the ICP (89-91). Gases such as helium, nitrogen, air and oxygen have been investigated in order to improve the analytical performance and to reduce the operation cost of the system. Recent work (92-97) has emphasized the use of low power mixed gas ICP's with particular interest in the nitrogen / argon cooled plasma. Work in our laboratory has shown that the nitrogen / argon cooled plasma is comparable to or better than the conventional pure argon plasma in terms of detection limit, stability, sensitivity and freedom from interference effects (97). Preliminary work using the mixed gas ICP with the FT spectrometer has demonstrated a tremendous

decrease in background which eases the dynamic range problem due to intense plasma background. In addition to this, the nitrogen / argon cooled plasma provides a more stable source when compared to the conventional ICP. In the following sections, the use of a mixed gas ICP to improve the performance of the ICP-FT spectrometer system will be briefly introduced.

(i) Near Infrared Region

As mentioned before, the detector used in this region is the silicon diode detector with a spectral response ranging from 500 to 1000 nm. Within this region, emission lines from the alkali metals are dominant. With the use of the conventional argon ICP, plasma background emission (Ar, O, H lines) is very intense. This renders the region useless for any analytical work. The problem is best illustrated in Figure 43. This spectrum was obtained with 500 ppm sodium aspirating into the conventional argon plasma. As it can be seen, the amplitude of the sodium emission lines (589.0 nm and 589.6 nm) is not large. In other words, the dynamic range problem is realized. Amplification of the signal is limited by the plasma background and the proportional noise indicated by the straight arrow in Figure 43. This spectrum was obtained without the Krohn-Hite electronic filter and

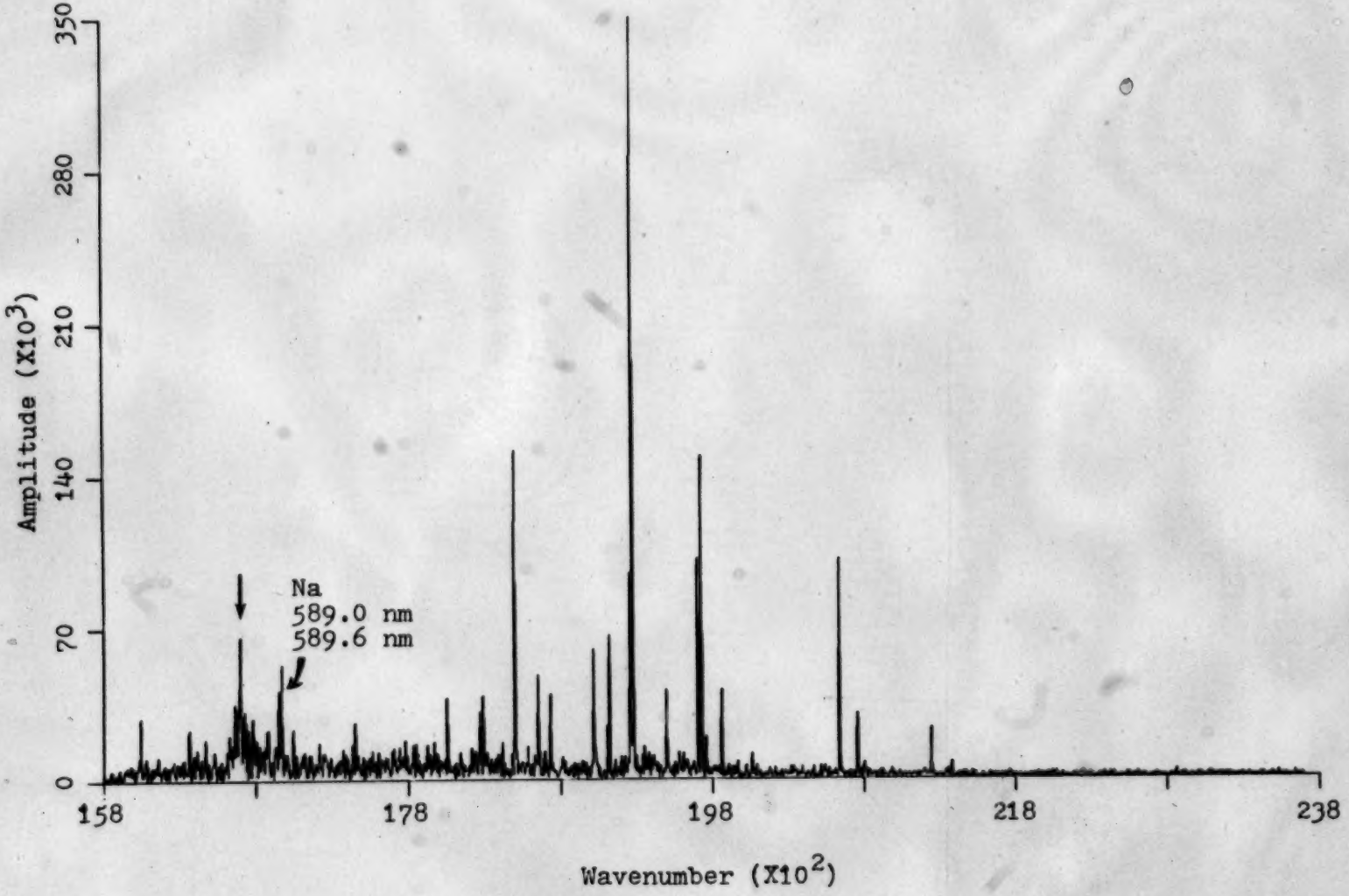


FIGURE 43. Sodium (500 ppm) spectrum obtained using a conventional argon ICP.

this is the reason why the proportional noise spike shows up in the spectrum. In this situation, determination of sub ppm level of the alkali metals is thus impossible. Introduction of nitrogen gas into the coolant stream of the plasma reduces the plasma background significantly. This is illustrated in Figure 44. This spectrum was obtained under the same conditions with 500 ppm Na aspirating. The only difference is the use of 50% nitrogen in the coolant stream of the plasma. In this case, the amplification of the sodium signal is no longer governed by the background. Analytical determination can then be performed in the sub ppm level. The multi-element alkali metal spectrum used later in this chapter was obtained with the aid of the nitrogen / argon plasma. One interesting factor that can be observed in Figure 44 is the disappearance of the proportional noise as we cross over from the argon plasma to the argon / nitrogen plasma. This further supports the fact that the argon plasma is rotating. The fact that the noise spike disappeared is likely due to the reduction in size of the argon / nitrogen plasma. The reduction in size prevents the assymmetrical rotation of the plasma and thus appears more stable as shown by the spectrum. In order to illustrate that quantitative analysis can be performed

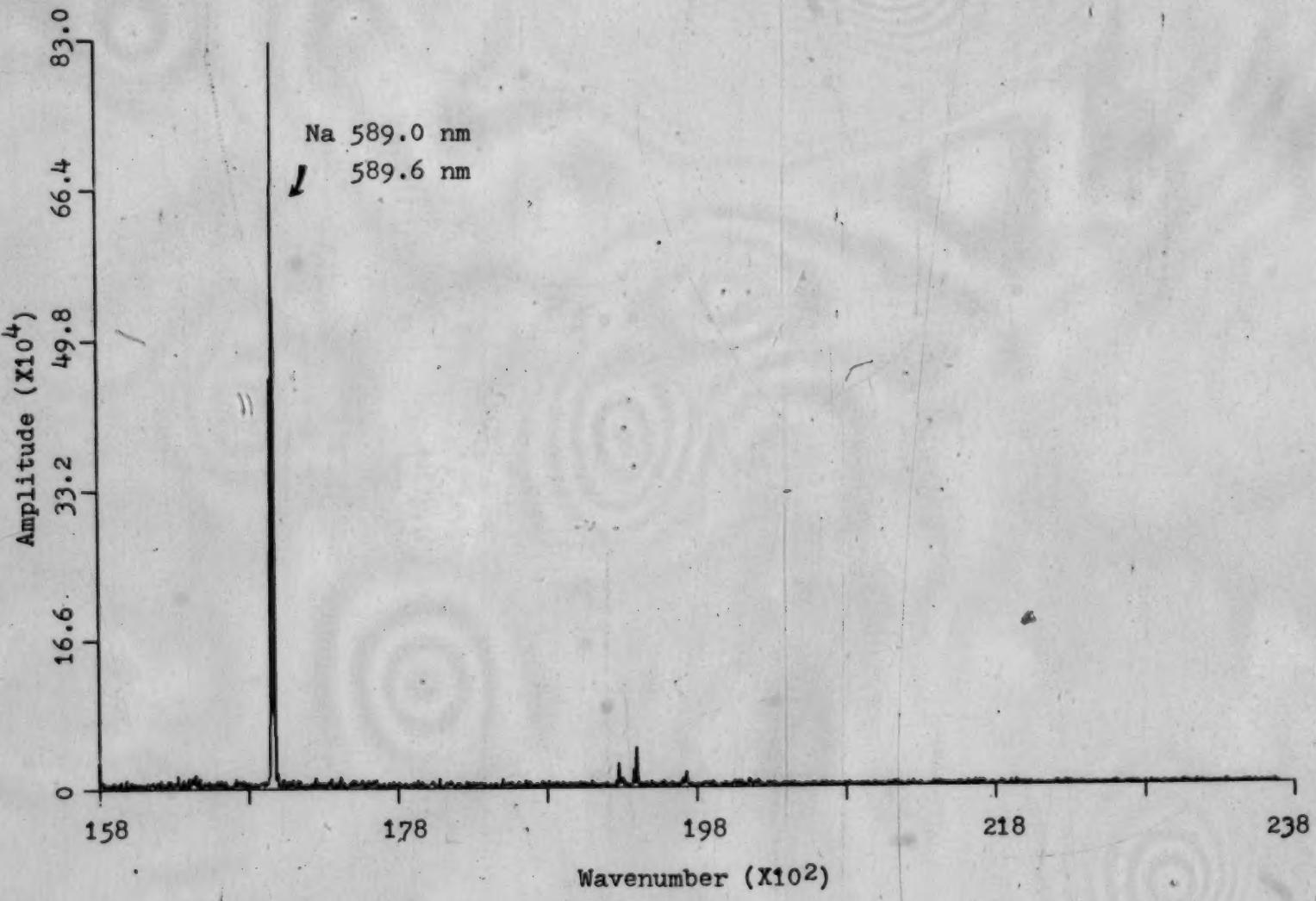


FIGURE 44. Sodium (500 ppm) spectrum obtained using a 50% argon / 50% nitrogen ICP.

with the argon / nitrogen plasma, a working curve of lithium covering over a concentration range of 0.1 ppm-10 ppm is shown in Figure 45.

(ii) Visible Region

The detector used in this spectral region is a photomultiplier tube with a spectral response extending from 200-650 nm. If this detector is used in conjunction with the conventional argon plasma, a typical spectrum obtained is shown in Figure 46. Intense argon emission lines combined with broadband emission due to nitrogen species are dominant in this region. Any good analytical work cannot be performed due to the dynamic range limitation. Introduction of 50% nitrogen / 50% argon as a coolant gas for the ICP has a remarkable effect in reducing the background to a minimum. This is shown in Figure 47 obtained using the same electronic amplification as for the spectrum shown in Figure 46. Note that there is some residual background and it is possible to further reduce this with the use of a 100% nitrogen cooled plasma. A working curve for calcium obtained using a 50% argon / 50% nitrogen ICP is shown in Figure 48. The concentration of calcium ranges from 0.1-50 ppm. This concentration range is virtually impossible to cover with the use of the conventional argon ICP when coupled to an FT spectro-

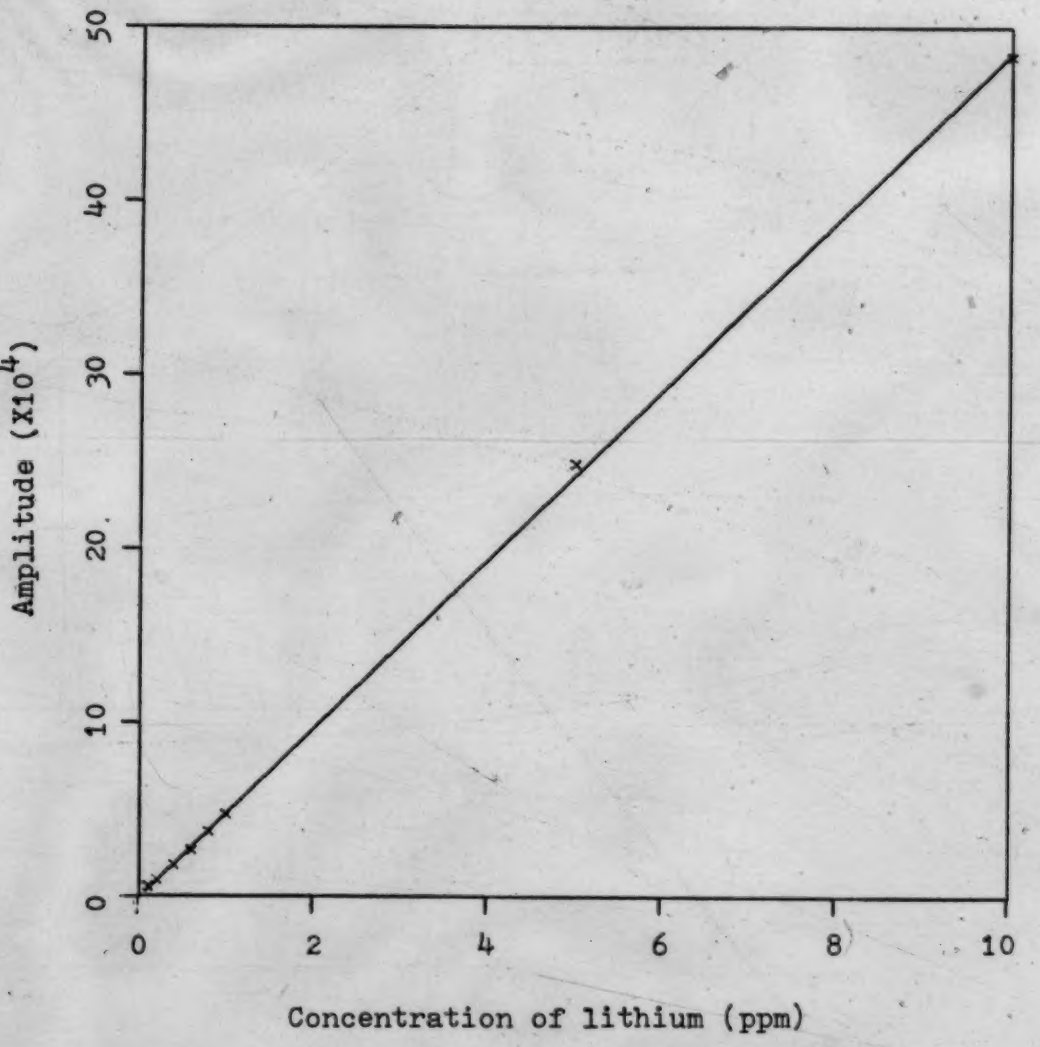


FIGURE 45. Analytical working curve for lithium obtained using an argon/nitrogen ICP.

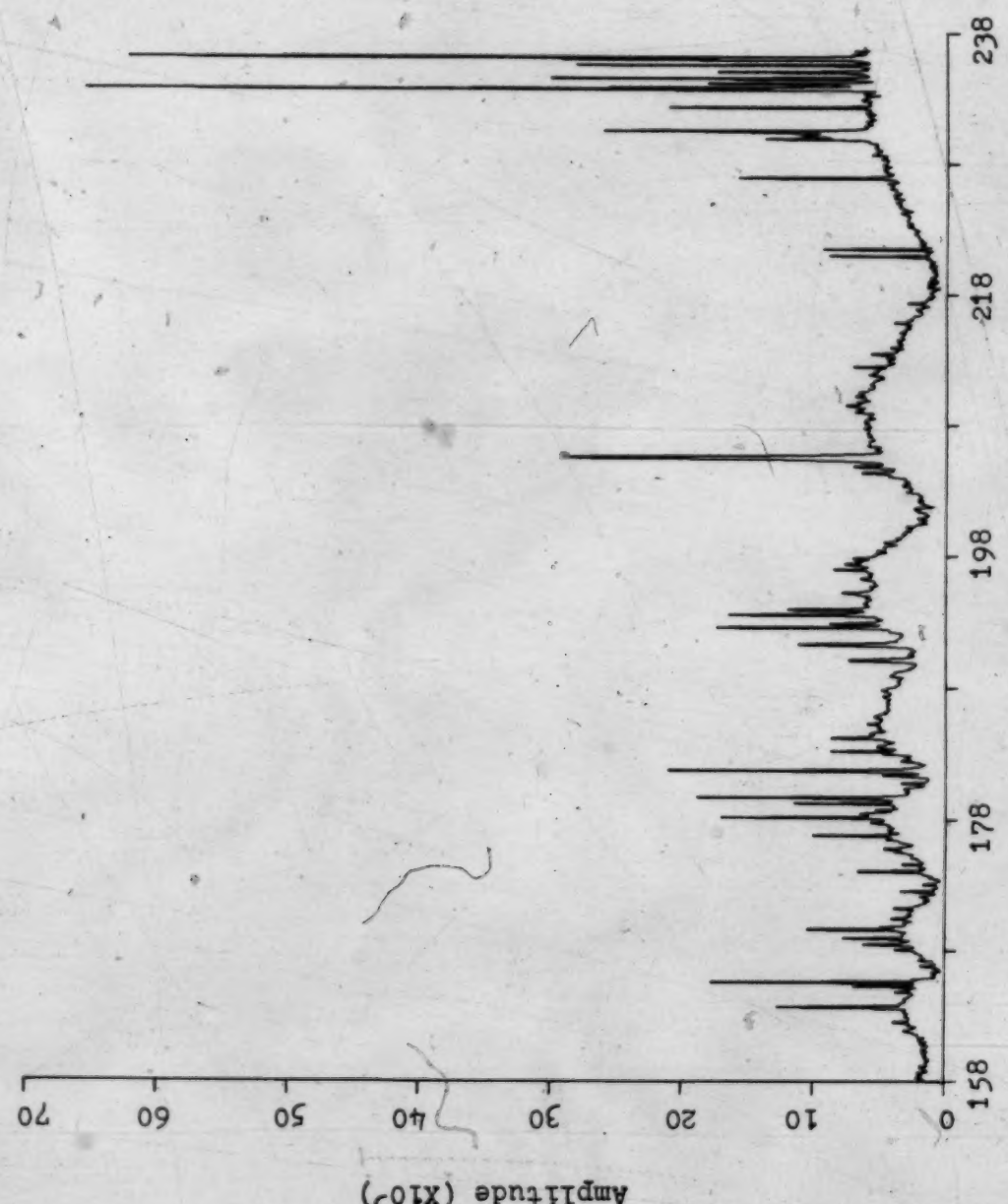


FIGURE 46. Background of the argon ICP in the visible region.

FIGURE 47. Background of the argon/nitrogen ICP in the visible region.

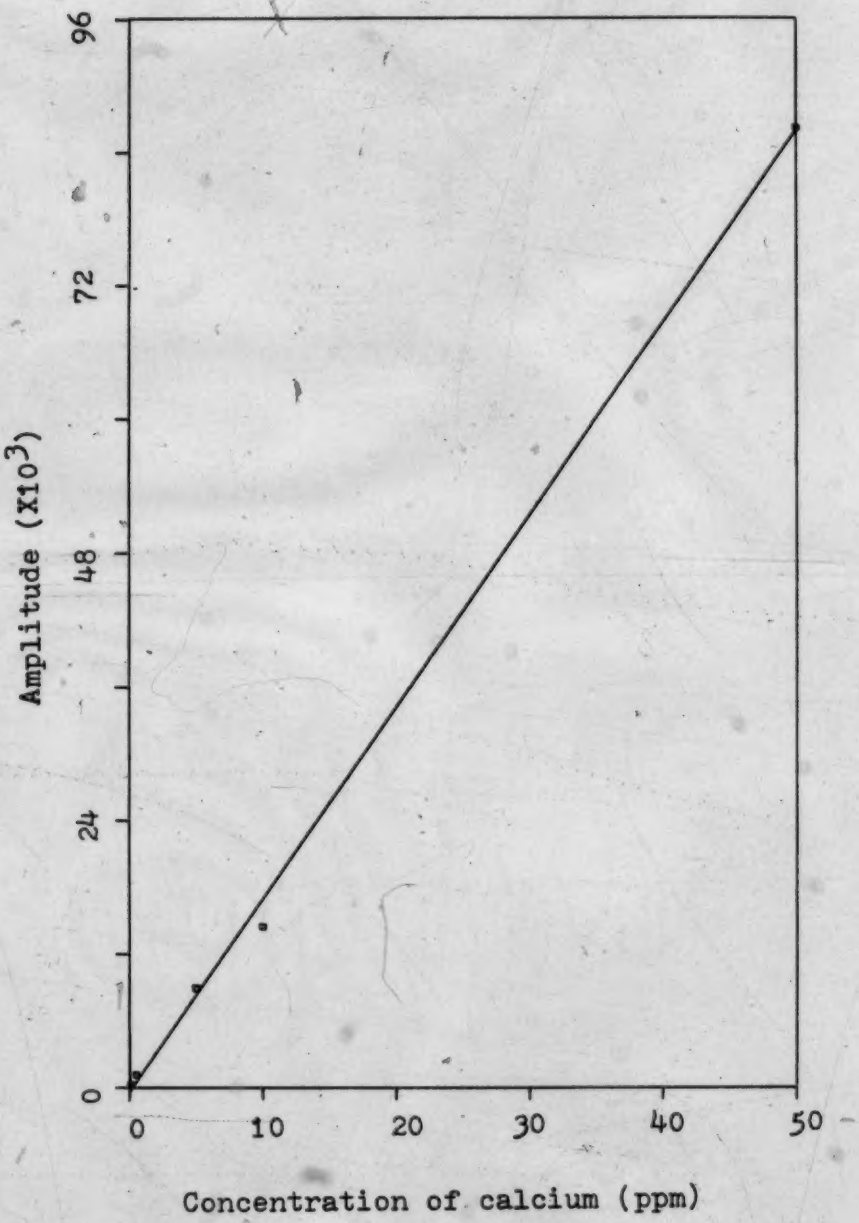


FIGURE 48. Analytical working curve of calcium obtained using a 50% argon/50% nitrogen ICP.

meter.

The use of nitrogen / argon mixture as the coolant gas for the plasma is not the only choice. An example of a spectrum obtained using a 50% helium / 50% argon ICP is shown in Figure 49. It consists of a 10 ppm calcium signal and a number of intense hydrogen emission lines. The presence of the hydrogen lines can be due to the hydrogen gas impurity in the helium gas supply or can be simply due to the hydrogen content of the water. In either case, it can be easily removed by filtration or desolvation techniques. In this way, a super clean plasma background can be obtained. The only major disadvantage of the use of a helium / argon ICP is the instability of the plasma. It is illustrated here simply to demonstrate that the argon / nitrogen ICP may not be the ultimate choice for the FT spectrometer system; further investigation is necessary. Besides, the optimum observation height, gas flow rates, power levels have still to be determined for the nitrogen / argon ICP. This investigation is best carried out using a photodiode array spectrometer and is currently underway in our laboratory. The work presented here by no means represents the optimum signals that can be obtained by the system. Further investigation must be carried out to fully extend

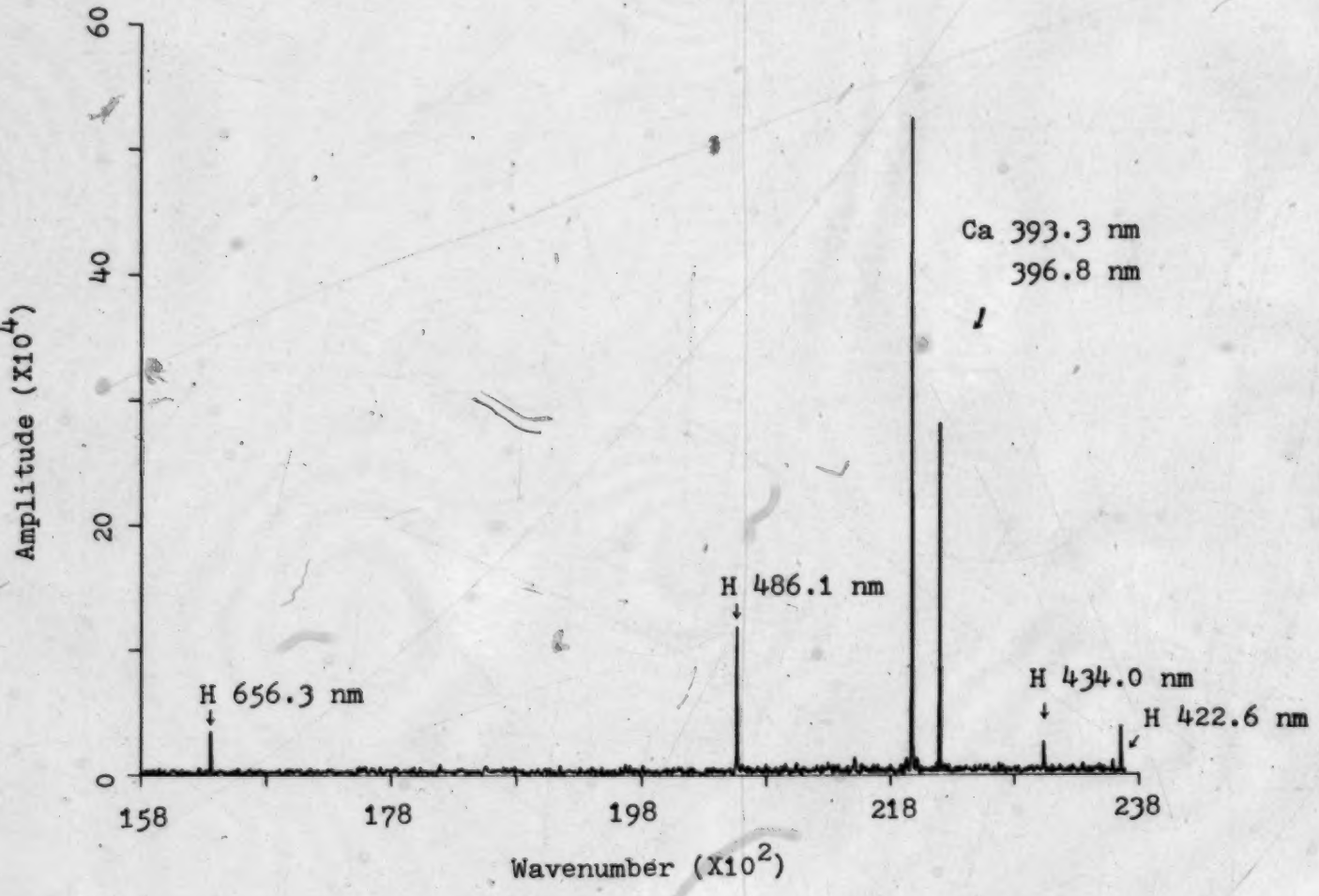


FIGURE 49. Calcium (10 ppm) spectrum obtained using a helium/argon ICP.

the capability of the ICP-FT spectrometer system.

(iii) Ultraviolet Region

Generally speaking, as pointed out by Hall (33), the conventional argon ICP provides an exceptionally clean spectral region for analysis with a solar blind PMT as a detector. The use of argon / nitrogen ICP will increase the molecular band emission due to nitrogen species. Thus, normally a conventional argon ICP is employed. A working curve of magnesium with concentration ranging from 0.1-50 ppm is shown in Figure 50 for illustration.

(d) Conclusion

The feasibility of the ICP-FT spectrometer system for good analytical work is hindered by the dynamic range problem present due to the multiplex property of the spectrometer. Through the use of a mixed gas ICP such as a 50% nitrogen / 50% argon plasma, the dynamic range limitation due to the strong background emission of the plasma has been reduced to a minimal level. Depending on the spectral region we are interested in, different plasma excitation sources can be utilized to reduce the background. This is summarized in Table 4. In addition, the argon / nitrogen ICP is a more stable source when compared to the conventional argon ICP.

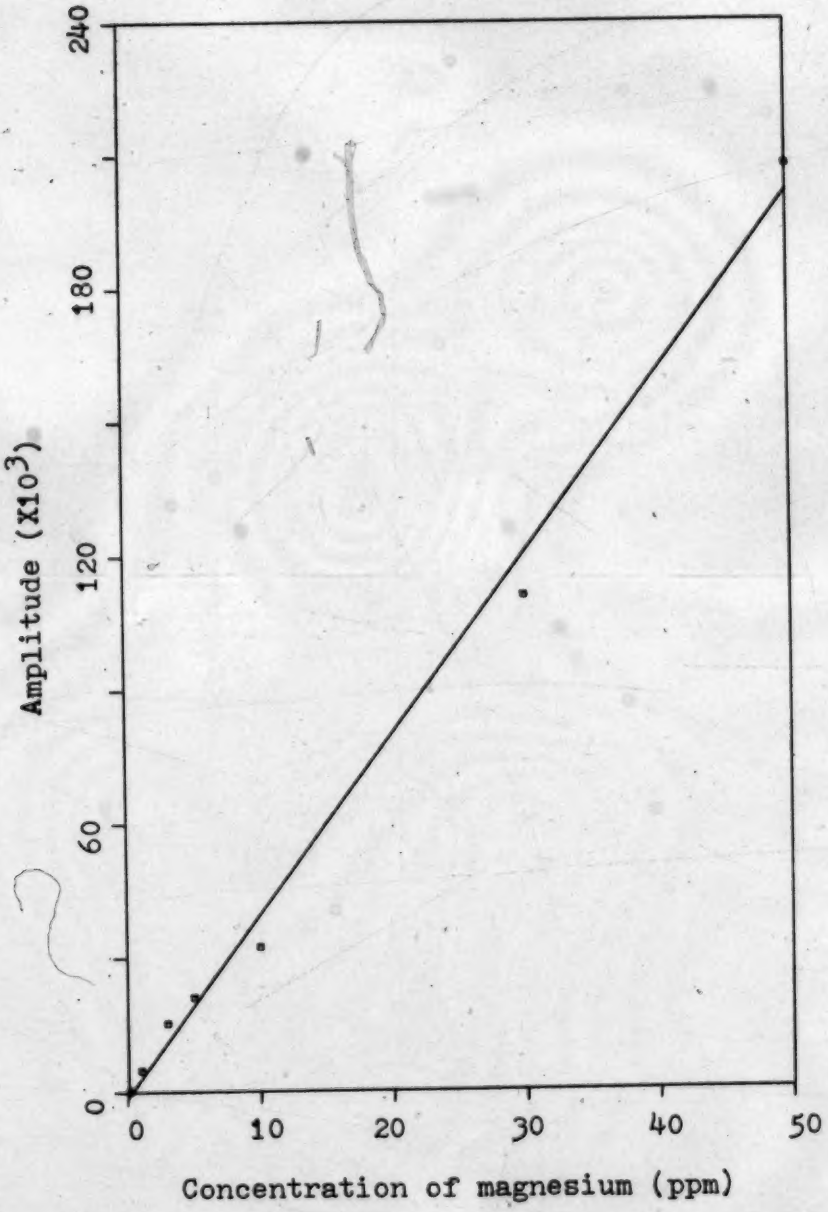


FIGURE 50. Analytical working curve of magnesium obtained using a conventional argon ICP.

TABLE 4. Recommended ICP source at different spectral regions.

| SPECTRAL REGION | ICP SOURCE | DETECTOR |
|---|---|---|
| Ultra-violet (160 nm - 320 nm) | Argon | Solar Blind PMT |
| Visible (320 nm - 600 nm) | Nitrogen / Argon or Helium / Argon | Visible PMT |
| Near Infrared (500 nm - 1000 nm) | Nitrogen / Argon | Silicon Diode |

However, other means of reducing the plasma background such as the use of a pure nitrogen plasma proposed by Barnes and Meyer (98) or the use of a microwave induced plasma which has a fairly clean spectral background (99) as compared to the conventional argon ICP cannot be overlooked. But, this will not improve the dynamic range problem imposed by the matrix of the sample. The use of optical filters combined with the availability of a good selection of spectral lines due to the wide spectral coverage of the spectrometer can in some way overcome the problem. For very complex matrices, optical isolation of the strong emission lines from weak emission lines must be performed. Techniques such as the selectively modulated interferometric dispersive spectrometer (100-102) or dual beam interferometer (103-105) can be employed. In the former case, the fixed mirror of the interferometer is replaced by a diffraction grating so that only a narrow band of spectral information is modulated and utilized by the spectrometer. In this case, the dynamic range problem will be completely eliminated. However, the multielement capability of the system is reduced or completely lost. However, the precise wavelength calibration inherited in the system can still be fully utilized. In other words, a precise slew scan type

spectrometer can be obtained.

In the case of a dual beam interferometer, the complementary outputs of the interferometer are used to cancel out the very intense emission signal present in the system. Thus, the weak emission spectral information can be detected. However, practical difficulties in exactly cancelling out the strong emission signals might arise.

In summary, the application of the ICP-FT spectrometer system to real sample analysis cannot be overlooked and the system will certainly extend to its full potential if the dynamic range limitation can be fully overcome.

D. Cross-correlation Masks for Processing Interferograms

The same concept of correlation techniques as applied to the spectral signals obtained using a photodiode array spectrometer can be utilized in a similar fashion for data obtained using a Fourier transform spectrometer. However, if correlation analysis is to be performed on signals in the spectral domain, at least two FFT's will be involved to convert the interferograms into spectra, one for the experimentally generated cross-correlation mask and one for the experimental signal. This is certainly not a very

efficient way of performing correlation analysis. There is no particular reason why cross-correlation techniques cannot be applied to time domain signals even though humans find these signals difficult to directly interpret. Hall (33) reported the use of experimentally generated interferograms as cross-correlation masks for extraction of analytical information from signal interferograms. In this case, selection of specific spectral features in the cross-correlation masks cannot be accomplished easily, in contrast to the correlation masks used in spectral domain, by means of threshold levels. Threshold levels can be implemented in a similar way only if the cross-correlation masks are Fourier transformed, threshold imposed and inverse Fourier transformed back to time domain signals. In addition, it is very difficult to obtain a very "clean" cross-correlation mask containing only the specific spectral features required experimentally. In most cases, background emission features are also included in the cross-correlation masks. Elimination of overlapping lines is also difficult. Further, phase differences between the cross-correlation masks and signals were corrected by performing a partial full cross-correlation function. Relative displacement (typically, ten data points along positive and negative $\tau$

displacements) between the signals and the correlation masks was performed in order to obtain the desirable correlation data. This increased the computation time for the cross-correlation operation. In this chapter, software generated cross-correlation masks will be utilized. This is possible only because of the precise wavenumber axis provided by the Fourier transform spectrometer.

Let us recall that the cross-correlation function at the $\tau = 0$ point can be expressed mathematically as the following:

$$C = \sum_n a_n b_n \qquad \text{(ix)}$$

where C is the cross-correlation data point at $\tau = 0$, b is the digitized signal which is an interferogram in this case and a is the cross-correlation mask. The correlation data point is obtained by the summation of the products of the point-to-point multiplication between the signal and the mask and it will contain the desirable analytical information as selected by the mask.

If monochromatic radiation is directed into a Michelson interferometer, a cosine waveform interferogram results. An example using a He-Ne laser as the source of radiation is depicted in Figure 51 with the dotted

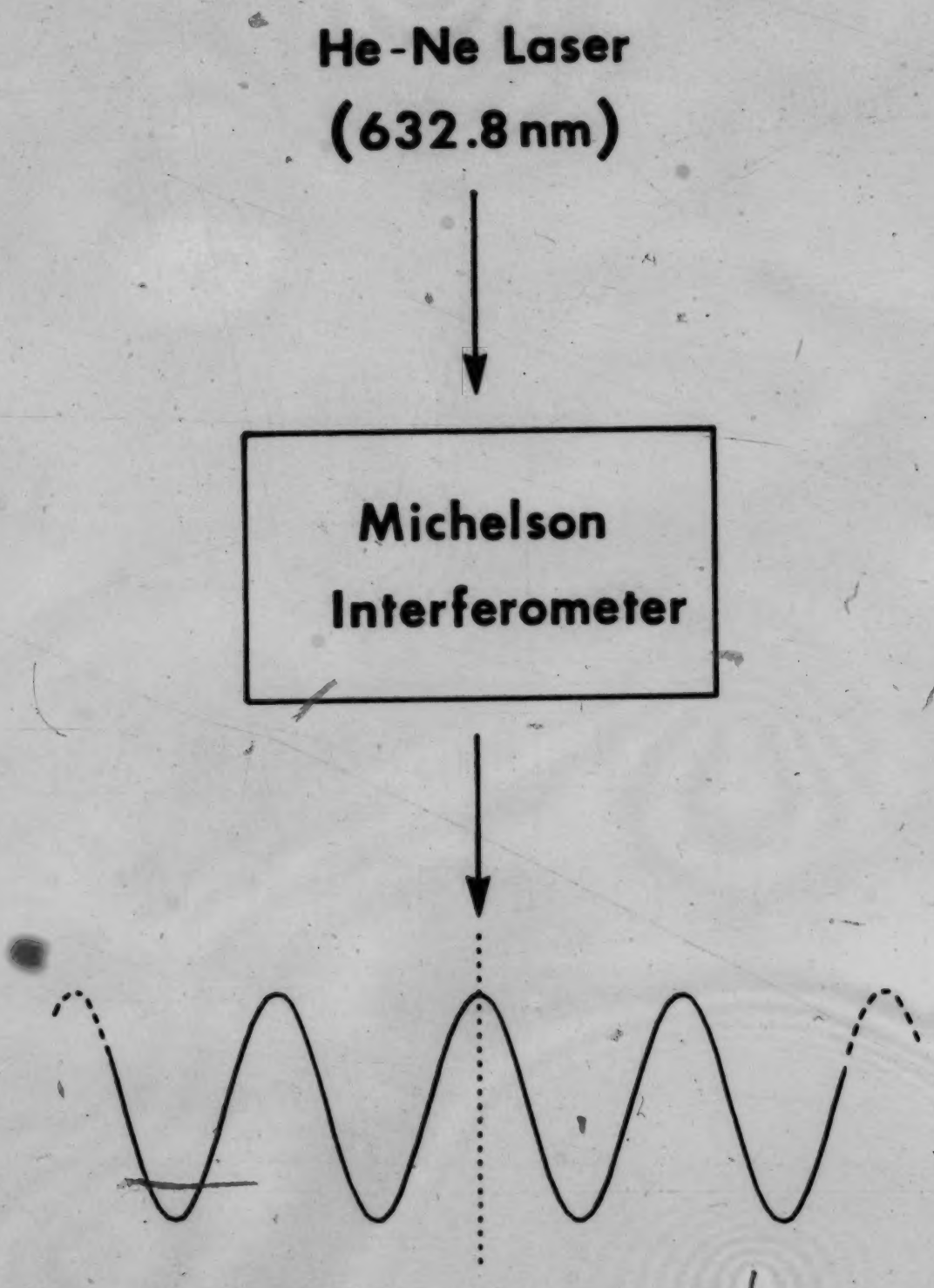


FIGURE 51. Interferogram resulting from a He-Ne laser.

line representing the zero path difference between the two mirrors in the interferometer. In an ideal case, that is no phase shift is present, the cosine wave originates at the zero path difference point. When the plasma system is coupled to the interferometer for simultaneous multielement analysis, the interferogram obtained is simply a waveform resulting from the summation of different cosine waves, each cosine wave corresponding to a particular spectral line. With a laser referenced interferometer, the exact waveform of the signals can be predicted, that is to say, for every spectral line, a precise cosine wave can be generated in the computer to be used as a cross-correlation mask. The idea of cross-correlation techniques as applied to interferograms is illustrated in Figure 52. The cross-correlation operation between an interferogram and a cross-correlation mask is simplified with the use of cosine waves (i.e. monochromatic signals). When correlation is performed between a signal and a mask that exactly match with each other, as shown in Figure 52(a), the product of every pair of data points will always turn out to be positive. A high correlation data point will result indicating the similarities between the signal and mask. As shown in Figure 52(b), if the same correlation mask is used for

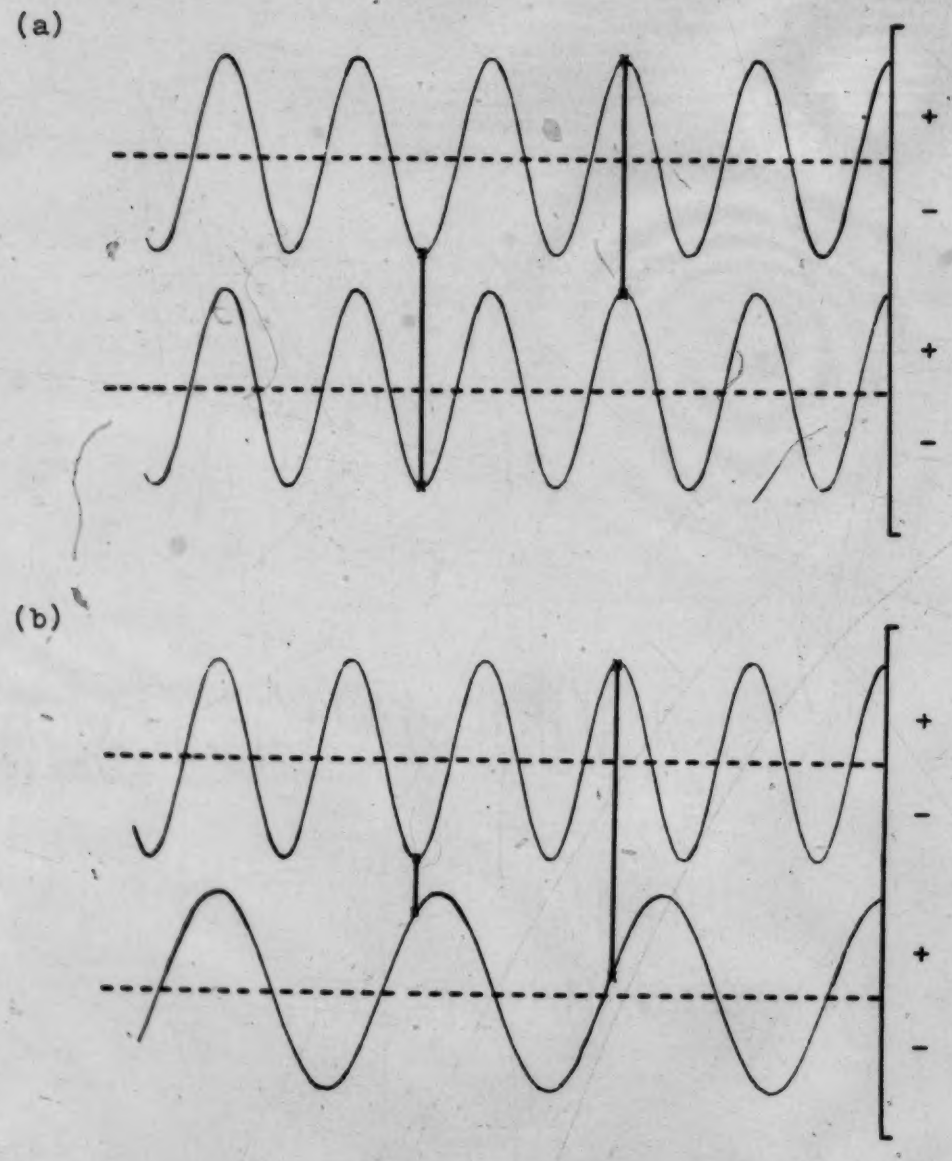


FIGURE 52. Cross-correlation between cosine waves of (a) same frequency and (b) different frequencies.

signals that do not correspond to the same frequency, the summation of the point-to-point products will average out to a very low correlation data point. Thus, cross-correlation analysis is analogous to the classical Fourier transform method, with only limited desirable spectral information being processed. Hall (33) has made an excellent comparison between correlation and Fourier transform processing methods and his work should be consulted for more details.

As can be seen from the figure, the phase relationship between the cross-correlation mask and the signal is very important in order to get the right information out of the signal. A phase correction routine is incorporated into the data processing step. It simply involves the generation of the appropriate cosine and sine waves as two different cross-correlation masks. Correlation analysis is then performed between these masks and the signal individually. Two correlation data points will be obtained, one for sine and one for cosine. The root mean square value of these two correlation data points will be the phase corrected correlation data point. The cosine and sine cross-correlation masks which are essentially synthetic interferograms are generated by the following expressions:

$$\cos(2\pi n\bar{\nu}\Delta s) \qquad \text{(x)}$$

$$\sin(2\pi n\bar{\nu}\Delta s) \qquad n=0,1,2,\ldots \qquad \text{(xi)}$$

where $\bar{\nu}$ is the wavenumber of the spectral line in interest, $\Delta s$ is the sampling interval and n is the point number of the interferograms. In our interferometer system, a He-Ne laser was employed to provide a sampling interval of 0.6328$\mu$.

A double sided interferogram is normally required for phase correction purposes when the interferogram is processed through the FFT route. This is not necessary in the case of cross-correlation techniques. Phase correction is accomplished by the use of cosine and sine waveforms. Thus, a single sided interferogram is sufficient. This immediately reduces the number of data points to be processed by correlation analysis in half as compared to the FFT route while maintaining the same degree of resolution. In this study, interferograms after the zero path difference point during the forward mirror movement will be utilized as opposed to the double sided interferograms.

In addition to the cosine and sine cross-correlation masks, the use of square wave synthetic interferograms as cross-correlation masks is also investigated. Square

synthetic interferograms are very much the same as the cosine and sine synthetic interferograms except they contain values of 1,0 and -1 only. They are obtained by converting all values of the cosine or sine synthetic interferograms that are greater than zero to 1's and -1 for values that are less than zero. That is to say, the amplitude information is discarded while retaining the frequency information of the cross-correlation masks. By doing this, the correlation process is simplified, as multiplication is replaced by addition or subtraction. This will certainly speed up the correlation process and in addition, less memory space is required to store these cross-correlation masks in a computer. In the following sections, the cross-correlation technique using both the analog (cosine and sine) and square synthetic interferograms as cross-correlation masks will be described.

E. Elemental Analysis Using Cross-correlation Techniques

Qualitative Aspects. A multielement interferogram containing sodium, potassium, rubidium, cesium and lithium information is shown in Figure 53. Obviously, the interferogram has no meaning at all as seen by human eyes. This interferogram was Fourier transformed

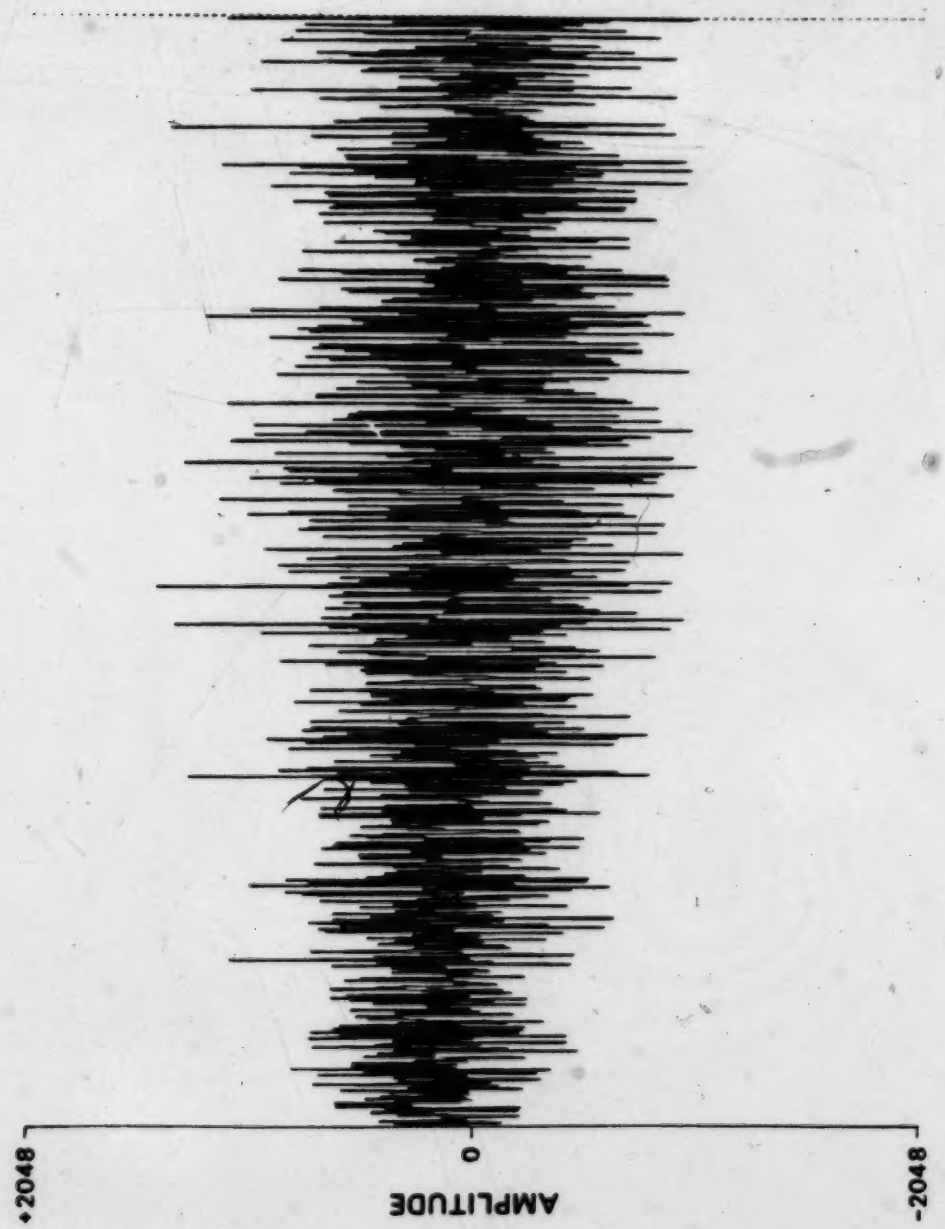


FIGURE 53. A multielement interferogram containing lithium, sodium, potassium, rubidium and cesium.

into its spectral domain as shown in Figure 54. In the spectral domain, it would then be possible to tell which elements are present. In this section, cross-correlation techniques for automatic elemental analysis of the signal in the Fourier domain will be illustrated.

As the multielement alkali metal interferogram was stored in the computer memory, synthetic interferograms or correlation masks, each corresponding to a particular wavelength of an element, were generated and correlated with the signal. The correlation masks of seventy elements were generated using the most sensitive ICP lines as reported by Boumans (106). These lines are included in Table 5. Each element has been assigned a code number arranged alphabetically for simplicity. There is no reason why the atomic number of the elements cannot be used. The present coding system was adopted simply because the ICP spectral lines of each element are listed alphabetically in Boumans paper. It must be kept in mind that the most sensitive ICP lines presented in Table 5 may not be true for the ICP-Fourier transform spectrometer system, especially when a mixed gas ICP is utilized. However, the table should be good enough for preliminary work. For future consideration, an atlas of ICP lines based on the interferometer system

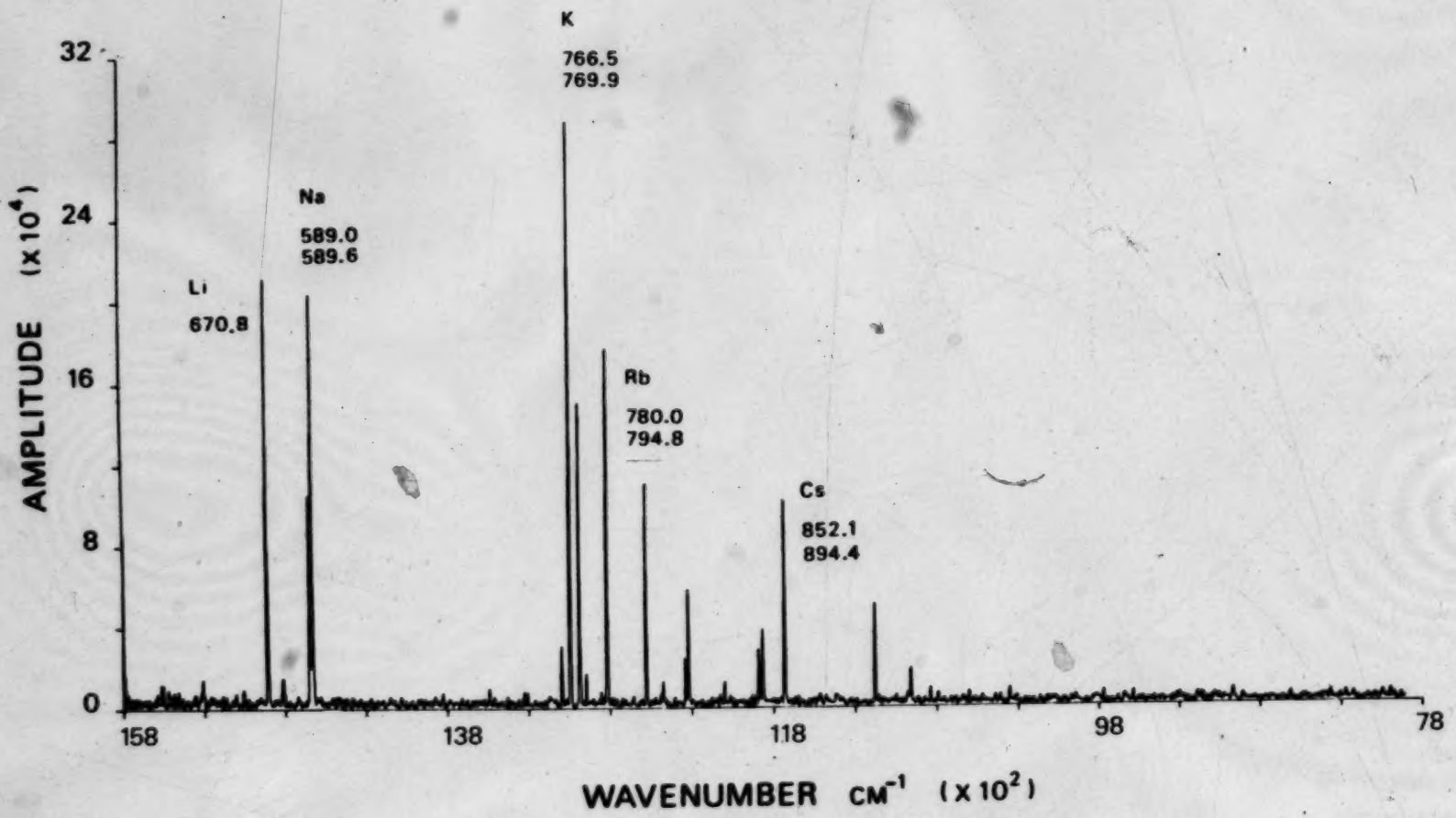


FIGURE 54. Multielement spectrum containing lithium, sodium, potassium, rubidium and cesium emission lines.

TABLE 5. Most sensitive ICP emission line for 70 elements.

| Element | Code Number | Wavelength (nm) | Element | Code Number | Wavelength (nm) |
|---|---|---|---|---|---|
| Ag | 1 | 328.068 | Na | 36 | 588.995 |
| Al | 2 | 396.152 | Nb | 37 | 202.932 |
| As | 3 | 197.197 | Nd | 38 | 430.358 |
| Au | 4 | 201.200 | Ni | 39 | 231.604 |
| B | 5 | 208.959 | Os | 40 | 206.721 |
| Ba | 6 | 455.403 | P | 41 | 213.618 |
| Be | 7 | 234.861 | Pb | 42 | 405.783 |
| Bi | 8 | 195.389 | Pd | 43 | 340.458 |
| C | 9 | 247.857 | Pr | 44 | 417.938 |
| Ca | 10 | 393.366 | Pt | 45 | 204.937 |
| Cd | 11 | 228.802 | Rb | 46 | 780.023 |
| Ce | 12 | 395.254 | Re | 47 | 227.525 |
| Co | 13 | 228.616 | Rh | 48 | 343.489 |
| Cr | 14 | 205.552 | Ru | 49 | 240.272 |
| Cs | 15 | 852.124 | Sb | 50 | 206.833 |
| Cu | 16 | 324.754 | Sc | 51 | 361.384 |
| Dy | 17 | 353.170 | Se | 52 | 196.026 |
| Er | 18 | 390.631 | Si | 53 | 251.611 |
| Eu | 19 | 420.505 | Sm | 54 | 356.827 |
| Fe | 20 | 259.940 | Sn | 55 | 197.080 |
| Ga | 21 | 294.364 | Sr | 56 | 407.771 |
| Gd | 22 | 342.247 | Ta | 57 | 214.687 |
| Ge | 23 | 199.824 | Tb | 58 | 350.917 |
| Hf | 24 | 202.818 | Te | 59 | 200.202 |
| Hg | 25 | 253.652 | Th | 60 | 401.913 |
| Ho | 26 | 345.600 | Ti | 61 | 334.941 |
| In | 27 | 325.609 | Tl | 62 | 351.924 |
| Ir | 28 | 216.942 | Tm | 63 | 346.220 |
| K | 29 | 766.490 | U | 64 | 385.958 |
| La | 30 | 394.910 | V | 65 | 309.311 |
| Li | 31 | 670.784 | W | 66 | 202.998 |
| Lu | 32 | 261.542 | Y | 67 | 371.030 |
| Mg | 33 | 279.553 | Yb | 68 | 369.419 |
| Mn | 34 | 257.610 | Zn | 69 | 206.200 |
| Mo | 35 | 202.030 | Zr | 70 | 339.198 |

similar to the one obtained by Fassel et al. for dispersive spectrometers (107) should be obtained.

The results of the cross-correlation process for all seventy elements are plotted in Figure 55. This is a plot of the cross-correlation function at $\tau = 0$ point versus an element axis where the elements are represented by their respective code numbers. From the plot, it can be seen that all the elements that were present in the sample show relatively high correlation results as compared with the others. In addition, indium, which was absent from the sample, also shows relatively high correlation data. This is because the indium line (325.61 nm), if present, will overlap with the lithium line (670.78 nm) because of alaising (32). However, the presence of indium in the sample is unlikely because the response of the silicon diode detector used to obtain the signal is minimal near 300 nm. Similar results were obtained using square synthetic interferograms as the cross-correlation masks. This is shown in Figure 56. The selectivity of the analog and the square synthetic interferograms appears to be comparable. The only difference is the slight increase in the absolute magnitude of the correlation data obtained using the square synthetic interferograms as the cross-correlation masks. This is because the square synthetic interferograms do

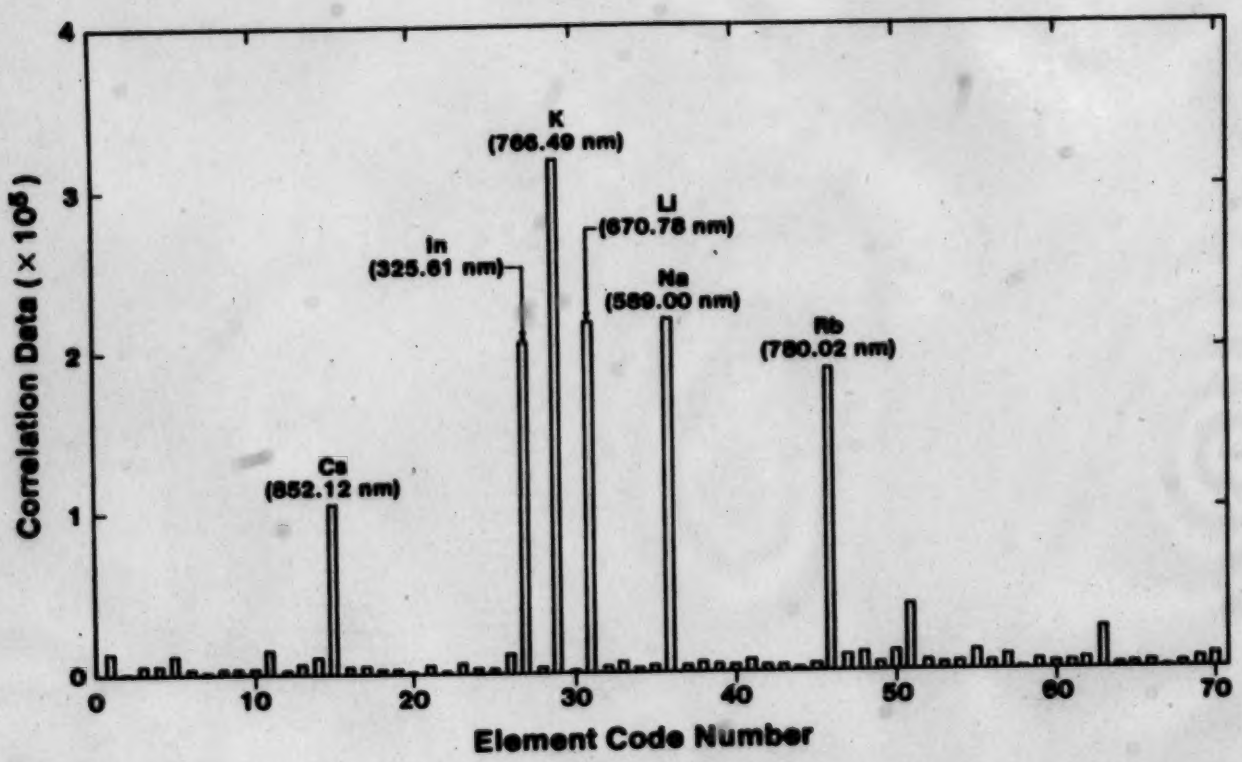


FIGURE 55. Results of cross-correlation analysis on the multielement alkali metal interferogram utilizing analog cross-correlation masks.

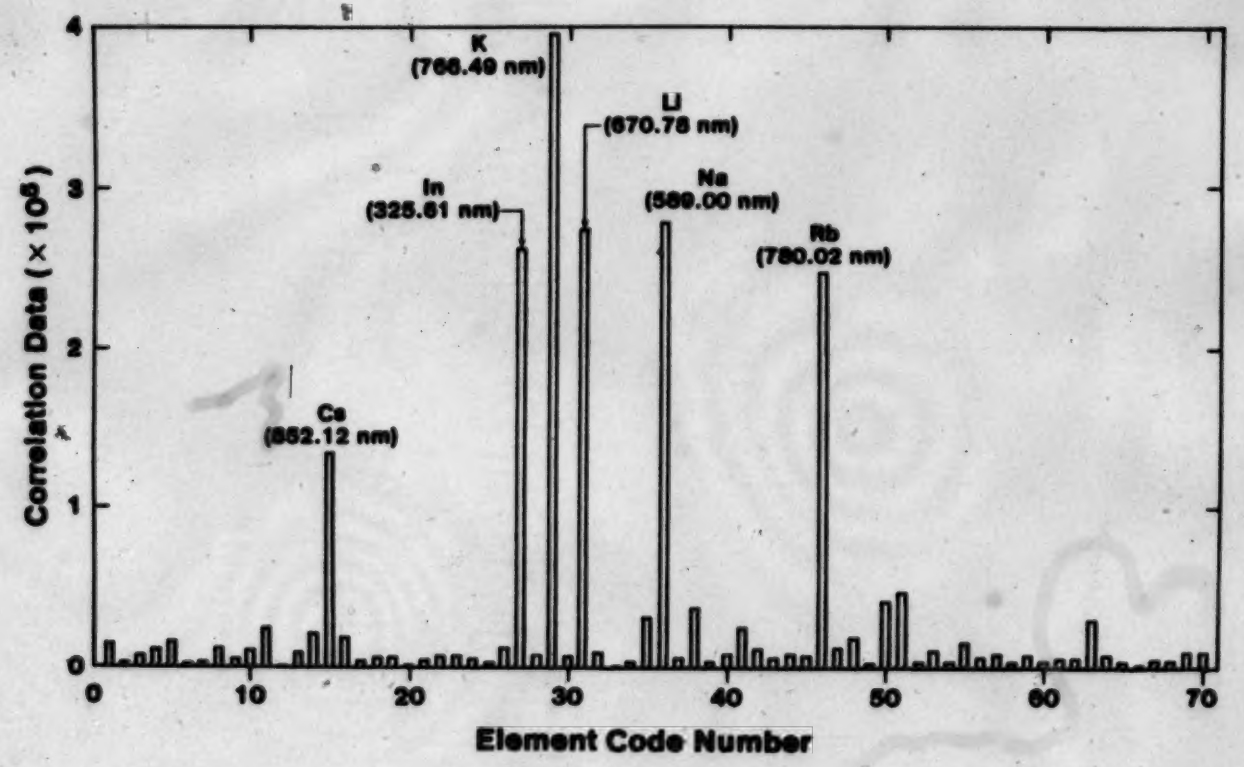


FIGURE 56. Results of cross-correlation analysis for the multielement alkali metal interferogram utilizing square cross-correlation masks.

not contain any value between 0 and -1; 0 and +1. The absolute magnitude of the correlation results represents the quantitative information about the sample analysed. This will be further discussed later in this chapter. In this way, the relative magnitude of the correlation data can be utilized to indicate the qualitative information of the signal. It can be implemented in an automatic fashion by a computer for spectral analysis. This is analogous to spectral search methods used in the infrared spectroscopy for compound identification. A spectral match between the signal and a library of spectra is performed in the spectral domain. With the correlation technique, spectral analysis can be accomplished in the Fourier domain utilizing a library containing various cross-correlation masks for each element.

The correlation technique was further investigated with the use of a more complex spectrum. The signal containing information about some transition metals is shown in Figure 57. These transition metals were cobalt, iron, nickel and vanadium. For the sake of illustration, this interferogram was Fourier transformed into the spectral domain and is shown in Figure 58. A fairly complex spectrum was obtained. The pure spectra of these elements, are shown in Figure 59 for reference.

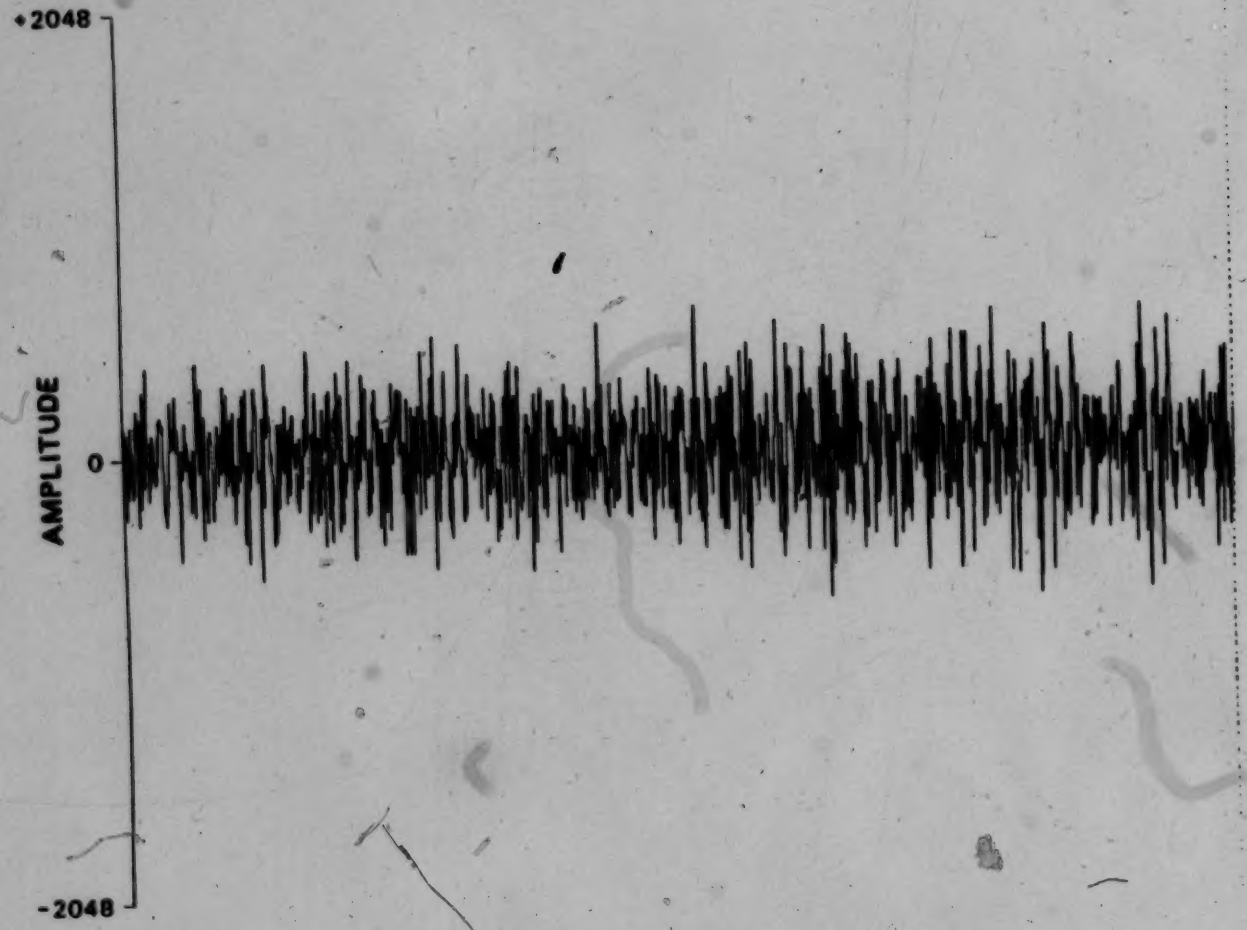


FIGURE 57. A multielement interferogram containing vanadium, cobalt, nickel and iron.

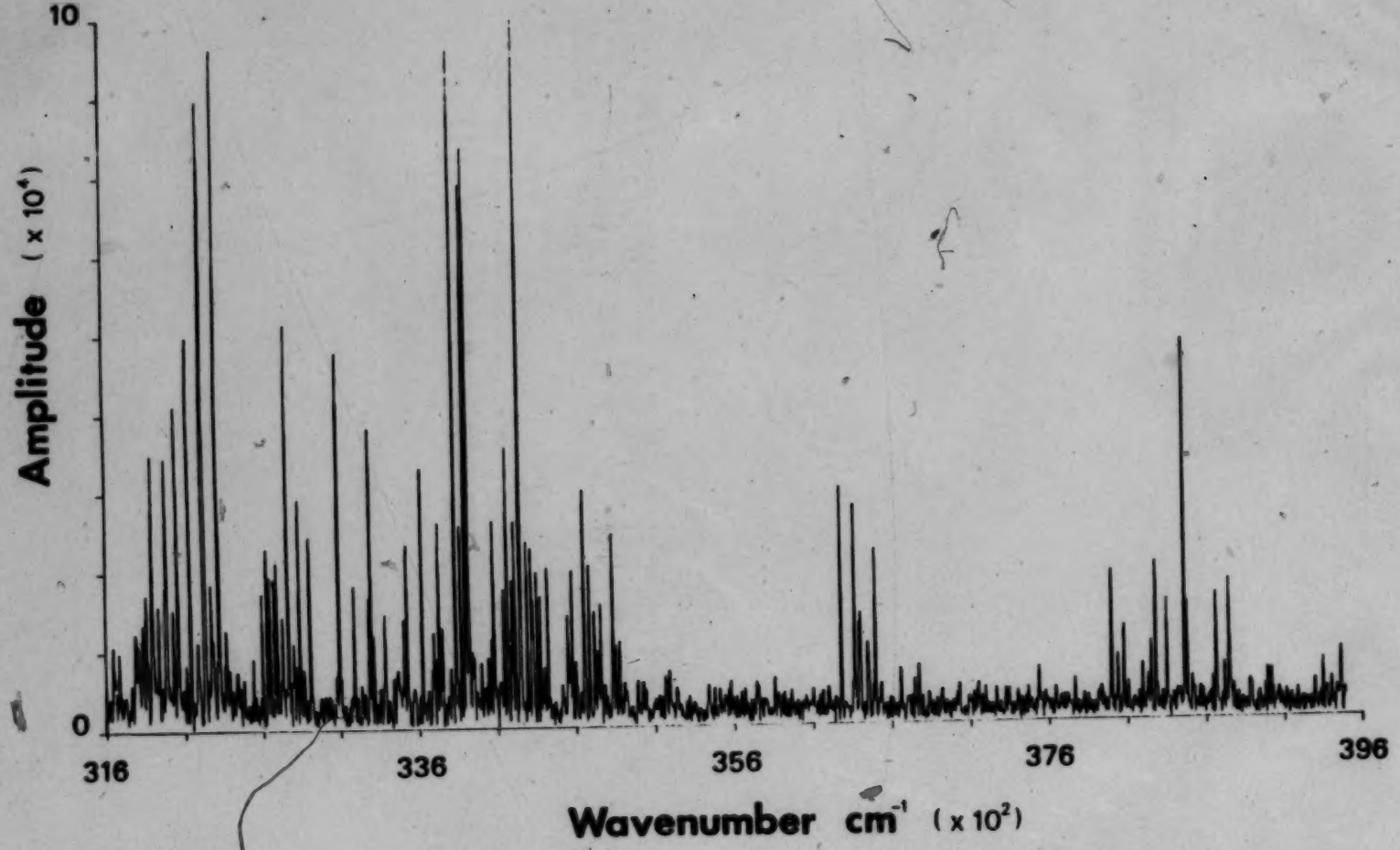


FIGURE 58. Multielement spectrum containing vanadium, cobalt, nickel and iron emission lines.

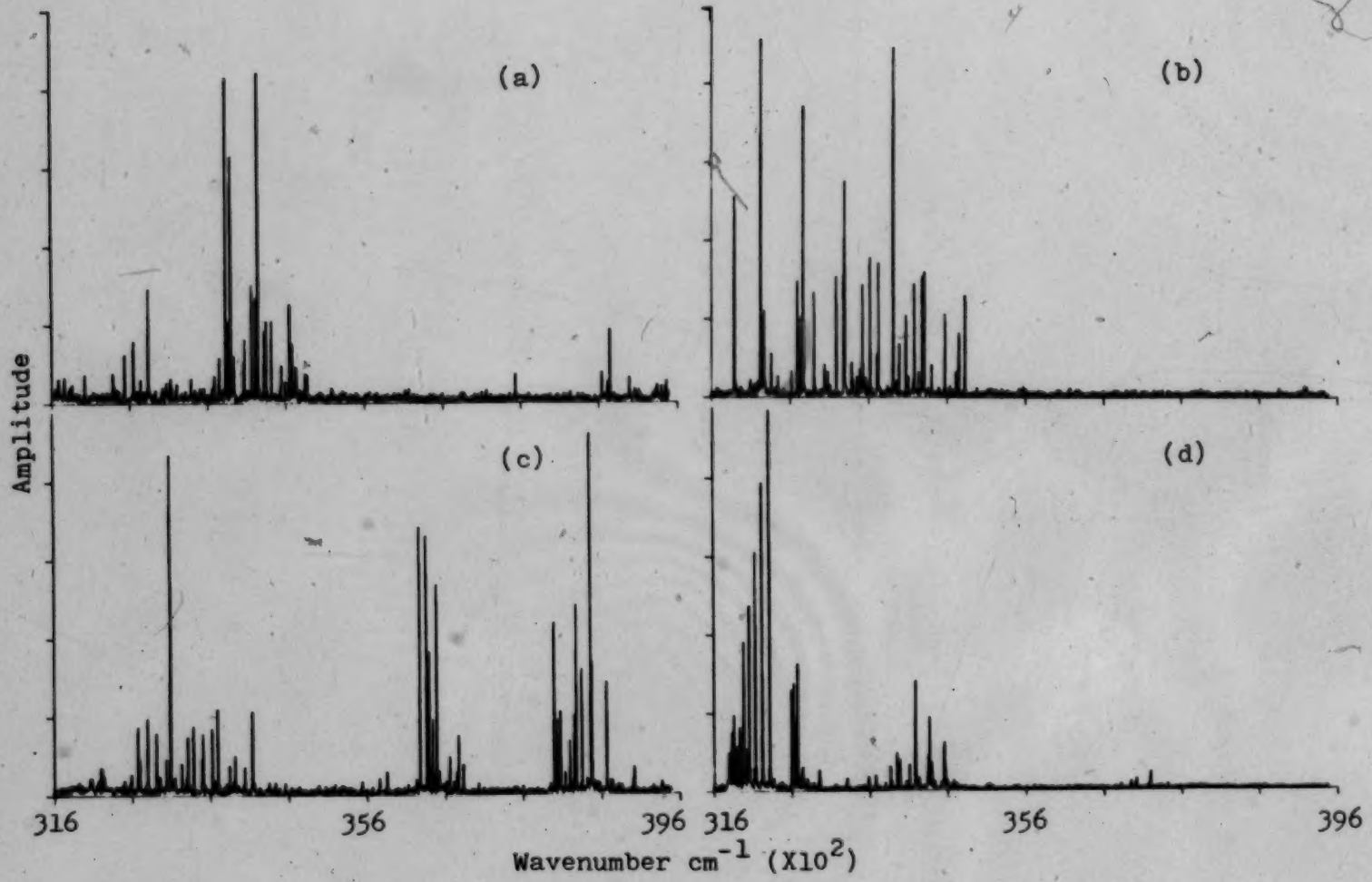


FIGURE 59. (a) Cobalt, (b) nickel, (c) iron and (d) vanadium spectra.

Note that in the case of correlation analysis neither the exact position of the spectral lines nor the degree of spectral overlap need be known. Cross-correlation analysis was applied to the time domain signal using cross-correlation masks generated according to the wavelengths listed in Table 5. These results were plotted as shown in Figure 60. The information obtained is erratic because neither sodium nor palladium was present. Besides, two out of the four elements that were present in the sample do not show relatively high correlation results as compared to the others. This problem was caused by the poor selection of wavelengths used to generate the cross-correlation masks. With the use of the solar blind filter and the visible PMT combination as the detector in obtaining this signal, the spectral response of the system was limited to within 240 nm to 360 nm region. The correlation analysis was then repeated using the cross-correlation masks generated by the wavelengths listed in Table 6. This table contains the most sensitive line for each element within the spectral window of 240 nm to 360 nm. Again, the wavelengths were extracted from the table published by Boumans (106). For some elements, there are no reasonably sensitive spectral lines within this region, the spectral line that is closest to the

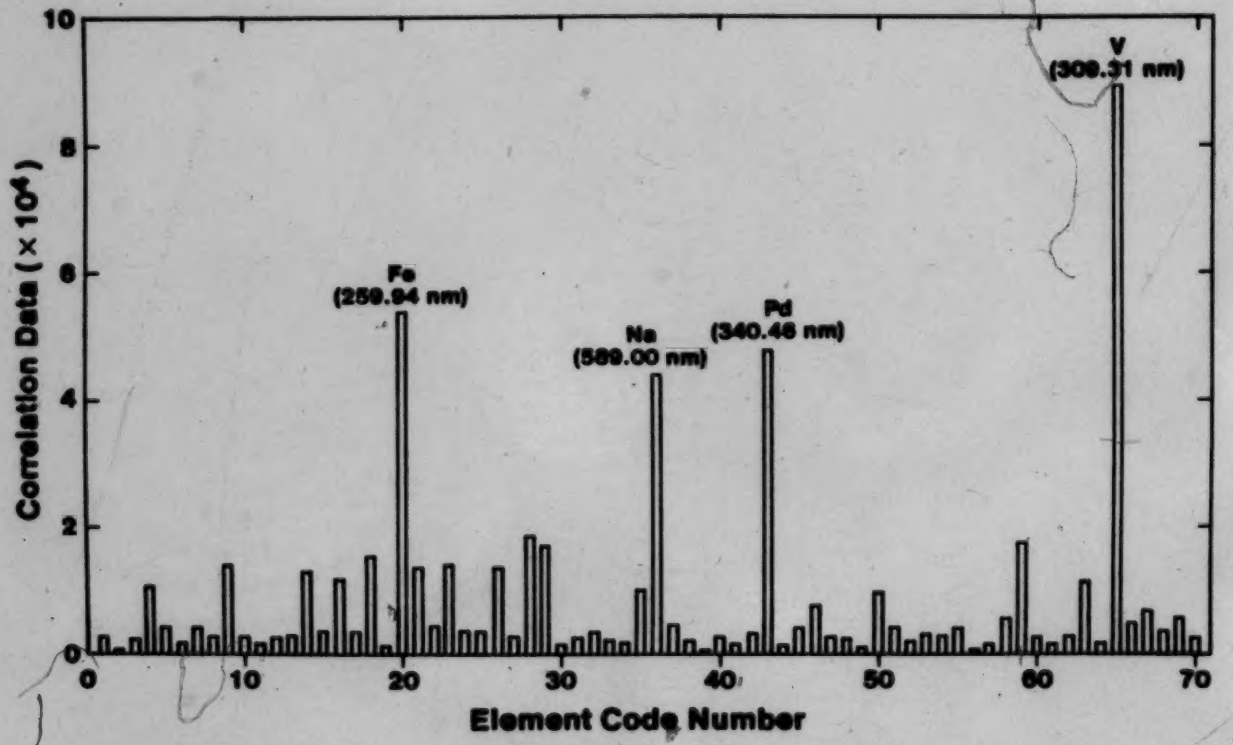


FIGURE 60. Results of cross-correlation analysis for the multielement transition metal interferogram using Table 5 for the generation of analog cross-correlation masks.

TABLE 6. Most sensitive ICP emission line for 70 elements within the spectral window of 240-360 nm.

| Element | Code Number | Wavelength (nm) | Element | Code Number | Wavelength (nm) |
|---|---|---|---|---|---|
| Ag | 1 | 328.068 | Na | 36 | 330.237 |
| Al | 2 | 309.271 | Nb | 37 | 309.418 |
| As | 3 | 278.022 | Nd | 38 | 386.333 |
| Au | 4 | 267.595 | Ni | 39 | 310.166 |
| B | 5 | 249.773 | Os | 40 | 253.800 |
| Ba | 6 | 234.758 | P | 41 | 253.565 |
| Be | 7 | 313.042 | Pb | 42 | 280.199 |
| Bi | 8 | 306.772 | Pd | 43 | 340.458 |
| C | 9 | 247.857 | Pr | 44 | 390.844 |
| Ca | 10 | 317.933 | Pt | 45 | 265.945 |
| Cd | 11 | 346.620 | Rb | 46 | 420.185 |
| Ce | 12 | 394.275 | Re | 47 | 346.046 |
| Co | 13 | 345.350 | Rh | 48 | 343.489 |
| Cr | 14 | 283.563 | Ru | 49 | 240.272 |
| Cs | 15 | 455.531 | Sb | 50 | 259.805 |
| Cu | 16 | 324.754 | Sc | 51 | 357.253 |
| Dy | 17 | 353.170 | Se | 52 | 206.279 |
| Er | 18 | 337.271 | Si | 53 | 251.611 |
| Eu | 19 | 381.967 | Sm | 54 | 356.827 |
| Fe | 20 | 259.940 | Sn | 55 | 283.999 |
| Ga | 21 | 294.364 | Sr | 56 | 346.446 |
| Gd | 22 | 342.247 | Ta | 57 | 240.063 |
| Ge | 23 | 265.118 | Tb | 58 | 350.917 |
| Hf | 24 | 339.980 | Te | 59 | 253.072 |
| Hg | 25 | 253.652 | Th | 60 | 339.204 |
| Ho | 26 | 345.600 | Ti | 61 | 334.941 |
| In | 27 | 325.609 | Tl | 62 | 351.924 |
| Ir | 28 | 254.397 | Tm | 63 | 346.220 |
| K | 29 | 404.414 | U | 64 | 367.007 |
| La | 30 | 394.910 | V | 65 | 309.311 |
| Li | 31 | 323.263 | W | 66 | 245.148 |
| Lu | 32 | 261.542 | Y | 67 | 360.073 |
| Mg | 33 | 279.553 | Yb | 68 | 328.937 |
| Mn | 34 | 257.610 | Zn | 69 | 334.502 |
| Mo | 35 | 313.259 | Zr | 70 | 339.198 |

region was chosen to complete the list. The results are shown in Figure 61. All four elements that were present in the sample show relatively high correlation, in addition, aluminium and palladium also show strong indication of their presence. This is because the aluminium line at 309.27 nm overlaps with the vanadium line at 309.31 nm and in the case of palladium (340.46 nm), there is a spectral overlap with a cobalt emission line at 340.51 nm. It must also be pointed out that the relatively high "background" for the rest of the elements tested is mainly caused by the complexity of the signal. Due to the large amount of emission lines that are available from the four elements present in the sample, spectral overlap is severe.

In order to distinguish the elements that were present in the sample from the elements that were not, but showed high correlation, a secondary correlation process is necessary. This simply means the utilization of more spectral lines of the suspected elements for correlation analysis. In this case, two additional spectral lines of each suspected element were used for the generation of the additional cross-correlation values. There is no particular reason why a total of three spectral lines were chosen. In complex situations where

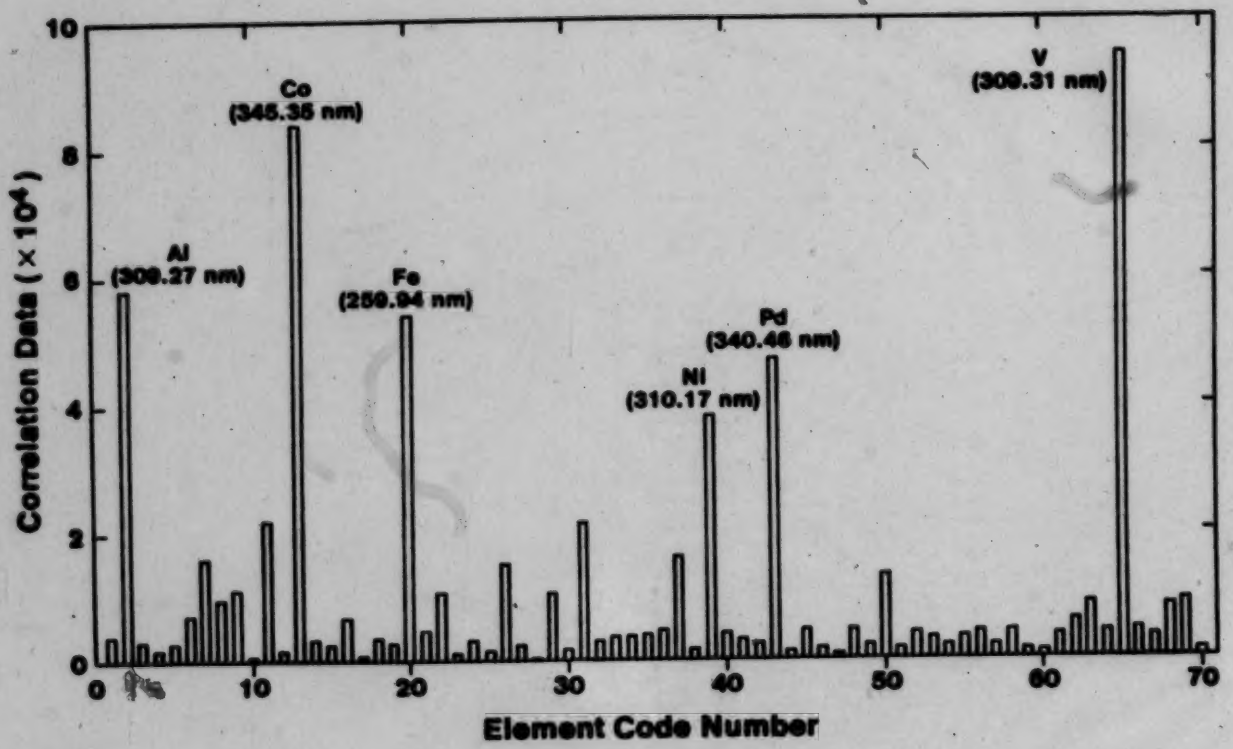


FIGURE 61. Results of cross-correlation analysis for the multielement transition metal interferogram using Table 6 for the generation of analog cross-correlation masks.

spectral overlap is more severe, more than three spectral lines for each element can be used to generate the cross-correlation masks for analysis. The wavelengths of three spectral lines for each element are shown in Table 7. Each spectral line has been assigned a code number as indicated in Table 7. Each of these spectral lines was used to generate a cross-correlation mask for analysis and thus each element has three correlation data points corresponding to each spectral line. The results of these are plotted as shown in Figure 62. In the case of aluminium and palladium, only the spectral lines (aluminium 309.27 nm and palladium 340.46 nm) that overlap with the lines originating from other elements which were present have high correlation data points. For the other spectral information tested for these elements none of them yields a high correlation result. In contrast, all four elements that were present in the sample show relatively high correlation for all the spectral information tested. In this way, one is able to pinpoint exactly which elements are present in the signal and automatically identify spectral overlap problems. As mentioned above, the absolute magnitude of the correlation data indicates the amplitude of the particular spectral information in the signal.

TABLE 7. Some ICP emission lines for aluminium, cobalt, iron, nickel, palladium and vanadium (240 nm - 360 nm).

| Element | Spectral Line | |
|---|---|---|
| | Code Number | Wavelength (nm) |
| Al | 1 | 309.27 |
| | 2 | 308.22 |
| | 3 | 257.51 |
| Co | 1 | 345.35 |
| | 2 | 340.51 |
| | 3 | 341.23 |
| Fe | 1 | 259.94 |
| | 2 | 302.06 |
| | 3 | 275.57 |
| Ni | 1 | 310.17 |
| | 2 | 341.48 |
| | 3 | 305.08 |
| Pd | 1 | 340.46 |
| | 2 | 342.12 |
| | 3 | 351.96 |
| V | 1 | 309.31 |
| | 2 | 310.23 |
| | 3 | 311.07 |

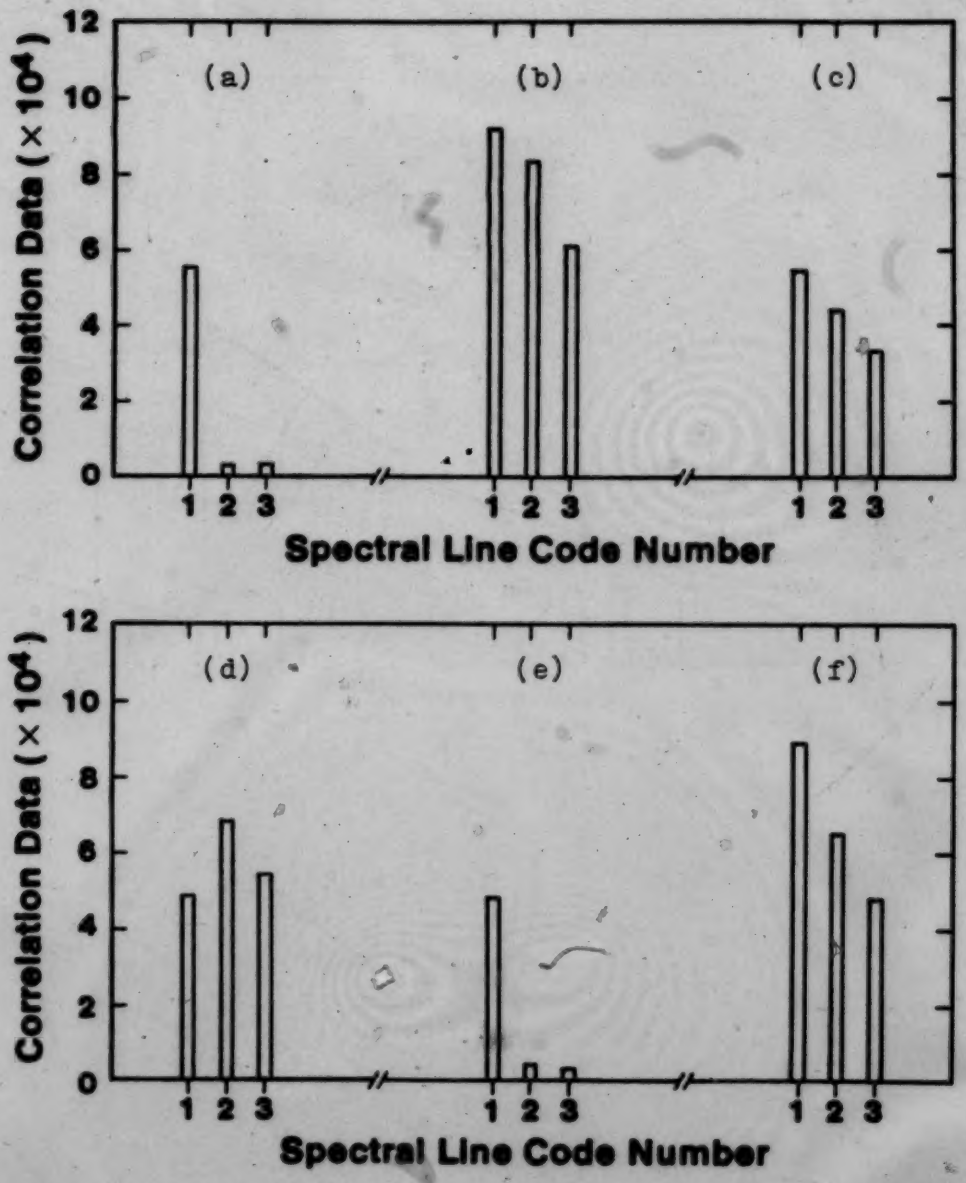


FIGURE 62. Secondary cross-correlation analysis results for (a) aluminium, (b) cobalt, (c) iron, (d) nickel, (e) palladium and (f) vanadium utilizing analog cross-correlation masks.

An alternative of performing the secondary correlation analysis is to combine the correlation results obtained from more than one correlation mask for each element. The results are shown in Figure 63. In this case, a code number of one represents the correlation data point obtained from the correlation mask generated using spectral line #1 for that particular element. A code number of two represents the summation of the correlation data points obtained from the correlation mask generated using spectral lines #1 and #2 for that particular element and so on.

As shown in Figure 63, in the case that high correlation is due to spectral overlap, the summation of all the correlation results obtained from three independent correlation analysis remains fairly constant as in the case of aluminium and palladium. Cobalt, iron, vanadium and nickel all show a staircase fashion increase in the correlation results. Thus, this can also be utilized as a mean for qualitative analysis. All the above analysis have been performed using the analog cross-correlation masks (i.e. cosines and sines). Similar results using the square synthetic interferograms as cross-correlation masks can be obtained. The results are illustrated in Figure 64,65 and 66.

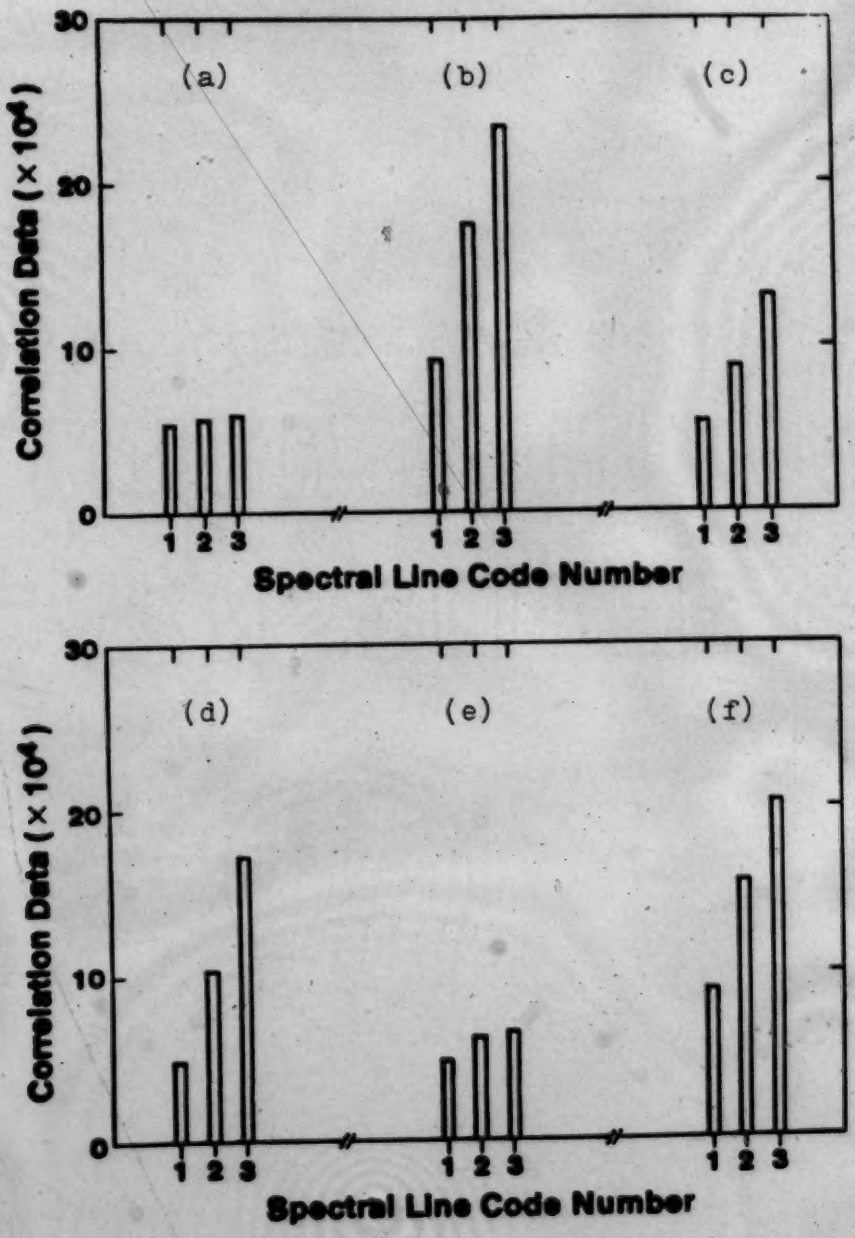


FIGURE 63. Results of the alternate secondary cross-correlation analysis for (a) aluminium, (b) cobalt, (c) iron, (d) nickel, (e) palladium and (f) vanadium utilizing analog cross-correlation masks.

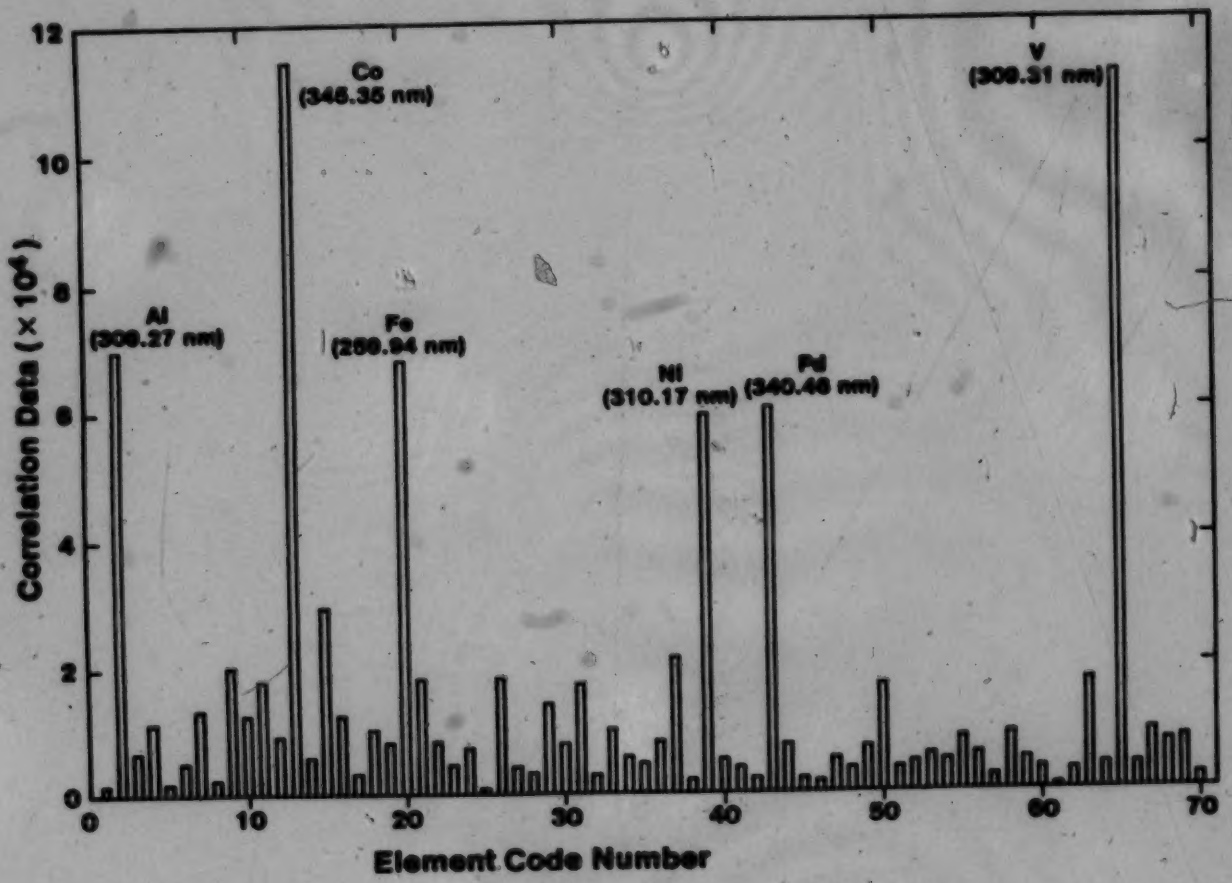


FIGURE 64. Results of cross-correlation analysis for the multielement transition metal interferogram using Table 6 for the generation of square cross-correlation masks.

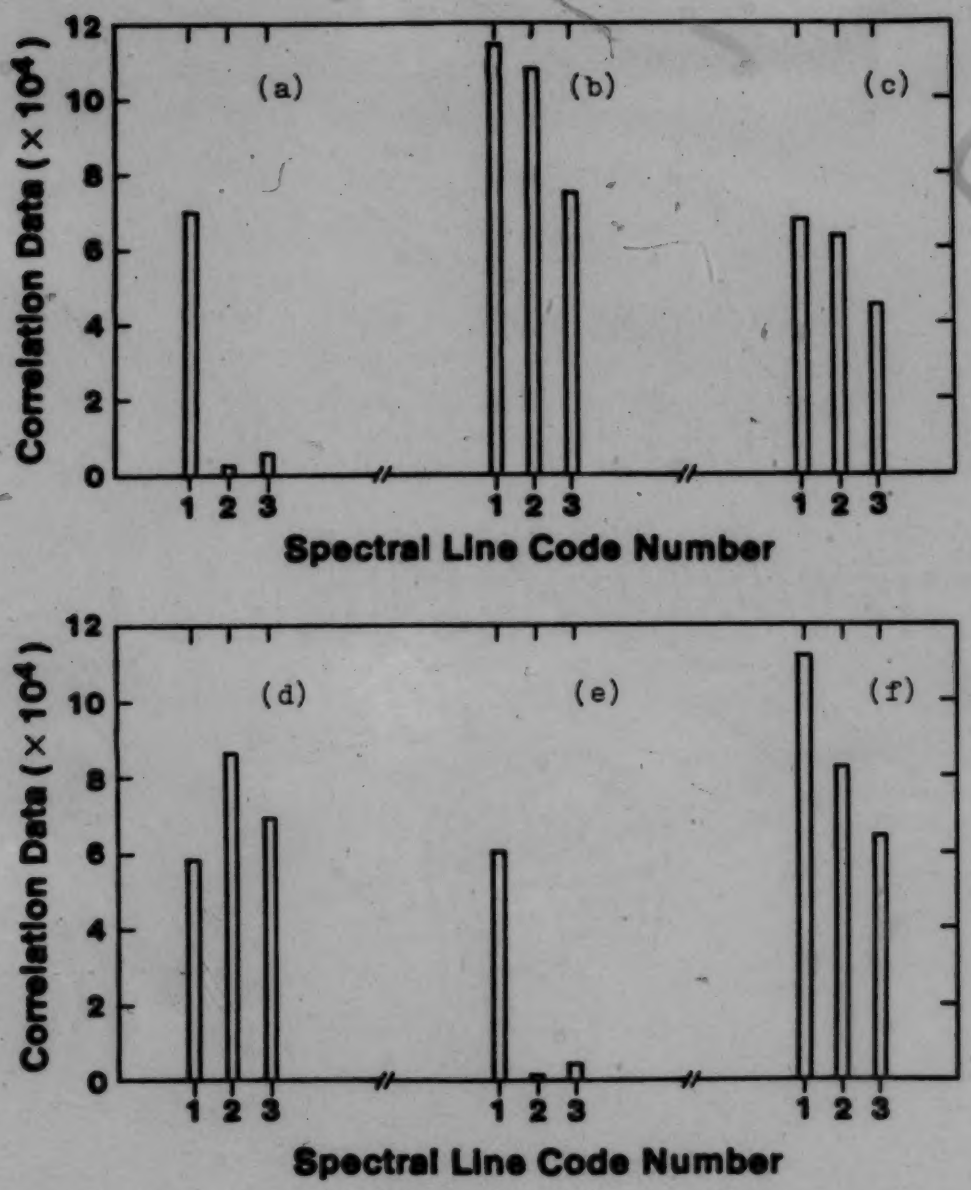


FIGURE 65. Secondary cross-correlation analysis results for (a) aluminium, (b) cobalt, (c) iron, (d) nickel, (e) palladium and (f) vanadium utilizing square cross-correlation masks.

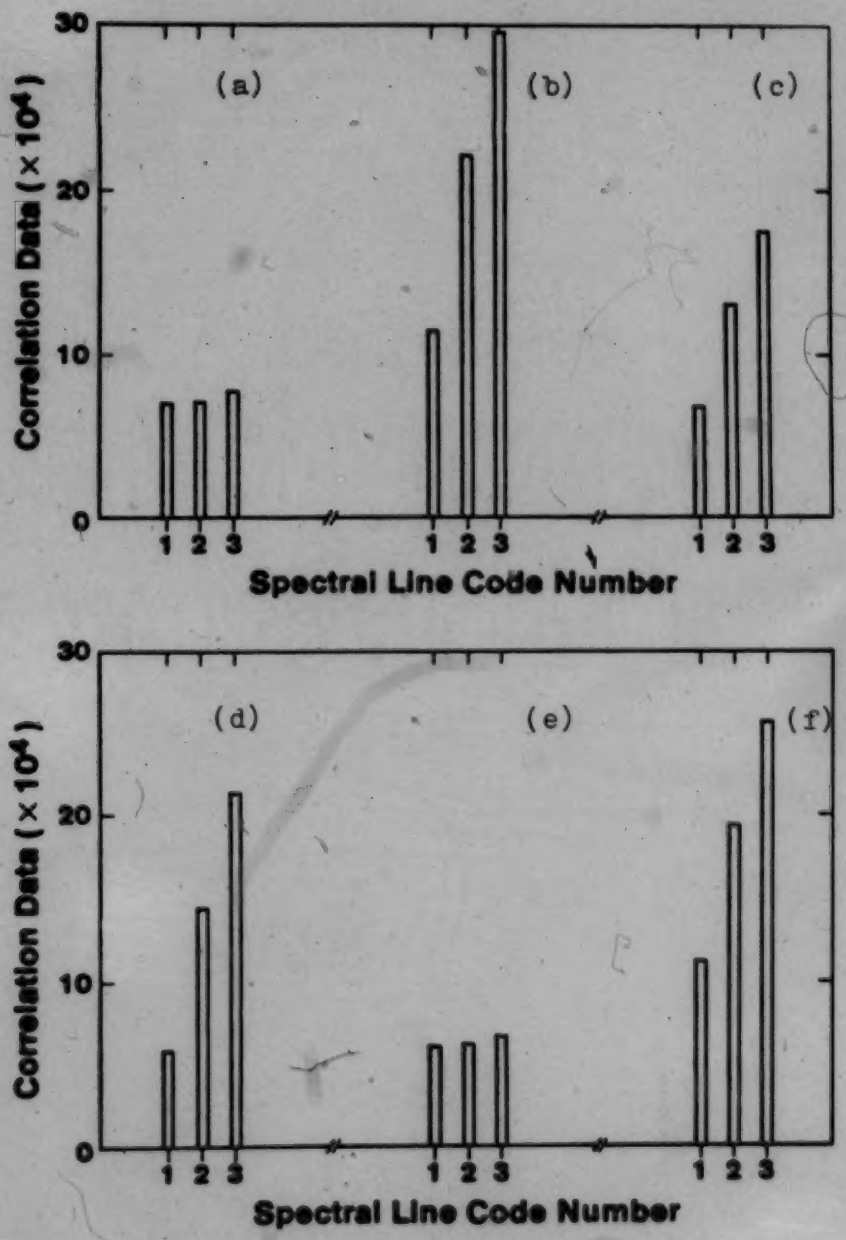


FIGURE 66. Results of the alternate secondary cross-correlation analysis for (a) aluminium, (b) cobalt, (c) iron, (d) nickel, (e) palladium and (f) vanadium utilizing square cross-correlation masks.

In situations where spectral analysis is difficult, cross-correlation analysis can be very helpful. Most of all, correlation analysis can be implemented essentially in an automatic fashion in a small computer system. Qualitative information can be obtained within a short period of time by performing the analysis using cross-correlation masks stored in a computer. In this case, neither knowledge of the spectral axis nor the degree of spectral overlap need be known once the library of correlation masks has been established.

Quantitative Aspects: As mentioned before, the absolute magnitude of a correlation data point represents the quantitative information at a particular spectral wavelength. Linear working curves for lithium with concentration ranging from 0.1 ppm to 10 ppm are shown in Figure 67. They were obtained using the analog and square synthetic interferograms corresponding to the lithium line at 670.78 nm as correlation masks. As indicated by the slopes of the graph, the results obtained using square synthetic interferograms as correlation masks have a better sensitivity over those obtained using analog synthetic interferograms. Both methods do demonstrate their abilities to extract quantitative information from analytical signals.

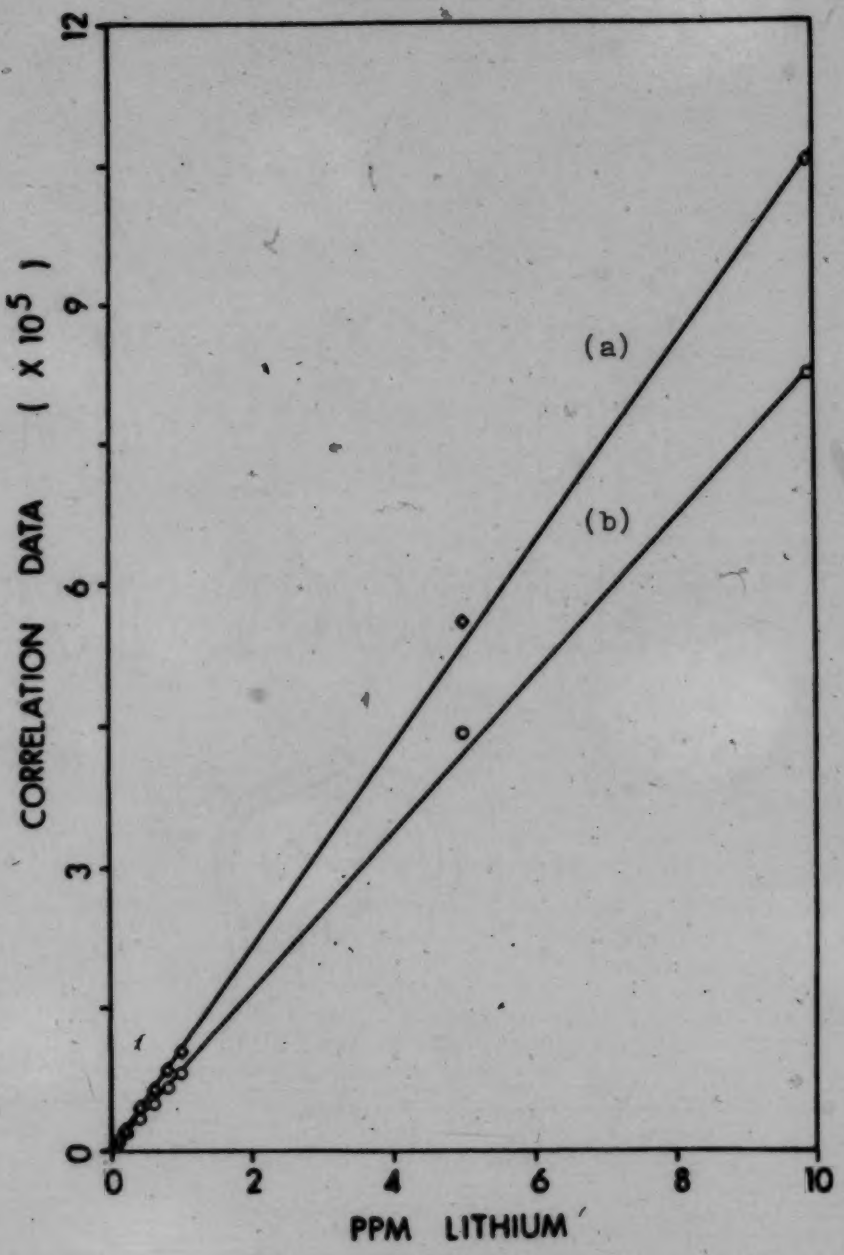


FIGURE 67. Linear analytical curves for lithium obtained by (a) square and (b) analog cross-correlation masks.

The effect of combining correlation data obtained from different correlation masks, each corresponding to the quantitative information at a particular spectral wavelength, is illustrated in Figure 68. This is a plot of correlation results versus the concentration of nickel with concentration ranging from 0 to 500 ppm. As more spectral information is utilized, the sensitivity as indicated by the slopes of the graph increases. However, one cannot simply utilize all the spectral information available in the signal as spectral interferences may be present. This is best illustrated with an example, determination of vanadium and nickel. Among the more sensitive lines of vanadium and nickel, the vanadium line at 310.23 nm overlaps with the nickel line at 310.17 nm. If the three most sensitive spectral lines of vanadium and nickel are utilized to establish an analytical calibration curve, the results illustrated in Figure 69 will be obtained. Correlation results using nickel and vanadium cross-correlation masks on solutions containing a constant amount of vanadium and an increasing amount of nickel are plotted as shown in Figure 69(a) and 69(b). Obviously, the vanadium cross-correlation masks are extracting nickel information because of the spectral overlap between the two elements. Thus, one has to be

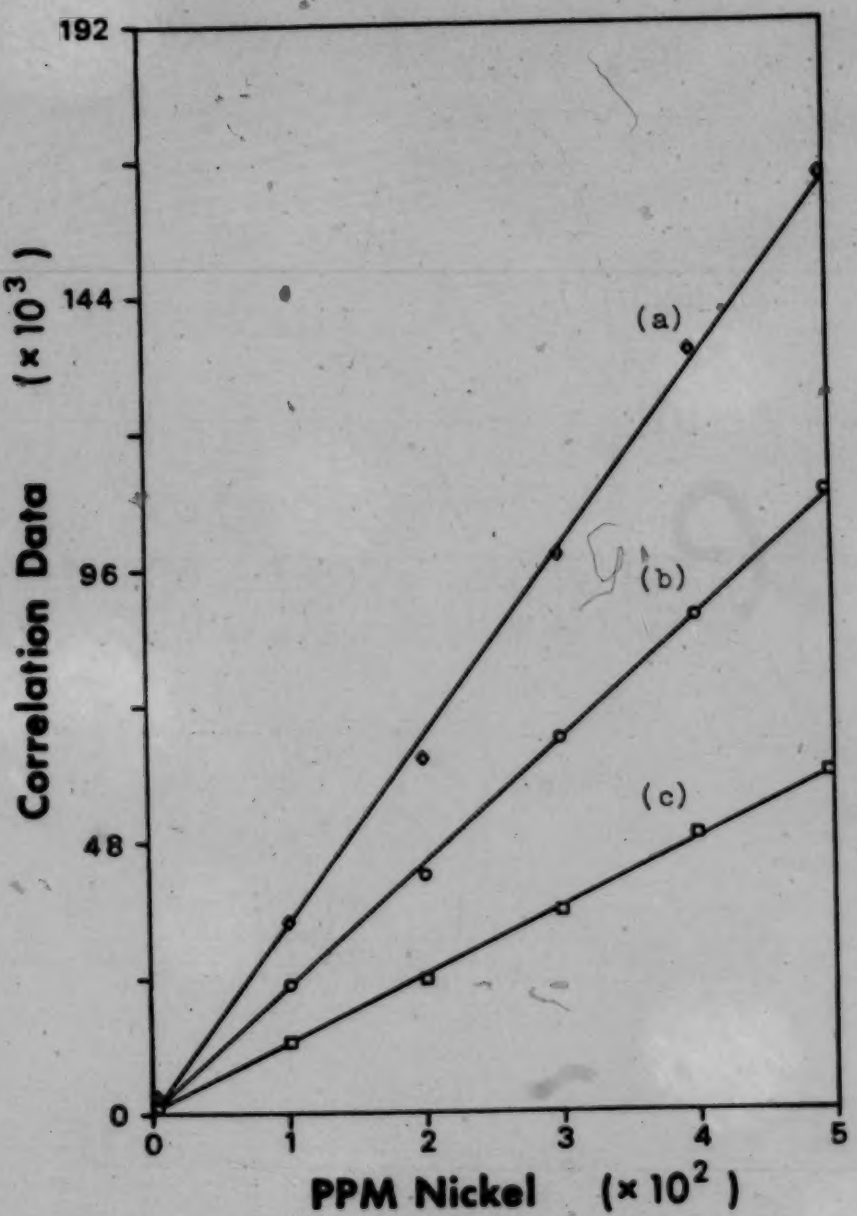


FIGURE 68. Linear analytical curves for nickel obtained by cross-correlation analysis with analytical information corresponding to (a) 310.17, 341.48, 305.08; (b) 310.17, 341.48; (c) 310.17 nm.

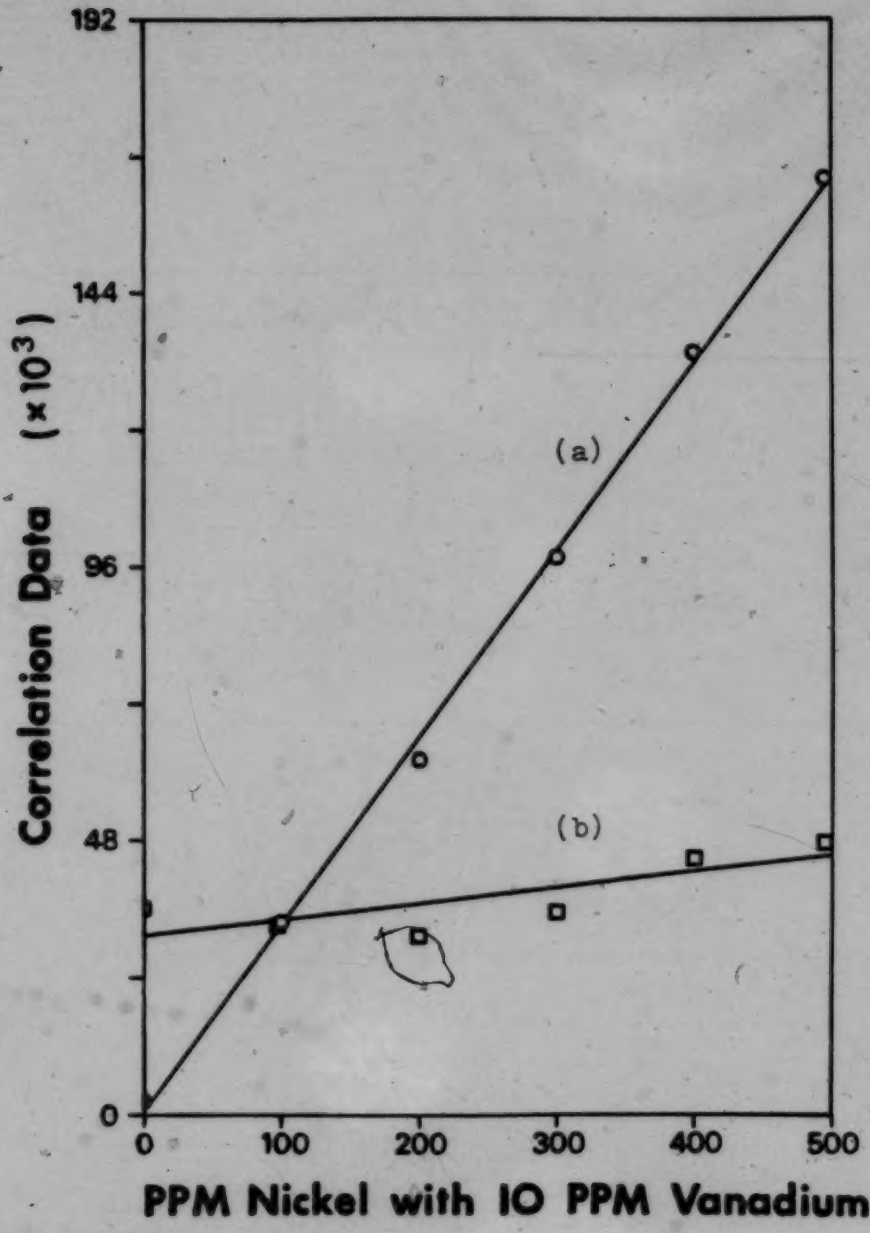


FIGURE 69. Detection of nickel and vanadium in the presence of each other with cross-correlation masks corresponding to (a) 310.17, 341.48, 305.08; (b) 309.31, 311.07, 310.23 nm.

careful about the choice of correlation masks. Upon elimination of the 310 nm spectral line for both nickel and vanadium, more desirable results are obtained as shown in Figure 70. Correlation analysis on vanadium shows a constant level of correlation data. In the case of nickel, a linear calibration curve with zero intercept is obtained. If a plot of correlation data obtained for a particular wavelength against the concentration shows a non-zero intercept, spectral interferences should be suspected. A final example is given for the determination of vanadium in the presence of cobalt, nickel and iron. A linear calibration curve for vanadium concentration ranging from 0 to 10 ppm is obtained as illustrated in Figure 71. The correlation data correspond to the vanadium information at 309.31 nm.

Precision is also an important consideration when dealing with the correlation analysis. A precision study on a solution of 10 ppm vanadium was carried out. The data are listed in Table 8. These numbers are the percent relative standard deviation of the 10 ppm vanadium signal over ten readings. The conventional peak analysis and correlation analysis based on both the analog and square correlation masks give comparable results.

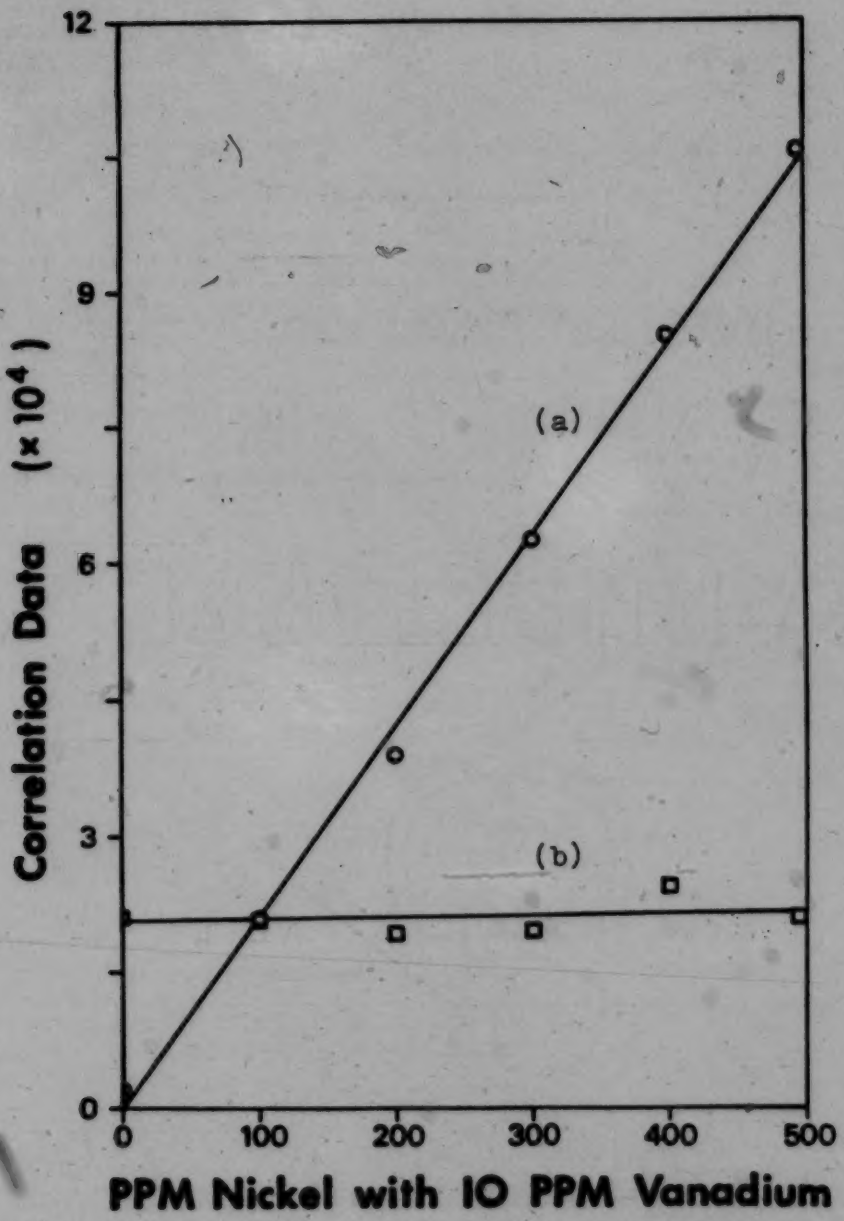


FIGURE 70. Detection of nickel and vanadium in the presence of each other with cross-correlation masks corresponding to (a) 341.48, 305.08; (b) 309.31, 311.07 nm.

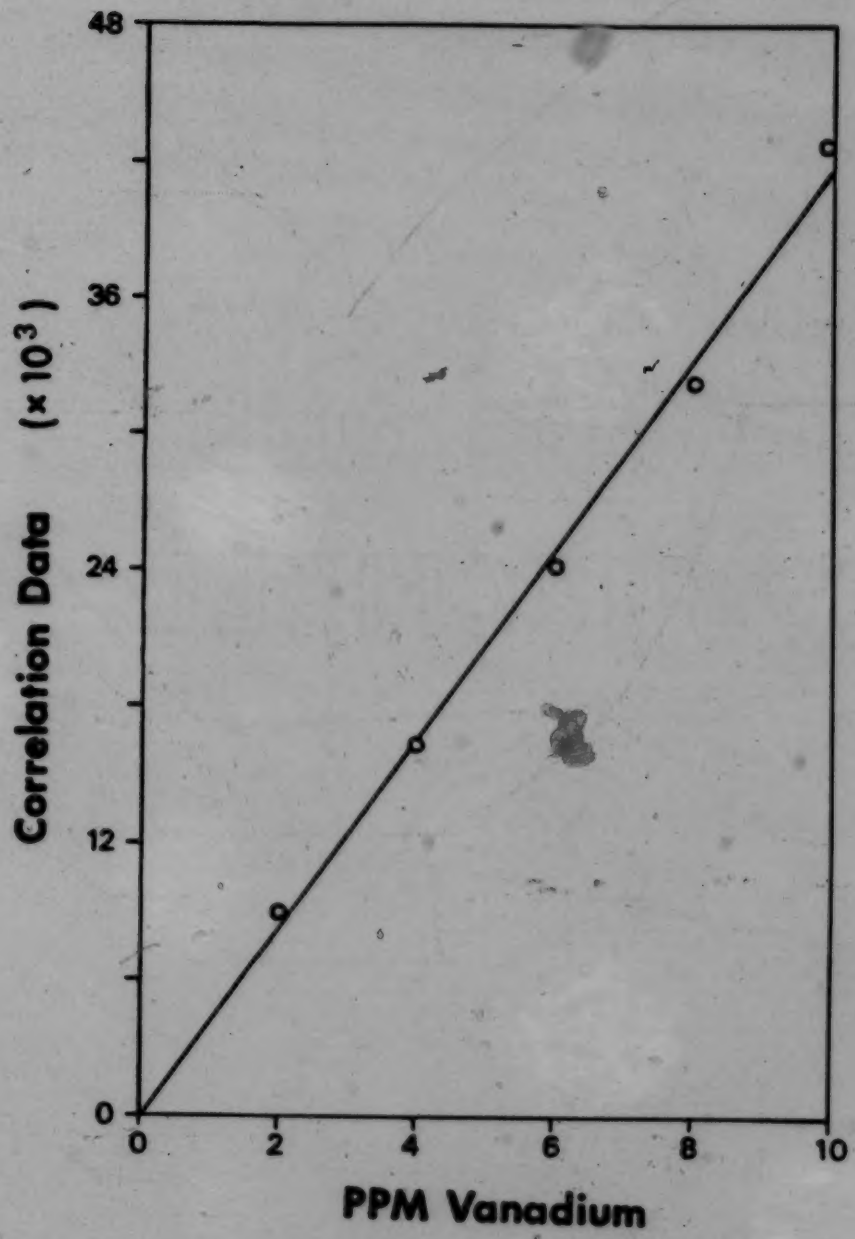


FIGURE 71. Analytical working curve for vanadium obtained in the presence of cobalt, nickel and iron by cross-correlation analysis.

TABLE 8. Percent relative standard deviation data for different data processing methods. (10 ppm vanadium, ten readings)

| Wavelength (nm) | Data Processing Method | | |
|---|---|---|---|
| | Conventional Peak | Analog Mask Correlation | Square Mask Correlation |
| 309.31 | 1.96 | 3.33 | 3.16 |
| 310.23 | 2.64 | 2.38 | 2.10 |
| 311.07 | 3.70 | 3.38 | 3.37 |

F. Conclusions

A final comparison between correlation analysis and the Fourier transform data processing method as applied to the ICP-FT spectrometer system is depicted in Figure 72. All the relevant analytical information can be obtained by correlation analysis without the necessity to convert the spectral data into the human interpretable spectral domain. Moreover, correlation based data processing of interferometric signals is simple when compared to the conventional fast Fourier transform data processing method and yet is a powerful technique. Because of its simplicity, the need for a large computer to carry out data processing for long interferograms disappears. Furthermore, the correlation analysis can be implemented essentially in an automatic fashion by a computer to perform qualitative and quantitative analysis within a very short period of time. The flexibility in the generation of cross-correlation masks fully utilizes the wide spectral coverage of the ICP-Fourier transform spectrometer system. Different spectral information can be obtained simply by using different cross-correlation masks. Background correction by correlation analysis is also possible. This can be accomplished by using an appropriate correlation mask that

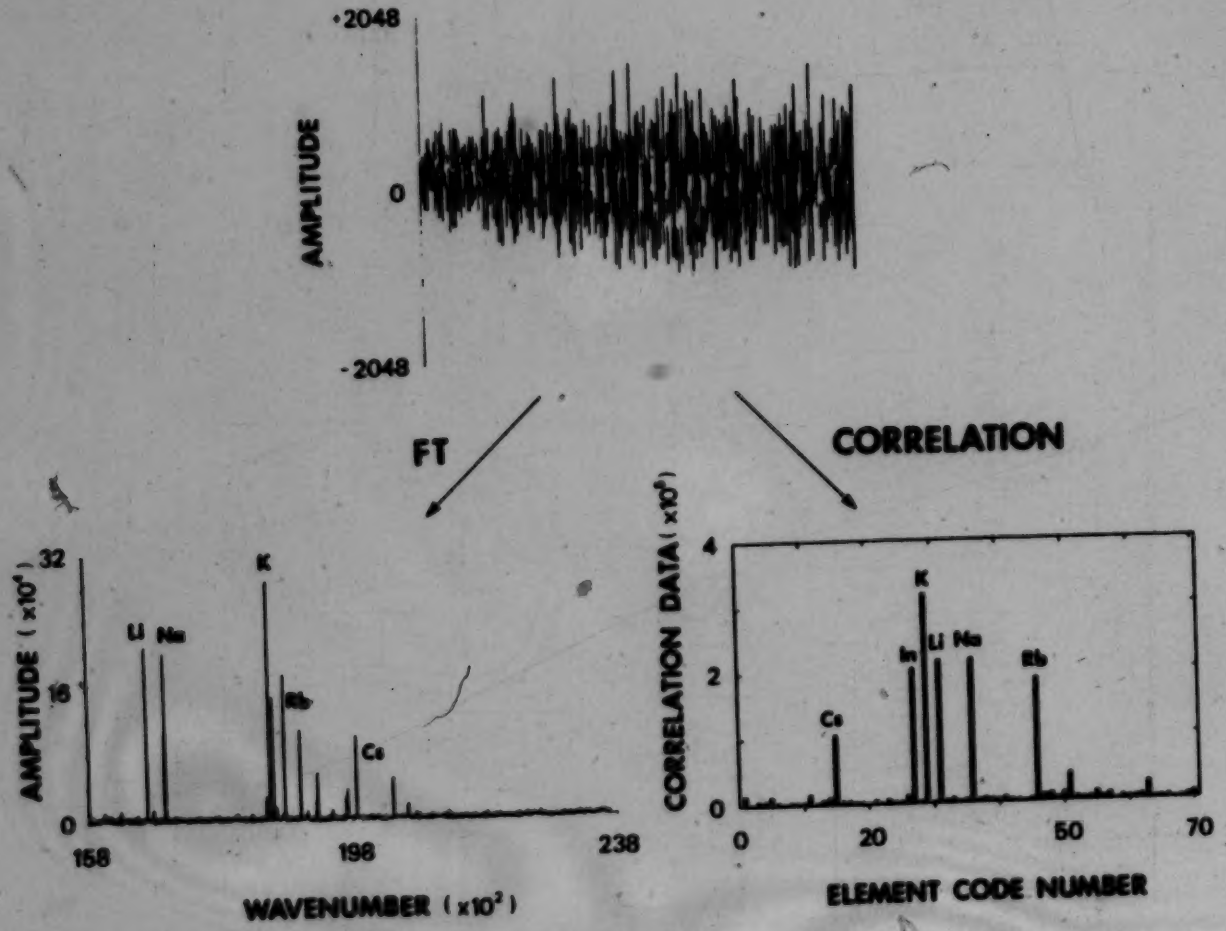


FIGURE 72. Comparison between Fourier transform and correlation data processing methods.

resembles closely in frequency the correlation mask used to extract the desirable analytical information.

With the advent of electronic multiplier chips, correlation analysis which is essentially a process of multiplications and accumulation can be accomplished in real time. In the next chapter, a correlation based real time data processing system using a microcomputer as a controller designed for the ICP-Fourier transform spectrometer system will be described.

# CHAPTER V

## A Real Time Correlation Based Data Processing System for Interferometric Signals

### A. Introduction to Real Time Data Processing Systems for Interferometric Signals

Recent hardware developments have resulted in the appearance of devices capable of essentially real time Fourier transformation of electrical (66) and optical (67) signals. The electro-optical system is particularly interesting in that a two dimensional Fourier transform of an optical image can be generated in a matter of milliseconds. High speed fast Fourier transformation is also available as computer firmware (68). Though the number of data points that the firmware can handle is limited at the present stage, the ultimate goal of performing fast Fourier transformation for a large block of data essentially in real time is not far away. These and future developments are likely to revolutionize the present data processing methods involving Fourier transformation. Applications of these devices to real time data processing for the ICP-Fourier transform spectrometer system may be possible in the near future. In this chapter, a real time data processing system based on the correlation approach will be described. It employs the use of the cross-correlation function at $\tau = 0$ point, in consequence of the success of the software implementation of the correlation

technique upon stored interfergrams described in Chapter IV.

As the fast Fourier transform algorithm for processing interferograms is not involved when correlation techniques are employed, the use of a microcomputer is sufficient for the correlation mathematical computation, even in the case of long interferograms. This can be achieved either in a software or hardware approach. In a software approach, interferograms stored in computer memories can be processed in exactly the same fashion as described earlier. However, correlation which is essentially a process of multiplications followed by accumulation can be hardware implemented more efficiently by utilizing high speed multiplier - accumulator electronic chips. The first prototype of a microcomputer based data processing unit designed for the ICP-Fourier transform spectrometer system will be presented. The basic idea is to use a microcomputer as a controller with a multiplier - accumulator electronic chip acting as the actual data processor. Cross-correlation masks are stored in computer memories and sent out to the multiplier - accumulator at appropriate times for processing. Multiplication between the acquired signal and the correlation mask followed by accumulation is performed in real time. Due to the fact that phase correction is necessary, two individual scans of the same signal are required for one correlation

data point (one for the cosine multiplication and one for the sine multiplication) because only one accumulator is available in the multiplier-accumulator chip.

This system is not meant to be a definitive configuration but was only constructed to test the basic idea of a simple hardware correlation processor.

B. Rockwell AIM 65/TRW Multiplier-Accumulator Data Processing System

A block diagram of the experimental system is shown in Figure 73. It can be subdivided into the following:

(a) Rockwell AIM 65 microcomputer.

(b) Interferometer control and measurement electronics.

(c) Start pulse and clock control circuitry.

(d) Analog to digital conversion circuitry.

(e) TRW multiplier-accumulator.

(f) Data multiplexing circuitry.

The microcomputer acts as a controller for the whole system and as the source of the correlation masks necessary for the data processing. The analog signal (interferogram) from the interferometer system is digitized by the analog to digital conversion circuitry. The computer keeps track of the end of conversion pulse for every signal and as soon as the analog to digital conversion is finished, the

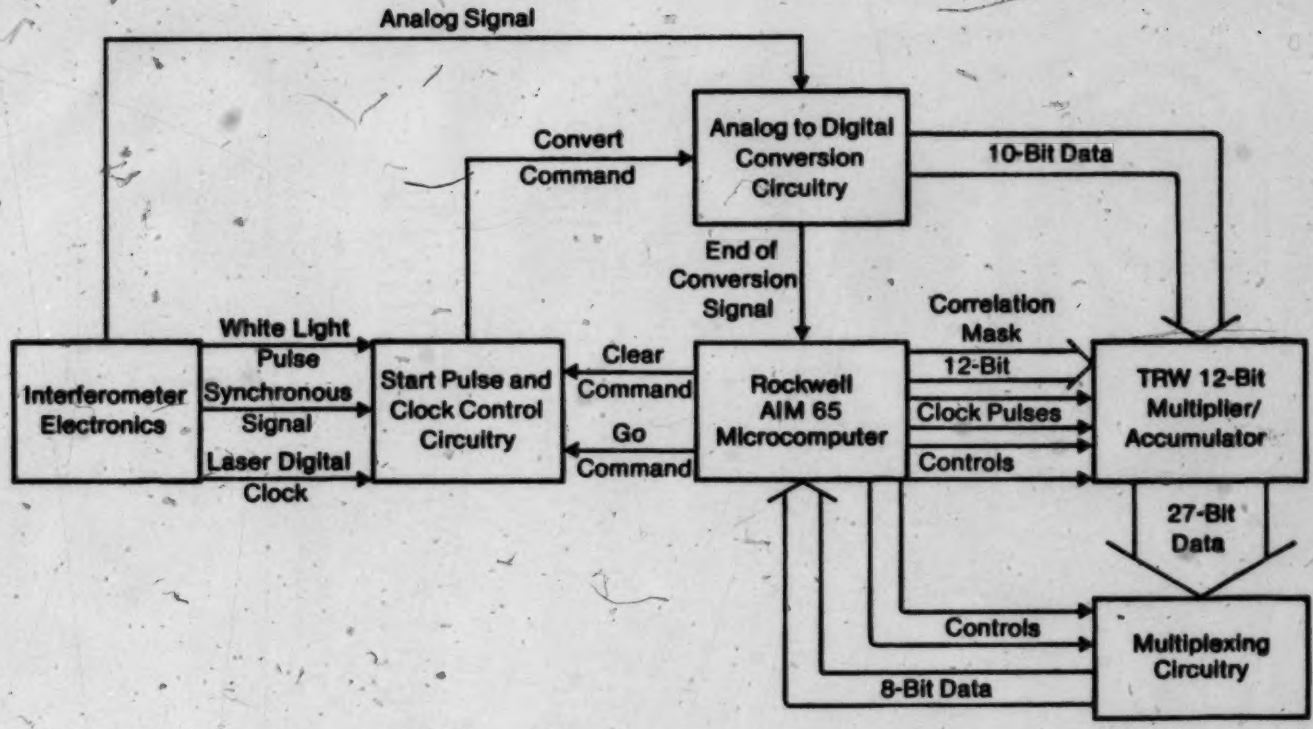


FIGURE 73. Block diagram of the Rockwell AIM 65 microcomputer/TRW multiplier-accumulator data processing system.

appropriate correlation mask data point is fed into the multiplier followed by the appropriate control and clock signals. At the end of a scan, as recognised by the computer, control signals are sent to the multiplexing circuitry in order to multiplex the final data into the computer in 8-bit data segments. This result will then be manipulated as required and output to display.

Start pulse and clock control circuitry which is controlled by the signals coming from the interferometer electronics is incorporated into the system so that the data acquisition/processing will start at the right moment.

Each of these subsystems will now be described in more detail in the following sections.

Rockwell AIM 65 Microcomputer: The "heart" of the data processing system is a Rockwell R6500 Advanced Interactive Microcomputer (AIM 65). It consists of two modules; a master module with a 20-column thermal printer, a 20-character display, and the microcomputer components; a standard keyboard module for communication between the computer and the operator. The R6502 Central Processing Unit (CPU) of the microcomputer operates at 1 MHz. Software support of the AIM 65 computer consists of an 8K MONITOR which includes an EDITOR; 8K BASIC and 4K ASSEMBLER. A typical computer like this with 4K RAM (Random Access

Memory) costs less than $1000 and thus significantly reduces the initial cost of the data processing system.

The interface of the computer with the rest of the system was accomplished through the R6522 Versatile Interface Adapter (VIA) which is available to the user at the Application Connector of the computer. The VIA consists of the following: two 8-bit I/O ports (A and B), four peripheral control/status lines (two for each port), two 16-bit counters/timers and an 8-bit shift register. Only the I/O ports and the control lines were utilized. The detailed configuration of the VIA is shown in Figure 74. Port A I/O lines (PA0-PA7) were used for data input into the computer. The accumulator output from the multiplier-accumulator chip was multiplexed into the computer in 8-bit segments through Port A. There are two peripheral control/status lines at Port A, namely CA1 and CA2. The CA1 line was set up so that the end of conversion signal (1→0 transition) from the analog-to-digital converter could be monitored. A positive pulse which acted as a multiply command signal to the multiplier-accumulator was generated at the CA2 line. Port B I/O lines (PB0-PB7) were used for output control signals and correlation masks. Correlation masks were sent from the computer to the multiplier-accumulator through the PB0 and PB1 lines. Accumulation and output register tristate

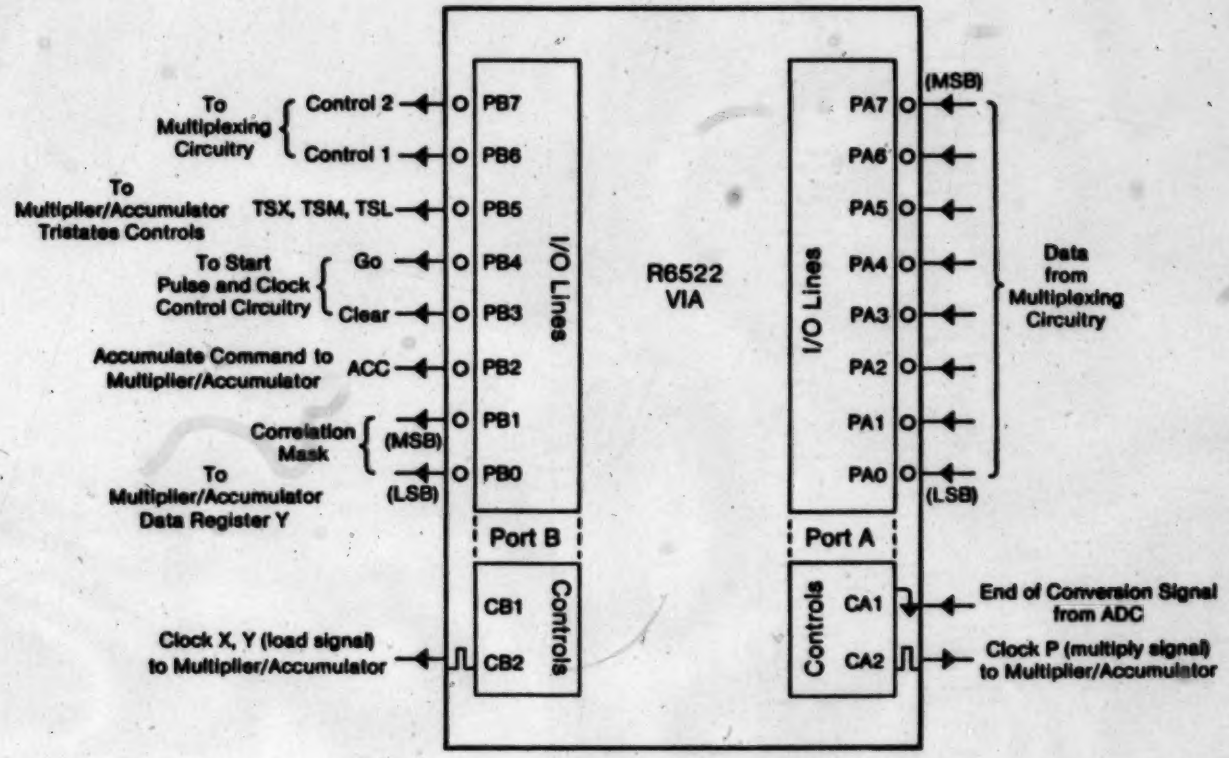


FIGURE 74. Rockwell AIM 65 microcomputer R6522 Versatile Interface Adapter configuration.

controls of the multiplier-accumulator were set by the PB2 and PB5 lines respectively. For multiplexing accumulator data into the computer, two control lines for the multiplexing circuitry were necessary. These were controlled by the computer utilizing the PB7 and PB6 I/O lines. In order to have the whole system running, a CLEAR command followed by a GO command which were software controllable must be issued through the PB3 and PB4 lines respectively. Only one of the two control/status lines at Port B were utilized. The CB2 line was set up to generate a positive pulse as a data loading command signal for the multiplier-accumulator.

The exact sequence of events during the operation of the system is shown schematically in Figure 75 and should be consulted during the discussion of the rest of the system.

Interferometer Control and Measurement Electronics: The interferometer electronics can be subdivided into two parts: a controlling part and a measuring part. The control electronics have been described in detail by Yuen (32) and later by Hall (33). Three digital signals from the control electronics were utilized. They were the white light pulse, the synchronous signal and the laser digital clock. Because of the fact that a single sided interferogram

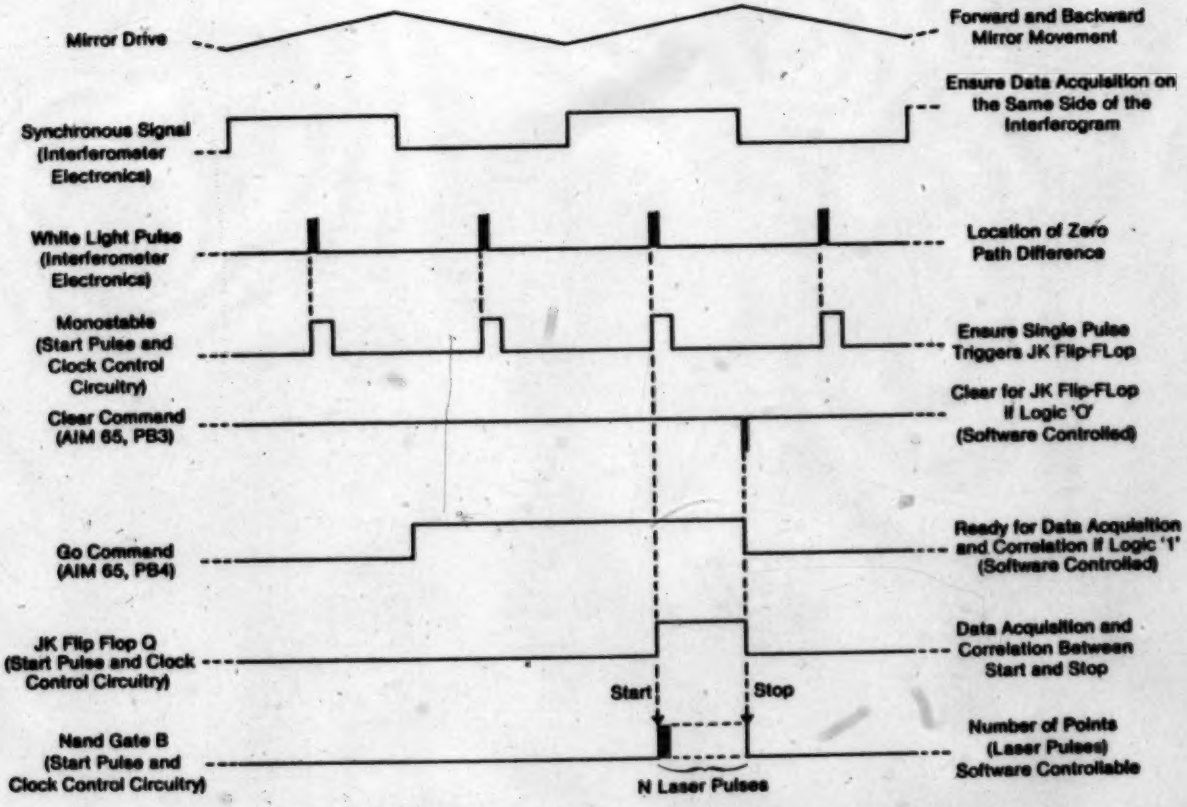
Mirror Drive
Forward and Backward Mirror Movement
Ensure Data Acquisition on the Same Side of the Interferogram
Synchronous Signal (Interferometer Electronics)
White Light Pulse (Interferometer Electronics)
Location of Zero Path Difference
Monostable (Start Pulse and Clock Control Circuitry)
Ensure Single Pulse Triggers JK Flip-FLop
Clear Command (AIM 65, PB3)
Clear for JK Flip-FLop If Logic '0' (Software Controlled)
Go Command (AIM 65, PB4)
Ready for Data Acquisition and Correlation If Logic '1' (Software Controlled)
JK Flip Flop Q (Start Pulse and Clock Control Circuitry)
Data Acquisition and Correlation Between Start and Stop
Start
Stop
Nand Gate B (Start Pulse and Clock Control Circuitry)
Number of Points (Laser Pulses) Software Controllable
N Laser Pulses

FIGURE 75. Timing diagram for the Michelson interferometer/Rockwell AIM 65 microcomputer system.

is sufficient for correlation analysis, the control electronics can be substantially simplified. The phase lock loop used to stabilize the mirror drive, the white light, the synchronous signal and the laser signal are sufficient for the full operation of the correlation data processing system. However, the three signal outputs were obtained directly from the control electronics circuitry to maintain the proper operation of the original system.

The white light pulse, together with the synchronous signal and the laser digital clock signal were connected directly into the start pulse and clock control circuitry. The white light pulse was used as the start pulse for the data acquisition and processing. The interferogram obtained after the zero path difference point between the two mirrors in the interfermeter as indicated by the appearance of white light pulses during the forward movement of the mirror was used as the signal for processing. This was recognized by the electronics with the aid of the synchronous signal. The laser digital signal was used as the conversion clock for the analog to digital conversion circuitry.

The measurement end of the interferometer electronics was described under the experimental section in Chapter IV. The analog bipolar signal was adjusted to be within a ±10 V range and was connected to the analog input of the analog

to digital conversion circuitry.

Start Pulse and Clock Control Circuitry: A schematic diagram of the start pulse and clock control circuitry is shown in Figure 76. The start pulse and the digital clock were all controlled by computer software. First, the comparator that converted the analog white light into pulses was set at a threshold so that normally three pulses were generated. Three instead of one were utilized because it was very difficult to maintain the threshold level to give only one pulse. This train of pulses was then converted into a single pulse by a monostable whose delay time was set to about ten milliseconds. This ensured that only one clock pulse would trigger the JK flip-flop which then started the data acquisition and processing. Refer to the timing diagram in Figure 75 for the exact sequence of events. The data acquisition and processing would start if and only if the computer issued a GO command (VIA PB4) and the white light pulse occurred during the forward movement of the mirror as distinguished by the synchronous signal. At this time, the laser digital clock appeared at the output of the NAND gates and thus triggered the conversion cycle of the analog-to-digital converter. If the computer did not issue a GO command, a logic level of '0' appeared at the output of the NAND B gate and the system would be at the waiting

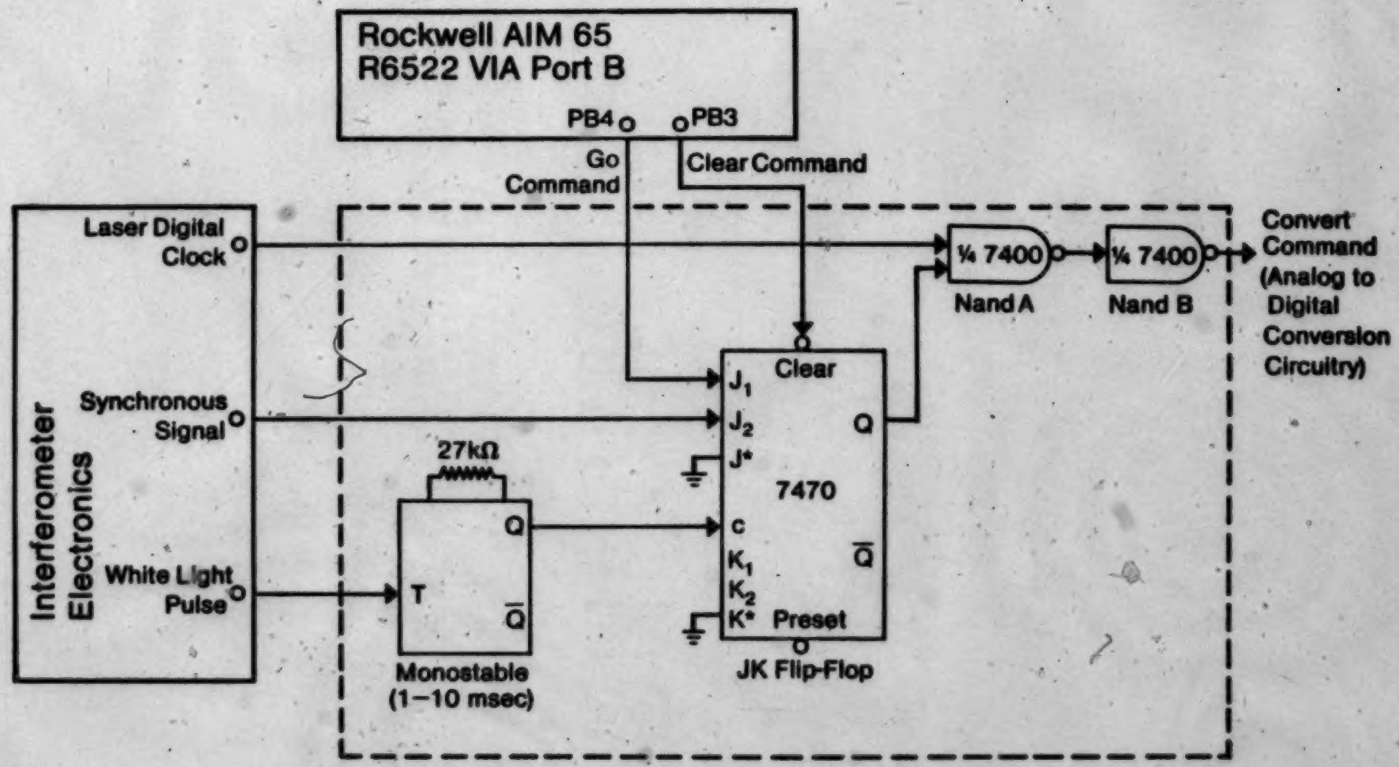


FIGURE 76. Start pulse and clock control circuitry.

stage. Whenever a signal was acquired and processed, the microcomputer would issue a CLEAR command through the VIA PB3 I/O line to clear the JK flip-flop to be ready for the next signal.

Analog to Digital Conversion Circuitry: The analog to digital conversion circuitry is shown in Figure 77. It consists of a 12-bit compatible sample and hold (Analog Devices, Sample and Hold SHA 1A) and a 10-bit analog-to-digital converter (Analog Devices, Analog-to-Digital Converter ADC 10Z-002). The settling time for the sample and hold is five microseconds and the conversion time for the analog-to-digital converter is twenty microseconds. They were wired according to the specifications recommended by Analog Devices (69,70).

The analog-to-digital converter operated under its internal clock during conversion of bipolar signals within ±10 V range. It was not calibrated against a standard reference voltage nor zero adjusted for this preliminary investigation. Obviously, a 12-bit analog-to-digital converter which has been calibrated and zero adjusted is a better choice for the system, but none were available in the laboratory for this application.

When the laser digital clock was used as the convert command for the analog-to-digital converter, the microcom-

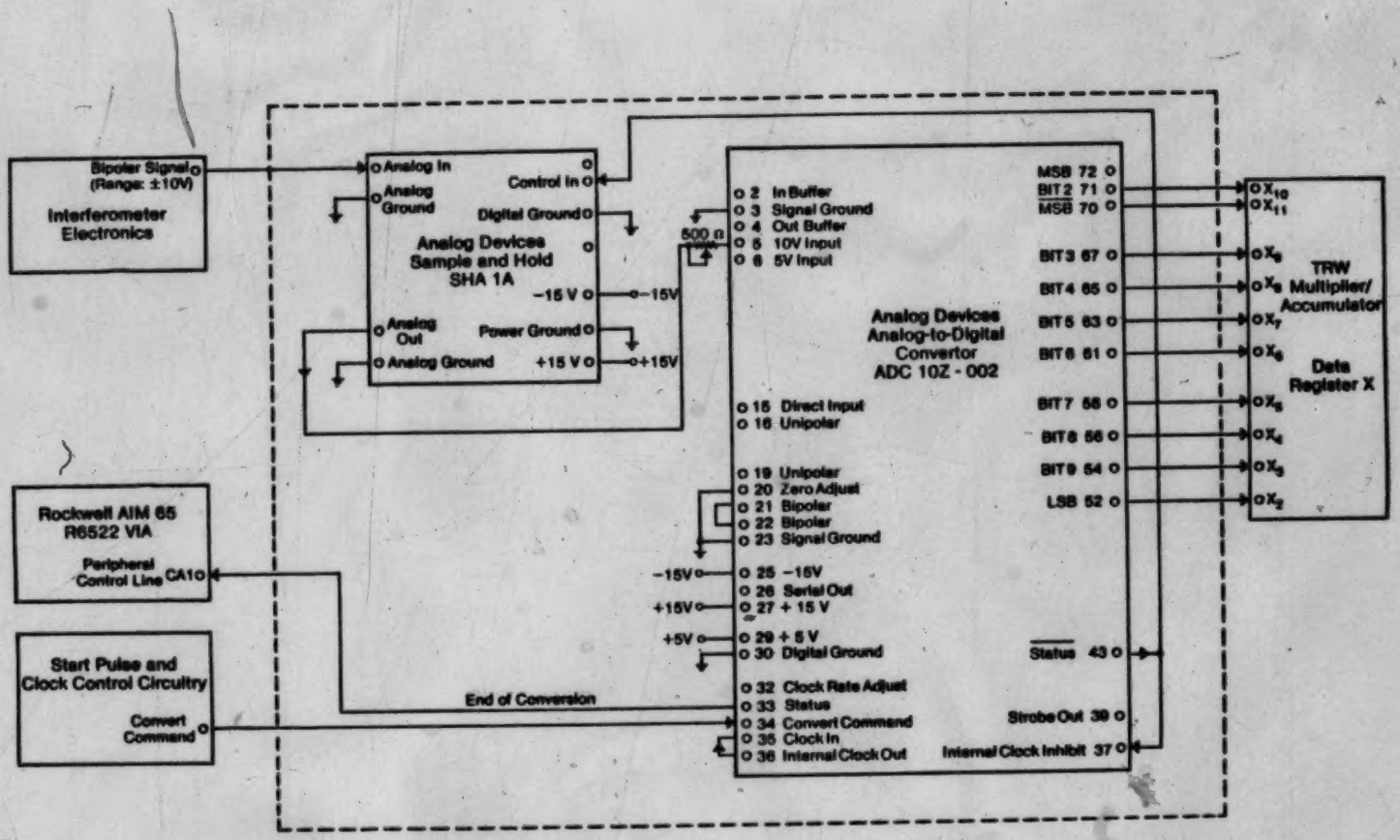


FIGURE 77. Analog to digital conversion circuitry.

puter kept track of the end of conversion. This was accomplished by the connection of the VIA CA1 line to the STATUS pin available in the analog-to-digital converter. In this way, the computer would generate appropriate correlation masks and control signals for data processing at the end of every conversion. The 10-bit digital output in two's complement format, corresponding to the analog signal, was continuously available to the data register X of the TRW multiplier-accumulator after every conversion.

TRW Multiplier-Accumulator: The 64-pin multiplier-accumulator chip, MAC (TRW, Inc., TDC 1009J) is a high speed TTL LSI device capable of performing a multiplication between two parallel 12-bit data and product accumulation in 95 nanoseconds (71). It consists of two 12-bit data registers, X and Y. Data are loaded into the registers X and Y at the rising edge of the clock pulses applied at CLK X and CLK Y respectively. Multiplication is performed between the two numbers in the data registers, followed by product accumulation at the rising edge of CLK P. The 27-bit output register is tristate controlled. It can be outputted in three segments, least significant 12-bit ($P_0$-$P_{11}$), most significant 12-bit ($P_{12}$-$P_{23}$) and extended most significant 3-bit ($P_{24}$-$P_{26}$). They are controlled by the TSL, TSM and TSX tristate control signals respectively.

A logic '0' at TSL, TSM, TSX will enable the output drivers.

The detailed configuration of the MAC is illustrated in Figure 78. The numerical system was configured in two's complement to be compatible with the analog-to-digital converter output. Since only 10-bit data were available from the analog-to-digital converter, the least significant two bits ($X_0$ and $X_1$) of the data register X were grounded. When the end of conversion signal was detected by the computer, a correlation mask data point was fed into the data register Y of the MAC through 2 VIA I10 lines (PB0 and PB1). The reason why only 2 lines were used for a 12-bit correlation mask will be explained later along with the computer software. Once everything was ready, the peripheral control line CB2 of the microcomputer would generate the data loading clock pulses (CLK X and CLK Y) so that data were entered into the registers. The peripheral control line CA2 would then generate the multiply command (CLK P) to finish off the multiplication and accumulation process for one data point. The whole cycle was repeated for another data point until finished.

Before data acquisition, it was necessary to preload the accumulator of the MAC with zeros. This was

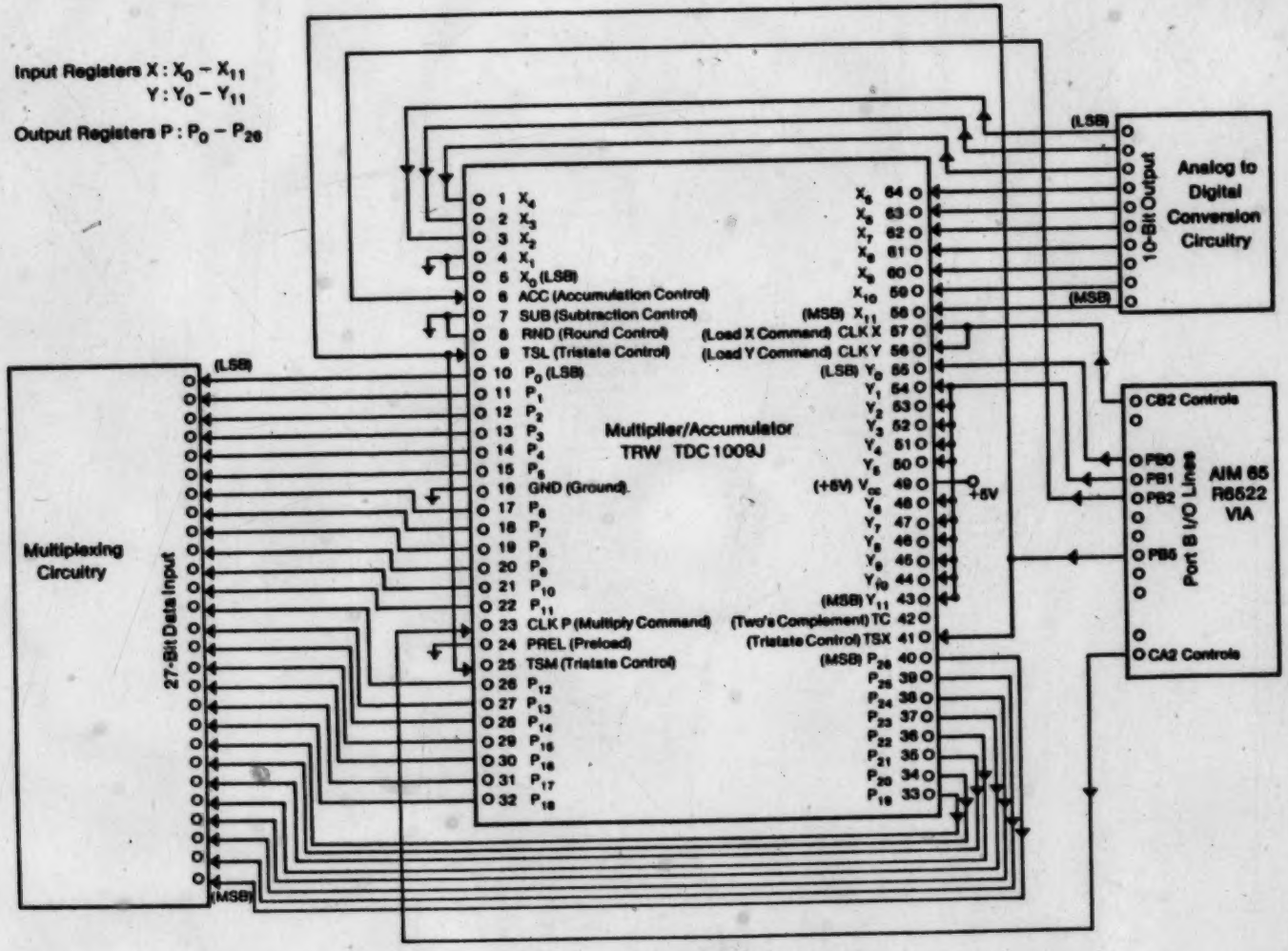


FIGURE 78. TRW multiplier-accumulator configuration.

achieved by the use of the non-accumulating mode of the MAC (logic '0' at ACC). Data register Y was filled with zeros through the use of PB0 and PB1 I/O lines. After the generation of the clock pulses (CLK X,Y, and CLK P), a zero product resulted in the accumulator. At this point, the MAC was configured back to its accumulating mode (logic '1' at ACC) to be ready for data acquisition. The 27-bit accumulator output drivers were opened at the end of one scan by the use of TSX, TSM, TSL command signals. The accumulator content was loaded into the computer through the multiplexing circuitry. This was necessary because the computer could only handle 8-bit data at one time.

Data Multiplexing Circuitry: The MAC output register (27-bit) was multiplexed into the computer as three 8-bit and one 3-bit data points. A block diagram of the data multiplexing circuitry is shown in Figure 79. It consists of a 2-line to 4-line decoder and an array of 27 tristates. The controls of the tristates were governed by the four output lines of the 2-line to 4-line decoder. The inputs to the 2-line to 4-line decoder were under computer control. A maximum of eight tristates were enabled at one time. The detail configuration of the 2-line to 4-line decoder which was made up of six NAND

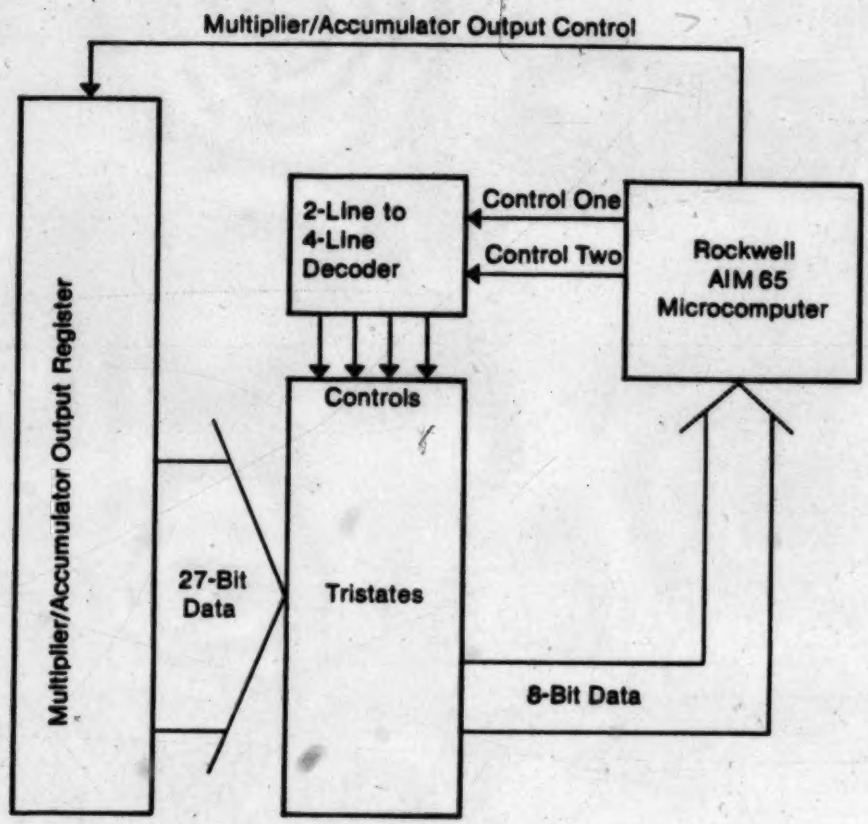


FIGURE 79. Block diagram of the data multiplexing circuitry.

gates is shown in Figure 80. The PB6 and PB7 I/O lines were the two control lines from the computer. Only one of these four outputs of the 2-line to 4-line decoder would be at a logic '0' which would open up to a maximum of eight tristates at one time. The data transfer from the MAC to the Port A of the computer is better understood with the aid of Figure 81. During the transfer of data, the output data register of the MAC was enabled and this was easily accomplished by feeding a logic '0' to the tristates controls (TSL, TSM, TSX) of the MAC through the PB5 line of the VIA.

Computer Software: The program was written in BASIC and ASSEMBLER languages. It was initiated under BASIC and would request a wavelength input for the calculation of correlation masks. Correlation masks were calculated in the form of square synthetic interferograms as described in Chapter IV and thus consisted of values +1, 0 and -1 only. The 12-bit binary equivalences of these numbers are shown in Table 9. As it can be seen, the information of the correlation masks can be transferred with the aid of only two I/O lines. The PB0 line of the VIA was used for the least significant bit and the PB1 line of the VIA was used for the most significant 11 bits of the correlation masks to be transferred from the computer

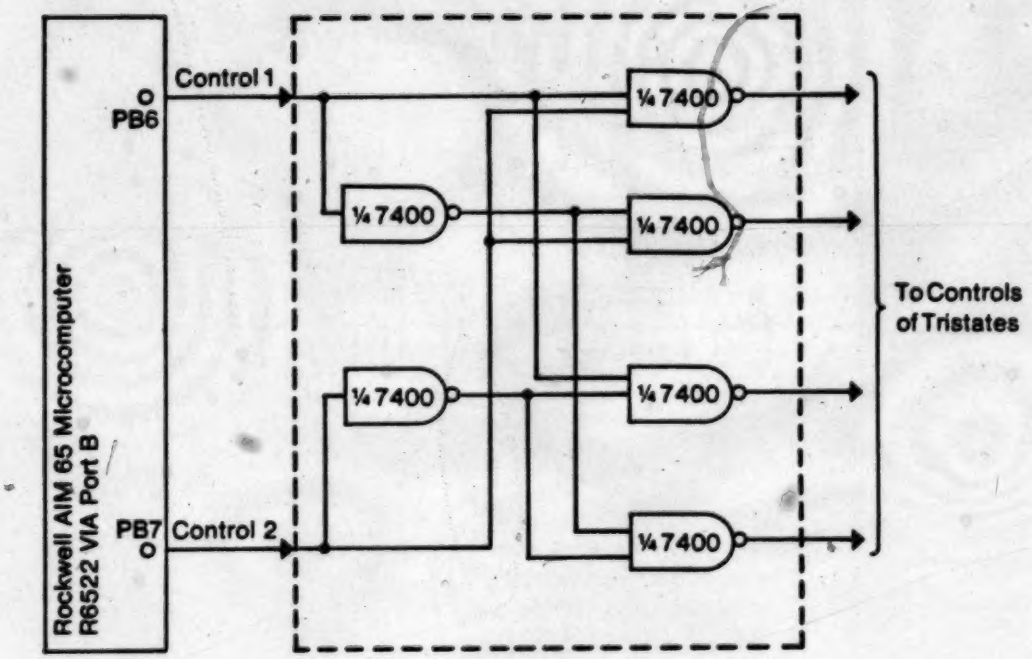


FIGURE 80. Two-line to four-line decoder of the data multiplexing circuitry.

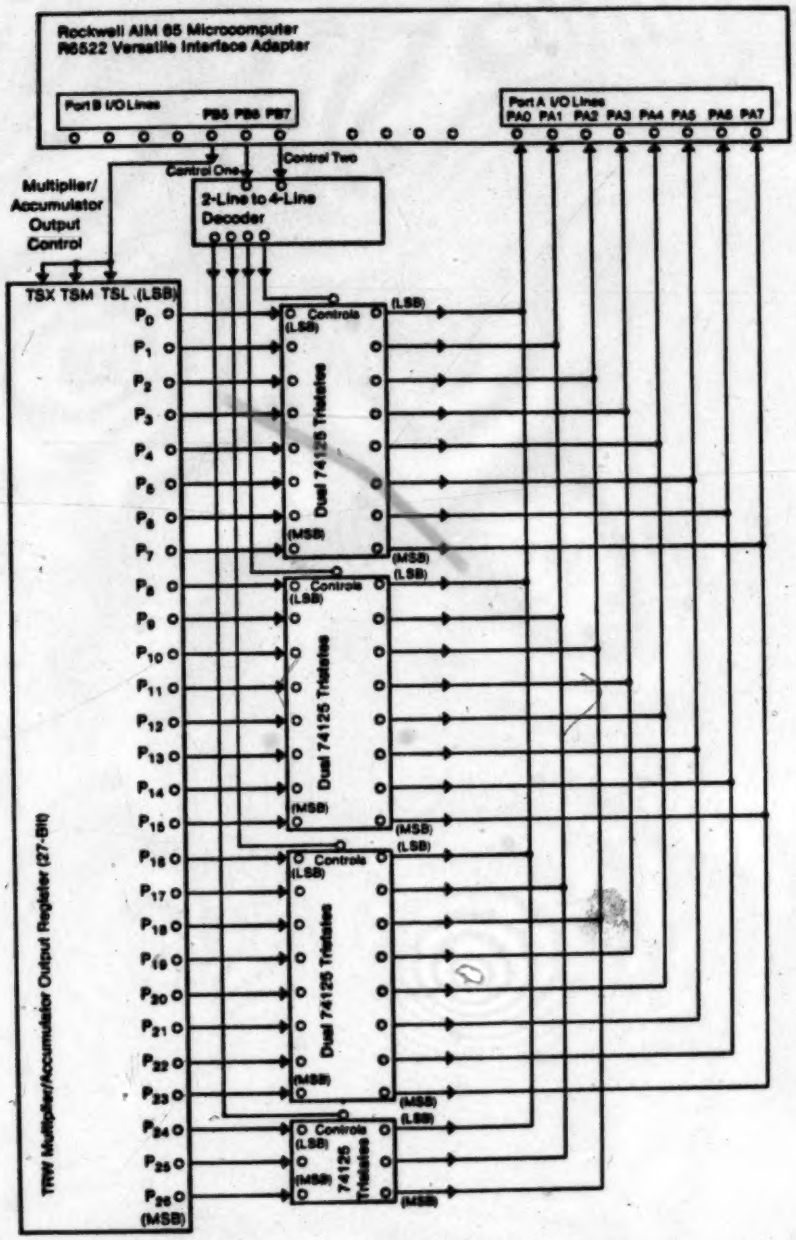


FIGURE 81. Multiplexing circuitry between the AIM 65 microcomputer and the TRW multiplier-accumulator.

TABLE 9. Binary equivalence of the correlation masks.

| Correlation Mask | 12-bit Binary Equivalence |
|---|---|
| +1 | 000000000001 |
| 0 | 000000000000 |
| -1 | 111111111111 |

to the MAC. The BASIC program stored the correlation masks (both sine and cosine) in decimal as shown in Table 10. The decimal equivalence also included the information for pins PB2 to PB7. These were the control signals used to operate the system. The memory location of the correlation masks are indicated in the memory map shown in Table 11.

The BASIC program then requested the ASSEMBLER subroutine which was entered into the computer with the aid of the Text Editor. The ASSEMBLER subroutine controlled the data acquistion and correlation data processing after preloading the accumulator of the MAC with zeros. The whole procedure was repeated twice, one for the cosine correlation and one for the sine correlation. The accumulator outputs stored in the memory by the ASSEMBLER subroutine were converted into the decimal mode by the BASIC program and outputed onto the display and printer. The whole process could be repeated for another set of data with the same or a new correlation mask. This program was initially set for acquiring 256-point interferograms and signal averaging capability was not available. However, the program can be modified to expand its capability.

Program flow charts and listings are included in

TABLE 10. Decimal equivalence of the correlation masks as generated by the BASIC program.

| Correlation Mask | VIA Port B I/O Lines | | | | | | | | Decimal (Hex) Equivalence |
|---|---|---|---|---|---|---|---|---|---|
| | PB7 | PB6 | PB5 | PB4 | PB3 | PB2 | PB1 | PB0 | |
| +1 | 1 | 1 | 1 | 1 | 1 | 1 | 0 | 1 | 253 (FD) |
| 0 | 1 | 1 | 1 | 1 | 1 | 1 | 0 | 0 | 252 (FC) |
| -1 | 1 | 1 | 1 | 1 | 1 | 1 | 1 | 1 | 255 (FF) |

TABLE 11. Memory map of the AIM 65 microcomputer.

| Type | Address | | | |
|---|---|---|---|---|
| | Hexidecimal | | Decimal | |
| | Start | End | Start | End |
| BASIC (internal use) | 0000 | 0211 | 0000 | 0529 |
| BASIC program | 0212 | 06FF | 0530 | 1791 |
| Assembler program | 0700 | 07FF | 1792 | 2047 |
| Text editor | 0800 | 0BFF | 2048 | 3071 |
| Correlation mask (cosine) | 0C00 | 0CFF | 3072 | 3327 |
| Correlation mask (sine) | 0D00 | 0DFF | 3328 | 3583 |
| Results | 0E00 | 0EFF | 3584 | 3839 |
| Index (used by Assembler) | 0F00 | 0F00 | 3840 | 3840 |
| Assembler symbol table | 0F01 | 0FFF | 3841 | 4095 |

Appendix III. For further details, the AIM 65 manuals (72,73) should be consulted.

C. Evaluation of the Rockwell AIM 65 / TRW MAC Data Processing System

Qualitative Aspects: The qualitative aspect of the system was tested out using a relatively simple signal, a He-Ne laser. The interferometric response was limited to the near IR-visible region because a silicon diode detector was used. The interferogram, which was a very simple cosine wave carrying the characteristic information about the laser was correlated with masks generated from the wavelengths indicated in Table 12. The lines for the alkali metals were used because they are the prominent lines present in this region. The resulting correlation data based on two repetitions of the signal are shown in Figure 82. It can be seen that the correlation mask corresponding to the wavelength of the He-Ne laser shows a relatively high correlation result while all the others do not.

The second test involved the use of the signal from a magnesium hollow cathode lamp. The spectrum of the magnesium hollow cathode lamp is shown in Figure 83. This spectrum was obtained after Fourier

TABLE 12. Some spectral lines in the near IR-visible region.

| Species | Spectral Line | |
|---|---|---|
| | Code Number | Wavelength (nm) |
| Na | 1 | 589.0 |
| | 2 | 589.6 |
| He-Ne Laser | 1 | 632.8 |
| Li | 1 | 670.8 |
| K | 1 | 766.5 |
| | 2 | 769.9 |
| Rb | 1 | 780.0 |
| | 2 | 794.8 |
| Cs | 1 | 852.1 |
| | 2 | 894.4 |

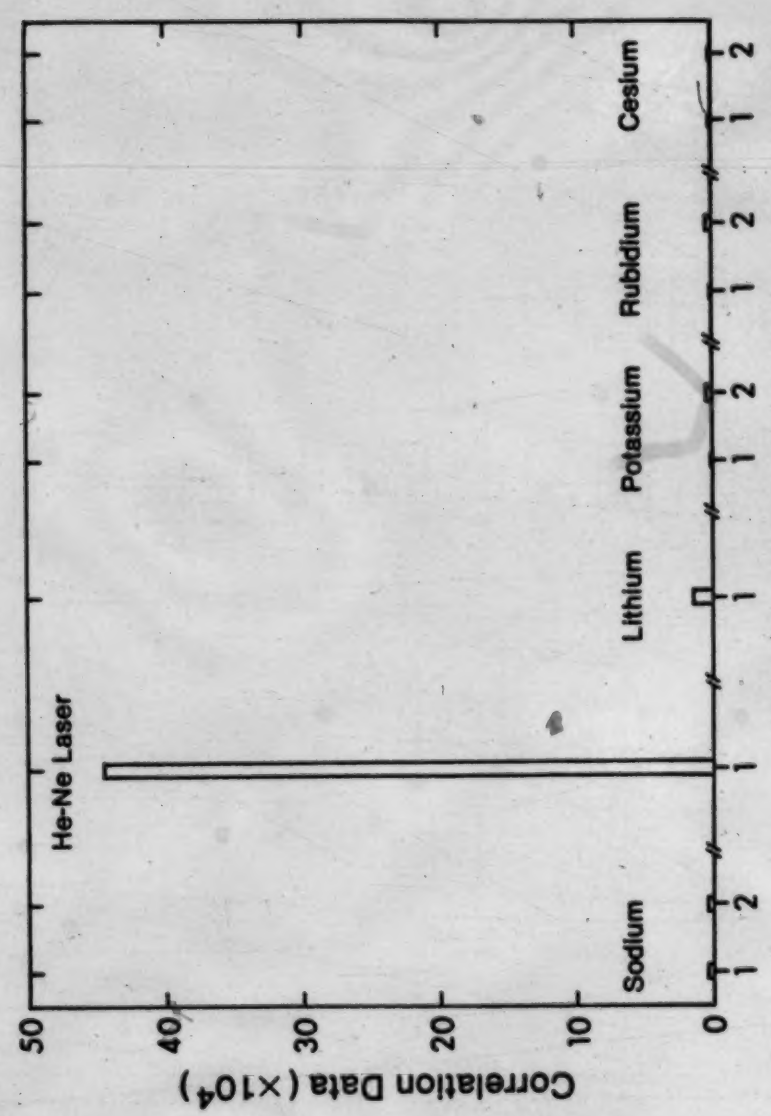


FIGURE 82. Cross-correlation analysis on a He-Ne laser signal.

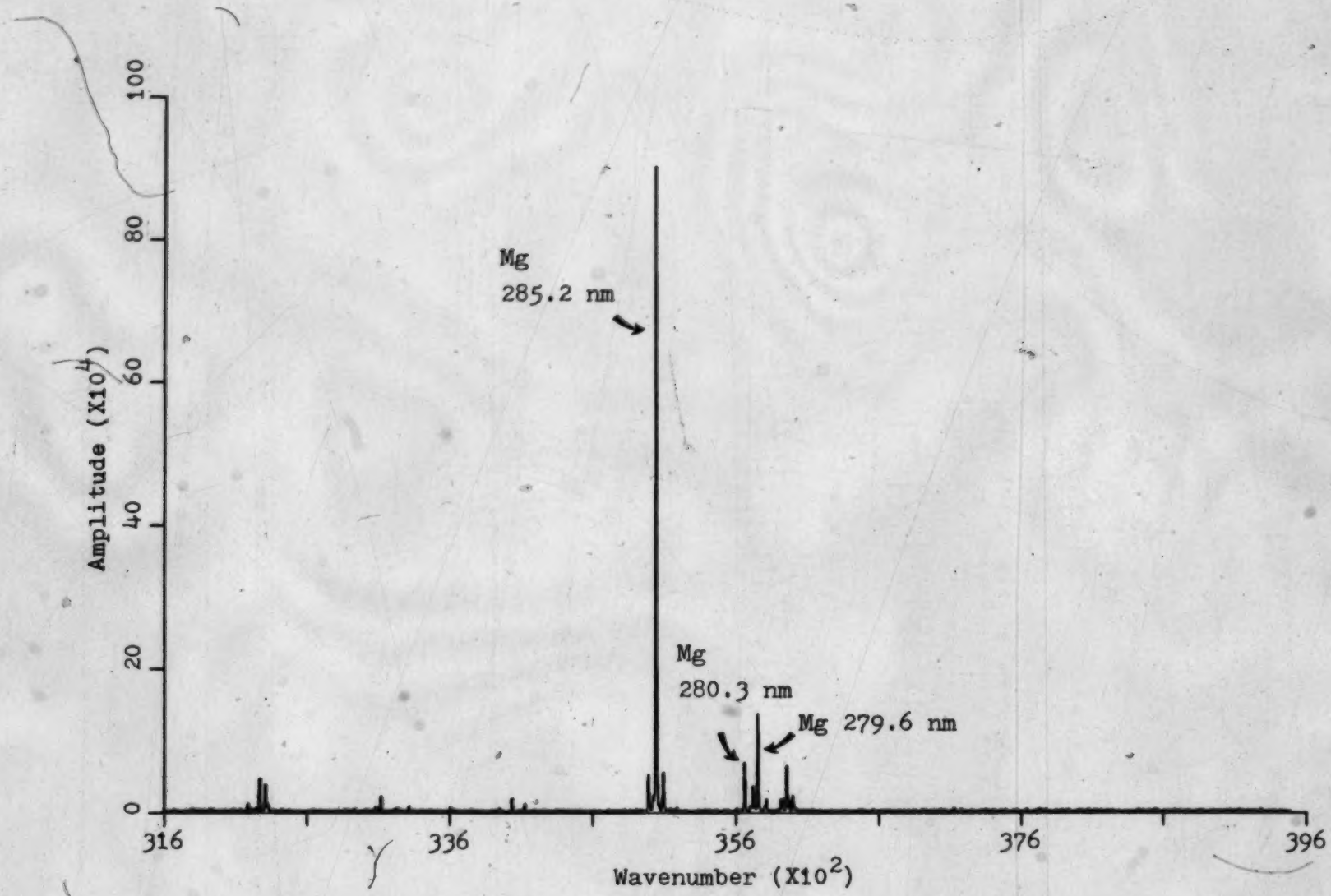


FIGURE 83. A magnesium hollow cathode lamp spectrum.

transformation of a 4096-point interferogram with the aid of the minicomputer used in the system described in Chapter IV. One has to keep in mind that the resolution of the signal obtained using the AIM 65 microcomputer (256-point interferogram) is not as good as the one obtained using the minicomputer (4096-point interferogram). The spectrum is shown here to indicate what spectral information is available from the magnesium hollow cathode lamp. From the spectrum, it can be seen that Mg 285.2 nm line is the prominant line present in the signal, followed by Mg 279.6 nm line and 280.3 line. This signal was obtained using the solar blind optical filter and the visible PMT detector. Correlation masks based on the wavelengths shown in Table 6 were generated and used to perform real time data acquistion / processing with this system. The correlation data are shown in Figure 84. There is no distinct indication that Mg is the major component because the wavelengths indicated in Table 6 correspond to the major emission lines available from the ICP not the hollow cathode lamp. With the signal obtained from the hollow cathode lamp,the 285.2 nm line instead of the 279.6 nm line is the prominent line. This, together with the lower resolution offered by the system accounts for the high "background" for the other elements. However, the secondary correlation process was able to sort out

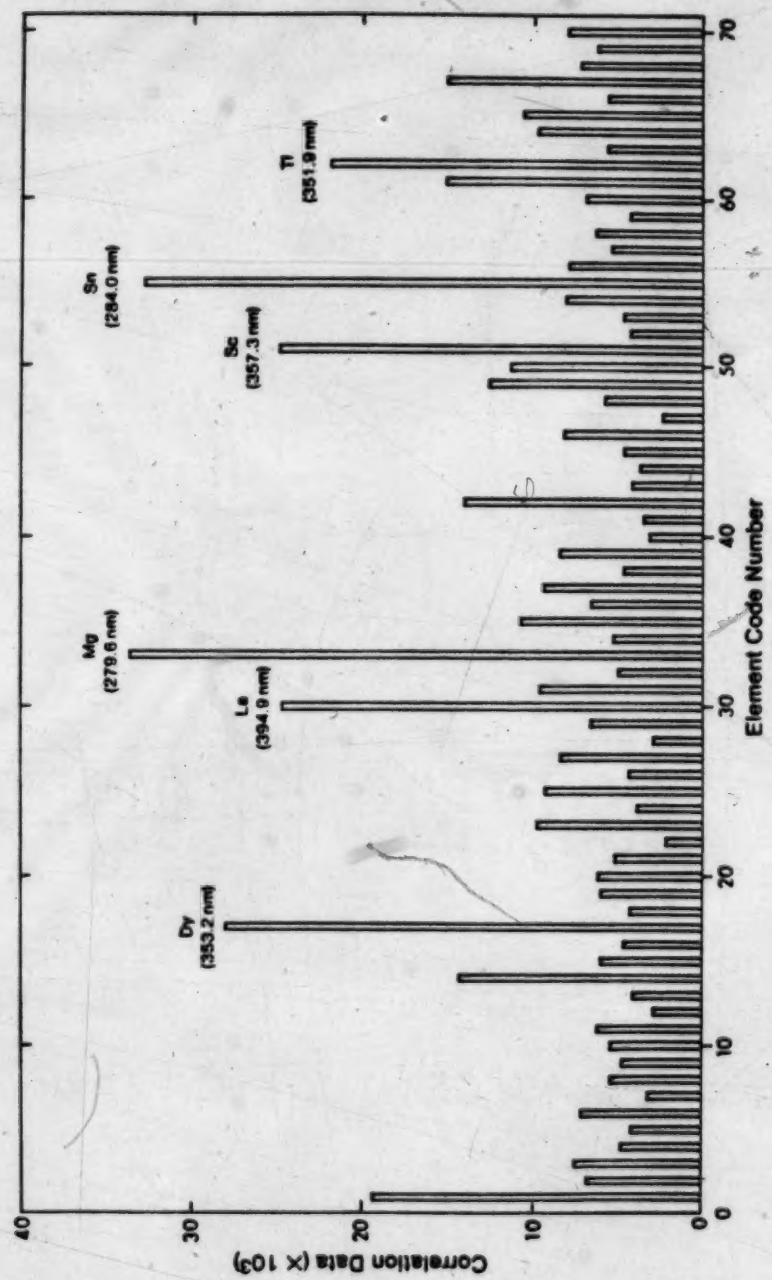


FIGURE 84. Cross-correlation analysis on a magnesium hollow cathode lamp signal.

the information present in the signal. The elements that showed relatively high correlation results, namely dysprosium, lanthanum, magnesium, scandium, tin and thallium were further correlated at secondary ICP lines. Dysprosium does not have any other intense lines present in this region and could not be further correlated. In the case of lanthanum, it is very unlikely that it was present due to the poor response of the detector for any spectral information outside the 240 nm - 360 nm region. The remaining six elements were then further tested with the secondary correlation analysis. The wavelengths used to generate the secondary cross-correlation masks can be found in Table 13. The secondary correlation results, as shown in Figure 85, clearly indicate the presence of magnesium information in the signal. From this example, the importance of the right choice of the spectral wavelengths used to generate cross-correlation masks is clear.

Quantitative Aspects: Linear working curves for He-Ne laser (632.8 nm) and magnesium (285.2 nm) signals are illustrated in Figures 86 and 87 respectively. These "analytical curves" were obtained using neutral density filters to alter the signal levels. Thus, the concentration axis in both cases are relative in scale and have no resemblence

TABLE 13. Most sensitive ICP spectral lines of magnesium, scandium, tin and thallium within the 240-360 nm window.

| Element | Spectral Line | |
|---|---|---|
| | Code Number | Wavelength (nm) |
| Mg | 1 | 279.6 |
| | 2 | 280.3 |
| | 3 | 285.2 |
| Sc | 1 | 357.3 |
| | 2 | 335.4 |
| | 3 | 357.6 |
| Sn | 1 | 284.0 |
| | 2 | 286.3 |
| | 3 | 270.7 |
| Tl | 1 | 351.9 |
| | 2 | 276.8 |
| | 3 | 291.8 |

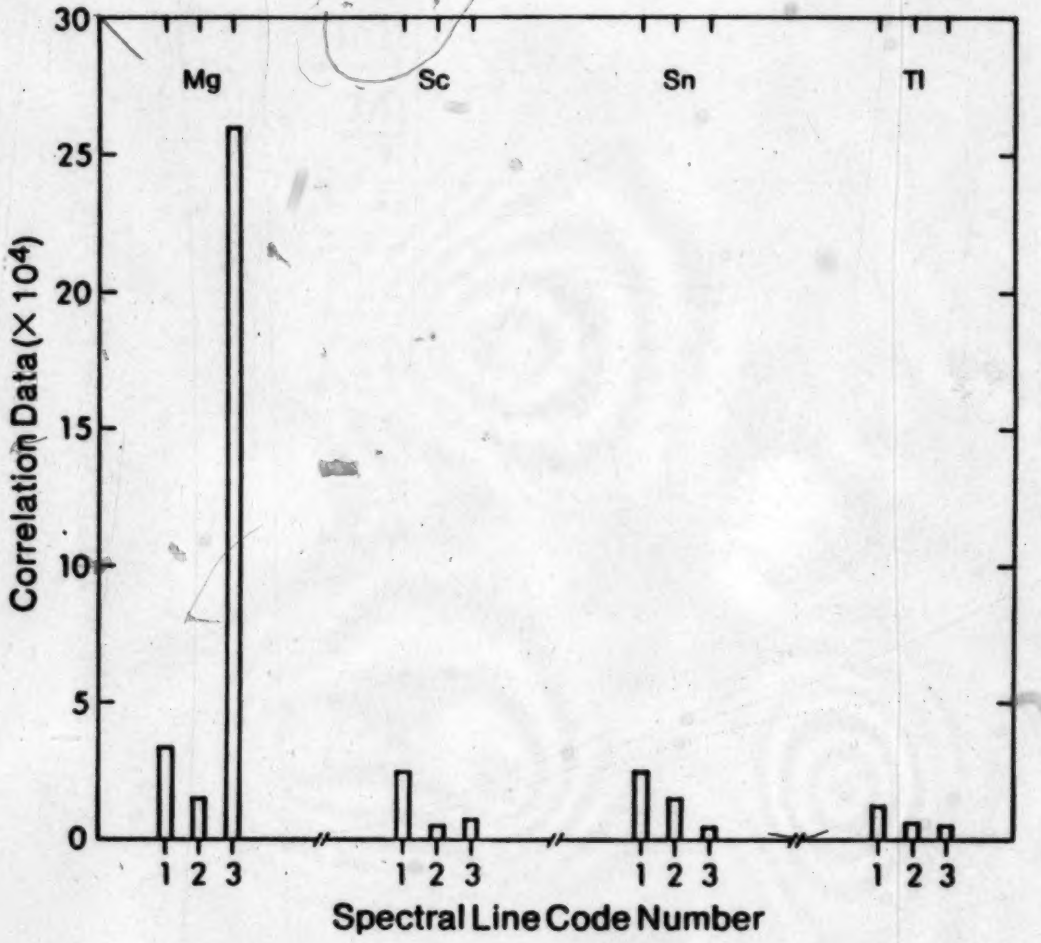


FIGURE 85. Secondary cross-correlation analysis on the magnesium hollow cathode lamp signal.

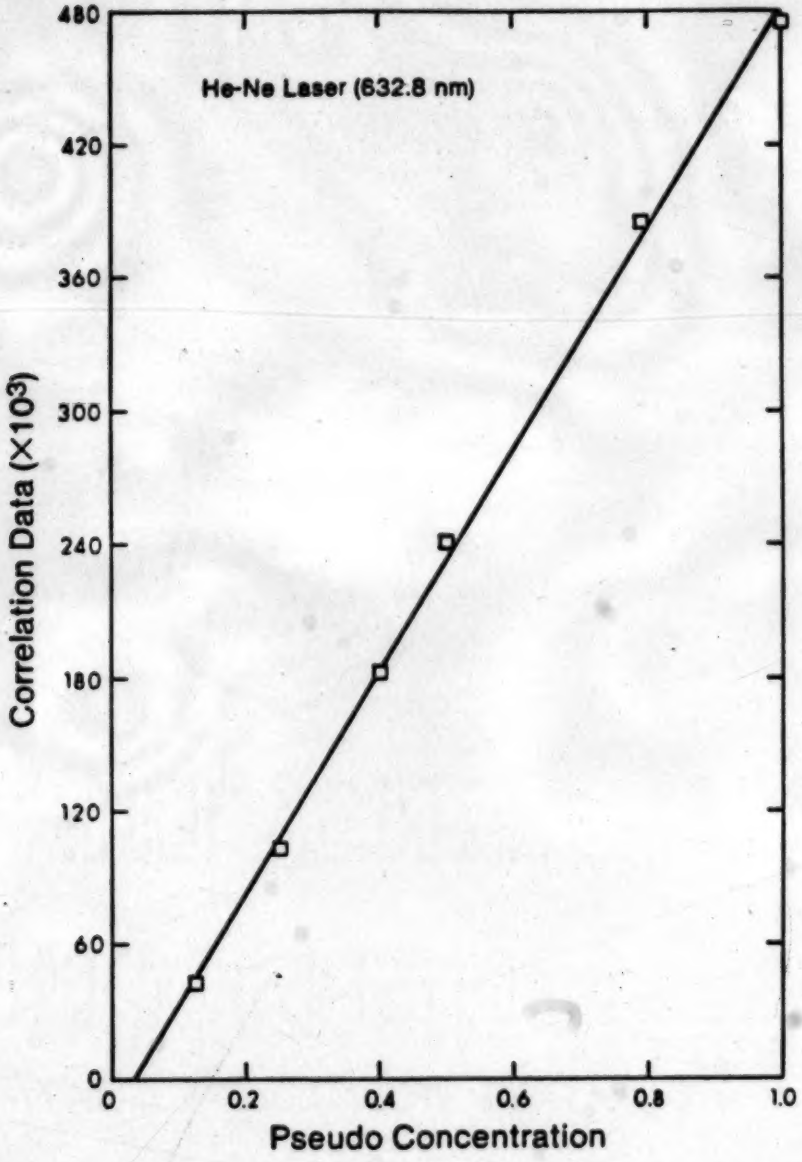


FIGURE 86. "Analytical working curve" for the He-Ne laser (632.8 nm).

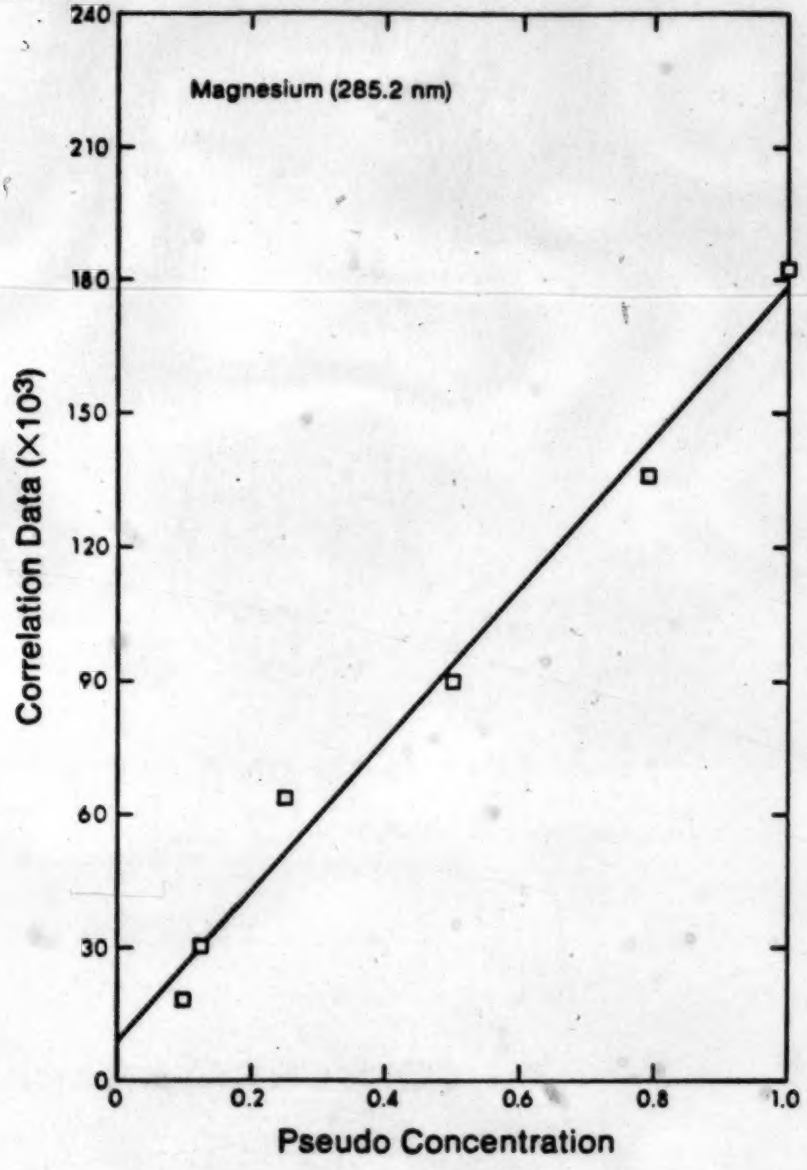


FIGURE 87. "Analytical working curve" for magnesium (285.2 nm).

at all to the actual level of the signals. These pseudo analytical curves are included to demonstate the quantitative aspect of this real-time data acquistion / processing system.

The precision of the data obtained with this system was typically in the range of 9 to 10 % relative standard deviation (rsd). It can at best attain a rsd of 4 to 5 % depending on the wavelength and the amplitude of the signal. This modest level of precision is limited by the fact that phase correction has not been performed on the same set of data. Any change in phase or amplitude between scans would contribute to the scattering of the readings. The solution to this problem is to implement phase correction on a single scan of signal with cosine and sine correlations performed simultaneously. This can be easily achieved with the use of two MAC's.

D. Conclusions and Prospects

At the present stage, the Rockwell AIM 65 micro-computer / TRW MAC system cannot function properly during the operation of the ICP due to radiofrequency interference originating in the plasma power supply. This is the reason why no actual ICP experimental data could be presented. This interference problem should be able to

be completely eliminated by properly packaging the whole system and also by the use of by-pass capacitors on every single electronic chip that has been used in this system. Further details on the use of by-pass capacitors can be obtained in reference 74. These have not been tried at this stage because the system requires a major modification to incorporate two MAC's into the system for better quantitative data.

All the results obtained are all based on a 256-point interferogram and the system can certainly be expanded to increase the resolution (i.e. decrease spectral interferences). There is actually no limitation on the length of interferograms that the system can handle, because the signal obtained is processed in real time and is not stored in the memory of the computer which normally imposes a limitation on the number of data points to be processed. However, in the case of long interferograms, the accumulator register of the MAC has to be checked for overflow.

The data processing system can be modified to a single channel slew scan type processor with the use of 2 MAC's or a multichannel direct reading type processor with the use of more than 2 MAC's. In the case of the latter design, one pair of MAC's would be dedicated for one

spectral line and true simultaneous multielement analysis can be accomplished. The use of the square synthetic interferogram correlation masks can be very beneficial to the system. The correlation masks have values of +1 and -1 with rare occasions that the value is exactly equal to zero. Thus, the zeros can be replaced by either +1 or -1 value with no substantial effect on the selectivity of the cross-correlation masks. A significant saving of computer memory for storing correlation masks can be achieved. High speed real time correlation analysis is possible if all the masks can be stored in ROM, instead of wasting computation time for the generation of the correlation masks. Moreover, correlation masks can be input into the MAC's more efficiently because one byte (8-bit) of data output will be able to feed 8 MAC's with correlation masks simultaneously. The AIM 65 microcomputer is limited by its 4K RAM and it should be expanded to increase its versatility. A large number of correlation masks can then be stored in ROM and recalled whenever they are necessary.

Based on these, a versatile, flexible and inexpensive real time correlation based data processor should be able to emerge for the ICP-Fourier transform spectrometer system. In fact, it should be treated as a general

purpose data processor for interferometric signals.

## CHAPTER VI

### Summary

In this study, the feasibility of automatically processing spectral data by cross-correlation techniques has been investigated. In particular, cross-correlation functions at $\tau=0$ point have been utilized. The basic approach involves cross-correlation of the raw spectral signal with a noise-free mask of the sought-for spectral pattern at zero phase shift. Various types of cross-correlation masks have been evaluated as to their effectiveness of spectral signal detection. These cross-correlation masks were either experimentally or computer software generated.

For an inductively coupled plasma - photodiode array spectrometer (ICP-PDA) system, several analog and binary spectral masks originating from high signal-to-noise ratio spectra of the sought-for elements were utilized to process the analytical information available. Both analog and binary cross-correlation masks clearly showed their effectiveness in extracting sought-for spectral information from complex multielement emission spectra. Spectral overlap problems were overcome by the use of highly selective cross-correlation masks. Furthermore, with the use of these cross-correlation masks, all the spectral information related to the sought-for chemical

species available from the system were fully utilized. In this way, the analytical data obtained were better than those obtained using the conventional single peak methods in terms of sensitivity and precision. Due to the limited spectral coverage of the ICP-PDA system, correlation analysis could not be utilized to its full potential, but the prospects of this technique certainly look good if photodiode array spectrometers, or in general, spectrometers based on image detectors can be developed with wide spectral coverage.

In the case of an inductively coupled plasma - Fourier transform spectrometer (ICP-FT) system, due to its inherent property of precise wavenumber calibration, analog and square cross-correlation masks were computer generated for use in the correlation analysis of interferograms. This, together with the wide spectral coverage provided by the Fourier transform spectrometer provide a high degree of flexibility in the use of the system. The cross-correlation masks are highly effective in obtaining quantitative and qualitative information directly from the interferograms obtained by the spectrometer. In carrying out elemental identification on the signals, a preliminary correlation operation is performed for all the elements. This procedure essentially shortens the list of elements that are suspected

to be present in the sample. Further investigations by correlation analysis on the suspected elements yield the final analytical results. A consequence of the simplicity of this correlation method, as compared to the usual FFT data processing method, is that a real time data processing system using a low cost microcomputer could be developed. The system utilizes a hardware multiplier and accumulator to carry out the actual correlation computation. The preliminary results obtained look promising and this approach warrants further investigations.

The comparable capability of the simplified cross-correlation masks, namely the binary masks for the ICP-PDA system and the square masks for the ICP-FT system when compared to the analog cross-correlation masks has certain advantages when implementing the correlation techniques. The correlation procedure becomes simple and fast, and binary and square masks are simple to store in read-only memories (ROM). This is important because storage of cross-correlation masks is necessary for high speed data processing.

In conclusion, spectral pattern recognition tasks are among the most difficult and complex operations to program and implement with electronic and computing technology. In fact we have some way to go before we

can rival the combination of the human brain and eye in such tasks. However, cross-correlation based procedures are beginning to provide a modest level of capability in automatic interpretation of complex data arrays and one can certainly foresee the important role of correlation techniques for data processing in simultaneous multielement analysis, or in general spectrochemical analysis.

## FOOTNOTES

[1] The notation used to label the axes throughout the thesis follows the version adopted in the computer graphics industry. For example, in Figure 3, the amplitude axis represents values ranging from 0 to 6000.

[2] In this particular example, the dynamic range problem is imposed by both the emission of the plasma background and the appearance of the noise spike. In cases where plasma background emission is low, such as in the solar blind spectral region, the dynamic range problem may be solely governed by the amplitude of the noise spike.

[3] The sodium lines appear between the lithium and potassium lines because of alaising (28).

## BIBLIOGRAPHY


1. L.R.P. Butler, H.G.C. Human and R.H. Scott, "Electrical Flames" in "Handbook of Spectroscopy", Vol. I, J.W. Robinson, Ed., CRC Press, Cleveland, Ohio 44128, 1974.
2. S. Greenfield, H.McD. McGeachin and P.B. Smith, Talanta, 22, 1 (1975).
3. S. Greenfield, H.McD. McGeachin and P.B. Smith, Talanta, 22, 553 (1975).
4. P.W.J.M. Boumans and F.J. deBoer, Spectrochim. Acta, 30B, 309 (1975).
5. P.W.J.M. Boumans, Optica Pura Y Aplicada, 11, 143 (1978).
6. G.I. Bobat, J. Inst. Elec. Eng., 94, 27 (1947).
7. T.B. Reed, J. Appl. Phys., 32, 821 (1961).
8. T.B. Reed, J. Appl. Phys., 32, 2534 (1961).
9. S. Greenfield, I.L.W. Jones and C.T. Berry, Analyst, 89, 713 (1964).
10. R.H. Wendt and V.A. Fassel, Anal. Chem., 37, 920 (1965).
11. M.W. Blades, Ph.D. Dissertation, The University of Alberta, Edmonton, Alberta, Canada, 1981.
12. T.E. Edmonds and G. Horlick, Appl. Spectrosc., 31, 536 (1977).
13. P.W.J.M. Boumans, Proc. Analyt. Div. Chem. Soc., 143, June 1977.
14. A.W. Witmer, J.A.J. Jansen, G.H. van Gool and G. Brouwer, Philips Tech. Rev., 34, 322 (1974).

15. F.G. Walthall, J. Res. U.S. Geol. Surv., 2, 61 (1974).
16. P.W.J.M. Boumans, R.F. Rumphorst, L. Willemsen and F.J. de Boer, Spectrochim. Acta, 28B, 227 (1973).
17. P.W.J.M. Boumans and G. Brouwer, Spectrochim. Acta, 27B, 247 (1972).
18. G. Horlick and E.G. Codding, Anal. Chem., 45, 1490 (1973).
19. G. Horlick and E.G. Codding, Appl. Spectrosc., 29, 167 (1975).
20. P.W. Fry, J. Phys. E., 8, 337 (1975).
21. D.A. Yates and T. Kuwana, Anal. Chem., 48, 510 (1976).
22. N. Furuta, Ph.D. Dissertation, The University of Tokyo, Tokyo, Japan, 1979.
23. M. Margoshes, Spectrochim. Acta, 25B, 113 (1970).
24. H.L. Felkel and H. Pardue, Anal. Chem., 50, 602 (1976).
25. A. Danielson and P. Lindblom, Physica Scripta, 5, 227 (1972).
26. H.L. Felkel and H.L. Pardue, Anal. Chem., 49, 1112 (1977).
27. H.A, Lewis and M.B. Denton, Journal of Automatic Chemistry, 3, 9 (1981).
28. G. Horlick, R.H. Hall and W.K. Yuen, "Atomic Emission Spectrochemical Measurements with a Fourier Transform Spectrometer" in "Fourier Transform Infrared Spectroscopy", Vol. 3, J.R. Ferraro and L.J. Basile, Eds., Academic Press, N.Y., (in press).

29. L.W. Chaney, L.T. Loh and M.T. Such, "A Fourier Transform Spectrometer for the Measurement of Atmospheric Thermal Radiation", Technical Report for ORA Project 05863, University of Michigan, Ann Arbour, 1967.

30. L.W. Chaney, S.R. Drayson and C. Young, Appl. Opt., 6, 347 (1967).

31. G. Horlick, Ph.D. Dissertation, University of Illinois, Urbana, Illinois, U.S.A., 1970.

32. W.K. Yuen, Ph.D. Dissertation, The University of Alberta, Edmonton, Alberta, Canada, 1978.

33. R.H. Hall, Ph.D. Dissertation, The University of Alberta, Edmonton, Alberta, Canada, 1979.

34. G.M. Hieftje, Anal. Chem., 44, 69A (1972).

35. G.M. Hieftje, R.I. Bystroff and R. Lim, Anal. Chem., 45, 253 (1973).

36. G. Horlick, Anal. Chem., 45, 319 (1973).

37. K.R. Betty, Ph.D. Dissertation, The University of Alberta, Edmonton, Alberta, Canada, 1977.

38. G. Horlick and G.M. Hieftje, "Correlation Methods in Chemical Data Measurement" in "Contemporary Topics in Analytical and Clinical Chemistry", Vol. 3, Eds., D.M. Hercules, G.M. Hieftje, L.R. Snyder and M.A. Evenson, Plenum, New York, 1978.

39. G.M. Hieftje and G. Horlick, Am. Lab., 13(3), 76 (1981).

40. J.W. Cooley and J.W. Tukey, Math. Comp., 19, 297 (1965).

41. R. Bracewell, "The Fourier Transform and Its Applications", McGraw Hill, New York, 1965.

42. D.C. Champeney, "Fourier Transforms and Their Physical Applications", Academic Press, London, 1973.

43. B. Liu, "Digital Filters and the Fast Fourier Transform", Halsted Press, New York, 1975.

44. N. Ahmed and K.R. Rao, "Orthogonal Transforms for Digital Signal Processing", Springer-Verlag, New York, 1975.

45. P.R. Griffiths, "Transform Techniques in Chemistry", Plenum, New York, 1978.

46. A. Zachor, J. Opt. Soc. Am., 56(10), VI (1966).

47. G. Horlick, Anal. Chem., 43, 61A (1971).

48. K.R. Betty and G. Horlick, Anal. Chem., 32, 31 (1978).

49. L.A. Powell and G.M. Hieftje, Anal. Chem. Acta, 100, 313 (1978).

50. D.G. Mitchell, K.W. Jackson and K.M. Aldous, Anal. Chem., 45, 1215A (1973).

51. K.W. Jackson, K.M. Aldous and D.G. Mitchell, Appl. Spectrosc., 28, 569 (1974).

52. K.W. Busch, N.G. Howell and G.H. Morrison, Anal. Chem., 46, 575 (1974).

53. K.M. Aldous, D.G. Mitchell and K.W. Jackson, Anal.

Chem., 47, 1034 (1975).

54. Y. Talmi, Anal. Chem., 47, 658A (1975).

55. Y. Talmi, Anal. Chem., 47, 699A (1975).

56. G.A. Mills, Ind. Eng. Chem., 42, 182 (1950).

57. B.J. Duffy and H.M. Hart, Chem. Eng. Progr., 48, 344 (1952).

58. J.V. Brunnock, D.F. Duckworth and G.G. Stevens, J. Inst. Petrol., 54, 310 (1968).

59. J.P. Walters, "A Synergic Approach to Graduate Research in Spectroscopy and Spectrochemical Analysis" in "Contemporary Topics in Analytical and Clinical Chemistry", Eds., D.M. Hercules, G.M. Hieftje, L.R. Synder and M.A. Evenson, Plenum, New York, 1978.

60. D. Hull, Ph.D. Dissertation, The University of Alberta, Edmonton, Alberta, Canada, 1981.

61. Reticon Corp., 910 Benicia Ave., Sunnyvale, CA 94086, The R5401 Binary to Analog Correlator.

62. R. Bystroff and T. Hirschfeld, Pittsburgh Conference on Analytical Chemistry and Applied Spectroscopy, Atlantic City, N.J., 1980, paper no. 338.

63. Y.W. Lee, T.P. Cheatham, Jr. and J.B. Wiesmer, Proc. IRE, 38, 1165 (1950).

64. Y.W. Lee, "Statistical Theory of Communication", John Wiley and Sons, New York, 1960.

65. F.H. Lange, "Correlation Techniques", D. Van Nostrand, Princeton, N.J., 1967.

66. Reticon Corp., 910 Benicia Ave., Sunnyvale, CA 94086, RC 5601 Discrete Fourier Transform.

67. S.T. Kowel, Optical Spectra, 7, 52 (1980).

68. Desert Microsystems, Incorporated, Pasco, Washington 99301, Fast Fourier Transform Firmwares.

69. Analog Devices Inc., Mass. 02062, Sample and Hold Module, SHA 1A, Document C098-10-4/71.

70. Analog Devices Inc., Mass. 02062, Low Cost General Purpose Analog to Digital Converter, Document C128-10-5/72.

71. TRW LSI Products, CA 90278, High Speed Multiplier-Accumulator, Document 109A-1/79.

72. Rockwell International Corp., CA 92803, AIM 65 Microcomputer User's Guide, 1979.

73. Rockwell International Corp., CA 92803, AIM 65 BASIC Language Reference Manuel, 1979.

74. H.V. Malmstadt, C.G. Enke and S.R. Crouch, "Experiments in Digital and Analog Electronics", E & L Instruments, Inc., Connecticut 06418, page I80, 1977.

75. G. Horlick, Appl. Spectrosc., 30, 113 (1976).

76. J. Connes, "Computing Problems in Fourier Spectroscopy" in "Aspen International Conference on Fourier

Spectroscopy", AFCRL-71-0019, Eds., G.A. Vanasse, A.T. Stair Jr. and D.J. Baker, 1970.

77. G. Guelachvili and J.P. Maillard, "Fourier Spectroscopy from $10^6$ Samples" in "Aspen International Conference on Fourier Spectroscopy", AFCRL-71-0019, Eds., G.A. Vanasse, A.T. Stair Jr. and D.J. Baker, 1970.
78. P.R. Griffiths, "Transform Techniques in Chemistry", Plenum, New York, 1978.
79. J.H. Davies, Anal. Chem., 42, 101A (1970).
80. R.C. Wieboldt, B.A. Hohne and T.L. Isenhour, Appl. Spectrosc., 34, 7 (1980).
81. D.M. Coleman and J.P. Walters, Spectrochim Acta, 33B, 127 (1978).
82. G. Horlick and W.K. Yuen, Anal. Chem., 47, 775A (1975).
83. Y. Talmi, R. Crosmun and N.M. Larson, Anal. Chem., 48, 326 (1976).
84. J.D. Ingle Jr., Anal. Chem., 49, 339 (1977).
85. C.Th.J. Alkemade, T. Hollander and K.E.J. Zijlstra, Spectrochim Acta, 34B, 85 (1979).
86. G.M. Hieftje and R.I. Bystroff, Spectrochim Acta, 30B, 187 (1975).
87. R. Belchamber and G. Horlick, Spectrochim. Acta, (in press).
88. G.L. Walden, J.N. Bower, S. Nikdel, D.L. Bolton and

J.D. Winefordner, Spectrochim. Acta, 35B, 535 (1980).

89. S. Greenfield, I.L.W. Jones, C.T. Berry and L.G. Bunch, Proc. Soc. Anal. Chem., 2, 111 (1965).

90. D. Truitt and J.W. Robinson, Anal. Chim. Acta, 49, 401 (1970).

91. D. Truitt and J.W. Robinson, Anal. Chim. Acta, 51, 61 (1970).

92. S. Greenfield and H. McGeachin, Anal. Chim. Acta, 100, 101 (1978).

93. S. Greenfield and D.T. Burns, Anal. Chim. Acta, 113, 205 (1980).

94. A. Montaser and J. Mortazavi, Anal. Chem., 52, 255 (1980).

95. L. Ebdon, D.J. Mowthorpe and M.R. Cave, Anal. Chim. Acta, 115, 171 (1980).

96. L. Ebdon, D.J. Mowthorpe and M.R. Cave, Anal. Chim. Acta, 115, 179 (1980).

97. E. Choot and G. Horlick, Pittsburgh Conference on Analytical Chemistry and Applied Spectroscopy, Atlantic City, N.J., 1981, paper no. 124.

98. R.M. Barnes and G.A. Meyer, Anal. Chem., 52, 1523 (1980).

99. A.T. Zander and G.M. Hieftje, Anal. Chem., 50, 1257 (1978).

100. J.J. Fitzgerald, T.L. Chester and J.D. Winefordner,

Anal. Chem., 47, 2330 (1975).

101. T. Dohi and T. Suzuki, Applied Optics, 10, 1359 (1971).

102. P. Connes, Rev. Opt., 38, 157 (1959).

103. H. Bar-Lev, Infrared Phys., 7, 93 (1967).

104. M.J.D. Low, Anal. Lett., 1, 819 (1968).

105. D. Kuehl and P.R. Griffiths, Anal. Chem., 50, 418 (1978).

106. P.W.J.M. Boumans, and M. Bosveld, Spectrochim. Acta, 34B, 59 (1979).

107. R.K. Winge, V. Peterson, V.A. Fassel and M. Floyd, Pittsburgh Conference on Analytical Chemistry and Applied Spectroscopy, Atlantic City, N.J., 1980, paper no. 397.

## APPENDIX I

### Alternate Methods of
### Recycling Fast Fourier Transform Algorithms

In this appendix, several recycling implementations other than the one presented in Chapter II when Scheme 2 is used as the primary FFT method will be illustrated. The computer software is identical to the one described in Chapter II and will not be repeated here.

Let us recall that Scheme 2 does produce real and imaginary output arrays and the imaginary array was ignored in the recycling method presented as Scheme 4 in Chapter II. It would seem that a recycling method as illustrated below:

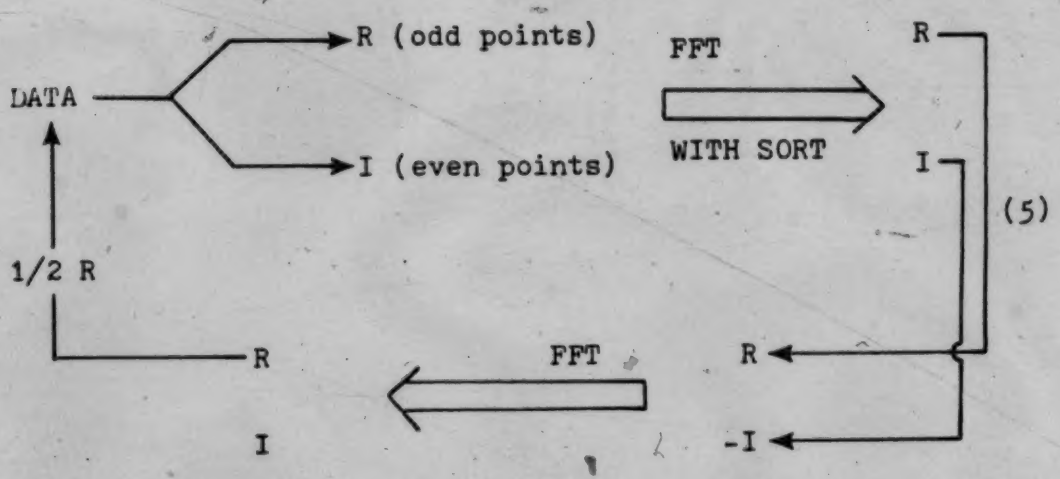


should also be valid. In this scheme the real output array is put into the real input array of the second FFT and the negative of the imaginary output array is put into the

imaginary input array of the second FFT and the FFT implemented in the normal way. The real, imaginary and amplitude output arrays for the second FFT are shown in Figure 88. This method works, but now the data occupy only half of the output arrays.

Another approach is to ignore the imaginary output of the first FFT and recycle using Scheme 1 to set up the second FFT. This is outlined below:

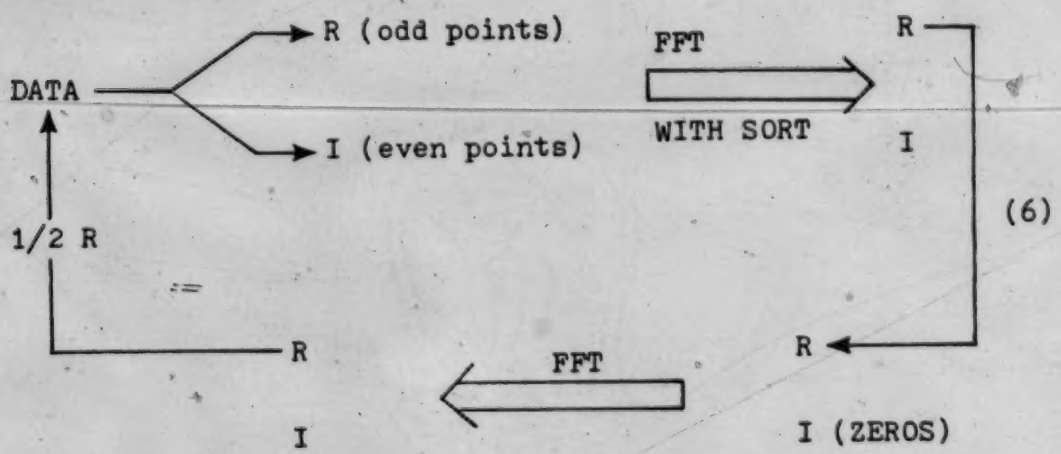


This also "works" as shown in Figure 89, but now the output arrays contain redundant information in the upper and lower halves.

Finally, a pseudo double sided interferogram similar to the interferograms generated by Fourier transform spectrometers can be constructed from the real output of

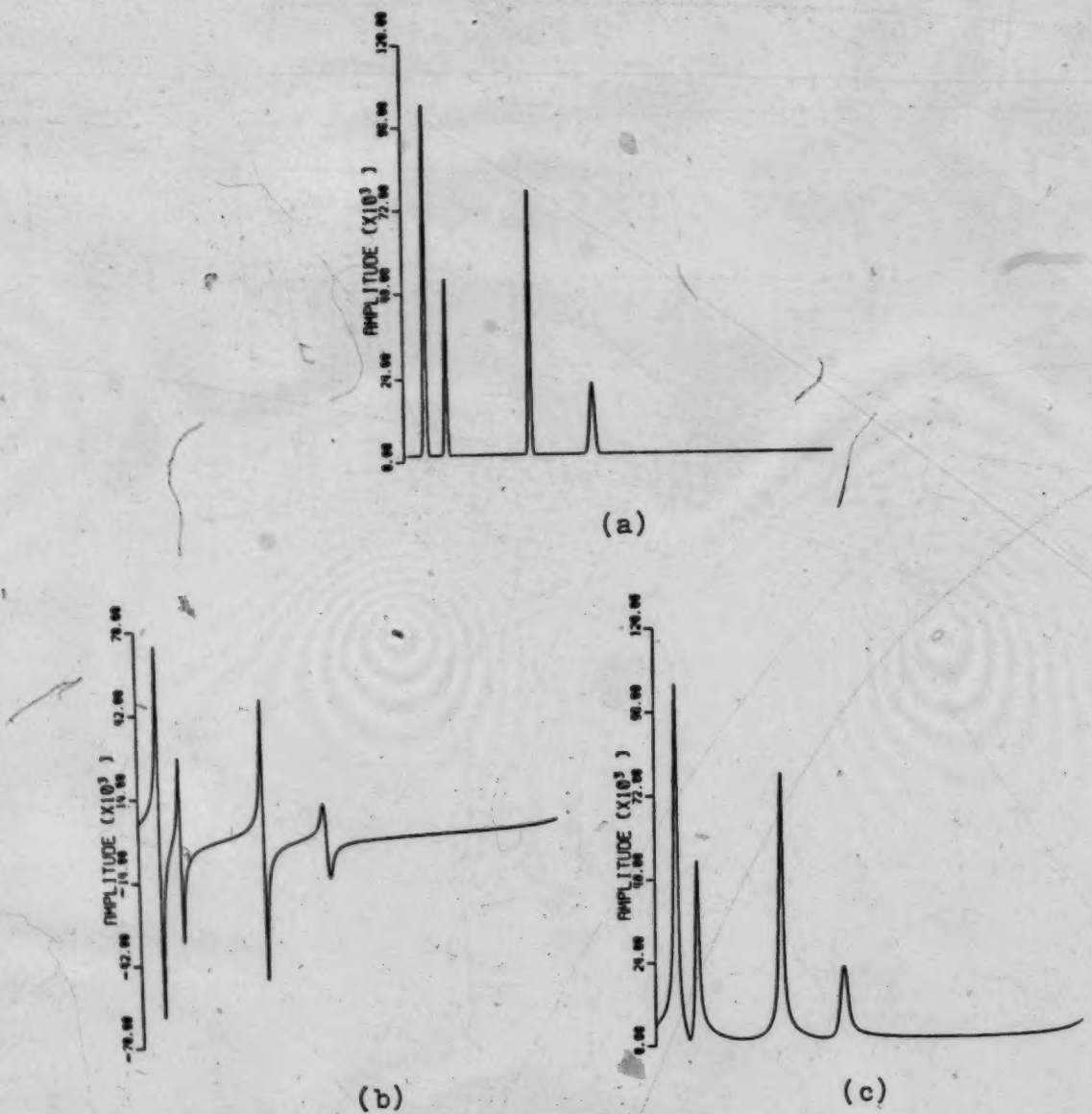


FIGURE 88. (a) Real, (b) imaginary and (c) amplitude output arrays for Scheme 5 inverse FFT implementation.

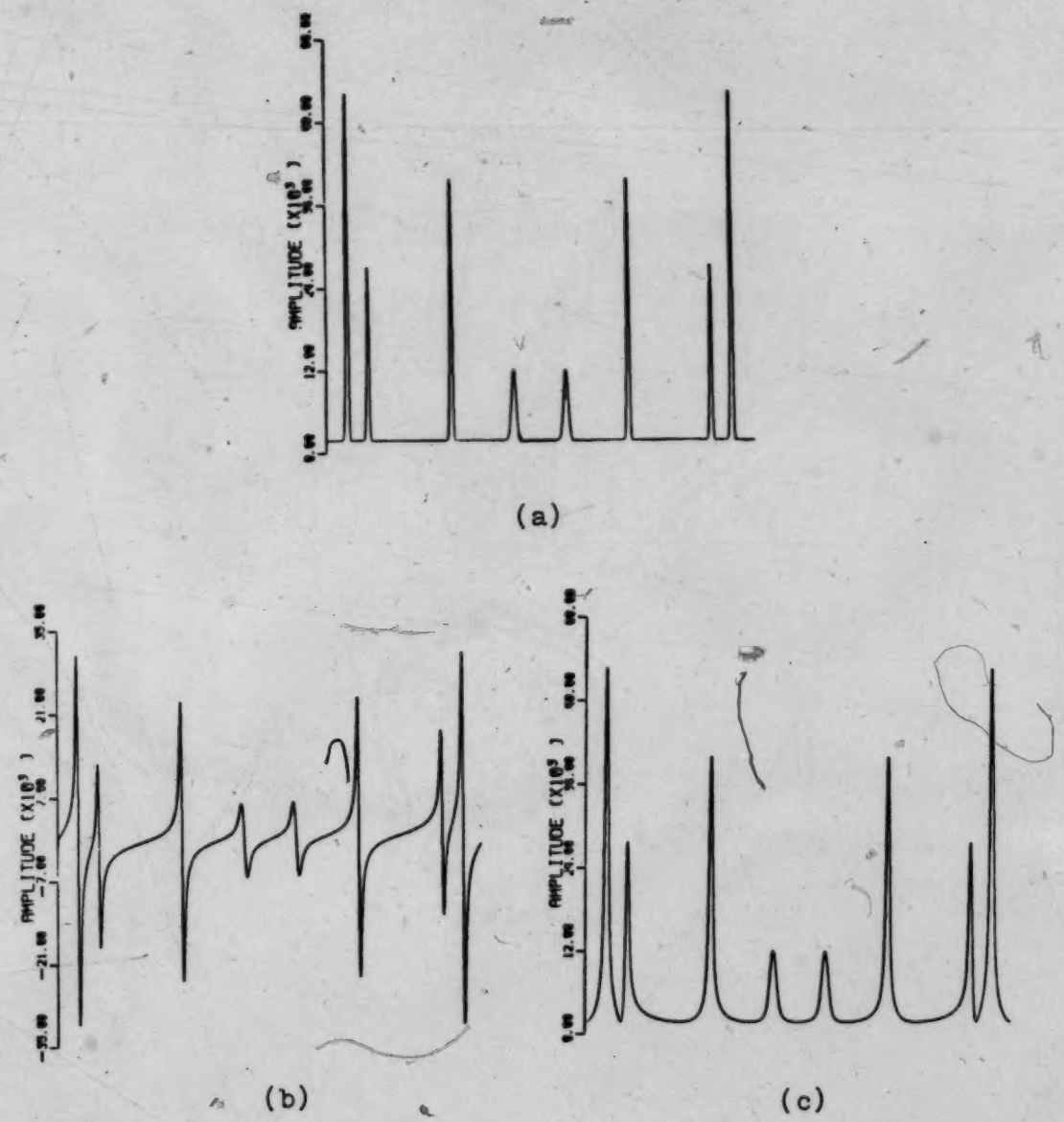


FIGURE 89. (a) Real, (b) imaginary and (c) amplitude output arrays for Scheme 6 inverse FFT implementation.

the Scheme 2 FFT. It is simply necessary to "reflect" it about the origin generating a new array, twice the number of the original data points as shown in Figure 90. The real, imaginary and amplitude output arrays for the second FFT when processed as outlined below:

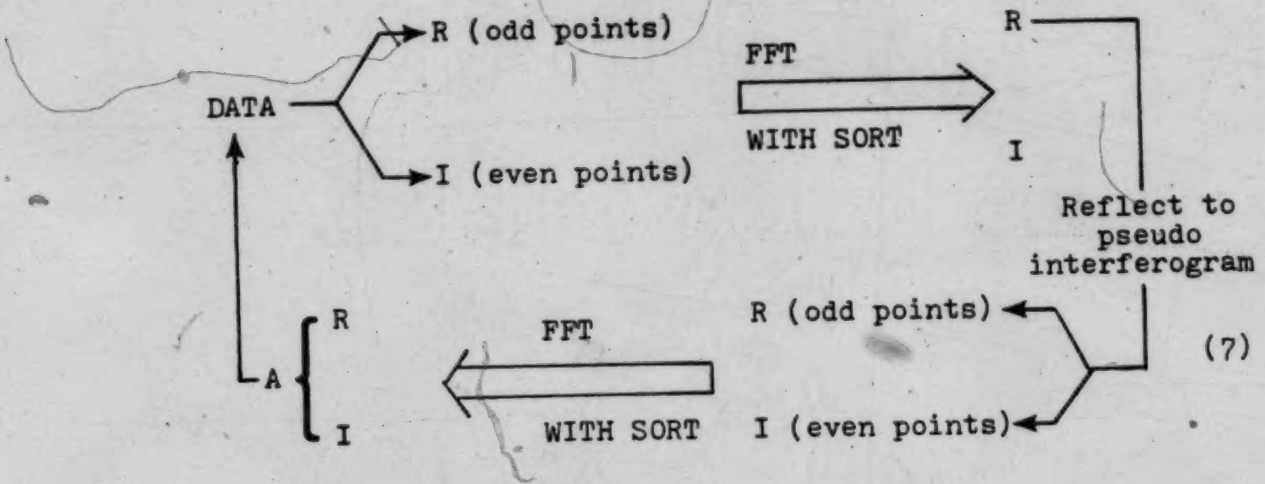


are shown in Figure 91. The amplitude array now contains the original data.

While Schemes 5-7 do represent somewhat unconventional inverse FFT routes they do clarify the information content of the various input and output arrays and illustrate that no one method is solely acceptable. In addition Scheme 7 illustrates the relationship of "double sided" interferogram type signals as generated by Fourier transform spectrometers to the output arrays when conventional spectra are transformed to the Fourier domain.

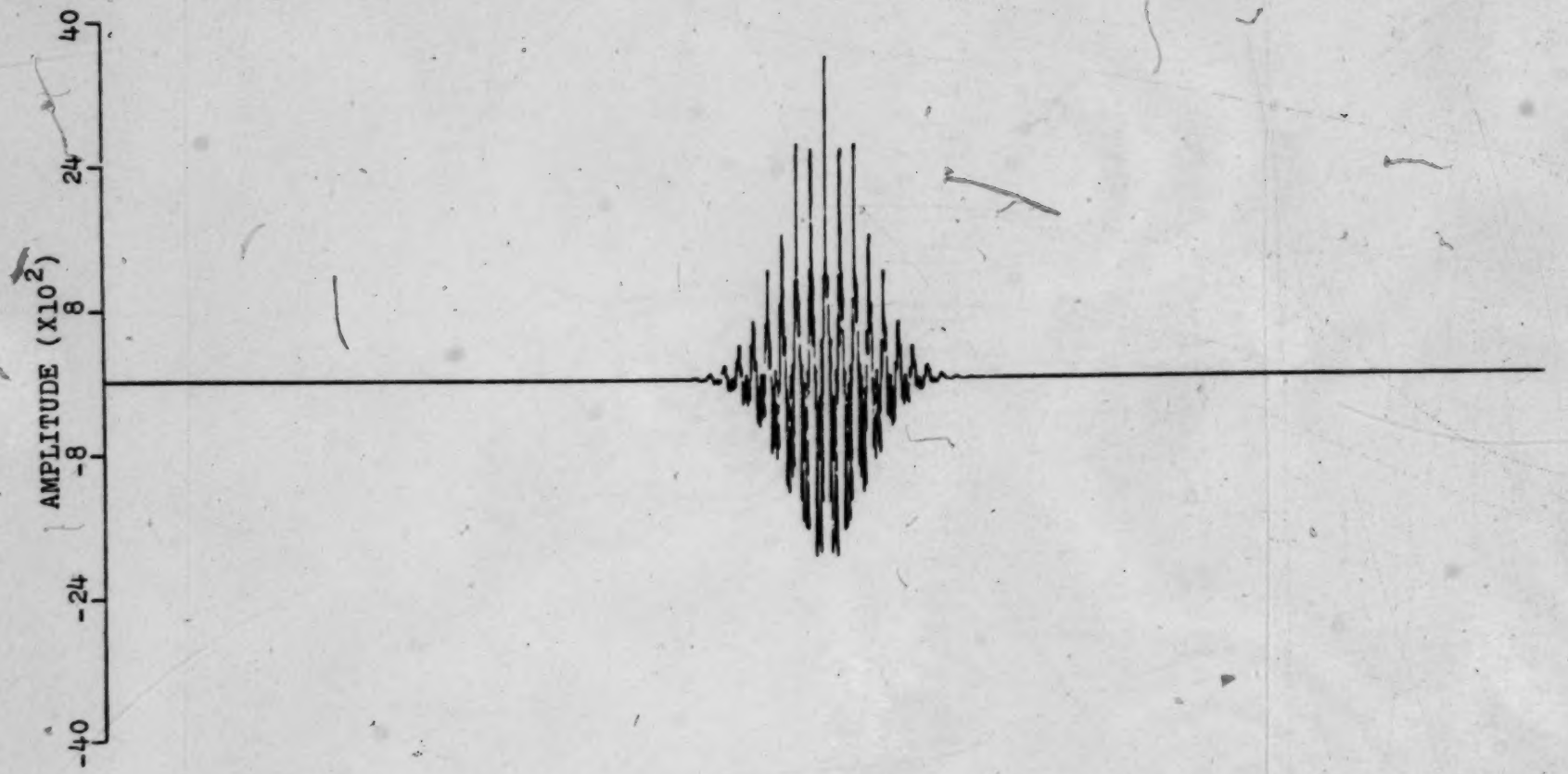


FIGURE 90. Pseudo interferogram obtained by reflecting the real output array of the Scheme 2 FFT about itself.

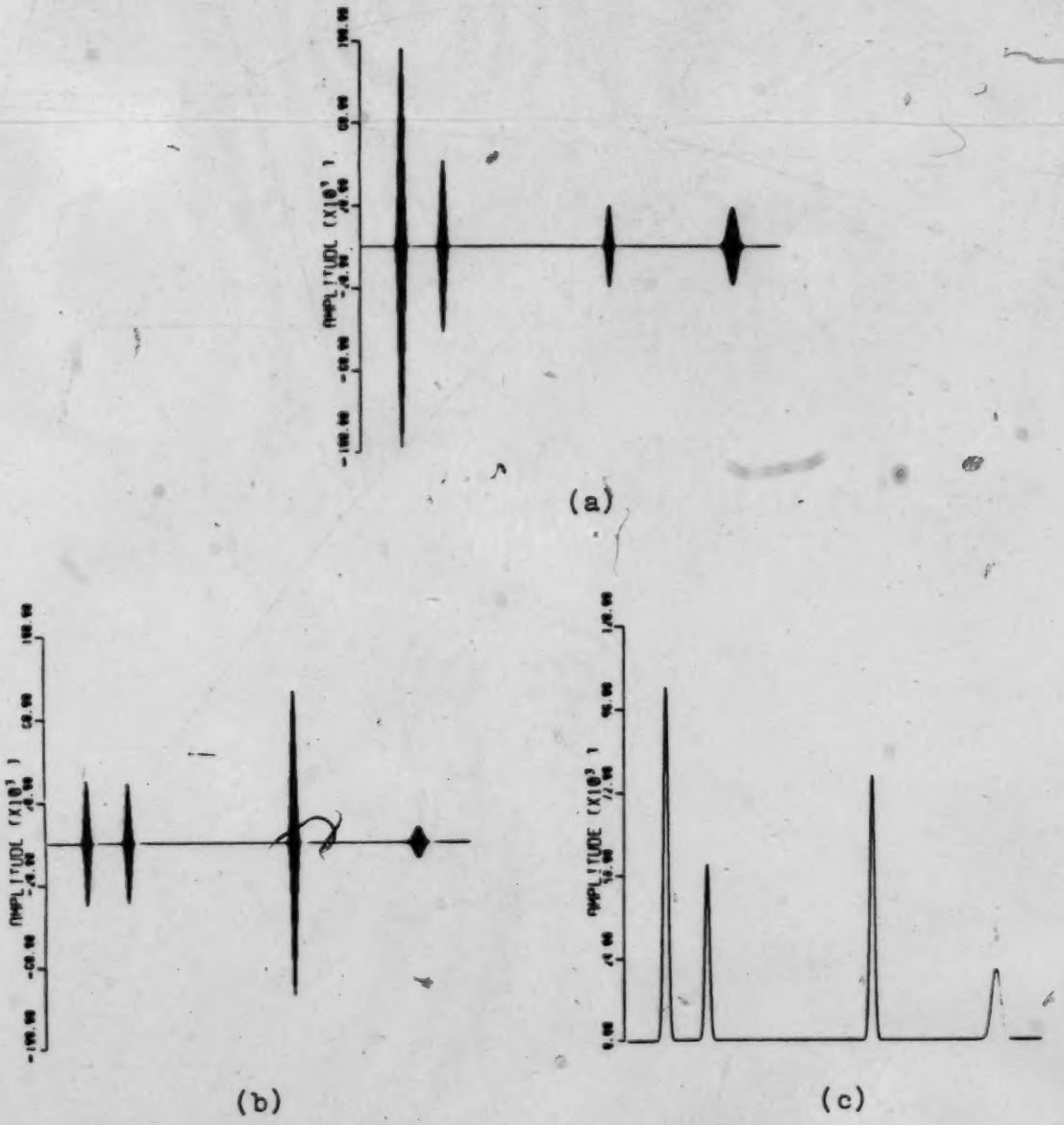

FIGURE 91. (a) Real, (b) imaginary and (c) amplitude output arrays for Scheme 7 inverse FFT implementation.

Several analogous manipulations of the real and imaginary output arrays for recycling when Scheme 1 was used to implement the first transform were investigated. None proved useful. In general, they generated severely overlapped information.

## APPENDIX II

### Modifications of the Michelson Interferometer

The Michelson interferometers in our research laboratory have evolved over more than 15 years. The original version of the interferometer was designed and built by Chaney (29,30) at the University of Michigan and was later adapted by Horlick (31) in 1969 at the University of Illinois. This design was then significantly modified into the present form by Yuen (32) and Hall (33). In this appendix, modifications that have been made to the interferometers since then, up to the time of writing will be described.

### A. Photomultiplier Tube Dynode Chain Circuitry

Two changes have been made on the dynode chain circuitry. The 0.05 microfarad capacitor was originally wired to the negative voltage supply (-HV) by mistake. The configuration has now been changed so that the capacitor is connected to the ground. This will ensure all the high frequency noise that is going through the dynode chain to be grounded. The other change is the conversion of the voltage output circuitry to the present current output configuration. This simply involves the removal of the load resistor and enables the current amplifier to be described later in this appendix to be utilized.

The final configuration of the photomultiplier tube dynode chain circuitry is shown schematically in Figure 92.

B. Photomultiplier Tube Housing

A 0.5 inch diameter UV grade quartz lens (Oriel A11-621-08) of focal length 13 mm is inserted between the entrance aperture of the PMT housing and the PMT. It is placed at a distance equal to its focal length from the aperture so that there is a significant increase in the amount of light that will reach the PMT. No experimental test has been carried out to see what is the difference between signal levels obtained with and without the lens.

C. Silicon Optical Detector

A new silicon diode detector from IR Industries, Inc. (catalog number: 8016L) is now being utilized. This detector provides better sensitivity than the old silicon diode because it has a large sensitive area and is equipped with a lens for focusing light onto the silicon diode. Again, no test has been done to check on the performance of these detectors.

D. Optical Filter Mount for the Detectors

Optical filters are invaluable for resolving dynamic

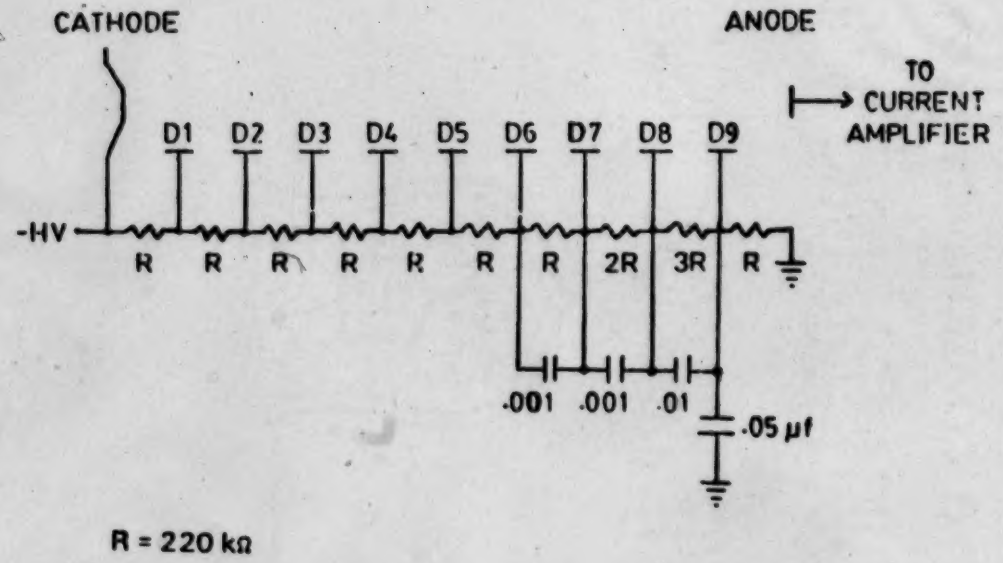


FIGURE 92. Modified photomultiplier tube dynode chain circuitry.

range problem imposed by the multiplex property of the Michelson interferometer (see Chapter IV). A mount designed for optical filters is attached to the detector mount. Optical filters such as those obtained from Oriel Corporation of America can be easily put in place in front of the detector. The optical mount can take any 1 inch diameter filters with thickness varying up to approximately 1 cm.

E. Micrometers on the Fixed Mirror Mount

The Michelson interferometer consists of a fixed mirror and a movable one. Final signal optimization is normally achieved by the alignment of the fixed mirror. In the case of UV signals, the alignment of this mirror is crucial and is not easy to achieve using a screw driver. Two differential micrometers obtained from Lansing Research Corporation, Ithaca, New York (model number: 22 505) are incorporated into the fixed mirror mount. Perfect alignment of this mirror can now be achieved very easily with the use of these micrometers.

F. Photomultiplier Tube Power Supply

The PMT is now powered by a high voltage supply obtained from Keithley Instruments (model number: 244).

The voltage can vary from -200 V to -2200 V.

G. Signal Measurement Electronics

The signal measurement channel has been redesigned with new electronic equipment . The current output from the detector is amplified with a Keithley 427 current amplifier before it is electronically filtered with a Krohn-Hite 3343 filter. The current amplifier can have a gain from $10^4$ to $10^{11}$ with d.c. suppression. Additional amplification can be obtained from the electronic filter (maximum 40 dB). This is usually configured as a bandpass filter. Final adjustment on the gain of the signal is provided by the PAR 225 low noise amplifier before the signal is input to the computer.

H. Old Mirror Drive System

The electrical wires that provide the power to move the mirror have been changed to smaller wires to provide smoother drive. In addition, some stop pins have been inserted into the mount to secure the springs in place.

I. New Mirror Drive System

Perhaps, the major modification to the interferometer system is at the mirror drive system. Two interferometer

systems are currently available in the laboratory. One with the old mirror drive system and the other with a new mirror drive system that is going to be described in this section.

A linear actuator (or linear moving coil motor) purchased from Kimco, Inc., San Marcos, California is used to drive the mirror in one of the two interferometer systems. This drive is capable of delivering a peak force of 8 pounds. With this new drive system, preliminary data show excellent stability even without the electronic phase locked loop and is certainly a great improvement over the old mirror drive.

# APPENDIX III

## Computer Software

A. Program Flow Chart and Listing for the Fast Fourier Transformation Program Based on the Cooley-Tukey Algorithm

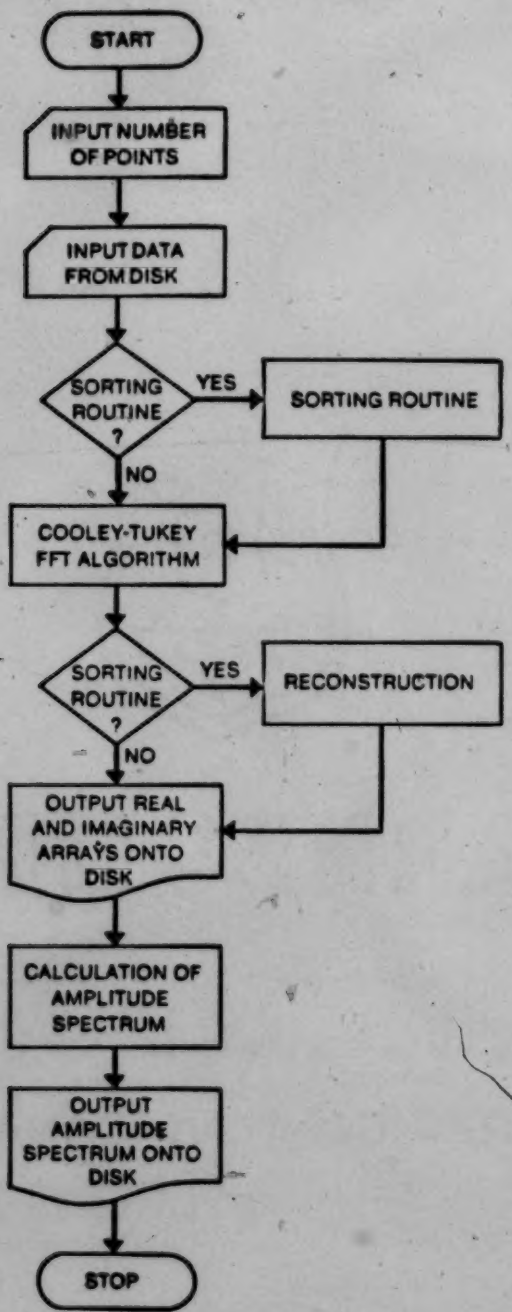


FIGURE 93. Flow chart for the FORTRAN FFT program.

```
C
C       THIS PROGRAM WILL PERFORM THE FAST FOURIER
C       TRANSFORMATION USING THE COOLEY-TUKEY
C       ALGORITHM
C
C       PROGRAM IS EXECUTED UNDER A RT-11 OPERATING
C       SYSTEM WITH A DEC PDP 11/10 MINICOMPUTER
C
C       SUBROUTINES REQUIRED:
C       (1)FORLIB
C       (2)SYSLIB
C
        DIMENSION X(4096),Y(4096),L(20)
C
C       COMPUTER REQUESTS AN INPUT TO INDICATE WHETHER
C       THE FFT IS WITH OR WITHOUT THE SORTING ROUTINE
C
C       SORTING FFT ROUTINE
C       - INPUT ONE DATA ARRAY
C       - ODD POINTS INTO REAL ARRAY X(N)
C       - EVEN POINTS INTO IMAGINARY ARRAY Y(N)
C       - REST FILLED WITH ZEROS
C       - FFT
C       - RECONSTRUCTION
C       - DATA OUTPUT
C
C       NON-SORTING FFT ROUTINE
C       - INPUT TWO DATA ARRAYS
C       - FFT
C       - DATA OUTPUT
C
        WRITE(7,100)
100     FORMAT(' ','0=SORT 1=NO SORT')
        READ(5,120) ISORT
120     FORMAT(I2)
C
C       COMPUTER REQUESTS INPUT OF NUMBER OF FFT POINTS
C       IN THE FORM OF 2**N
C
C       MAXIMUM NUMBER OF DATA POINTS IS 4096 (N=12)
C       FOR THIS PROGRAM
C       LIMITATION IS DUE TO THE SIZE OF THE COMPUTER
C       MEMORY
C
        WRITE(7,140)
140     FORMAT(' ','INPUT N (2**N)')
        READ(5,120) N2POW
        NP=2**N2POW
C
C       DATA INPUT
C
C       ONE INPUT ARRAY FOR SORTING ROUTINE
C       TWO INPUT ARRAYS FOR NON-SORTING ROUTINE
```

```
C
      CALL ASSIGN(10,'DK:DATA.DAT',-1,'OLD','NC',1)
      READ(10)(X(I),I=1,NP)
      IF(ISORT.EQ.0) GO TO 9
      READ(10)(Y(I),I=1,NP)
9     ENDFILE 10
      CALL CLOSE(10)
C
C     SORTING OF DATA ARRAY FOR SORTING FFT ROUTINE
C
C     ODD DATA POINTS INTO REAL ARRAY
C     EVEN DATA POINTS INTO IMAGINARY ARRAY
C     REST FILLED WITH ZEROS
C
      IF(ISORT.EQ.1) GO TO 12
      NPT=NP/2
      N=NP
      DO 2 I=1,NPT
      X(I)=X(I*2-1)
2     Y(I)=X(I*2)
      DO 3 I=NPT+1,NP
      Y(I)=0.0
3     X(I)=0.0
C
C     ***************************
C     COOLEY-TUKEY FFT ALGORITHM
C     ***************************
C
12    NTHPOW=2**N2POW
      N4POW=N2POW/2
      IF(N4POW)60,63,60
60    DO 61 IPASS=1,N4POW
      NXTLTH=2**(N2POW-2*IPASS)
      LENGTH=4*NXTLTH
      SCALE=6.2831853/FLOAT(LENGTH)
      DO 61 J=1,NXTLTH
      ARG=FLOAT(J-1)*SCALE
      C1=COS(ARG)
      S1=SIN(ARG)
      C2=C1*C1-S1*S1
      S2=C1*S1+C1*S1
      C3=C1*C2-S1*S2
      S3=C2*S1+S2*C1
      DO 61 ISQLOC=LENGTH,NTHPOW,LENGTH
      J1=ISQLOC-LENGTH+J
      J2=J1+NXTLTH
      J3=J2+NXTLTH
      J4=J3+NXTLTH
      R1=X(J1)+X(J3)
      R2=X(J1)-X(J3)
      R3=X(J2)+X(J4)
      R4=X(J2)-X(J4)
      FI1=Y(J1)+Y(J3)
      FI2=Y(J1)-Y(J3)
```

```
      FI3=Y(J2)+Y(J4)
      FI4=Y(J2)-Y(J4)
      X(J1)=R1+R3
      Y(J1)=FI1+FI3
      IF(J-1)64,62,64
64    X(J3)=C1*(R2+FI4)+S1*(FI2-R4)
      Y(J3)=-S1*(R2+FI4)+C1*(FI2-R4)
      X(J2)=C2*(R1-R3)+S2*(FI1-FI3)
      Y(J2)=-S2*(R1-R3)+C2*(FI1-FI3)
      X(J4)=C3*(R2-FI4)+S3*(R4+FI2)
      Y(J4)=-S3*(R2-FI4)+C3*(R4+FI2)
      GO TO 61
62    X(J3)=R2+FI4
      Y(J3)=FI2-R4
      X(J2)=R1-R3
      Y(J2)=FI1-FI3
      X(J4)=R2-FI4
      Y(J4)=R4+FI2
61    CONTINUE
63    IF(N2POW-2*N4POW)65,66,65
65    DO 67 J=1,NTHPOW,2
      R1=X(J)+X(J+1)
      R2=X(J)-X(J+1)
      FI1=Y(J)+Y(J+1)
      FI2=Y(J)-Y(J+1)
      X(J)=R1
      Y(J)=FI1
      X(J+1)=R2
67    Y(J+1)=FI2
66    DO 68 J=1,13
      L(J)=1
      IF(J-N2POW)69,69,68
69    L(J)=2**(N2POW+1-J)
68    CONTINUE
      IJ=1
      L1=L(13)
      NTHPOW=L(12)
      ISQLOC=L(11)
      J=L(10)
      N2P1=L(9)
      N2=L(8)
      NP2MJ=L(7)
      L8=L(6)
      N2POW=L(5)
      N4POW=L(4)
      LENGTH=L(3)
      NXTLTH=L(2)
      IPASS=L(1)
      DO 601 J1=1,L1
      DO 601 J2=J1,NTHPOW,L1
      DO 601 J3=J2,ISQLOC,NTHPOW
      DO 601 J4=J3,J,ISQLOC
      DO 601 J5=J4,N2P1,J
```

```
      DO 601 J6=J5,N2,N2P1
      DO 601 J7=J6,NP2MJ,N2
      DO 601 J8=J7,L8,NP2MJ
      DO 601 J9=J8,N2POW,L8
      DO 601 J10=J9,N4POW,N2POW
      DO 601 J11=J10,LENGTH,N4POW
      DO 601 J12=J11,NXTLTH,LENGTH
      DO 601 JI=J12,IPASS,NXTLTH
      IF(IJ-JI)610,610,601
610   R=X(IJ)
      X(IJ)=X(JI)
      X(JI)=R
      FI=Y(IJ)
      Y(IJ)=Y(JI)
      Y(JI)=FI
601   IJ=IJ+1
C
C     **********************************
C     COOLEY-TUKEY FFT ALGORITHM ENDS
C     **********************************
C
C     RECONSTRUCTION FOR THE SORTING FFT ROUTINE
C
      IF(ISORT.EQ.1) GO TO 19
      ARG=3.1415927/FLOAT(N)
      C1=COS(ARG)
      S1=-SIN(ARG)
      C1JX=1.
      S1JX=0.
      N2=N/2
      N2P1=N2+1
      DO 70 J=2,N2P1
      NP2MJ=N+2-J
      SORR1=X(J)+X(NP2MJ)
      SORI1=Y(J)-Y(NP2MJ)
      R=C1JX
      C1JX=C1JX*C1-S1JX*S1
      S1JX=R*S1+S1JX*C1
      SORR2=X(J)-X(NP2MJ)
      SORI2=Y(J)+Y(NP2MJ)
      SORR3=C1JX*SORR2-S1JX*SORI2
      SORI3=C1JX*SORI2+S1JX*SORR2
      Y(J)=0.5*(SORI1-SORR3)
      X(J)=0.5*(SORR1+SORI3)
      IF(J-N2P1)71,70,71
71    Y(NP2MJ)=0.5*(-SORI1-SORR3)
      X(NP2MJ)=0.5*(SORR1-SORI3)
70    CONTINUE
      X(1)=X(1)+Y(1)
      Y(1)=0.
C
C     DATA OUTPUT ONTO THE DISK
C
C     REAL ARRAY OUTPUT UNDER THE FILE NAME
```

```
C       -REAL.DAT
C       IMAGINARY ARRAY OUTPUT UNDER THE FILE NAME
C       -IMAG.DAT
C
19      CALL ASSIGN(10,'DK:REAL.DAT',11,'NEW','NC',1)
        WRITE(10)(X(I),I=1,NP)
        ENDFILE 10
        CALL CLOSE(10)
        CALL ASSIGN(10,'DK:IMAG.DAT',11,'NEW','NC',1)
        WRITE(10)(Y(I),I=1,NP)
        ENDFILE 10
        CALL CLOSE(10)
C
C       CALCULATION OF THE AMPLITUDE SPECTRUM
C
        DO 311  I=1,NP
        X(I)=SQRT(X(I)*X(I)+Y(I)*Y(I))
311     CONTINUE
C
C       AMPLITUDE SPECTRUM OUTPUT ONTO THE DISK UNDER
C       THE FILE NAME
C       -AMPL.DAT
C
        CALL ASSIGN(10,'DK:AMPL.DAT',11,'NEW','NC',1)
        WRITE(10)(X(I),I=1,NP)
        ENDFILE 10
        CALL CLOSE(10)
C
C       PROGRAM ENDS
C
C       ***************
C       ROGER C. L. NG
C       ***************
C
C       SUPERVISOR: DR. GARY HORLICK
C
C       JUNE 1980
C       CHEMISTRY DEPARTMENT
C       UNIVERSITY OF ALBERTA
C       EDMONTON,ALBERTA
C       CANADA
C
        STOP
        END
```

B. Computer Software for the AIM 65 / TRW Multiplier - Accumulator Data Processing System

(a) Program flow chart and listing for the main program in BASIC.

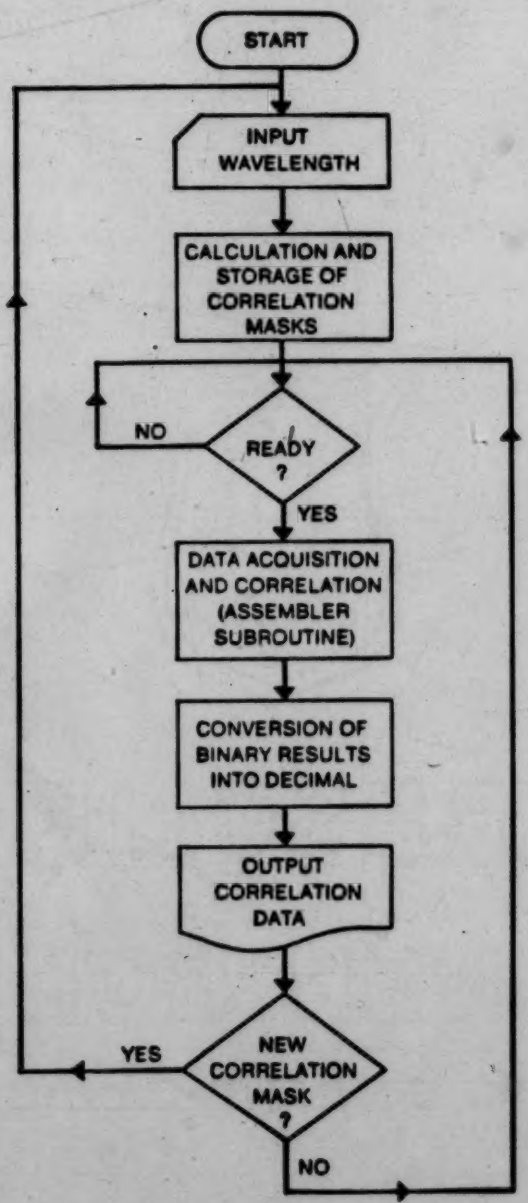


FIGURE 94. Flow chart for the BASIC program.

```
 10 INPUT"WAVELENGTH,NM";W
 15 W=3975.99/W
 20 FOR I=0 TO 255
 25 A=I*W
 30 R=COS(A)
 40 K=0
 50 IF R<0 THEN J=255
 60 IF R=0 THEN J=252
 70 IF R>0 THEN J=253
 80 IF K=1 THEN 130
 90 POKE 3072+I,J
100 K=1
110 R=SIN(A)
120 GOTO 50
130 POKE 3328+I,J
140 NEXT
150 POKE 4,0:POKE 5,7
155 PRINT"WAITING"
160 GET A$
170 IF A$="" THEN GOTO 160
175 PRINT"BE PATIENT"
180 DUM=USR(I)
190 I=0
200 IF I=0 THEN GOTO 230
210 C2=C1
220 I=4
230 A=PEEK(3584+I)
240 B=PEEK(3585+I)
250 C=PEEK(3586+I)
260 D=PEEK(3587+I)
270 C1=D*1.6777216E07+C*6.5536E04+B*2.56E02+A
280 IF C1>6.7108864E07 THEN C1=C1-1.34217728E08
290 IF I=0 THEN 210
300 RES=SQR(C1*C1+C2*C2)
```

```
310 PRINT!RES
320 PRINT"0=NEW MASK 1=NEW DATA"
330 INPUT I
340 IF I=0 THEN 10
350 GOTO 150
```

(b) Program flow chart and listing for the subroutine program in ASSEMBLER.

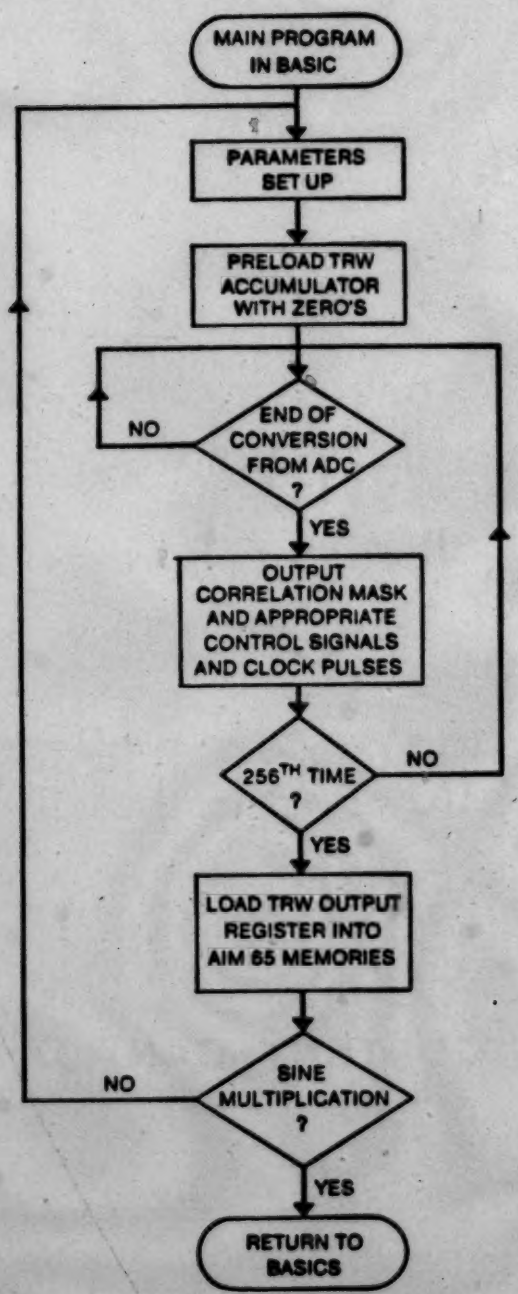


FIRURE 95. Flow chart for the ASSEMBLER program.

```
        *=$0700
        LDA #$00          ;INDEX FOR SINE OR COSINE
        STA $0F00         ;MULTIPLICATION
LOOP    LDX #$00          ;X REGISTER AS POINTER
        LDY #$FF          ;Y REGISTER AS NUMBER OF POINTS
        LDA #$FF          ;PORT B FOR OUTPUT
        STA $A002
        LDA #$00          ;PORT A FOR INPUT
        STA $A003
        LDA #%11001100    ;CA1, CB1 INPUT, FALLING EDGE MODE
        STA $A00C         ;CA2, CB2 OUTPUT, MANUEL PULSE MODE
        LDA #%11100000    ;PRELOAD MULTIPLIER WITH ZEROS
        STA $A000
        LDA #%11101100    ;GENERATE CLOCK X,Y WITH CB2
        STA $A00C
        LDA #%11001100
        STA $A00C
        LDA #%11001110    ;GENERATE CLOCK P WITH CA2
        STA $A00C
        LDA #%11001100
        STA $A00C
        LDA #%11111100    ;READY
        STA $A000
LONE    LDA $A00D         ;CHECK FOR END OF CONVERSION ON CA1
        AND #%00000010
        BEQ LONE          ;YES, GO AHEAD
        LDA $0F00         ;LOAD CORRELATION MASK AND CONTROL
        BEQ LTWO          ;SIGNALS ONTO PORT B
        LDA $0D00,X
        JMP LTHR
```

```
LTWO    LDA $0C00,X
LTHR    STA $A000
        LDA #%11101100    ;GENERATE CLOCK X,Y AND P
        STA $A00C
        LDA #%11001100
        STA $A00C
        LDA #%11001110
        STA $A00C
        LDA #%11001100
        STA $A00C
        LDA $A001         ;CLEAR INTERRUPT FLAG
        INX               ;INCREMENT POINTER
        DEY               ;DECREMENT COUNTER
        BNE LONE          ;REPEAT IF NOT FINISHED
        LDA $0F00         ;LOAD ACCUMULATOR OF MULTIPLIER
        BEQ LFIV          ;INTO AIM 65
        LDX #$04
        JMP LSIX
LFIV    LDX #$00
LSIX    LDA #%11100100    ;LOAD MULTIPLIER WITH ZEROS TO
        STA $A000         ;ENSURE NO FURTHER ACCUMULATION
        LDA #%11101100
        STA $A00C
        LDA #%11001100
        STA $A00C
        LDA #%11001100    ;LOAD PRODUCT IN 8-BIT SEGMENT
        STA $A000         ;WITH LEAST SIGNIFICANT FIRST
        LDA $A001
        STA $0E00,X
```

```
        LDA #%01001100
        STA $A000
        LDA $A001
        STA $0E01,X
        LDA #%10001100
        STA $A000
        LDA $A001
        STA $0E02,X
        LDA #%00001100
        STA $A000
        LDA $A001
        AND #%00000111
        STA $0E03,X
        LDA $0F00       ;CHECK IF COSINE MULTIPLICATION,
        BNE LFOU        ;REPEAT WITH SINE MULTIPLICATION
        INC $0F00
        JMP LOOP
LFOU    RTS             ;RETURN TO BASIC
```